STUDIES ON REMOVAL OF FLUORIDE AND ARSENIC FROM CONTAMINATED WATER

Ph.D. THESIS

by

VINEET KUMAR RATHORE

DEPARTMENT OF CHEMICAL ENGINEERING
INDIAN INSTITUTE OF TECHNOLOGY ROORKEE
ROORKEE-247667 (INDIA)
JUNE, 2018

STUDIES ON REMOVAL OF FLUORIDE AND ARSENIC FROM CONTAMINATED WATER

A THESIS

Submitted in partial fulfilment of the requirements for the award of the degree

of

DOCTOR OF PHILOSOPHY

in

CHEMICAL ENGINEERING

by

VINEET KUMAR RATHORE

DEPARTMENT OF CHEMICAL ENGINEERING
INDIAN INSTITUTE OF TECHNOLOGY ROORKEE
ROORKEE-247667 (INDIA)
JUNE, 2018

INDIAN INSTITUTE OF TECHNOLOGY ROORKEE
ROORKEE

CANDIDATES DECLARATION

I hereby certify that the work which is being presented in the thesis entitled **"STUDIES ON REMOVAL OF FLUORIDE AND ARSENIC FROM CONTAMINATED WATER"** in partial fulfilment of the requirements for the award of the degree of Doctor of Philosophy and submitted in the Department of Chemical Engineering of the Indian Institute of Technology Roorkee, Roorkee is an authentic record of my own work carried out during a period from July, 2012 to June, 2018 under the supervision of Dr. P. Mondal, Associate Professor, Department of Chemical Engineering, Indian Institute of Technology Roorkee, Roorkee.

The matter embodied in this thesis has not been submitted by me for the award of any other degree of this or any other Institute.

(VINEET KUMAR RATHORE)

This is to certify that the above statement made by the candidate is correct to the best of my knowledge.

(P. MONDAL)
Supervisor

Date: June , 2018

DEDICATED TO
ALMIGHTY GOD AND MY
FAMILY

ABSTRACT

Water is a vital component of life and also an important building block for the ecosystem. In the last few decades, due to growth in human population and industries, this component of the ecosystem is facing some serious challenges and has become scarce in its usable form as drinking water. Groundwater is most important source of drinking water and irrigation for more than 50 % of the global population. The rapid increase in global population and industrial activities has caused overexploitation of groundwater, which in turn has resulted in a drastic degradation of its quality. More and more cases of groundwater contamination with inorganic pollutants, salinity, heavy metals, etc., are coming into light day by day.

Arsenic and fluoride are two of such contaminants, which have posed greatest threat to the human beings. It is estimated that, worldwide the number of people suffering from high arsenic and fluoride content in drinking water is about ten million and a hundred million, respectively. The consumption of drinking water having excess quantities of these contaminants results in several types of diseases and health related problems like bone and skeletal fluorosis due to fluoride and different types of cancers due to arsenic. Because of these probable severe adversities in drinking water, WHO has issued guideline value of 10 μg/L and 1500 μg/L for arsenic and fluoride, respectively. Also, the maximum permissible limits, as per the Indian Standard (IS 10500) are recommended as 10 μg/L and 1500 μg/L for arsenic and fluoride, respectively. There are many countries around the world like India, China, Mexico, Argentina, and Pakistan, where these contaminants are reported to coexist in groundwater. The co-occurrence of both these contaminants in the groundwater of many areas in Rajnandgaon District, Chhattisgarh, India has been reported to be well above the permissible limits. Co-occurrence of these pollutants may create more serious effects on human health.

Natural clays have excellent capacities to accumulate both anionic as well as cationic pollutants either through ion exchange or adsorption or both. Laterite soil, in particular, is considered as good adsorbent as it has high content of aluminum oxide (Al_2O_3 ~ 21%), iron oxide (Fe_2O_3 ~ 47%) and silica (SiO_2 ~ 28%) as well as has arsenic and fluoride removal capacity. The removal efficiency of laterite can also be improved by its surface modification. Further, both arsenic and fluoride can exist as negatively

charged species in solution under certain conditions but their speciation chemistry is different. Thus, the presence of both species in solution may influence the individual removal of these species.

In many of the recently published papers, metal oxides and metal hydroxides are reported to be potential candidates for the adsorptive removal of arsenic and fluoride from water. These adsorbents are abundantly available in nature in the form of various types of minerals and can also be synthesized in a laboratory easily. In particular, oxides and hydroxides of aluminum are studied extensively for the remediation of arsenic and fluoride bearing water. Alumina is one of the most broadly studied adsorbents for the removal of fluoride from water.

It is also reported in many of the literature that the spent adsorbent can be reused several times with the help of regeneration process; however, the limitation of the regeneration is that it subsequently decreases the adsorption capacity of the material with every cycle of usage and it needs to be discarded after certain number of cycles. Further, regeneration also creates some pollutants. The regeneration step can be neglected in the case of low cost adsorbents as they are mostly made from such raw materials that have almost no commercial value and their regeneration can be even more costly than the actual cost of the production. Thus, the concerns related to the disposal of spent adsorbent still remain unanswered.

Apparently, it seems that the solidification of spent adsorbent derived from low cost material may be an attractive route for its management. In reality, spent adsorbent management issue is not well studied, which is very important for the applicability of the adsorbents. Frequently, it has been observed that the spent adsorbent/sludge is disposed on the ground leading to possible contamination of surface water and groundwater sources through seepage. Further, surface modification increases the cost of the adsorption process and produces many environmental consequences. Thus, to get a suitable adsorbent for sustainable utilization, the life cycle analysis of the adsorbent is important.

In the present study, adsorptive removal of arsenic and fluoride has been carried out with the help of 2 different types of adsorbents, i.e., Acid base treated laterite soil (ABTL) and aluminum oxide/hydroxide nanoparticles (AHNP). For both the adsorbents,

the effects of various process parameters like initial pH of the solution, dose of adsorbent, contact time and initial concentration of ions have been studied. In case of ABTL as adsorbent, optimum conditions for maximum removal of both the contaminants (arsenic and fluoride) in the single component system are found as pH 5, adsorbent dose 20 g/L, contact time 300 min with an initial concentration of arsenic as 500 µg/L and fluoride as 10000 µg/L, respectively. Adsorption isotherm data was well described with Langmuir model and under the optimum conditions, the Langmuir maximum adsorption capacity of ABTL is found to be 769 µg/g and 526 µg/g for arsenic and fluoride, respectively. Adsorption followed pseudo second order kinetics for both the contaminants in single component. Further, binary adsorption experiments were also performed at the same optimum conditions with varying concentrations of arsenic and fluoride. In the binary adsorption studies, the adsorption of arsenic does not get affected much as the concentration of fluoride is increased, while fluoride shows antagonistic behavior and its adsorption decreases as the concentration of arsenic is increased. The extended Freundlich model is found to best represent the apparent equilibrium adsorption phenomena in binary system.

In case of AHNP adsorbent, the optimal conditions for maximum removal of arsenic and fluoride are found as pH 7, adsorbent dose 2 g/L and 8 g/L for arsenic and fluoride, respectively, and contact time 300 min for the single component system. The adsorption process is well explained by Langmuir isotherm and follows pseudo second order kinetics for both arsenic and fluoride. The Langmuir maximum adsorption capacity of AHNP is found as 833.33 µg/g for arsenic and 2000 µg/g for fluoride at optimum conditions. Binary adsorption study was performed at the same optimum conditions using AHNP also with varying the concentrations of arsenic and fluoride. In the binary adsorption studies, arsenic showed slightly synergistic behavior as the concentration of fluoride is increased, while fluoride shows antagonistic behavior and its adsorption decreases as the concentration of arsenic is increased. Among different bi-component isotherms, the modified competitive Langmuir isotherm is found to well describe the bi-component system. The performance of both the adsorbents has also been tested successfully with the help of a real groundwater sample having arsenic 512 µg/L and fluoride 6300 µg/L along with other ions in batch mode of operation.

The performance of both the adsorbents has also been tested in the column mode of operation. For this study, a column made of Perspex was used which had an internal diameter of 1 cm and the influent was introduced in up flow direction by a peristaltic pump. The bed height was taken as 20 cm for both the adsorbents and initial concentrations of arsenic and fluoride were taken as 500 µg/L and 10000 µg/L respectively. In these studies, the effect of flow rate of the influent was studied from 17 ml/hr to 50 ml/hr for ABTL adsorbent and from 17 ml/hr to 100 ml/hr for AHNP.

To further describe the adsorption mechanism, various column adsorption kinetic models were applied to fit the experimental data. Thomas model and Yoon Nelson model showed good correlation for the adsorption of both arsenic and fluoride for both the adsorbents. The Thomas model estimated the maximum adsorptive capacity of the ABTL adsorbent as 60.37 µg/g for arsenic and 384 µg/g for fluoride whereas for AHNP adsorbent it was 18323.7 µg/g for arsenic and 13390.89 µg/g for fluoride in the column mode of operation. The Yoon Nelson model estimated the time required to reach 50 % breakthrough curve (τ). For ABTL adsorbent, the value of τ are found to be 9292.87 min for arsenic and 2719.83 min for fluoride, whereas, for AHNP adsorbent, values of τ are found as 44153.5 min for arsenic and 12102.75 min for fluoride. The Adam-Bohart model assessed the adsorption performance of the columns at different flow rates of the influent and predicted the adsorption capacity coefficient and thus the column performance. The increase in flow rate of the influent speeded up the exhaustion of the column.

After adsorption, the spent adsorbents have been stabilized as clay bricks. The effects of concentration of spent adsorbent and sintering temperature have been investigated on the properties of bricks and leaching of arsenic and fluoride. The bricks have been tested for various properties like density, percentage water absorption, shrinkage, compressive strength, and efflorescence. The maximum values of density and shrinkage of the bricks formed are found as 2.3 g/cm^3 and 10.2 % respectively, whereas the percentage water absorption and compressive strength of the bricks are found to range between 11 % to 14 % and 35 kgf/cm^2 to 150 kgf/cm^2 respectively. All the test results are in accordance with the criteria set by Indian Standards for building bricks. The leaching test of arsenic and fluoride from the bricks reveals that their maximum

values in leachate are 510 µg/L and 2100 µg/L respectively, which are below the permissible limits as per USEPA standards.

Life cycle assessment (LCA) of defluoridation of water using laterite soil based adsorbents has been carried out. The scope of LCA study consists of cradle to grave approach (i.e., starting from the acquisition of raw materials to the management of spent adsorbent). Environmental impacts associated with the defluoridation process are interpreted with the help of CML 2001 and TRACI methods using GaBi 6.0 software. All calculations are based on the amount of adsorbent required to reduce the fluoride concentration from 10000 µg/L to 1500 µg/L of 720 L water. The results from life cycle impact assessment reveal that the overall impacts are highest for TTL followed by ABTL and ATL. The fluoride adsorption capacity of adsorbents is found as the key factor influencing environmental impacts. Further, through sensitivity analysis, loading capacity of the vehicle and the distance between the mining and the processing site are found to play important role in environmental degradation, which can be reduced by selecting a vehicle with lower loading capacity due to its higher fuel economy.

ACKNOWLEDGEMENT

I take the opportunity to express my deepest gratitude to all those, who have made it possible for me to submit this work in the hands of the learned elite.

I express my deep sense of gratitude, indebtedness and respect towards my revered guide **Dr. P. Mondal**, Associate Professor, Department of Chemical Engineering, Indian Institute of Technology, Roorkee, who provided wholehearted co-operation, never ending inspirations and guidance, all blended with the personal touch throughout the duration of this work. His painstaking efforts during experimentation, invaluable suggestions and through discussions have immensely contributed towards the completion of this work.

Heartily thanks to all the members of my Student Research Committee (SRC), especially Prof. Shri Chand and Prof. A. A. Kazmi for their time and invaluable input to the present research.

I take this opportunity to put on record my respects to Prof. S. Sinha, Head of the Department, for providing various facilities during the course of the present research.

I also thank Dr. Ravi Shankar, Dr. Lokendra Singh Thakur, Dr. Anil Kumar Varma, Mr. Amit Kumar Chaurasia, Mr. Pushpraj Patel and Mr. Sounak Mukherjee and all my dear juniors and friends of IIT Roorkee who were always there with me for issues related to work and beyond.

I extend my thanks to all the staff members of Institute Instrumentation Center, IIT Roorkee. Special thanks to Dr. Bhupendra Singh and Mr. S. D. Sharma for their support and assistant to complete this work. Thanks are also due to Mr. Arvind Kumar, Mr. Satpal Singh and other technical staff of the Chemical Engineering Department, IIT Roorkee who helped me during the course of experimental work and analysis of samples.

I like to gratefully acknowledge Ministry of Human Resource Development, Government of India and Dean of Students Welfare, IIT Roorkee, for providing funds to support this research. The institute, Indian Institute of Technology Roorkee is great and the environment is supportive for the researchers.

Sincere thanks to Mrs. Mondal who was so cooperative to me and always encouraged to strive forward in hard times.

Finally, I wish to express my handful of regards and owe respect towards my esteemed father Mr. Vishnu Prasad Rathore for his endless motivations and thank my mother, brother and sisters. I extend special thanks to my beloved wife Neetu who stood with me when I was dealing with dire situations and my son Darsh who made me forget the stress of work after getting to home.

(VINEET KUMAR RATHORE)

CONTENTS

LIST OF FIGURES

LIST OF PHOTOGRAPHS

LIST OF TABLES

NOMENCLATURE

b_L	Langmuir constant related to rate of adsorption (L/g)
C	Constant related to intra-particle diffusion (μg/g)
C_{ad}	Concentration of the adsorbate (arsenic or fluoride) on the adsorbent (μg/g)
cal	Calculated values of specific uptake of i^{th} component
C_e	Concentration of the adsorbate (arsenic or fluoride) in the solution at equilibrium (μg/L)
$C_{e1.5}$	Concentration of fluoride equal to 1500 μg/L
C_o	Initial concentration of arsenic or fluoride (μg/L)
D_f	Film diffusion coefficients (cm^2/sec)
D_p	Pore diffusion coefficients (cm^2/sec)
exp	Experimental values of specific uptake of i^{th} component
k_1	Rate constant for pseudo first order adsorption (sec^{-1})
k_2	Rate constant for pseudo second order adsorption (g/μg.min)
K_F	Freundlich constants adsorption capacity and favorability
K_{id}	Rate constant for intra particle diffusion (μg/g.$sec^{1/2}$)
n	Freundlich constants which show the favorability of adsorption.
n_m	Number of readings in the model
n_p	Number of parameters in the model
$Q_{1.5}$	Fluoride adsorption capacity of adsorbent at an equilibrium dissolved fluoride concentration of 1500 μg/L
q_e	Amount of arsenic or fluoride adsorbed at equilibrium (μg/g)
q_{max}	Langmuir constants related to adsorption capacity
r	Radius of the adsorbent particle (cm)
R_L	Separation factor related to Langmuir isotherm
t	Time (min)

$t_{1/2}$	Time required to bring down the concentration of the adsorbate to half of its initial concentration
δ	Thickness of water film adhered to the adsorbent particle (cm)
η	Competitive effect of the adsorbate species present in the solution

RESEARCH PUBLICATIOS

Published in International Journal

1. **Vineet Kumar Rathore** and Prasenjit Mondal, "Life cycle assessment of defluoridation of water using laterite soil based adsorbents", in Journal of Cleaner Production, 180 (2018) 716 – 727
2. **Vineet Kumar Rathore** and Prasenjit Mondal, "Stabilization of arsenic and fluoride bearing spent adsorbent in clay bricks: Preparation, characterization and leaching studies" in Journal of Environmental Management, 200 (2017) 160 – 169
   (The findings of this paper were recognized by "**Current Science**" and published as news item under the column "Science Last Fortnight" in its VOL. 113, NO. 6, 25 SEPTEMBER 2017 Edition)
3. **Vineet Kumar Rathore** and Prasenjit Mondal, "Competitive Adsorption of Arsenic and Fluoride onto Economically Prepared Aluminum Oxide/Hydroxide Nanoparticles: Multicomponent Isotherms and Spent Adsorbent Management" in Industrial and Engineering Chemistry Research, 56 (2017) 8081 – 8094
4. **Vineet Kumar Rathore**, Dileep Kumar Dohare and Prasenjit Mondal, "Competitive adsorption between arsenic and fluoride from binary mixture on chemically treated laterite", in Journal of Environmental Chemical Engineering, 4 (2016) 2417 – 2430

International/National Conference

1. **Vineet Kumar Rathore** and Prasenjit Mondal, Adsorptive removal of arsenic from aqueous solution using aluminum oxide/hydroxide nanoparticles and management of spent adsorbent, in The International Conference on Nano for Energy and Water (NEW 2017) held at University of petroleum and Energy Studies, Dehradun (India) on February 22-24, 2017
2. **Vineet Kumar Rathore** and Prasenjit Mondal, Defluoridation of water using aluminum oxide/hydroxide nanoparticles: Optimization of process parameters and management of spent adsorbent, in The 12th International Symposium on Southeast Asian Water Environment (SEAWE2016) held at Hanoi, Vietnam on November 28-30, 2016.

3. **Vineet Kumar Rathore**, Prasenjit Mondal and Niran Bagchi, Life cycle assessment of defluoridation of ground water using laterite soil based adsorbents, in Indian Conference on Life Cycle Management (ILCM) 2016 held at FICCI, Federation House, New Delhi on 17-18 October 2016
4. **Vineet Kumar Rathore**, Lokendra Singh Thakur, Prasenjit Mondal and N. Bagchi, System thinking and life cycle assessment for development of sustainable urban water systems in Indian Conference on Life Cycle Management (ILCM) 2015 held at FICCI, Federation House, New Delhi on 14-15 September 2015
5. **Vineet Kumar Rathore**, Sneha Malhotra, Dileep Kumar Dohare, Prasenjit Mondal and N. Bagchi, Preparation of laterite soil based low cost adsorbent for treatment of contaminated groundwater: Life cycle assessment, in Indian Conference on Life Cycle Management (ILCM) 2014 held at FICCI, Federation House, New Delhi on 29-30 September 2014
6. Pragya Mishra, **Vineet Kumar Rathore**, Faisal Akram and Prasenjit Mondal, Removal of fluoride from water by treated laterite soil, at Ist International Forum on Asian Water Environment Technology held on 18-20 December 2013 at Jawaharlal Nehru University Convention Center, New Delhi

Patent

1. Submitted a patent report titled "Development of a Novel Water Filtration Unit Containing Hybrid Adsorbents for Simultaneous Removal of Arsenic and Fluoride from Contaminated Water" to Intellectual property right (IPR) Cell of IIT Roorkee for possible consideration.

CHAPTER 1

INTRODUCTION

Contamination of arsenic and fluoride in groundwater is a major challenge for 21st century around the globe. Prolonged consumption of contaminated ground water containing these elements have resulted in various health problems such as different types of arsenic related cancers, bone and skeletal fluorosis in many countries [Mohan and Pittman Jr. 2007, Jagtap et al. 2012]. The severity of health impacts is maximum when both these elements co-exist in ground water. In some countries such as India, China, Mexico, Argentina and Pakistan, both these elements have been found to co-exist in some places [Indu et al. 2007, Wen et al. 2013, Armienta and Segovia 2008, Gomez et al. 2009, Mahmood et al. 2007]. Around ten million and hundred million people suffer from high arsenic and fluoride content in groundwater globally [Li et al. 2014, Essadki et al. 2009]. Considering the health impacts of these elements, the maximum contaminant level (MCL) for arsenic and fluoride in drinking water has been fixed as 10 µg/L and 4000 µg/L respectively by USEPA, whereas, as per the Indian Standards maximum permissible limit are 50 µg/L and 1500 µg/L respectively [USEPA, IS 10500]. WHO has also provided guideline values as 10 µg/L for arsenic and 1500 µg/L for fluoride [WHO 2011].

Natural geogenic processes like dissolution of arsenic and fluoride mineral bearing rocks, volcanic activity etc. and anthropogenic sources such as metal semiconductor, glass, fertilizer etc. producing industries are prominent sources of arsenic and fluoride contamination in groundwater. Various techniques like ion exchange, reverse osmosis, chemical reduction, electrodialysis, distillation, biological processes, adsorption and other processes have been investigated by different researchers for the removal of arsenic and fluoride from water [Ding et al. 2015, Teychene et al. 2013, Jagtap et al. 2012, Choong et al. 2007]. Amongst these techniques, adsorption has gained more interest due to low energy requirement, low initial cost, possibility of reusing the spent adsorbent via regeneration and simplicity of design [Singh et al. 2008].

Since the economic condition of the common people in most of the affected countries is poor, extensive research is going on to produce low cost adsorbents including different types of natural clays and soils [Moghal et al. 2016]. Natural clays have excellent capacity to accumulate both anionic and cationic pollutants either through

ion exchange or adsorption or both [Moghal et al. 2017]. Iron and aluminum compounds present in these adsorbents have been found responsible for arsenic and fluoride removal. Natural laterite having high content of aluminum oxide (Al_2O_3 ~ 21%), iron oxide (Fe_2O_3 ~ 47%) and silica (SiO_2 ~ 28%) have arsenic and fluoride removal capacity [Maiti et al. 2009]. Further, surface modification of this soil can improve the adsorption capacity for arsenic and fluoride [Maiti et al. 2010].

A large amount of literature is also available on aluminum, iron, manganese, zirconium, cerium, and lithium based adsorbents for defluoridation and arsenic removal from water [Hashim et al. 2011, Mohan and Pittman Jr. 2007, Jagtap et al. 2012, Patra et al. 2018]. Use of nanoparticles for the remediation of heavy metals and microbes from water has also been studied [Pradhan et al. 2017, Pal et al. 2007, Banerjee et al. 2012, Mohammod et al. 2011]. Aluminum oxide is reported to have good removal capacity for cadmium and zinc [Sen et al. 2008, Bhargavi et al. 2015]. In particular, oxides and hydroxides of aluminum are extensively studied for the remediation of fluoride bearing water. Similarly, arsenic removal with aluminum compounds being used as adsorbents is also reported by several researchers [Tchieda et al. 2016, Tripathy et al. 2008]. It is noteworthy that in most of the literature reported for the adsorptive removal of arsenic or fluoride, the studies were performed for single-component system. Hence, there is an urgent requisite for the development of a new adsorbent having the ability to treat both the contaminants together.

Only few literatures are available for the removal of arsenic and fluoride simultaneously using chemically synthesized adsorbents [Tang et al. 2010, Zhang et al. 2010, Jing et al. 2012, Deng et al. 2012] but interaction between arsenic and fluoride ions is not explained in these literature with the help of binary adsorption isotherms, which prevails in reality.

Further, by reviewing the literature on arsenic and fluoride removal from water through adsorption process, it seems that most of the reports are based on batch scale study. However, to assess the suitability of any adsorbent its performance in column reactor is essential.

After adsorption, the concerns related to the disposal of spent adsorbent still remain unanswered. The spent adsorbent management issue is not well studied, which is

very important for the applicability of the adsorbents. Frequently, it has been observed that the spent adsorbent/sludge is disposed openly on ground leading to possible contamination of groundwater and surface water sources through seepage [Rouf and Hossain, 2003]. Apparently, it seems that the solidification of spent adsorbent derived from low cost material may be an attractive route for its management. Very few literature are available on the Solidification/Stabilization (S/S) of arsenic bearing spent adsorbent like activated alumina, iron oxide coated cement, zeolite or perlite supported magnetite, MgO etc. [Singh and Pant, 2006, Kundu and Gupta, 2008, Verbinnen et al., 2015, Tresintsi et al., 2014], however these reports do not provide any information about its applicability for fluoride bearing spent adsorbent.

To assess the environmental sustainability of process, its Life Cycle Assessment (LCA) is normally practiced. The LCA study helps in identifying hot spots of a process that have to be improved so that the overall impacts can be minimized [Togarcheti et al. 2017]. However, there is very few literatures on the LCA of adsorptive removal of As or F or both from water. On the basis of the above backdrop the aim and objectives of the present investigation have been decided as stated below.

Aim and Objectives

The main aim of the present study is to investigate the adsorptive removal of arsenic and fluoride from synthetic solution as well as from real groundwater samples through adsorption on a low cost laterite soil based adsorbent and Aluminum Oxide/Hydroxide Nanoparticles (AHNP) based adsorbent. It also aims to investigate on the safe disposal of arsenic and fluoride containing spent adsorbent in the form of clay bricks. The last aim of the study is to perform the LCA of the defluoridation process to understand its environmental implications. Point wise objectives are as follows:

1. To synthesize laterite soil based low cost adsorbents and identification of the most efficient one for arsenic and fluoride removal.
2. To synthesize AHNP adsorbent for arsenic and fluoride removal.
3. To optimize process conditions (viz. initial pH of the solution, adsorbent dose, contact time and initial concentration of ions) for individual removal of arsenic and fluoride using the selected adsorbents separately.

4. To perform kinetic evaluation and isotherm study for the individual adsorption of arsenic and fluoride by the adsorbents separately.

5. To perform competitive adsorption study (simultaneous removal of arsenic and fluoride) on both the adsorbents in batch mode of operation with synthetic solution.

6. To carry out the performance analysis of the adsorbents with real ground water samples.

7. To prepare clay bricks from spent adsorbents, characterize them and perform leaching tests for arsenic and fluoride.

8. To study the effect of influent flow rate on adsorption of arsenic and fluoride simultaneously in column operation with synthetic solutions for the selected adsorbents.

9. To perform economic evaluation of the adsorbents.

10. To perform LCA of the defluoridation process by laterite soil based adsorbents.

CHAPTER 2

LITERATURE REVIEW

Literature review has been carried out regarding the removal of arsenic and fluoride from water. Sources of these contaminants in ground water, their toxic effects and health impacts in various places in India and across the globe have been reviewed for understanding the severity of the problem.

Several processes employed for the removal of arsenic and fluoride from water has been reviewed. Some important processes are reported hereunder for a brief comparison and selection of the most suitable method(s). Adsorption is one of the most widely studied and explored process for the treatment of water. Different types of adsorbents, including low cost clay material and nano-material based adsorbents have been reviewed for the removal of these ions along with others normally available with these in contaminated water. Further, spent adsorbent management and Life Cycle Analysis of the adsorption process have also been reviewed.

Details of literature review for the present investigation are provided below through Section 2.1 to section 2.5.

2.1 STATUS OF CONTAMINATION OF GROUNDWATER BY ARSENIC AND FLUORIDE

Previous investigations narrate that, in aqueous environment, arsenic exists predominantly as inorganic oxy-anions of trivalent arsenite (As (III)) or pentavalent arsenate (As (V) [Smedley and Kinniburgh 2002]. Trivalent arsenite (As (III)) species viz. $H_3AsO_3^0$, H_2AsO^{3-}, $HAsO_3^{2-}$ and AsO_3^{3-} mostly occur in reducing anaerobic environments such as groundwater, while pentavalent arsenate (As (V)) species viz. H_3AsO_4, H_2AsO^{4-}, $HAsO_4^{2-}$ and AsO_4^{3-} are dominant in oxygen rich aerobic environments such as surface water [Greenwood and Earnshaw 2012]. Although inorganic arsenic species are present in abundance, the presence of organic arsenic species, i.e. monomethylarsonic acid (MMA) and dimethylarsinic acid (DMA) has also been reported in natural water [Bednar et al. 2002 and Xu et al. 2008].

On the other hand, most of the fluoride is associated with monovalent cations such as NaF and KF in water soluble form, while the others formed with divalent cations

such as CaF_2 and PbF_2 are generally insoluble. Fluoride occurs abundantly in the earth's crust as a component of rocks and minerals. Naturally fluoride is present as a natural constituent of rocks in the form of fluorite, cryolite (Na_3AlF_6), fluorspar or calcium fluoride (CaF_2), apatite or rock phosphate ($Ca_3F(PO_4)_3$), magnesium fluoride (MgF_2) and as a replacement of ions in the crystal lattice of mica and many other minerals [Das et al. 1998 and Das et al. 1999]. It is released into the groundwater by slow dissolution of such rocks and minerals [Biswas et al. 2009, Goswami and Purkait 2011]. Whenever carbonate and bicarbonate rich water passes through such type of rocks, fluoride ion is released and percolates to the ground water and increases its concentration [Saxena and Ahmed 2001].

The contamination of arsenic and fluoride in water occurs mainly because of natural geological sources such as erosion of rocks, weathering of mineral, volcano emission; and anthropogenic sources such as effluents from industries like glass, metal, semiconductor, pesticides, electroplating, mines (acid mine drainage) etc. [Balasubramanian et al. 2009, Liu et al. 2012, Moghal et al. 2017]. Wastewater from these industries, discharged over the land or in surface water, would percolate through soil and later reach to the groundwater sources [Sen et al. 2004, Sen et al. 2002]. Such contaminated surface water stream can also cause different types of health impacts when these are consumed by living beings [Reddy and Cameselle 2009, Reddy 2010, Dugo et al. 2007, Wasewar 2010]. Recently, the availability of these pollutants in food items is also observed and has been a very serious issue, which is supposed to be due to the presence of these pollutants in water used for irrigation purpose.

Arsenic is a carcinogenic compound; its prolonged consumption may cause different health impacts like skin, liver, lung and kidney cancer [Basha et al. 2008]. Fluoride is an essential micronutrient required for human beings to strengthen teeth and skeleton, while its concentration higher than 1500 µg/L may cause teeth disintegration, skeleton fluorosis, renal and neuronal disorders along with myopathy [Ayoob and Gupta 2006]. Considering the health impacts of these pollutants, the regulatory bodies around the world have fixed the Maximum Contaminant Level (MCL) value for these pollutants in drinking water at a lower level. Permissible limits of arsenic and fluoride for drinking water as per some world and Indian regulatory bodies are presented in Table. 2.1.

Table. 2.1 Permissible limits of arsenic and fluoride for drinking water [Ahmaruzzaman 2011 & Villanueva et al. 2014]

Contaminant	Limits for drinking water (µg/L)		
	Indian standard IS 10500:2012 (Acceptable limit)	**WHO (Guideline value)**	**USEPA (Maximum Contaminant Level (MCL))**
Arsenic	10	10	10
Fluoride	1000	1500	4000

WHO: World Health organization, USEPA: United States Environmental Protection Agency

However, the permissible limit of these pollutants in the treated industrial effluents is relatively higher since it is diluted significantly when it enters the surface water stream. Table 2.2 shows the permissible limits of these pollutants in treated wastewater as per CPCB standard.

Table. 2.2 General standards for discharge of arsenic, fluoride in environment in India [CPCB Standard 1986]

Contaminant	Standards (maximum, µg/L)			
	Inland surface water	**Public sewers**	**Land for irrigation**	**Marine coastal area**
Arsenic	200	200	200	200
Fluoride	2000	15000	-	15000

Worldwide co-occurrence of arsenic and fluoride in groundwater including India is reported by several authors, some of such reports are summarized in Table 2.3.

Table 2.3 Co-occurrence of arsenic and fluoride in groundwater around the world

Arsenic concentration (µg/L)	Fluoride concentration (µg/L)	Place (s)	Reference
360-683	18500-35400	Nagarparkar, Pakistan	Brahman et al. 2014
100-3830	13800-49300	Tharparkar, Pakistan	Brahman et al. 2013
4-5280	1330-28400	La Pampa, Argentina	Smedley et al. 2002
<0.2-60.87	<170-6510	Diabase Intrusions, Newark Basin, Southeastern Pennsylvania, USA	Senior and Sloto 2006
<10-1900	160-22100	Kasur and Lahore districts, Punjab, Pakistan	Farooqi et al. 2007a
76-1093	400-3360	Hangjinhouqi, Western Hetao plain, Inner Mongolia	He et al. 2009
5.1-259.5	10-750	Middle Gangetic Plain of Ghazipur District, Uttar Pradesh, India	Kumar et al. 2010a
0.21-11.15	90-97000	Tea garden belt of Darrang district, Assam, India	Borah et al. 2010
<10-21	<1000-3000	Monojili, Assam. India	Chaurasia et al. 2012
0.1-11.6	100-3400	Jhansi district of Bundelkhand region, India	Singh et al. 2013a
0.6-56.4	350-1060	Lakhimpur District, Assam, India	Hazarika and Bhuyan 2013

ND-117	1150-6730	Laguna El Cuervo, Mexico	Reyes-Gómez et al. 2015
75-134	4800-5900	Meoqui City, Chihuahua, México	Piñón Miramontes et al. 2003
0-250	500-12000	Coronel Moldes, Chacopampean plain Argentine, Argentina	Gomez et al. 2009
<1-100	20-2740	Alluvial aquifer, Korea	Kim et al. 2012
N.D. -12.7	6000-134000	Vulcano Island, Italy	Aiuppa et al. 2000
148-985	3700-27000	Kourikasa, Rajnandgaon District, Chhattisgarh, India	Patel et al. 2017
10-5300	51-7340	Chaco Pampean plain, Argentina	Nicolli et al. 2012

(N.D. - Below detection limit)

From Table 2.3, it is clear that both arsenic and fluoride are present in contaminated groundwater of many countries and in some places the concentrations of these pollutants are higher than their respective permissible limits.

2.2 TREATMENT TECHNIQUES FOR THE REMOVAL OF ARSENIC AND FLUORIDE FROM WATER

Arsenic species, physio-chemical properties of water and concentration of other ions like SO_4^{2-} , PO_4^{2-} , Fe etc. influence the selection of removal process. Generally, arsenic removal technologies are based on the following principles:

i. Chemical oxidation of As (III) to As (V) which is followed by coagulation, sedimentation and filtration
ii. Microbial oxidation of As (III) to As (V) and its removal with the help of manganese and iron oxides
iii. Ion exchange (by using anion and cation exchange resins)
iv. Adsorption

v. Membrane separation

Adjustment of solution pH is essential for optimized performance of these arsenic treatment technologies as it influences the speciation of arsenic in water [Bissen and Frimmel 2003]. The traditional fluoride removal technologies from drinking water include addition of lime along with fluoride precipitation. The coagulation and precipitation processes with calcium [Yin et al. 2015], activated alumina [Ghorai and Pant 2005] and Fe (III) [Tressaud 2006] have been studied extensively.

2.2.1 Important Techniques Used for the Removal of Arsenic and Fluoride from Water

Different techniques including physicochemical, electrochemical and biological processes have been used for the removal of arsenic and fluoride from water as presented in Figure 2.1.

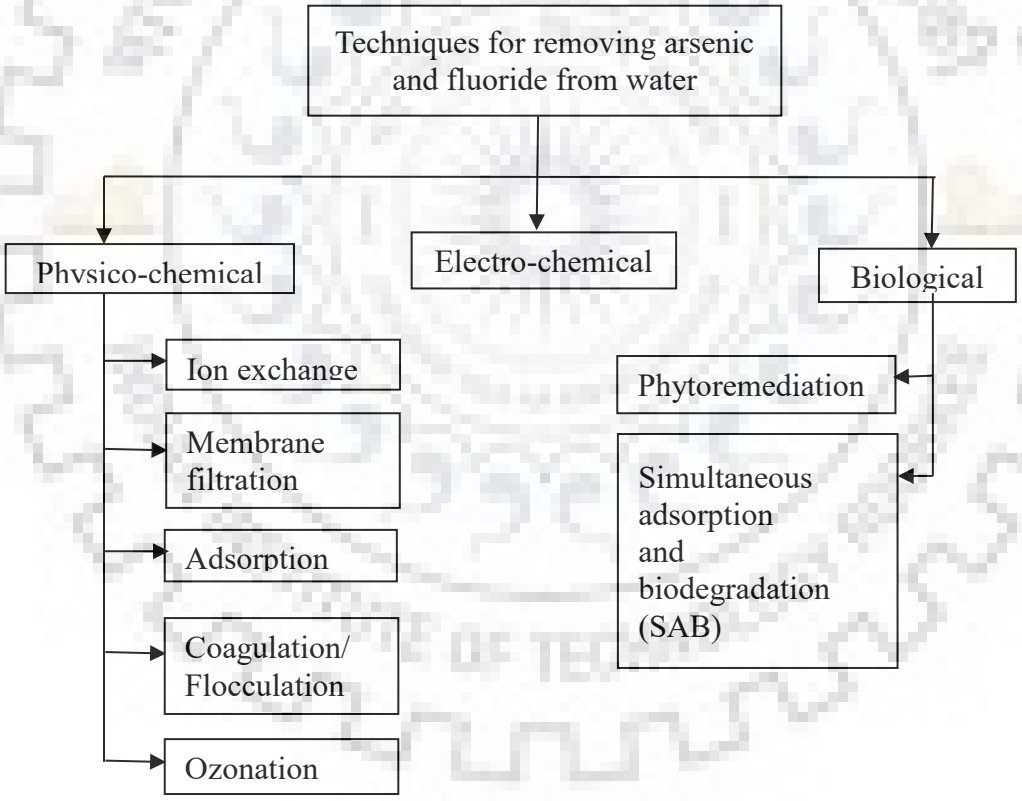

Figure 2.1 Some important techniques for the removal of arsenic and fluoride from water

For the removal of arsenic, a peroxidation stage has been used in many cases to oxidize As (III) to As (V) to facilitate its removal as the solubility of As (V) is less than that of As (III). Merits and demerits of the physico-chemical, biological and electrochemical techniques are presented in Table 2.4.

Table 2.4 Merits and demerits of the most common water treatment technologies for arsenic and fluoride removal

Technique	Merits	Demerits	Reference
Ion-Exchange	Simple design with flexibility High efficiency	Efficiency largely depends on pH Performance depends on interfering ions Expensive process Produces toxic liquid wastes	Velazquez-Jimenez et al. 2015
Membrane filtration	High efficiency Suitable to remove other pollutants	Expensive High capital and operating cost	Habuda-Stanić et al. 2014
Adsorption	Simple design and operation Less cost	Efficiency is dependent on pH and interfering ions Spent adsorbent management issue	Velazquez-Jimenez et al. 2015
Coagulation / Flocculation	Simple process	Efficiency is dependent on pH and interfering ions Costly chemicals required Secondary sludge formation	Habuda-Stanić et al. 2014
Electrochemical	Coagulants are produced in- situ Less sludge production High efficiency	Not well proven Requires skilled labor Polarization problems	Velazquez-Jimenez et al. 2015

2.2.2 Best Available Techniques (BATs) for Arsenic and Fluoride Removal from Water

According to USEPA and National Environment Services Center, West Virginia University (WVU) the best available techniques for removal of arsenic and fluoride are listed in Figure 2.2.

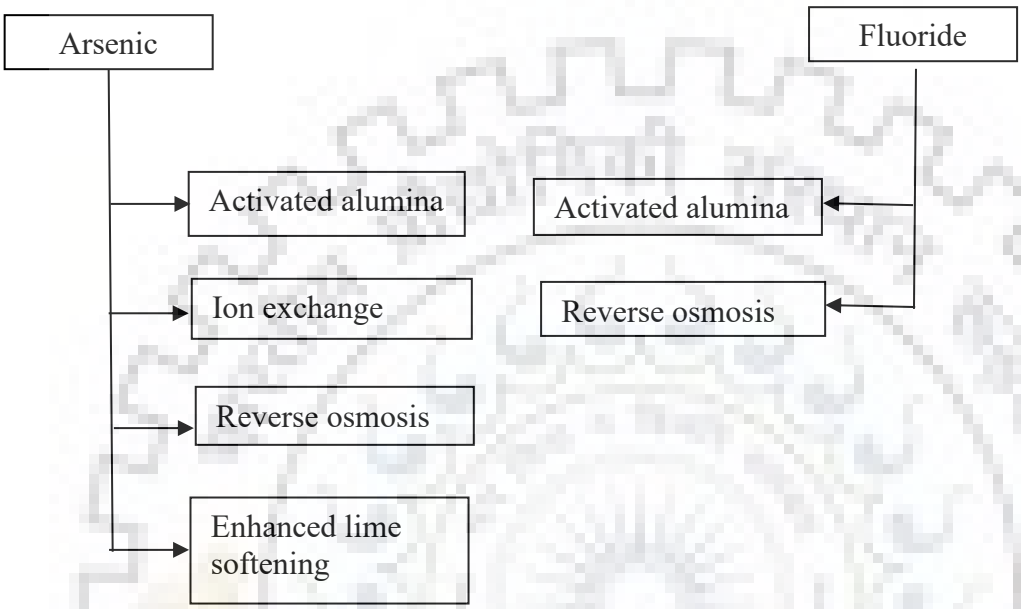

Figure 2.2 Best available techniques for arsenic and fluoride removal

2.2.3 Scope of Adsorption Technique Using Low Cost Adsorbents for Treatment of Arsenic and Fluoride Contaminated Water

Various techniques like ion exchange, reverse osmosis, chemical reduction, electrodialysis, distillation, biological processes, adsorption [Jagtap et al. 2012, Choong et al. 2007] and other processes have been investigated by different researchers to remove arsenic and fluoride from water. Amongst these techniques, adsorption has gained more interest due to low energy requirement, low initial cost, possibility of reusing the spent adsorbent via regeneration and simplicity of design. Since the economic conditions of the common people of most of the suffering countries are poor, extensive research is going on to produce low cost adsorbents including different types of natural clay soils.

Natural clays have excellent capacities to accumulate both anionic as well as cationic pollutants either through ion exchange or adsorption or both [R. Srinivasan

2011]. Various geological minerals like calcinated bauxite, iron oxide coated sand, ferruginous manganese ore, beidellite, sepiolite, zeolite, raw and acidified/acid treated laterite have been reported for arsenic removal [Ayoob et al. 2007, Gupta et al. 2005, Chakravarty et al. 2007, Bektas et al. 2011, Glocheux et al. 2013]. Similarly, acid treated spent bleaching earth, red mud, activated titanium rich bauxite, raw laterite soil (0.5 mm size), raw and mechanochemically activated kaolinites, raw and acid treated waste mud, granular red mud, lanthanum modified bentonite clay, granular acid-treated bentonite etc. have been reported as adsorbent for removal of fluoride in literature [Mahramanlioglu et al. 2002, Kemer et al. 2009, Meenakshi et al. 2008, Ma et al. 2011]. Iron and aluminum compounds present in those adsorbents have been found responsible for the removal of arsenic and fluoride [Mohan et al. 2007, Jagtap et al. 2012].

In case of natural laterite, it has high content of aluminum oxide (Al_2O_3 ~21%), iron oxide (Fe_2O_3 ~47%) and silica (SiO_2 ~28%) and has arsenic and fluoride removal capacity [Maiti et al. 2009]. The removal efficiency of laterite can also be improved by its surface modification [Maiti et al. 2010, Maiti et al. 2011]. Further, both arsenic and fluoride can exist as negatively charged species in solution under certain conditions but their speciation chemistry is different. Thus, presence of both species in solution may influence the individual removal of these species. However, there is hardly any literature available on simultaneous removal of both arsenic and fluoride using natural clay soils or surface modified laterites. Only few literature is available on simultaneous removal of arsenic and fluoride using chemically synthesized adsorbents [Tang et al. 2011, Deng and Yu 2012] but interaction between arsenic and fluoride ions is not explained in these literature with the help of binary adsorption isotherms which prevails in reality.

2.2.4 Scope of Adsorption Technique Using Nanoparticles as Adsorbents for Treatment of Arsenic and Fluoride Contaminated Water

In many of the recently published papers, metal oxides and metal hydroxides have been reported to be potential candidates for the adsorptive removal of arsenic and fluoride from water [Mohan et al. 2007, Jagtap et al. 2012]. These adsorbents are abundantly available in nature in the form of various types of minerals and can also be synthesized in the laboratories easily. In particular, oxides and hydroxides of aluminum are extensively studied for the remediation of fluoride bearing water as they have positively charged surface, which enables the adsorption of negatively charged fluoride

ions due to electrostatic attraction. On the other hand, arsenic is reported to be removed primarily by metal oxides and hydroxides by ligand exchange mechanism. Further, it is a known fact that nanomaterials possess more surface area and porosity, which favours adsorption. Thus, efforts are on to develop nano adsorbents based on metal oxide /oxy hydroxides.

Alumina is one of the most widely studied metal oxide adsorbents for the defluoridation of water. The research for adsorptive removal of fluoride with alumina shows different kinds of compounds which are synthesized with different techniques to give these specific characteristics. Similarly, arsenic removal with aluminum compounds being used as adsorbents is also reported in several researches [Tchieda et al. 2016, Tripathy and Raichur, 2008]. However, there is very few literature over the removal of As and F using nano adsorbents based on alumina.

2.3 ADSORPTIVE REMOVAL OF ARSENIC AND FLUORIDE FROM WATER

Mechanism of adsorption process and the important work done around the world on the removal of arsenic and fluoride individually as well as simultaneously are provided and analyzed below to identify the scope of the present investigation.

2.3.1 Work Done on the Adsorptive Removal of Fluoride from Water by Low Cost Adsorbents

Iriel et al. 2018, tested soil based adsorbent to remove fluoride from synthetic or real wastewater in batch reactor in the pH range of 4-8. The equilibrium time was 30 min with a specific uptake of 480 µg/g. Pseudo second order kinetics explained the process. Adsorption data was successfully explained through Dubinin-Ataskhov model determining that the fluoride adsorption onto soil particles mainly followed a physical mechanism.

Talat et al. 2018, used by coconut husk activated carbon (surface area 1448 m^2/g) column reactor to remove fluoride from water. Effect of bed height, flowrate and fluoride concentration on its removal was studied. High adsorption capacity 6500 µg/g was achieved with F^- concentration 10000 µg/L and 100 ml/hr as flowrate at pH 5. Bed Depth Service Time (BDST) was found more suitable among different breakthrough

curve models to explain the phenomena. Regeneration of the adsorbent was done using NaOH solution.

Khan et al. 2017 studied on the fluoride removal from water using organometallic polymeric adsorbents. The adsorption followed the pseudo-second-order kinetics. Specific uptake as per Langmuir isotherm was achieved as 25000 µg/g. Column study was also performed to assess its performance.

Mehta et al. 2016 used marble waste powder (MWP) with specific surface area of 7.18 m^2/g as adsorbent for fluoride removal from aqueous solution. Specific uptake at pH 7 with 180 min contact time was found as 1200 µg/g. Pseudo second order kinetic model and Freundlich isotherm explained the kinetics and adsorption equilibrium.

Waghmare et al. 2015 studied the behavior of modified calcium and aluminum zeolite (CAZ) as novel adsorbents for fluoride removal from drinking water. In this study, the best suited results for fluoride ion was presented with the help of zeolite modified with aluminum sulphate and calcium sulphate in the ratio as 2:1. The fluoride was removed from drinking water at the wide range of pH between 4 and 8. The adsorption isotherm was fitted well by Freundlich model. The Langmuir maximum adsorption capacity of CAZ was found to be 8038.5 µg/g.

Dayanand et al. 2014 synthesized CaO loaded mesoporous Al_2O_3 (20 wt. % CaO loading) and used it as an adsorbent for removing fluoride from aqueous solution. The new adsorbent $CaO_2@Al_2O_3$ exhibited better fluoride removal capacity than that of commercial Al_2O_3 over a wider range of pH. It improved the rate of adsorption significantly.

Maiti et al. 2011 used chemical treated laterite for fluoride removal from aqueous system. Specific uptake of acid–base treated laterite (TL) at 15, 32 and 42 °C, as per Langmuir isotherm is found as 36300, 37900, and 39100 µg/g respectively. They computed by external mass transfer (K_f) and pore diffusion coefficient (D_e) to interpret the kinetics of the process.

Biswas et al. 2010 used synthetic iron (III)–aluminum (III)–chromium (III) ternary mixed metal oxide for fluoride removal from aqueous solution. The process was found endothermic and spontaneous (ΔH^0 = +19.819 kJ/mol, ΔG^0 = -12.856 to -16.902

kJ/mol, ΔS^0 = + 0.115 kJ/mol.K) which takes place with increasing entropy (ΔS^0 = + 0.115 kJ/mol.K). Pseudo second order rate equation and Langmuir isotherm explains the adsorption process. Specific uptake as per Langmuir isotherm was 31889 µg/g.

Sujana and Anand 2010 synthesized iron and aluminum based mixed metal hydroxides and used it for fluoride removal from water. The adsorbent with Fe:Al (1:1 molar ratio) exhibited maximum adsorption capacity for fluoride. The adsorbent was characterized by various techniques such as TGA, XRD, TEM, SEM-EDX and FTIR.

Biswas et al. 2009 synthesized iron (III)–tin (IV) mixed metal oxide (HITMO) and used for defluoridation of water. The adsorption followed pseudo second order kinetics well and the overall rate is found to be multi-stage controlled. The Langmuir isotherm well describes the equilibrium data and Langmuir maximum adsorption capacity is reported as ~10500 µg/g.

Maliyekkal et al 2008 reported magnesia amended activated alumina (MAAA) for removal of fluoride from drinking water. Adsorptive removal of fluoride onto MAAA was found to be pH dependent and a decreasing trend in adsorption was observed at higher values of pH. Among the kinetic models employed, pseudo second order model described the kinetic data well. The adsorption was well described by Sips model and the maximum sorption capacity deduced through Sips equation was 10120 µg/g.

Maliyekkal et al. 2006 studied the adsorption potential of manganese oxide coated alumina (MOCA) for removal of fluoride from drinking water. The Langmuir equilibrium model was found to well describe the fluoride sorption on MOCA. The maximum fluoride uptake capacity for MOCA was found to be 2850 µg/g and followed pseudo second order kinetics.

Ghorai et al. 2005 investigated the defluoridation of water by activated alumina. Adsorption isotherm was well described by Langmuir equation and maximum adsorption capacity was found to be 2410 µg/g. The adsorption process followed pseudo first order kinetics.

2.3.2 Work Done on Adsorptive Removal of Fluoride from Water by Nanoparticle Based Adsorbents

Zhou et al. 2018 synthesized layered Al-Zr-La tri-metal hydroxide (AZL) and used it for the adsorbent showed high adsorption capacity. As per Langmuir isotherm the maximum specific uptake was found as 90480 µg/g at 35 °C and pH 3.0.

Ekka et al. 2017 studied defluoridation of water using ionic liquid-functionalized alumina as a novel adsorbent. The adsorption process followed the pseudo second order kinetics and from Langmuir adsorption isotherm. The maximum adsorption capacity was found to be 25000 µg/g from.

Christina and Viswanathan 2015 developed two Fe_3O_4 nanoparticle based sorbents namely (FNPSA) and (FNPSOPR). The Fe_3O_4 nanoparticles were immobilized in sodium alginate matrix individually and with saponified orange peel respectively. Both the adsorbents followed Langmuir isotherm model and the maximum specific uptke was found as 58240 µg/g and 80330 µg/g respectively,

Dayanand et al. 2015 synthesized MgO nanoparticle loaded mesoporous Al_2O_3 and used it for defluoridation study. Loading of MgO nanoparticle on mesoporous Al_2O_3 enhanced the fluoride adsorption capacity from 56 % to 90 % with initial fluoride concentration of 10000 µg/L. Kinetics followed the pseudo second order model, which suggests the chemisorption mechanism. The maximum adsorption capacity of the adsorbent was found as 37350 µg/g.

He et al. 2014 studied defluidation of water using an optimized Zr based nanoparticles embedded polysulfone blend hollow fiber membrane in the pH range of 3 to10. The maximum adsorption capacity of the optimized membrane was 60650 µg/g.

Zhao et al. 2010 studied the defluoridation of aqueous media by using hydrous aluminum oxide embedded with Fe_3O_4 nanoparticle (Fe_3O_4@$Al(OH)_3$). The Langmuir maximum adsorption capacity of the material was calculated as 88480 µg/g at pH 6.5. The kinetics followed a pseudo second order rate equation.

Further, some important findings on the adsorptive removal of fluoride from water are summarized in Table 2.5.

Table 2.5 Recent advancements for fluoride removal from water

Adsorbent	Mode of operation	Optimum pH	Sorption dose (g/L)	Contaminant concentration (µg/L)	Contact time (min)	Uptake capacity (µg/g)	References
Lanthanum–carbon	Batch	7 ± 0.2	5 to 30	1000–80000	60	9960	Vences-Alvarez et al. 2015
Lanthanum-loaded magnetic cationic hydrogel	Batch	7.0 ± 0.2	0.3	29300	120	136780	Dong and Wang 2016
Iron nano impregnated adsorbent	Batch	7	2.5	4000	25	2180	Ali et al. 2015
Al (III)–Zr (IV) binary oxide adsorbent	Batch	2	1	50000–150000	240	114540	Zhu et al. 2015
Aluminium fumarate metal organic framework	Batch	7	0.75	30000	1440	600000	Karmakar et al. 2016
Mg–Fe–La trimetal composite	Batch	7	0.5	10000–150000	180	112170	Wang et al. 2015
Sulphate doped hydroxyapatite	Batch	7	0.5	2000–100000	1440	28300	Chen et al. 2016

Bone char	Batch	7	2	5000–80000	1440	5920	Rojas-Mayorga et al. 2015
Neem (*Azadirachta indica*) leaf powder	Batch	5.0–7.0	1.0–5.0	3000–15000	60	4700	Bharali and Bhattacharyya 2015
Natural calcium-rich attapulgite	Batch	8	0.5	5000–2000000	1440	140000	Yin et al. 2015
Hydroxyapatite	Batch	12.5	0.4–4	8690 ± 1840	240	12400	Melidis 2015
Regenerated aluminium oxide-coated media	Batch	7 ± 0.05	12	40000–60000	432000	34240	Buamah et al. 2016
Tea waste loaded with Al/Fe oxides	Batch	4.0–8.0	0.4–8.0	5000–200000	120	18520	Cai et al. 2015
Zirconium-impregnated fibrous protein	Batch	6.54	1	2000 – 50000	360	12600	Deng and Yu 2015
Sorghum and canola	Batch	5	2–14	10000–100000	10–180	7800 and 8240	Zazouli et al. 2015
Lamb and chicken bones	Batch	6–7	15 and 20	10000	120	122 and 226	Ismail and AbdelKareem 2015

Magnetite-chitosan composite	Batch	7	0.25–2	1000–10000	60	9430	Mohseni-Bandpi et al. 2015
Alumina-based composite	Batch	7.43	0.4	53000	1080	17570	Waghmare et al. 2015
Chemically activated cotton nut shell carbon	Batch	7	1.75	2000–10000	180	1503	Mariappan et al. 2015
Jajarm bauxite	Batch	7	15	2300–2700	90	590	Malakootian et al. 2015
Ultrasonically prepared aluminium hydroxide	Batch	3 to 9	4	>20000	300	3800	Gai et al. 2015
Hydroxyapatite (HAP) nanowires	Batch	7	0.5	200000	720	40650	He et al. 2016
Alumina-modified expanded graphite composite	Batch	4	0.2	5000	120	1180	Jin et al. 2015
3D hierarchical amorphous aluminium oxide microspheres	Batch	7	0.5	5000–150000	720	126900	Kang et al. 2015

Mg-/Fe-layered double hydroxides	Batch	7	1	5000–75000	600	50900	Kang et al. 2013
Aluminium alginate beads	Batch	2	1	19000–190000	240	75200	Kaygusuz et al. 2015
Chitosan beads	Batch	7	1	>20000	80	17470	Prabhu and Meenakshi 2015
Ce–Fe bimetal oxide adsorbent	Batch	2.9–10.1	0.3–1.5	10000	40	60970	Tang and Zhang 2016
Chitosan/montmorillonite/ZrO_2 nanocomposite	Batch	4	0.1	20000	60	23000	Teimouri et al. 2015
Lanthanum-impregnated green sand	Batch	6 to 9	6	15000	240	3740	Vivek Vardhan and Srimurali 2016
Aluminium-impregnated coconut fibre	Batch	5	0.05	1000-10000	40	3190	Mondal et al. 2015
Hydrothermally modified limestone powder	Batch	7.10–7.50	3.3	>10000	180	6450	Gogoi and Dutta 2016
Marble waste powder	Batch	7	8	10000	180	1200	Mehta et al. 2016

Al_2O_3/TiO_2 nano composite	Batch	7	0.002	2000	30	1900	Suriyaraj et al. 2015
Cerium-loaded mesoporous zirconium phosphate	Batch	6	0.01	>50000	60	20500	Dash et al. 2015
Fe_3O_4 superparamag netic nanoparticles with zirconium oxide	Batch	2.5	1	20000	60	145200	Riahi et al. 2015
Industrial based adsorbent (cement)	Batch	7	30	30000	60	1720	Bibi et al. 2015a, b

2.3.3 Work Done on Adsorptive Removal of Arsenic from Water by Low Cost Adsorbents

Bahar et al. 2018 investigated on the removal of As (V) from aqueous solution using coir pith ash (CPA) as adsorbent in batch reactor. Effects of process variables on As (V) removal were studied. Adsorption kinetics and equilibrium were explained by pseudo second order kinetic model and Langmuir and Dubinin–Radushkevich (D–R) isotherms respectively. The maximum adsorption capacity was found as 36500 µg/g.

Ghosal et al. 2018 studied on the removal of As (V) and As (III) from water by using novel iron/olivine composite as adsorbent. The maximum adsorption capacity for As (V) and As (III) as per Langmuir isotherm were found as 5250 and 2830 µg/g, respectively. Adsorption kinetics followed pseudo second order model.

Malwal and Gopinath 2017 used silica stabilized magnetic chitosan beads for adsorptive removal of arsenic from water as adsorbent. It was characterized by FTIR, TGA and SEM and XRD. Performance of the hybrid chitosan beads was compared with only chitosan beads for arsenic removal. Kinetic and equilibrium study were also performed. Further, the adsorption efficiency of the chitosan beads and the hybrid beads were calculated as 1699 µg/g.

Tchieda et al. 2016 studied removal of arsenic by alumina based adsorbents. For the adsorption isotherms, the Langmuir isotherm model fitted best to the experimental data. Adsorption uptake slightly < 20000 µg/g was shown for the synthesized alumina; APS and TiO_2-coated alumina calcinated at 450°C provided similar values of about 9000 µg/g.

Lan et al. 2016 used potassium ferrate for aqueous arsenic (As) and antimony (Sb) removal. In this study potassium ferrate was reported as a viable agent to remediate arsenic and antimony combined pollution. The maximal adsorption capacity towards arsenic was 162020 µg/g of potassium ferrate at pH 6.5 and towards antimony it was 129930 µg/g of potassium ferrate at pH 4.0.

Aredes et al. 2014 used natural iron oxide minerals as adsorbent for the adsorptive removal of arsenic from water. Higher adsorption was observed at pH lower

than isoelectric points (IEPs) of the minerals. Both physical and chemical adsorption was reported.

Tabelin at al. 2014 used three natural geologic materials such as pumiceous tuffs, coastal marine sediments and partly-weathered volcanic ashes to capture boron and arsenic from aqueous solutions. They also characterized the adsorbents. Both Langmuir and Freundlich isotherms described the equilibrium for arsenic removal while for boron the Henry-type model (linear) was followed. Adsorbents with more Al and Fe showed more As removal.

Baig et al. 2013 studied for removal of arsenic in saturated sand filters (SSF (a) and SSF (b)) which contained raw and iron-coated honeycomb briquette cinders (HBC and Fe-HBC). The samples were collected at different sampling time (ST) (5–120 min) during various treatment days (TD) 1, 6, 12, 18 and 24 to assess filters' performance from tap water which was spiked with 200 µg/L of As(V) and As(III) into SSF(a) and SSF(b), respectively. It is reported that the removal efficiencies of arsenic in SSF (a) and SSF (b) was obtained > 95% and > 85% till TD-12 and then decreased to ~78% and ~ 60%, respectively, on TD-24.

Canales et al. 2013 studied the removal of arsenic by an Australian laterite with particles size ranging between 38 µm and 25 µm. it is reported that particle size influenced both equilibrium and kinetic characteristics of arsenic adsorption. The equilibrium adsorption capacity of laterite increased from ~ 100 µg/g for laterite particles coarser than 4 µm, to ~ 160 µg/g for laterite particles between 75 µm and 4 µm. It increased to over 200 µg/g for laterite particles finer than 75 µm. The kinetic adsorption data fitted well pseudo second order kinetic model especially to finer particles.

Bektas et al. 2011 used low cost and locally available natural minerals like beidellite, zeolite and sepiolite for the adsorptive removal of arsenic from aqueous solutions. The adsorption process was described well by pseudo second order model. The adsorption capacities of these three modified minerals are reported to range between 476 to 841 µg/g at different temperatures.

Maiti et al. 2010 used Acid activated laterite (AAL) for the adsorptive removal of arsenic from water. The data fitted better to pseudo second order kinetic model. The removal was also studied in continuous fixed bed column mode of operation. In column

mode, AAL was able to treat 200 bed volume (~ 21 L) of arsenic contaminated groundwater (with total arsenic: 378 µg/L) at a breakthrough concentration of 50 µg/L arsenic and column height of 20 cm (weight of adsorbent: 125 g).

Mamindy-Pajany et al. 2009 used hematite and goethite for the adsorptive removal of arsenic. The adsorption of arsenic on both the adsorbents was greatly dependent on pH of the solution and the maximum adsorption is reported to be in acidic pH for As (V). The adsorption capacity of the material is found to be ~125 µg/g for both the adsorbents.

Maji et al. 2008 also reported the removal of arsenic on natural laterite soil. The kinetics showed that adsorption of arsenic by laterite soil was well described by pseudo second order. In the column study, the rate of movement of adsorption zone through the bed was 0.80 cm/h, and 47.12 % of the total column saturated at breakthrough. The value of adsorption rate coefficient (K) was obtained as 1.21 L/(mg h) and the adsorption capacity coefficient (N) as 69.22 mg/L.

Mohapatra et al. 2007 used kaolinite, montmorillonite and illite as adsorbents for the removal of arsenic. The adsorption data fitted well with Langmuir isotherm and Langmuir maximum adsorption capacity of 860, 640 and 520 µg As (V)/g of kaolinite, montmorillonite and illite, respectively. A decrease in the adsorption of As (V) was observed with increase in the adsorption temperature.

2.3.4 Work Done on Adsorptive Removal of Arsenic from Water by Nanoparticle Based Adsorbents

Yu et al. 2018 synthesized yttrium doped iron oxide magnetic adsorbent for arsenic (arsenate and arsenite) removal from water. The adsorbent was aggregation of nano-sized irregular particles with rough surface and porous structure. It was characterized through different instrumental methods and point of zero charge was determined as about 7.0. The maximum adsorption capacities of As (III) and As (V) at neutral pH were 84220 and 170480 µg/g, respectively. Freundlich isotherm well explained the adsorption equilibrium.

Chatterjee and De 2017 doped chemically treated iron ore slime (IOS) in polysulfone hollow fiber membrane and used it for adsorptive removal of arsenic from

groundwater. It was characterized and observed that incorporation of IOS in membrane reduces porosity but increases hydrophobicity and arsenic removal capacity.

Huong et al. 2016 removed arsenic from water using graphene oxide-$MnFe_2O_4$ magnetic nanohybrids as magnetically separable adsorbent. Freundlich isotherm and pseudo second order model explain the equilibrium and kinetics of the adsorption process.

Andjelkovic et al. 2015 synthesized a three-dimensional (3D) graphene-iron oxide nanoparticle aerogel composite for removing arsenic from contaminated water. It was characterized and its characteristic pore network in the 3D architecture as well as high surface-to-volume ratio showed outstanding performance.

Raul et al. (2014) worked on arsenic removal from water using iron oxide hydroxide nanoflower. It showed maximum arsenic sorption capacity of 475 μg/g. Regeneration of the spent adsorbent was done by using dilute HCl.

Kilianová et al. 2013 studied the removal of arsenate from aqueous solution by ultrafine superparamagnetic iron(III) oxide nanoparticles. As reported, ~ 100 % arsenate removal was achieved when the Fe/As ratio was kept equal to 20/1 and pH ranging from 5 to 7.6. The arsenates were completely removed within several minutes of treatment.

Observations of some other report on adsorptive arsenic removal from water are summarized in Table 2.6.

Table 2.6 Recent advancements for arsenic removal from water

Adsorbent	Mode of operation	Optimum pH	Sorbent dose (g/L)	Contaminant concentration (µg/L)	Contact time (min)	Uptake capacity (µg/g)	Refrences
Al–Fe (hydr)oxides	Batch	5.0–9.0	0.2	0 to 15000	1440	71430	Qiao et al. 2014
Iron oxide-coated pumice and sepiolite	Batch	7	2	500	5040	579 and 309	Öztel et al. 2015
Nickel/nickel boride nanoparticles	Batch	3.3–11.5	10	5000 to 500000	1440	23400	Çiftçi and Henden 2015
Polyaniline/Fe^0 composite nanofibres	Batch	7	0.1	1000	1440	232600	Bhaumik et al. (2015)
i. Hydrated cement ii. Marble powder (waste) iii. Brick powder (waste)	Batch	8	10–40	100–1000	60	i. 1920 ii. 40 iii. 40	Bibi et al. (2015)
Akaganeite decorated graphene oxide composite	Batch	3–10	0.003	100	15	77500	Chen et al. (2015)

Chitosan/$Cu(OH)_2$ and chitosan/CuO	Batch	1–12	0.050	20000-100000	300	3900	Elwakeel and Guibal (2015)
Goethite/parabutlerite nanocomposites	Batch	7	0.01	500–85000	1440	37090	Fang et al. (2015)
Nanoiron/oyster shell composites	Batch	6.8	1.5	18000	1440	800	Fan et al. (2015)
Fe_3O_4-graphene macroscopic composites	Batch	4.0–10.0	0.010	5000	1440	471	Guo et al. (2015)
Iron-impregnated biochar	Batch	5.8 ± 0.2	0.1	100-55000	1440	2160	Hu et al. (2015)
Mg-Al layered double hydroxides	Batch	7.0 ± 0.1	0.024	30000	1440	125800	Huang et al. (2015)
Ferrihydrite	Batch	3.0–9.0	1.0	10000–200000	17280	142860	Jiang (2015)
Acid mine drainage sludge (AMDS)	Batch	2–10	0.1	20000	10080	18250 and 4970	Lee et al. (2015)

Denim fibre scraps	Batch	7–9	10	30000	1440	1500	Mendoza-Castillo et al. (2015)
Chitosan-based electrospun nanofibre membrane (CS-ENM)	Batch	3.3–11	0.5	50–130000	1440	30800	Min et al. (2015)
Activated alumina, Titanium dioxide (TiO2) and granular ferric hydroxide (GFH)	Batch	8.2	0.003	200	4320	7000, 13000 and 5000	Lescano et al. (2015)
Iron oxide nanoparticles	Batch	2-11	150	973 – 973960	60	149840	Morillo et al. (2015)
Fe(III) salts	Batch	7	0.020	25–100	120	55	Ouzounis et al. (2015)
Zr(IV) oxide	Column	7	0.2	1000000	7200	20000	Padungthon et al. (2015)

Macroporous polymer impregnated with hydrous iron oxide	Batch	2–12	100	78	120	31000	Taleb et al. (2015)
Akhtenskite-coated waste goethite	Batch	3.5	1-10 g	10000	50	8030	Shih et al. (2015)
Fe–Mn binary oxide-impregnated chitosan bead	Batch	7.0 ± 0.1	1	5000–60000	2160	39100	Qi et al. (2015)
Pine cone biochar	Batch	2–12	10 and 100	50000–200000	480	5.7 and 7.0	Van Vinh et al. (2015)
MIL-53(Fe)	Batch	6–10	1	5000-15000	960	21270	Vu et al. (2015)
Iron manganese bimetal oxides	Batch	3.0–12.0	0.2	100000	1440	67890	Wen et al. (2015)
Hydrous cerium oxide-modified graphene (GNP-HCO)	Batch	4–7	0.1	10000	720	62330 and 41310	Yu et al. (2015)
Montmorillonites	Batch	3–12	0.5	1000–2500000	1440	10600	Zehhaf et al. (2015)

2.3.5 Work done on Simultaneous Removal of Arsenic and Fluoride from Water

Limited work has been reported on simultaneous removal of arsenic and fluoride through adsorption.

Qiao et al. 2014 reported the Al-Fe (hydr)oxides for simultaneous removal of arsenate and fluoride. The adsorption capacity of the Al-Fe (hydr)oxides increased with increasing Al content in the adsorbents. The highest adsorption capacity of 4Al : Fe for arsenate and fluoride removal was due to highest surface hydroxyl group density besides its largest pHpzc.

Liu et al. 2012 used iron and aluminum binary oxide (FeAlOxHy) for the simultaneous removal of arsenate and fluoride. Iron oxyhydroxide (FeOxHy) showed a better removal capability for As (V) as compared to fluoride. The introduction of aluminum to FeOxHy (for producing FeAlOxHy) improved the fluoride removal capacity.

Li et al. 2011 used highly ordered mesoporous alumina and calcium doped alumina for arsenic and fluoride removal. These materials exhibited extremely high fluoride removal capacities. The highest defluoridation capacity value reached up to 450000 µg/g. The reported materials also showed good arsenic removal ability. It is reported that, 1 g of mesoporous alumina can treat 200 kg of arsenic contaminated water and reduce the concentration of arsenate from 100 µg/L to 1 µg/L.

Observations of some other report on adsorptive arsenic removal from water are summarized in Table 2.7.

Table 2.7 Recent advancements for simultaneous arsenic and fluoride removal from water

Adsorbent	Mode of operation	Optimum pH	Sorbent dose (g/L)	Contaminant concentration, Arsenic (µg/L)	Contaminant concentration, Fluoride (µg/L)	Contact time (min)	Uptake capacity, Arsenic (µg/g)	Uptake capacity, Fluoride (µg/g)	Reference
Goethite	Batch	3	0.5 to 5	50130	25600	1440	3250	850	Tang et al. 2010
Fe–Ce oxide	Batch	5	6	1000000	2.5×10^6	1440	46450	---	Zhang et al. 2010
Titanium and lanthanum oxides impregnated granular activated carbon	Batch	5	1	30000	10000	1440	28500	80000	Jing et al. 2012
Cerium impregnated fibrous protein	Batch	3	1	74920	37980	1440	172316	106154	Deng et al. 2012

2.3.6 Mechanism of Adsorptive Removal of Arsenic and Fluoride from Water

Various model equations can define the adsorption capacity and predict efficiency of adsorbent, as discussed below.

Kinetic models for single component adsorption

In order to study the kinetics for the adsorption of arsenic and fluoride in single component system in batch reactor, pseudo first order, pseudo second order as well as intra particle diffusion models have been used in literature where the kinetic parameters have been computed using the linear forms of different models, which are briefly described below:

Pseudo first order rate equation or linearized first order (Lagergren) equation can be written as:

$$\ln(q_e - q_t) = \ln q_e - k_1 t \tag{2.1}$$

The pseudo second order kinetic model in its linear form can be represented as:

$$\frac{t}{q_t} = \frac{1}{k_2 q_e^2} + \frac{t}{q_e} \tag{2.2}$$

To investigate the pore diffusion in adsorption (intraparticle diffusion) and to understand the implication of data for improved adsorbent and process design Webber and Morris model is used. This model describes the intraparticle uptake of adsorbate. According to Weber and Morris model, the transient uptake of the solute varies almost proportionately with the half power of time ($t^{1/2}$) for most of the adsorption processes. According to this model the relationship between q_t and $t^{1/2}$ is written as

$$q_t = K_{id} t^{\frac{1}{2}} + C \tag{2.3}$$

Further, in order to determine the rate limiting step for the adsorption process, the value of pseudo first order kinetics rate constant (k_1) is obtained from the slope of the pseudo first order kinetic model. The pore diffusion constant and film diffusion constant can be calculated using the following equations [Mondal et al. 2009]:

$$t_{1/2} = \frac{0.03\, r^2}{D_p} \tag{2.4}$$

$$t_{1/2} = \frac{0.23\, r\, \delta}{D_f} \times \left(\frac{C_{ad}}{C_e}\right) \quad (2.5)$$

The Eq. (2.4) and (2.5) are called half time equations.

The value of $t_{1/2}$ can be calculated as follows:

$$t_{1/2} = \frac{-[\ln(0.5)]}{k_1} \quad (2.6)$$

For a suitable value of δ the value of D_p and D_f can be calculated from Eq. (2.4) and (2.5) by putting the value of $t_{1/2}$ obtained from Eq. (2.6) [Mondal et al. 2009].

Isotherm models for single component adsorption

To explain the equilibrium adsorption of arsenic and fluoride in single component system, Langmuir and Freundlich isotherm models are normally used. Isotherm constants are computed using the linear forms of these equations and interpretation are made on the basis of some factors/ constants as described below.

Langmuir isotherm model: Langmuir isotherm assumes a mono layer adsorption on adsorbent surface with energetically identical sorption sites [Mondal et al. 2009]. The linear form of the Langmuir isotherm equation is given by:

$$\frac{C_e}{q_e} = \frac{1}{q_o b_L} + \frac{C_e}{q_o} \quad (2.7)$$

The feasibility of Langmuir isotherm can be checked by a separation factor R_L, which can be calculated by the following equation:

$$R_L = \frac{1}{1+b_L C_o} \quad (2.8)$$

The value of separation factor R_L, indicates the isotherms' type and the nature of the adsorption process. Generally, if $R_L > 1$, it is unfavorable for adsorption whereas, linear for $R_L = 1$, favorable for $0 < R_L < 1$ and irreversible when $R_L = 0$.

Freundlich isotherm model: Freundlich adsorption isotherm describes equilibrium adsorption on heterogeneous surfaces and therefore does not assume mono layer capacity. The Freundlich isotherm expression in its logarithmic form is given by the following equation:

$$\ln q_e = \ln K_F + \frac{1}{n}\ln C_e \quad (2.9)$$

The value of 1/n obtained from the slope of Eq. (2.9) should lie between 0 and 1 for favorable adsorption process [Zhu et al. 2015].

Isotherm models for binary adsorption

Equilibrium adsorption in binary system can be studied using non modified competitive Langmuir model, modified competitive Langmuir model, extended Langmuir model and extended Freundlich model, which are briefly described below.

Non modified competitive Langmuir model: This isotherm model is used for the competitive adsorption models for i^{th} component in a system having n components. It can be written as:

$$q_{e,i} = \frac{q_{o,i} b_{L,i} C_{e,i}}{1+\sum_{j=1}^{N} b_{L,j} C_{e,j}} \quad (2.10)$$

Modified competitive Langmuir isotherm: In this isotherm, an additional term η is introduced to show the competitive effect of the adsorbate species present in the solution [Aksu et al. 1999]. It is written as:

$$q_{e,i} = \frac{q_{o,i} b_{L,i} \left(\frac{C_{e,i}}{\eta_i}\right)}{1+\sum_{j=1}^{N} b_{L,j} \left(\frac{C_{e,j}}{\eta_j}\right)} \quad (2.11)$$

Extended Langmuir isotherm: According to assumptions in this isotherm, when all the sites of adsorbent are available for both the adsorbates (ions) and both the ions have non interacting effect [Srivastava et al. 2006], the equilibrium adsorption of any species can be written as:

$$q_{e,i} = \frac{q_{max} b_i C_{e,i}}{1+\sum_{j=1}^{N} b_j C_{e,j}} \quad (2.12)$$

Extended Freundlich: This isotherm was proposed by Fritz and Schluender [Fritz and Schluender, 1974], which is an extension of Freundlich model for binary mixtures. It can be written as:

$$q_{e,1} = \frac{K_{F,1} C_{e,1}^{\left(\frac{1}{n_1}\right)+x_1}}{C_{e,1}^{x_1} + y_1 C_{e,2}^{Z1}} \quad (2.13)$$

$$q_{e,2} = \frac{K_{F,2} C_{e,2}^{\left(\frac{1}{n_2}\right)+x_2}}{C_{e,2}^{x_2} + y_2 C_{e,1}^{Z2}} \quad (2.14)$$

The accuracy and adequacy of data fitted for adsorption isotherm can be tested by calculating MPSD (Marquardt's Percent Standard Deviation) value. The MPSD error function can be calculated as [Marquardt, 1963]:

$$\text{MPSD} = 100 \sqrt{\frac{1}{n_m - n_p} \sum_{i=1}^{n} \left(\frac{\left(\sum_{i=1}^{N} q_{e,i,exp}\right) - \left(\sum_{i=1}^{N} q_{e,i,cal}\right)}{\sum_{i=1}^{N} q_{e,i,exp}} \right)^2} \quad (2.15)$$

Kinetic models for column adsorption for the removal of arsenic and fluoride

Some important models normally used to understand the kinetics of column adsorption and its performance are described below.

Thomas model: The Thomas model is one of the most commonly applied model in column studies. It helps in estimation of maximum adsorption capacity of the adsorbent in column mode of operation. It can be written as follows:

$$\ln\left[\frac{C_o}{C_t} - 1\right] = \frac{k_{Th} q_{max} m}{Q} - k_{Th} C_o t \quad (2.16)$$

Yoon Nelson model: Yoon Nelson model is another model which is employed to estimate the time, which the column takes to get 50 % exhausted. The linearized form of this model can be written as follows:

$$\ln\left[\frac{C_t}{C_o - C_t}\right] = k_{YN} t - \tau k_{YN} \quad (2.17)$$

Adam Bohart model: Adam Bohart model is applied to estimate the behaviour of the column breakthrough in its initial stage. It is helpful in the estimation of saturation concentration of contaminant in the column. The linearized equation of this model can be written as follows:

$$\ln\left[\frac{C_t}{C_o}\right] = k_{AB} C_o t - \frac{k_{AB} N_o Z}{U_o} \quad (2.18)$$

Where, the value of U_o can be calculated as follows:

$$U_o = \frac{\text{Flow rate of the solution}}{\text{Cross sectional area of the column}} \quad (2.19)$$

2.4 MANAGEMENT OF SPENT ADSORBENTS

Spent adsorbent management is an important issue of any adsorption process. Different approaches such as regeneration, solidification, cementation etc. have been reported in literature. Regeneration is favorable when the adsorbent cost is high whereas for low cost adsorbents the solidification route is more suitable. Few literatures are available on the management of spent adsorbents after the removal of arsenic/fluoride from water as stated below.

2.4.1 Work Done on Management of Spent Adsorbents

Li et al. 2018 studied regeneration of nano composite based spent adsorbent after methylene blue (MB) and Pb (II) removal in batch reactor. The fresh adsorbent was a sandwich structured adsorbent with having magnetic property. The spent adsorbent was readily magnetically separated from the solution and then regenerated through Fenton-like reaction for MB and using acidic desorption process for Pb (II). It showed considerable regeneration even after fifth cycle.

Ismail and Abdelkareem, 2015 used waste lamb and chicken bones for defluoridation of water and managed the spent adsorbent through resuming as concrete mix. It was found that up to 7.5 % of spent adsorbent can be added with sand to make concrete to retain its compressive strength in desirable value. Leaching of fluoride was also tested and found ok.

Kundu and Gupta, 2008 investigated the cement and lime-based solidification / stabilization (S/S) of arsenic (As (III)) containing spent iron oxide coated cement (IOCC) adsorbent. Leachability indices and effective diffusion coefficients were used to evaluate the S/S effectiveness. Less leaching of arsenic was obtained.

2.5 LIFE CYCLE ASSESSMENT (LCA)

Life-cycle assessment (LCA, also known as Eco balance, life-cycle analysis, and cradle to grave analysis) is a technique to estimate the environmental impacts

associated with products' entire life from cradle to grave (i.e., from the acquisition of raw material, materials processing, manufacture of product, distribution, use, repair and maintenance, and disposal or recycling. The LCA of any process can be performed as per the protocol of the International Organization for Standardization (ISO 14040:2006, ISO 14044:2006), which consists of four phases: (1) Defining the goal and scope of problem, (2) Life cycle inventory analysis, (3) Life cycle impact assessment, and (4) Interpretation of results (IS/ISO 14040:2006). Very few literatures are available on the LCA of adsorption processes. Some of these are summarized below.

2.5.1 Work Done on the LCA Studies of Adsorptive Removal Process

Arena et al. 2016 performed LCA for the production of activated carbon from coconut shells in Indonesia. Human Toxicity Potential, Global Warming Potential and Acidification Potential were identified to play a key role in the overall environmental performance of the production chain. It was found electricity consumption in crushing and tumbling units produces more environmental impacts. Use of biomass energy can reduce the impacts significantly.

Yami et al. 2015 evaluated the environmental impacts of defluoridation process using adsorbents such as bone char, aluminum oxide amended wood char, activated alumina and treated alum. Raw material acquisition, adsorbent preparation and process as well as waste management were considered in the LCA study. Eco-Indicator and TRACI were used to evaluate the impacts.

Dominguez-Ramos et al. 2014 performed environmental sustainability assessment for the removal of arsenic from water through adsorption and ion-exchange processes. They used activated alumina as adsorbent and two ion exchange resins for comparison and to understand the effect of integration of these methods for water treatment. LCA inventory was obtained through modeling and simulation. Through LCA results it was interpreted that the integration of these two methods in water treatment can increase material, energy and water requirement. Spent material was found to be the main burden for the environment.

Hajila et al. 2013 performed LCA of the activated carbon (AC) preparation from olive-waste cake. Impregnation, pyrolysis of impregnated precursor and dry were identified as main steps responsible for creating more environmental impacts. The global warming potential was found as 11.10 kg CO_2 eq/kg AC.

CHAPTER 3

EXPERIMENTAL SET-UP AND INSTRUMENTATION

Present investigation was carried out on adsorptive removal of arsenic and fluoride from synthetic solution and real groundwater with the objectives as mentioned in Chapter 1. Adsorptive removal of arsenic and fluoride from synthetic and real groundwater was carried out in batch reactor through adsorption process (Figure 3.1). Continuous adsorption studies (column studies) were also carried out in order to remove arsenic and fluoride from synthetic solution (Figure 3.2). After adsorption of the contaminants (arsenic and fluoride), the spent adsorbents were immobilized in the form of clay bricks (Figure 3.3). In this chapter, the design considerations viz., composition of synthetic solution and real groundwater, range of experimental parameters considered, details of the experimental setups, limitations of the setups and specifications of auxiliary and analytical instruments used, have been described.

3.1 TYPES OF AQUEOUS SOLUTIONS CONSIDERED

Considering the co-existence of arsenic and fluoride in groundwater in many parts of India and globally, the removal studies were conducted with both synthetic solutions as well as real groundwater.

3.1.1 Synthetic Solution Containing Arsenic and Fluoride

The composition of the synthetic solution was decided on the basis of published literature. Recently in 2015, the coexistence of arsenic and fluoride, above their permissible limits, has been reported in the groundwater in many places of Rajnandgaon district of Chhattisgarh in India [Patel et al., 2015]. The composition of the groundwater as reported in this literature in the identified area is represented in Table 3.1.

Table 3.1 Composition of groundwater in Kaudikasa village, Ambagarh Chowki area, Rajnandgaon District, Chhattisgarh [Patel et al., 2015].

Component	Range of concentration of contaminant in reported area (µg/L)	Mean value of concentration of contaminant in reported area (approximately, in µg/L)
Arsenic	148 to 985	550
Fluoride	3700 to 27000	12000
Sulphate	14000 to 84000	40000
Chloride	14000 to 195000	69000
Nitrate	2700 to 134000	28000
Iron	900 to 2250	1630
Sodium, potassium, calcium, magnesium (Total hardness)	103000 to 529000	250000

From Table 3.1, it seems that the mean value of arsenic and fluoride are more than their permissible limits as per Indian standard (IS 10500). It is also evident that the mean concentrations of other cations and anions are below their respective permissible limits. Further, the effects of other anions on the removal of arsenic and fluoride can be counteracted by other cations. Thus, only arsenic and fluoride are included in the synthetic solution sample and their concentrations for the present investigation are considered as shown in Table 3.2.

Table 3.2 Concentrations of arsenic and fluoride in synthetic solution

Component	Concentration of contaminants taken during the optimization of process variables	Range of concentration of contaminants taken (for ABTL) during the isotherm studies	Range of concentration of contaminants taken (for AHNP) during the isotherm studies
Arsenic (µg/L)	500	100 to 1000	100 to 1000
Fluoride (µg/L)	10000	5000 to 15000	5000 to 30000

The arsenic and fluoride concentrations in most of the groundwater samples, reported by Patel et al. 2015, are below 500 µg/L and 10000 µg/L, respectively with the mean values of arsenic and fluoride as 550 µg/L and 12000 µg/l, respectively. Considering these facts, the concentrations of arsenic and fluoride in the synthetic samples are considered as 500 µg/l and 10000 µg/l, respectively, to investigate the effects of process variables on the removal of these pollutants. However, to cover the whole range of concentrations of arsenic and fluoride, their values in the synthetic solutions are also varied from 100 to 1000 µg/L for arsenic and from 5000 to 30000 µg/L for fluoride, respectively.

3.1.2 Real Groundwater Containing Arsenic, Fluoride and other Ions

The characteristics of real groundwater, collected from hand pump of Kaudikasa village, Rajnandgaon District, Chhattisgarh, India (20° 71′ N and 80° 77′ E) used in the present investigation, have been shown in Table 3.3. Photo 3.1 shows the location and collection of groundwater from real site.

Table 3.3 Characteristics of real groundwater used in the present investigation

Parameters	Concentration (µg/L)
pH	6.8
Temperature (°C)	27.2
Electric conductivity (µS/cm)	1169
Arsenic	512
Fluoride	6300
Iron	3500
Nitrate	42000
Phosphate	3000
Total hardness	105000
Dissolved oxygen	4000
Turbidity (NTU)	17

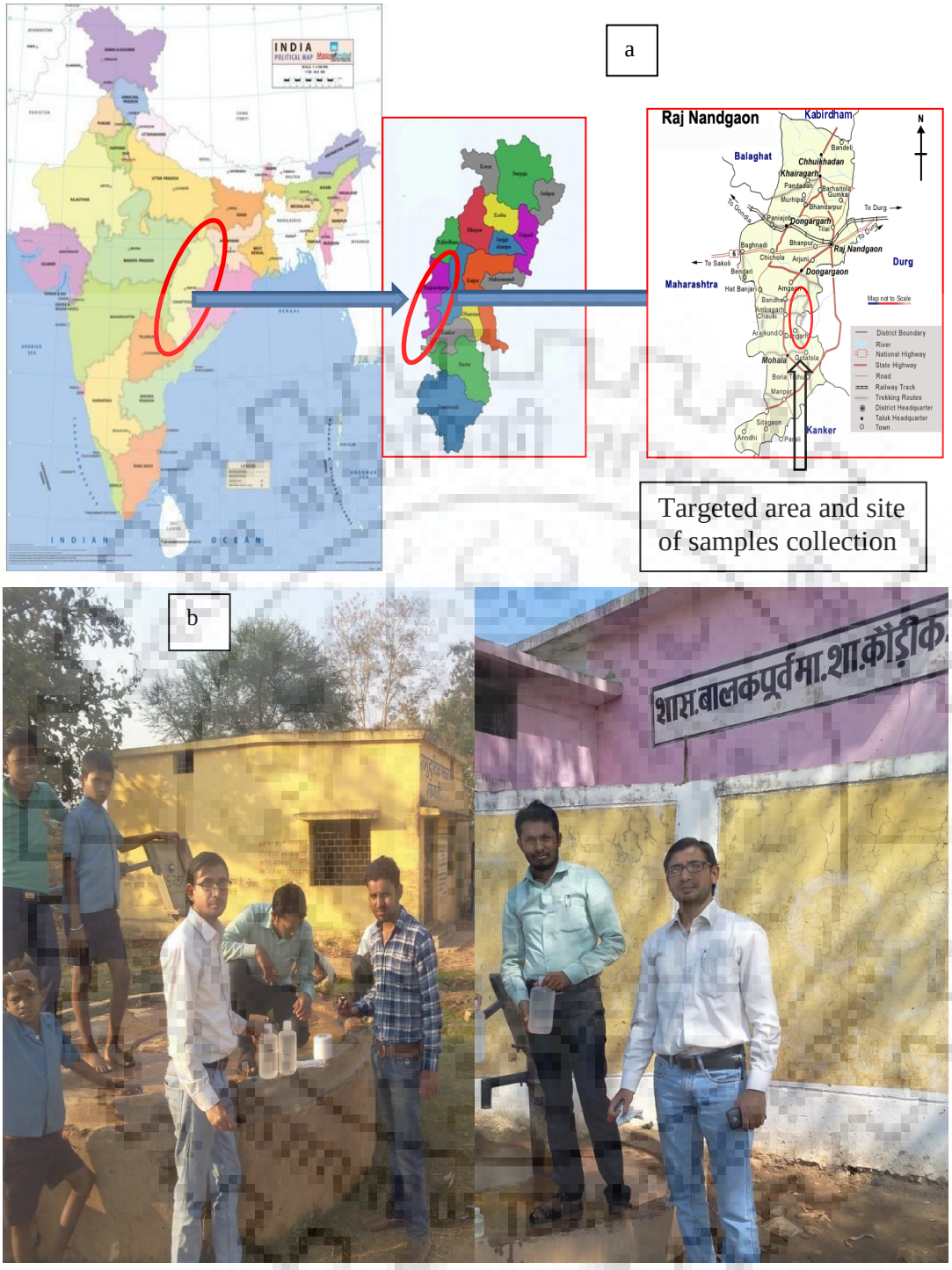

Photo 3.1 Location of contaminated area (a) and collection of real groundwater samples (b)

3.2 DESIGN CONSIDERATIONS

Design considerations of the batch and continuous studies to obtain accurate and reliable experimental data for the removal of arsenic and fluoride from synthetic solution

and real groundwater which was collected from Kaudikasa village, Rajnandgaon District, Chhattisgarh, India, are discussed below:

3.2.1 Adsorption Study In Batch Reactor

Batch study was undertaken for the optimization of process parameters for the removal of arsenic and fluoride from synthetic solution and real groundwater using adsorption process. Effects of individual process parameter on the removal of arsenic and fluoride were studied to find out the optimum process conditions. After optimization of the process parameters, the data was used to extract design parameters like rate constants and isotherm constants and to study the adsorption kinetics and adsorption capacity of the adsorbents. Considering the requirement of the sample for the analysis of arsenic and fluoride, 50 ml of the sample volume was taken for each experiment.

3.2.2 Adsorption Study In Column Reactor

Continuous study was carried out for the simultaneous removal of arsenic and fluoride from synthetic groundwater in up-flow column reactor. Material of construction of the column reactor was Perspex to avoid any contamination (chemical or bacterial) from the column reactor material. To maintain the constant feed of synthetic solution to the column reactor, peristaltic pump was used.

3.2.3 Management of Spent Adsorbents

Post adsorption of the contaminants, one of the major problem arises is management of the spent adsorbent. The spent adsorbents may also be regenerated, but in the present case, the route of regeneration of the spent adsorbents was not adopted. This was due to two major reasons:

1) The regeneration of the adsorbents decreases the adsorbing capacity of the adsorbents with every cycle of adsorption and regeneration of the material. Moreover, the regeneration process also produces many secondary pollutants which often contain harmful chemicals containing the adsorbate itself.

2) The regeneration of the adsorbents adds up additional cost to the overall process of the water treatment. In the present process, the major focus was on

development of low cost adsorbents which may be used in practical application to mitigate the problem of arsenic and fluoride contaminated groundwater.

The spent adsorbent obtained after the removal of arsenic and fluoride was managed in the form of clay bricks. The bricks were formed by blending the spent adsorbents with the clay in definite ratios and were also sintered at different temperatures to assess the applicability of this method. The bricks were tested for various physical properties for checking their suitability as building material. Leaching tests were performed to ensure the proper immobilization of the contaminants in the bricks.

3.2.4 Life Cycle Assessment of the Adsorbents

The LCA of defluoridation process is carried out to evaluate impacts that arise due to various processes including mining of the raw material, transportation, physical and chemical processing and finally management of the spent adsorbent by S/S in the form of clay bricks. The present study includes the performance of LCA study and comparison of environmental impacts of three types of adsorbents prepared from a locally/easily available natural material. The raw material for remediation of fluoride containing water was also selected such that it is available easily in many parts of India and globally. The LCA study of the adsorbent was carried out to understand the environmental sustainability of the adsorbent. The impacts associated with the defluoridation process were evaluated with the help of GaBi (Version 6.0) software.

3.3 TYPES OF EXPERIMENT CONDUCTED AND RANGE OF PARAMETERS SELECTED

Experiments conducted in the present study have been divided into 15 different set of experiments which have been presented in Table 3.4. The ranges of process and input variables are provided in Table 3.5.

Table 3.4 Different studies conducted in the present work

Type of experiment	Arsenic	Fluoride	Type of water/adsorbent
Screening of laterite based adsorbents			
Selection of best laterite based adsorbent	×	√{1}	Synthetic solution
Batch study (Individual ions) with ABTL / AHNP			
Effect of pH	√{2}/√{2*}	√{6}/√{6*}	Synthetic solution
Effect of adsorbent dose	√{3}/√{3*}	√{7}/√{7*}	
Effect of contact time	√{4}/√{4*}	√{8}/√{8*}	
Effect of initial ionic concentration	√{5}/√{5*}	√{9}/√{9*}	
Batch study (Simultaneous removal) ABTL/ AHNP			
At optimized conditions	√{10}/√{10*}		Synthetic solution
At optimized conditions	√{11}/√{11*}		Real groundwater
Column study (Simultaneous removal) ABTL/ AHNP			
At optimized conditions	√{12}/√{12*}		Simulated groundwater
Spent adsorbent management study through brick formation			
Effect of percentage of ABTL and sintering temperature on brick quality	√{13}		Spent ABTL
Effect of percentage of AHNP and sintering temperature on brick quality	√{14}		Spent AHNP
LCA for defluoridation of water			
LCA for defluoridation of water	√{15}		Laterite based adsorbents

√ = Experiment number

* = Experiments performed with AHNP as adsorbent

Table 3.5 Range of process and input parameters for different set of experiments conducted in the present study

Adsorption experiments								
Exp. set no.	**Variation in process parameter**				**Flow rate (ml/h)**	**Variation in input parameter**		**Type of water**
	pH	**Adsorbent dose (g/L)**	**Contact time (min)**	**Temperature (°C)**		**As_o (µg/L)**	**F_o (µg/L)**	
√{1}	7	10	300	25	--	--	10000	Synthetic solution
√{2}/√{2*}	3-9 / 4-9*	10/2*	300/300*	25/25*	--	500/500*	--	Synthetic solution
√{3}/√{3*}	5/7*	2-30 / 0.5-3.5*	300/300*	25/25*	--	500/500*	--	Synthetic solution
√{4}/√{4*}	5/7*	20/2*	15-780/15-300*	25/25*	--	500/500*	--	Synthetic solution
√{5}/√{5*}	5/7*	20/2*	300/300*	25/25*	--	100-1000/100-1000*	--	Synthetic solution
√{6}/√{6*}	3-9/4-9*	10/2*	300/300*	25/25*	--	--	10000/10000*	Synthetic solution
√{7}/√{7*}	5/7*	2-30/0.5-9*	300/300*	25/25*	--	--	10000/10000*	Synthetic solution
√{8}/√{8*}	5/7*	20/8*	15-780/15-300*	25/25*	--	--	10000/10000*	Synthetic solution
√{9}/√{9*}	5/7*	20/8*	300/300*	25/25*	--	--	5000-15000/5000-30000*	Synthetic solution

√{10}/ √{10*}	5/7*	20/8*	300/300*	25/25*	--	0-500/0-500*	0-10000/0-10000*	Synthetic solution
√{11}/ √{11*}	6.8/6.8*	20/8*	300/300*	25/25*	--	512	6300	Real groundwater

Adsorption experiments

Exp. set no.	**Variation in process parameter**					**Flow rate (ml/h)**	**Variation in input parameter**		**Type of water**
	pH	**Bed height (cm)**	**Mass of adsorbent (g)**	**Contact time (min)**	**Temperature (°C)**		**As_o (µg/L)**	**F_o (µg/L)**	
√{12}/ √{12*}	5/7*	25/25*	25/10*	--	25/25*	17-50/17-100*	500/500*	10000/10000*	Synthetic solution

Fixed Parameter:
For batch study:
Agitation speed: 150 rpm
* = Experiments performed with AHNP as adsorbent

Spent adsorbent management experiments		
Exp. set no.	**Variation in process parameter**	**Variation in input parameter**
	Percentage of the spent adsorbent	**Sintering temperature**
√{13}	0 to 30 % spent ABTL	800 to 1000 °C
√{14}	0 to 30 % spent AHNP	800 to 1000 °C
Life cycle assessment study		
	Software used	**Impact analysis methods**
√{15}	GaBi	CML2001, TRACI

3.4 DETAILS OF EXPERIMENTAL SETUP AND LCA STUDY

3.4.1 Setup for Arsenic and Fluoride Removal in Batch Reactors

The adsorption setup for batch scale experiments for the removal of arsenic and fluoride from synthetic and real groundwater has been schematically presented through Figure 3.1 and pictorially represented through Photo 3.2. The setup consists of a horizontally rotating platform with clamps for holding the bottles containing synthetic solution or contaminated groundwater. The bottles used for the experiments were of 100 ml capacity and made of HDPE. Shaking was carried out at 150 rpm and constant temperature.

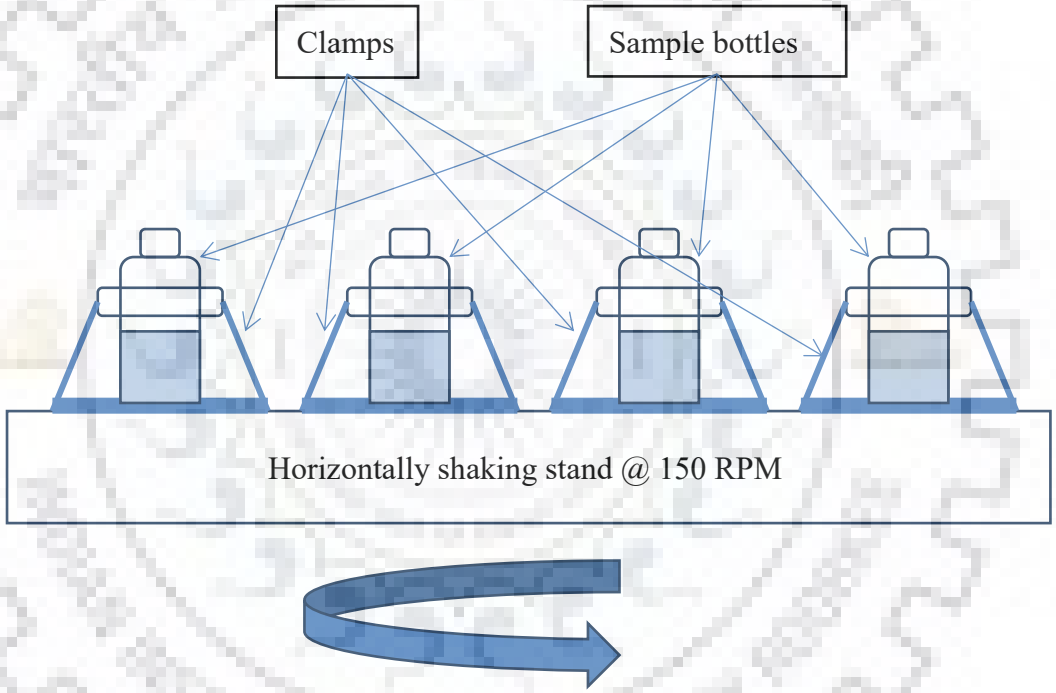

Figure 3.1 Schematic diagram of batch reactor setup

Photo 3.2 Photo of batch reactor setup

3.4.1.1 Instrumentation and control

The shaking speed of the platform and the temperature were controlled with the help of a digital controller.

3.4.1.2 Limitations of the setup

The shaking was carried out in horizontal manner hence the adsorbent gets settled down at lower shaking speeds. Replicate experiments were carried out in different bottles of similar size and dimension.

3.4.2 Setup for Arsenic and Fluoride Removal in Column Reactor

Schematic diagram of the setup has been shown in Figure 3.2 and photograph of the setup has been given in Photo 3.3. The setup consists of a simple tubular column made of Perspex glass with internal diameter 1 cm and a small hole at height of 20 cm to collect the samples of effluent. The bottom of the column was fitted with a mesh made of non-reacting polymeric material to keep the adsorbents in the column.

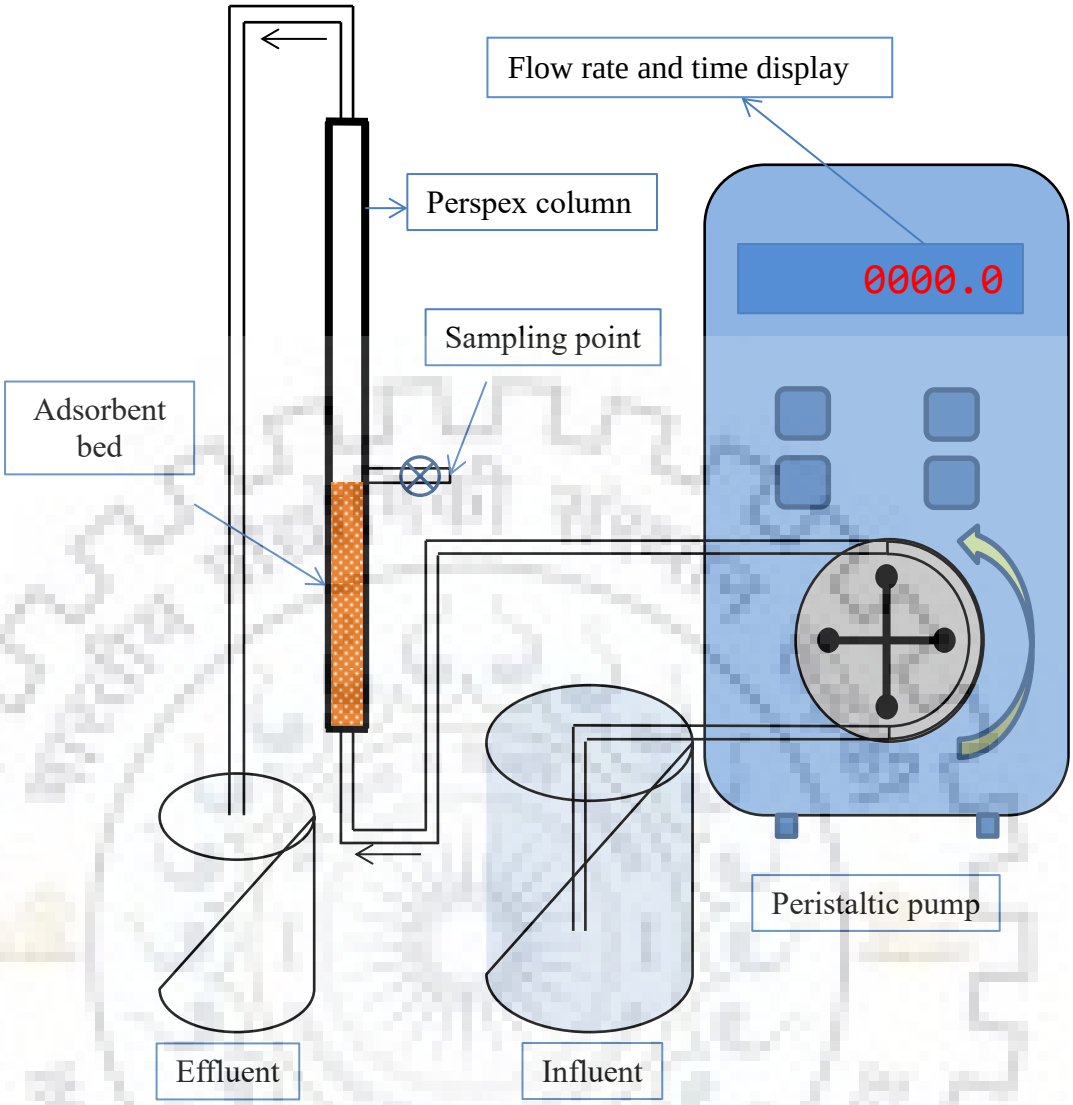

Figure 3.2 Schematic diagram of column reactor setup

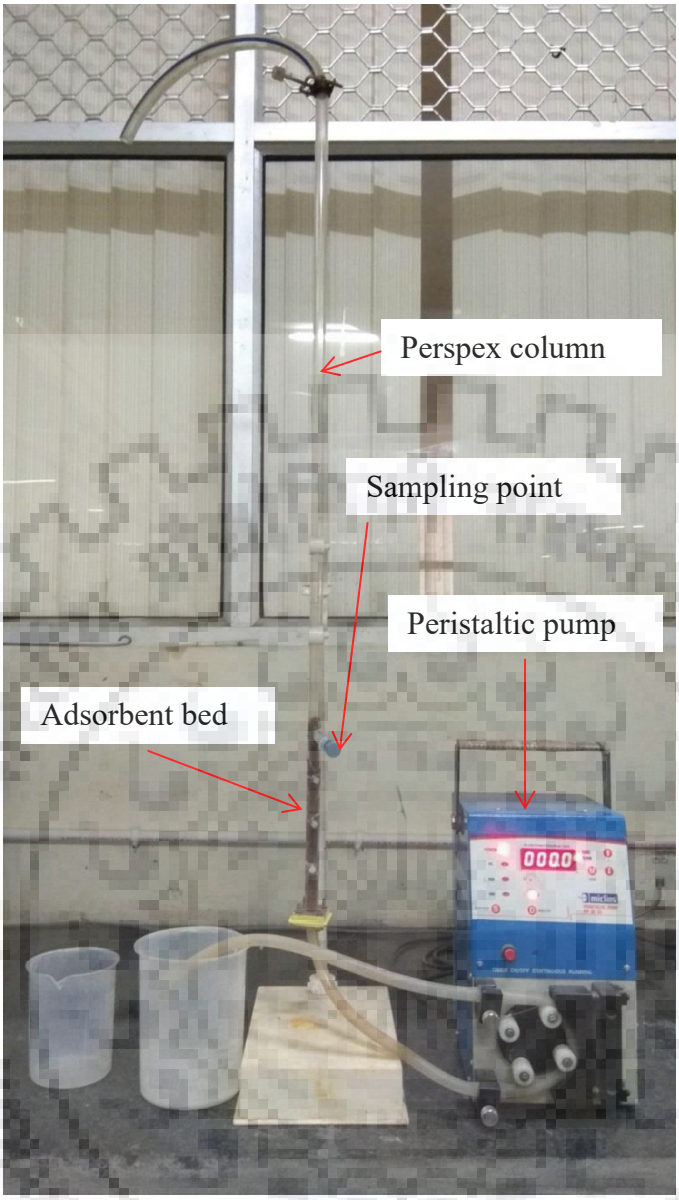

Photo 3.3 Photo of column reactor setup

3.4.2.1 Instrumentation and control

Feed flow rate was controlled by calibrated peristaltic pump (Miclins PP 20 and Miclins PP 20 Ex) procured from Miclins India, Mumbai.

3.4.2.2 Limitations of the setup

The column reactor set up had no arrangements for temperature and pH control.

3.4.3 Setup for the Manufacturing of Clay Bricks for the Management of Spent Adsorbents

For the preparation of the bricks, small metallic mould (made of iron) was used. The mould was made such that the internal dimensions of the bricks remain approximately 60 mm × 33 mm × 27 mm. The schematic diagram of the mould is shown through Figure 3.3. The photograph of the mould is given as Photo 3.4.

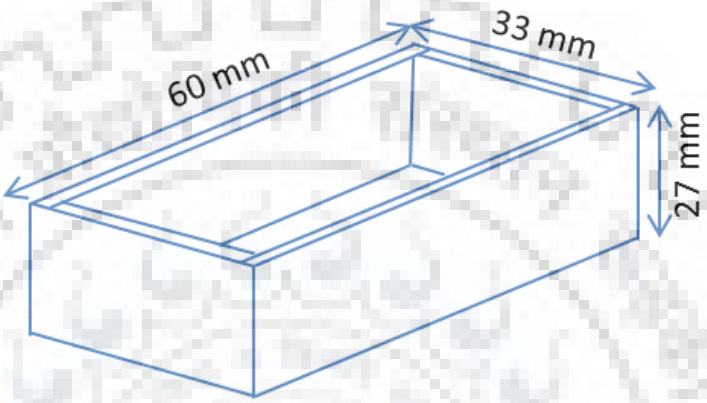

Figure 3.3 Schematic diagram of the mould used for making bricks

Photo 3.4 Photo of brick mould

3.4.3.1 Instrumentation and control

The brick formation was done manually. However, temperature controlled furnace (Metrex Scientific Instruments Pvt. Ltd., New Delhi) was used to maintain the sintering temperature.

3.4.3.2 Limitation of the setup

No automatic control system was used for the mixing of spent adsorbent and clay.

3.4.4 LCA Study of Adsorptive Removal Process

LCA of the defluoridation process was performed to assess the environmental implications of the process. Life cycle models were built with the help of GaBi 6.0 software and the impacts associated with each of the processes were evaluated with the help of GaBi professional database 2016. A life cycle impact analysis of the whole process was obtained using two different methods namely, Centrum voor Milieukunde, Leiden 2001 (CML 2001) and Tool for Reduction and Assessment of Chemicals and other Environmental Impacts (TRACI). All the inputs and emissions were calculated on the basis of appropriate material and energy balances. Due to lack of availability of data for Indian conditions for some of the processes, all the data presented in the study are given according to German context except the transportation data which is presented in Global (GLO) context.

3.5 ANALYTICAL INSTRUMENTS USED FOR THE PRESENT INVESTIGATION

Analytical instruments used in the present study are Inductively Coupled Plasma-Mass Spectrometry (ICP-MS), fluoride ion selective electrode, ion meter, Fourier Transform Infrared Spectroscopy (FTIR), XRD, Field Emission Scanning Electron Microscopy (FE-SEM). Details of important instruments are provided in Appendix A. Photographs of some sophisticated instruments used in the present investigation are provided in Appendix B and important calibration curves used in the present investigation are provided in Appendix C.

3.6 AUXILIARY EQUIPMENTS USED IN THE PRESENT INVESTIGATION

Auxiliary equipment used in the present study were pH meter, dissolved oxygen (DO) meter, hot air oven, Milli-Q water unit, distilled water plant, muffle furnace, weighing balance etc.

CHAPTER 4

EXPERIMENTAL PROGRAM AND DATA ACQUISITION

All the experiments were carried out as per the plan reported in Chapter 3 and were grouped under four major divisions/types such as synthesis and characterization of laterite based and aluminum oxide/hydroxide nanoparticles (AHNP) based adsorbents; removal of ions through adsorption by these adsorbents; management of the spent adsorbents; and life cycle assessment of the defluoridation process with laterite soil based adsorbents. In the first type of experiments, modification of the surface of laterite soil has been done through different techniques and AHNP has been prepared through electrochemical process and all the adsorbents have been characterized. Second type of experiments deal with the removal of ions from synthetic as well as real groundwater samples through batch and column reactors using laterite soil based and AHNP based adsorbents, respectively. The third type of experiments includes spent adsorbents management through brick formation and their characterization. In further type of experiment, life cycle assessment of laterite soil based adsorbents has been performed.

The experimental program undertaken for the present study is summarized in Figure 4.1. The techniques for characterization of synthetic solution and real groundwater, calibration of measuring instruments and set-up, design of experiments, experimental procedure and data recording for the above experimental scheme are discussed hereunder.

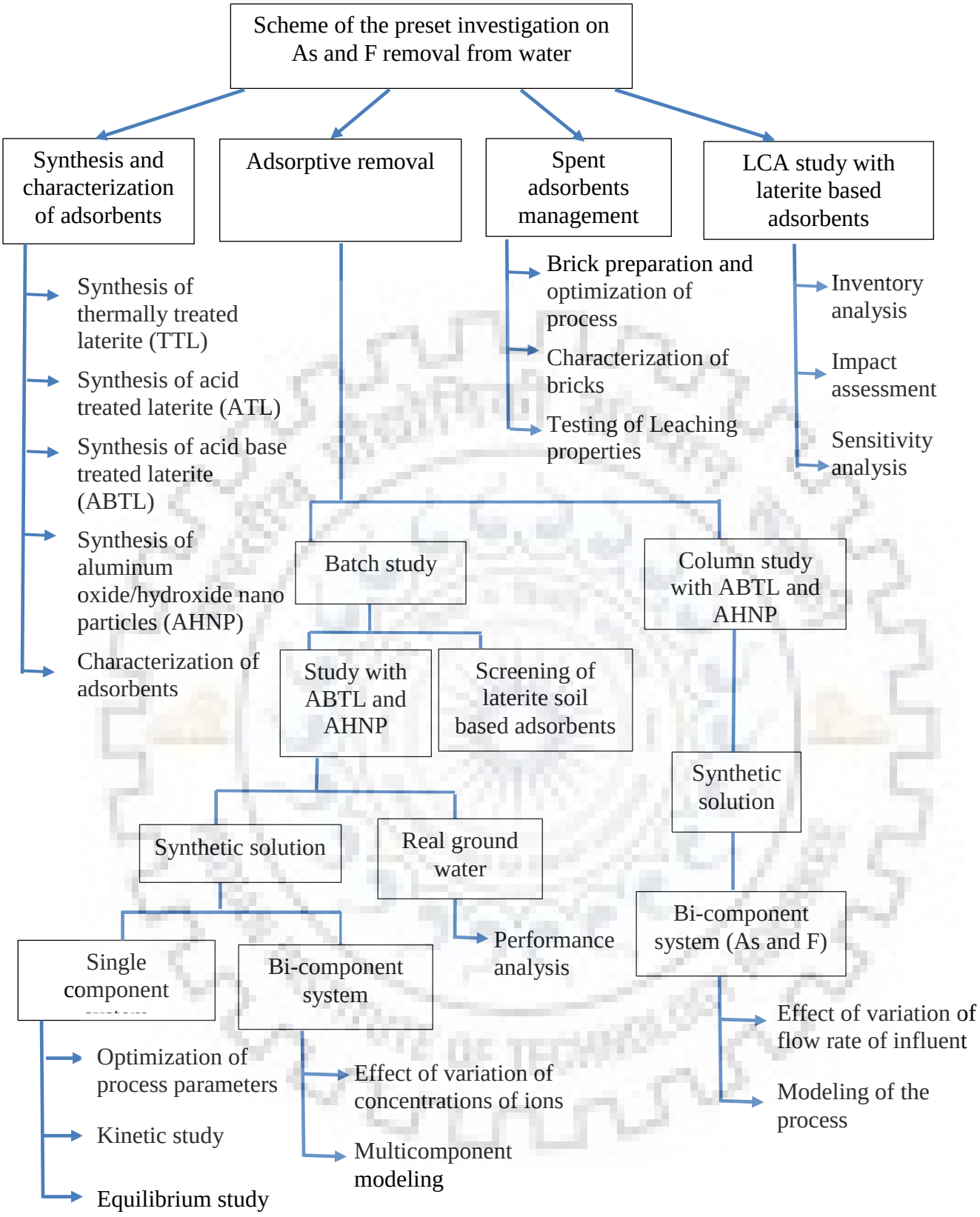

Figure 4.1 Experimental scheme for the present investigation

4.1 PREPARATION OF SYNTHETIC SOLUTIONS

All reagents used in present investigation were of analytical grade. Details of some important reagents are provided in Appendix D.

4.1.1 Synthetic Arsenic Solution

Stock solution of arsenite having concentration of 100000 µg As (III)/L was prepared by dissolving 1.734 g $NaAsO_2$ (Loba chemie) as detailed in Appendix E, in Milli-Q water. It was further diluted as per the requirements.

4.1.2 Synthetic Fluoride Solution

Stock solution of fluoride having concentration of 1000000 µg/L was prepared by dissolving 2.211 g of NaF (Sigma Aldrich) as detailed in Appendix E, in Milli-Q water. It was further diluted as per the requirements.

4.2 COLLECTION OF REAL GROUNDWATER

Arsenic and fluoride contaminated groundwater site was selected on the basis of published literature [Patel et al. 2015]. Based on this information, real groundwater samples were collected from hand pump of Kaudikasa village, Rajnandgaon District, Chhattisgarh, India. The sampling, on site analysis of some of the parameters and preservation of the samples was carried out as per the Indian Standard (IS 3025, Part 1). Before collecting the samples, the groundwater from the hand pump was purged for at least 10 min to drain off the water from the pipe and to retrieve the real groundwater from aquifer.

4.3 CHARACTERIZATION OF THE SYNTHETIC SOLUTION AND REAL GROUNDWATER

Characterization of synthetic solution and real groundwater, mentioned in section 3.1.1 and 3.1.2 were carried out as stated below.

Concentrations of arsenic was measured by Inductively Coupled Plasma Mass Spectroscopy (ICP-MS, Perkin Elmer, model ELAN-DRC-e) as per the standard method USEPA 200.8 [Creed et al., 1994]. Concentration of fluoride was measured by ion meter (Orlab India, model-OR930) coupled with fluoride ion selective electrode (Cole Parmer,

USA) [McQuaker and Gurney, 1977]. In order to prevent the interference of other ions in fluoride detection, Total Ionic Strength Adjustment Buffer (TISAB) was added to each sample in volumetric ratio of 1:1. The TISAB was prepared by adding 58 g of NaCl, 57 mL of glacial acetic acid, and 4 g of trans-1,2-diaminocyclohexane-N, N, N′, N′-tetra-acetic acid (CDTA) in approximately 500 mL of Millipore water. The pH of the solution was adjusted between 5 and 5.5 by adding approximately 125 mL of 6N NaOH. Finally, Millipore water was added to it for making the volume up to 1000 mL. Toshcon (Toshniwal India, model CL 46) pH meter was used to measure the solution pH. The calibration curves for measuring arsenic and fluoride contents are shown in Appendix C. Other characteristics of the groundwater sample like pH, turbidity, DO, total hardness, nitrate, and phosphate were analyzed onsite with the help of water testing kit (Jal-TARA water testing kit; supplied by Taralife Sustainability Solutions Pvt. Ltd., New Delhi) validated by UNICEF, whereas for the testing of other metals and ions like As, Fe, and F, the samples were transported to laboratory after preserving them by acidifying to pH < 2 (by adding 2 mL of concentrated HNO_3 per liter groundwater) for As and Fe at 4 °C (IS 3025); for fluoride no acid was added.

4.4 PREPARATION OF ADSORBENTS

For the adsorptive removal of arsenic and fluoride, two different types of adsorbents have been synthesized, namely, surface modified laterite based adsorbents and aluminum oxide/hydroxide nanoparticles based adsorbents. The synthesis of both type of the adsorbents have been discussed below.

4.4.1 Preparation of Laterite Soil Based Adsorbents

The laterite soil based adsorbents were prepared with an aim to produce a low cost adsorbent for the treatment of arsenic and fluoride contaminated groundwater. For the preparation of the adsorbent, laterite soil was taken from Burdwan District of West Bengal, India (GPS Location: 23.25N, 87.85E) and was washed, crushed, dried and sieved to get clean laterite particles of 1–1.7 mm size.

Raw laterite soil as such does not have very high adsorption capacity for either of the contaminants. Therefore, in order to overcome this problem, the surface of the raw laterite soil was modified by both physical as well as chemical treatment to increase its

adsorption capacity. The surface modification techniques adopted in the present case for the preparation of surface modified adsorbents are as follows.

4.4.1.1 Preparation of thermally treated laterite (TTL)

For preparing TTL, raw laterite soil was crushed in a jaw crusher so as to make particles of proper size (1 – 1.7 mm diameter particle size) and then it was washed thoroughly with tap water and subsequently with distilled water in order to remove all the dust, clay and other organic matters present on the surface of it. Then the laterite soil was heated in hot air oven at 105 °C for 6 hours. This material was assigned as TTL.

4.4.1.2 Preparation of acid treated laterite (ATL)

For preparing ATL, 50 g TTL was added in excess quantity of 2N HCl (200 ml) and the solution was heated at 70 °C for 3 hours with thorough agitation on a magnetic stirrer. Thereafter, the solution was heated at 110 °C without stirring so as to distill the excess free HCl (approximately 60 %). The acid treatment of the laterite is also helpful in development of positive charges on its surface due to the formation of amorphous silica from the destruction of the soil structure and/or dissolution of Al layers and subsequent attachment of H^+ ions with the silica (impurities) present on the adsorbent surface, which facilitates the adsorption of F^- ions from the solution [Maiti et al. 2010, Jozefaciuk 2002]. Finally, the solution was allowed to cool down to room temperature and the solid mass was separated from the solution by filtration, washed several times with distilled water till the pH of the wash water is ~7 and was dried in hot air oven at 110 °C. This material was assigned as ATL.

4.4.1.3 Preparation of acid-base treated laterite (ABTL)

For preparing ABTL, 200 ml of 2N HCl was added to 50 g TTL and the solution was heated at 70 °C for 3 hours with thorough agitation on a magnetic stirrer. Thereafter, the solution was heated at 110 °C without stirring so as to distill the excess free HCl (approximately 60 %). Then 200 ml distilled water was added to this followed by addition of base (in the form of 4N NaOH solution). It was added drop-wise at room temperature under constant stirring and the final pH of the mixture was adjusted to nearly 6.5. The addition of base was done in order to hydrolyze the iron and aluminum ions leached out during acid treatment to the slurry, in the form of respective metal

hydroxides [Maiti et al 2011]. The so formed metal hydroxides were then allowed to precipitate over the residual laterite mass at the bottom by keeping the mixture undisturbed for 24 hours. After all the precipitates got settled on the laterite mass at the bottom, the clear liquid formed as the top layer was decanted. The mixture was further washed several times with distilled water till the wash water was free from chloride ions. Residual chloride in wash water was determined by titrating it with $AgNO_3$ in presence of potassium chromate with phenolphthalein as indicator. Finally, the solid mass was filtered. The filtrate was discarded and the residue (solid mass) was kept in the oven to dry at 110 °C. The dried mass was assigned as ABTL.

4.4.2 Preparation of Aluminum Oxide/Hydroxide Nanoparticles Based Adsorbent (AHNP)

For preparing aluminum oxide/hydroxide nanoparticles, electrolysis was carried out in Millipore water with two aluminum plates (size 10 cm × 10 cm × 0.1 cm) as anode and cathode. AR grade NaCl (1 g/L) was used as an electrolyte. Power was supplied in the form of DC with a current density of 195 A/m^2 to this system.

The electrolysis process was allowed to proceed for 2 h, after which the power supply was turned off and nanoparticles of aluminum hydroxide were allowed to precipitate at the bottom of the reactor. The reaction was halted after 2 h of operation so as to remove the layer of oxides, which gets deposited on the surface of the electrodes. These precipitates were separated from the solution by centrifugation and washed several times with deionized water to remove the traces of electrolyte (NaCl) added during the electrolysis process. The precipitates were dried at 105 °C for 24 h and crushed to obtain particles of desired size (1 - 1.7 mm). Finally, the precipitates were subjected to calcination in an electric furnace at 700 °C so as to partially convert it into aluminum oxide and used for adsorption.

4.5 CHARACTERIZATION OF ADSORBENTS

All the adsorbents were characterized for mineralogical composition and morphological properties with various techniques like BET surface area, FTIR, XRD, FESEM-EDX. Surface area and pore volume of the samples were measured by N_2 adsorption/desorption isotherm using Micromeritics ASAP 2020 instrument by Brunauer–Emmett–Teller (BET) method and Barrett–Joyner–Halenda (BJH) method

respectively, using the software of Micromeritics. Liquid nitrogen was used as cold bath (–196 °C). The crystal structure was studied by X-ray diffractometer (BRUKER D8 advance, with Cu Kα, l = 1.54 Å, scanning rate is 1° min^{-1}) and the data was analyzed through PANalytical X'Pert HighScore software version 1.0e using database of X-ray powder diffraction patterns maintained by the International Center for Diffraction Data (ICDD) as well as published literature. Field Emission Scanning Electron Microscope (QUANTA 200 FEG from FEI, Netherlands and Carl Zeiss Ultra Plus, GEMINI, Germany) equipped with Energy-dispersive X-ray spectrometer was used to see the surface morphology and surface chemical composition of the particles. The functional groups present in the sample (organic and inorganic) were analyzed by Fourier transform infrared spectroscopy. FTIR spectra of both the adsorbents were taken in the wave number range of 4000–400 cm^{-1}, by Thermo Scientific Nicolet 6700 FTIR spectrometer coupled with OMNIC software (version 6.2) using spectroscopic grade KBr pallets in a mass ratio of 1:10 (sample: KBr) to record spectra. For the determination of point of zero charge (pH_{pzc}) of AHNP, 50 mL of 0.01 M NaCl solution was taken into each of the 10 LDPE bottles of 250 mL capacity. The initial pH of solutions of all the bottles was adjusted in the range of 2-11 by using 0.1 M HCl or 0.1 M NaOH. Further, 0.1 g of aluminum oxide/hydroxide nanoparticles was added to each of the bottles and was agitated at 150 rpm in an incubator shaker at room temperature. After 24 h, the final pH values of solutions were measured and the difference between the final pH (pH_f) and initial pH (pH_i) values, i.e., ΔpH (where, $\Delta pH = pH_f - pH_i$) was plotted against the initial pH of the solution. The point of intersection of the resulting curve with the X-axis, at which ΔpH = 0, provided the point of zero charge.

4.6 CALIBRATION OF MEASURING INSTRUMENTS

Calibration of instruments is very essential to get reliable data in the experiments. The procedure for the calibration of pH meter, ICP-MS and ion selective electrode meter are mentioned below and detail of instrument has been given in Appendix A.

4.6.1 Calibration of pH Meter

Calibration of pH meter was done using pH buffers of value 4, 7 and 9.2 as per the instruction manual provided by the manufacturer.

4.6.2 Calibration of Conductivity Meter

Calibration of conductivity meter was done as per the instruction manual provided by the manufacturer.

4.6.3 Calibration of Ion Meter and Fluoride Ion Selective Electrode

Calibration of ion selective electrode meter was done as per the instruction manual provided by the manufacturer using standard solutions of respective metal salts (calibration curve in Appendix C).

4.6.4 Calibration of ICP-MS

Calibration of ICP-MS was done as per the instruction manual provided by the manufacturer using standard solutions of respective metal salts (calibration curve in Appendix C).

4.6.5 Calibration of Peristaltic Pumps

Calibration of peristaltic pump was done as per the instruction manual provided by the manufacturer.

4.7 CALIBRATION OF EXPERIMENTAL SETUP

For batch experiments the temperature of incubator cum shaker was calibrated with the help of a pre-calibrated thermometer. For column study, variable speed peristaltic pump required calibration before the starting of experiments in column reactor. Calibration of the peristaltic pump was done by the instruction manual provided by the manufacturer.

4.8 EXPERIMENTAL PROCEDURE AND DATA RECORDING

Experiments were conducted as per the program shown in Figure 4.1. Each experiment was repeated thrice and the average reading was recorded with 2 % error. Detail procedure and recording of data for various experiments undertaken in the present study are described below.

4.9 ADSORPTIVE REMOVAL STUDIES

Experiments on the adsorptive removal of arsenic and fluoride from synthetic solution as specified in Table 3.5 of Section 3.3 were conducted in batch reactor to optimize the operating conditions for both the adsorbents. Further the removal of both the contaminants was assessed from real groundwater at the optimized conditions.

4.9.1 Studies on the Adsorptive Removal of Arsenic and Fluoride from Synthetic Solution by Laterite Soil Based Adsorbents in Batch Reactor

The removal of arsenic and fluoride from the synthetic solution was studied with the help of surface modified laterite soil based adsorbents in batch reactors. The operating parameters for the adsorption experiments were kept similar for all the adsorbents.

4.9.1.1 Comparison of the laterite soil based adsorbents and selection of the best one

The adsorption experiments were performed taking all the three types of surface modified laterite soils and their fluoride removal capacities were determined (initial pH of solution 7, adsorbent dose as 10 g/L, contact time as 300 minutes and initial fluoride concentration as 10000 µg/L). Since the arsenic removal capacity of laterite soil based adsorbents is relatively high and concentration of arsenic present in water is less (in ppb level). Thus, only fluoride removal capacity is considered for selecting the type of adsorbent. The detailed results are presented in the Section 5.1. Based on the experiments, it was found that ABTL has the highest adsorption capacity for fluoride. Thus, it was selected as best adsorbent among the laterite based adsorbents and considered for further studies.

4.9.1.2 Studies on the removal of arsenic/fluoride by ABTL in single component system

For the single component system, the removal of arsenic and fluoride were taken individually and the various operating parameters affecting the adsorption like pH, adsorbent dose, initial ion (arsenic or fluoride), contact time and temperature were optimized through sequential optimization. The procedure for conducting the experiments is described below.

4.9.1.2.1 *Studies on the removal of arsenic/fluoride at various pH*

The initial pH of solution plays important role in adsorptive removal of pollutants from water as it affects both the surface charge/surface functional groups of adsorbents as well as the solution phase chemistry of pollutant. Adsorptive removal of both arsenic and fluoride were studied for pH range 3 to 9 by ABTL and from pH range 4 to 9 for AHNP in order to assess both the acidic and basic scenario. The adsorption capacity of ABTL for fluoride is found to be lesser than AHNP in the preliminary experiments. Hence a wider range of pH has been considered for ABTL (from 3 to 9) as compared to AHNP (from 4 to 9). The dependency on pH of arsenic and fluoride to get adsorbed on adsorbent surface has been explained with the help of speciation chemistry of these ions as well as with the help of surface charge of the adsorbent at different values of initial pH of solution. The speciation chemistry of arsenic and fluoride are given in the speciation diagram prepared with the help of Visual MINTEQ Ver.3.1 software.

4.9.1.2.2 *Studies on the removal of arsenic/fluoride at various adsorbent dose*

The amount of adsorbent dose required to bring down the concentration of the contaminants was carried out in this study. The adsorbent dose study using ABTL was carried out from 2 g/L to 30 g/L at pH 5, 500 µg/L initial arsenic or 10000 µg/L initial fluoride with 300 min contact time effect.

4.9.1.2.3 *Studies on the removal of arsenic/fluoride with respect to contact time*

The study for the optimization of contact time was carried out by varying the contact time of the adsorbent from 15 minutes to 800 minutes. The studies were conducted at pH 5, 20 g/L adsorbent dose, 500 µg/L initial arsenic or 10000 µg/L initial fluoride concentration. Moreover, this study also helped to understand the kinetics of the process and determine the order of the kinetics.

4.9.1.2.4 *Studies on the removal of arsenic/fluoride with respect to initial ion concentration*

To study the effect of initial concentration of ions on their percentage removal, the concentration of the arsenic ions was varied from 100 µg/L to 1000 µg/L and for

fluoride from 5000 µg/L to 15000 µg/L at pH 5 and adsorbent dose as 20 g/L. Moreover, this study also helped to estimate the adsorption isotherm constants.

4.9.1.2.5 *Kinetic studies*

In order to study the kinetics for the adsorption of arsenic and fluoride in single component system, pseudo first order, pseudo second order as well as intra particle diffusion models were used and the kinetic parameters were computed using the linear forms of these models, which are briefly described in Section 2.3.5.

4.9.1.2.6 *Isotherm studies*

To explain the equilibrium adsorption of arsenic and fluoride in single component system, Langmuir and Freundlich isotherm models were used. Isotherm constants were computed using the linear forms of these equations and interpretation were made on the basis of some factors/constants, which are described in Section 2.3.5.

4.9.1.3 Studies on the simultaneous removal of arsenic and fluoride by ABTL in bi-component system

The binary adsorption experiments were conducted at pH 5 for 300 min with 20 g/L adsorbent dose and the initial concentration of arsenic and fluoride were varied as shown in Table 4.1.

Table 4.1 Variations in the initial concentration of arsenic and fluoride for bi-component system.

$C_{o,\ fluoride}$ (µg/L)	$C_{o,\ arsenic}$ (µg/L)
5000	0
7500	0
10000	0
0	100
5000	100
7500	100
10000	100
0	300
5000	300
7500	300
10000	300
0	500
5000	500
7500	500
10000	500

In general, a mixture of adsorbates can exhibit three different types of behavior, namely

(a) Synergism (the effect of mixture is greater than the single component in the mixture)

(b) Antagonism (the effect of mixture is less than that of each of the components in the mixture)

(c) Non-interaction (the mixture has no effect on the adsorption of each of the adsorbents in the mixture).

In this study, the interaction between arsenic and fluoride has been explored based on these three types of behaviors.

4.9.1.3.1 *Multicomponent isotherm modeling*

Equilibrium adsorption in binary system was studied using various multicomponent isothermal models like non modified competitive Langmuir model, modified competitive Langmuir model, extended Langmuir model and extended Freundlich model. The details of these models are discussed in Section 2.3.5.

4.9.1.3.2 *Calculation of the error function*

The accuracy and adequacy of data fitted for binary adsorption isotherms models (non modified competitive Langmuir model, modified competitive Langmuir model, extended Langmuir model and extended Freundlich model) were tested by calculating MPSD (Marquardt's Percent Standard Deviation) formula using MS Excel 2007. The details of MPSD error function and its formula is mentioned in Section 2.3.5.

4.9.2 Studies on the Removal of Arsenic and Fluoride from Real Groundwater by ABTL in Batch Reactor

The study for the removal of arsenic and fluoride from real groundwater was carried out at the optimized conditions (initial pH of solution 6.8, adsorbent dose as 20 g/L and contact time as 300 minutes) which were found out with the help of above mentioned studies.

4.9.3 Studies on the Adsorptive Removal of Arsenic and Fluoride from Synthetic Solution by ABTL Adsorbent in Column Reactor

Experiments were conducted to study the simultaneous removal of arsenic and fluoride from synthetic solution in a column reactor by ABTL. The schematic diagram of the rector has been shown in Figure 3.2 of Section 3.4.2. The flow of the synthetic solution was in upward direction and was controlled with the help of a peristaltic pump.

4.9.3.1 Studies on the effect of flow rate of influent on simultaneous removal of arsenic and fluoride

For the simultaneous removal of arsenic and fluoride, the amount of ABTL used in the column was 25 g and the bed height was taken as 20 cm. The flow rate of the

solution was varied from 17 ml/hr to 50 ml/hr with 500 µg/L arsenic and 10000 µg/L fluoride concentration.

4.9.3.2 Analysis of column adsorption data and modeling of the column adsorption process

The effect of flow rate of influent on the performance of ABTL adsorbent has been studied and the breakthrough curves are obtained. The changes in the nature of breakthrough curves are interpreted with the help of mathematical modeling. Dynamic response of the adsorption column was determined by the breakthrough time and shape of the breakthrough curve. The mathematical analysis of the parameters associated with column breakthrough curves has been carried out. The dynamic behavior of the column has been predicted and analyzed with the help of three models i.e. (i) Thomas model (ii) Yoon-Nelson model and (iii) Adam-Bohart model.

4.9.4 Studies on the Adsorptive Removal of Arsenic and Fluoride from Synthetic Solution by AHNP in Batch Reactor

The removal of arsenic and fluoride from the synthetic solution by AHNP was studied in a similar way to that of ABTL.

4.9.4.1 Studies on the removal of arsenic/fluoride by AHNP in single component system

For the single component system, the removal of arsenic and fluoride were taken individually and various operating parameters affecting the adsorption like pH, adsorbent dose, initial ion (arsenic or fluoride), contact time and temperature were optimized through sequential optimization similarly to ABTL adsorbent. The procedure for conducting the experiments is described below.

4.9.4.1.1 *Studies on the removal of arsenic/fluoride at various pH*

The initial pH of solution plays important role in adsorptive removal of pollutants from water in case of AHNP also as it also affects both the surface charge/surface functional groups of adsorbents as well as the solution phase chemistry of pollutant. Adsorptive removal of both arsenic and fluoride were studied for pH range 4 to 9 in order to assess both the acidic and basic scenario. The dependency on pH of arsenic and

fluoride to get adsorbed on adsorbent surface of AHNP has also been explained with the help of speciation chemistry of these ions as well as with the help of surface charge of the adsorbent at different values of initial pH of solution.

4.9.4.1.2 *Studies on the removal of arsenic/fluoride at various adsorbent dose*

The amount of adsorbent dose required to bring down the concentration of the contaminants was carried out in this study. The adsorbent dose study using AHNP was carried out from 0.5 to 3.5 g/L in case of arsenic and 0.5 g/L to 9 g/L in case of fluoride at pH 7, 500 µg/L initial arsenic concentration or 10000 µg/L initial fluoride concentration with 300 min contact time.

4.9.4.1.3 *Studies on the removal of arsenic/fluoride with respect to contact time*

The study for the optimization of contact time was also carried out similar to ABTL by varying the contact time of the adsorbent with the arsenic and fluoride containing solution from 15 minutes to 300 minutes. The studies were conducted at pH 7, 2 g/L adsorbent dose for arsenic and 8 g/L for fluoride, 500 µg/L initial arsenic or 10000 µg/L initial fluoride concentration. This study was also carried out to understand the kinetics of the process and determine the order of the kinetics.

4.9.4.1.4 *Studies on the removal of arsenic/fluoride with respect to initial ion concentration*

The study of effect of initial ion concentration on the percentage removal of the contaminant was also performed similar to ABTL. To conduct this study, the initial concentration of arsenic ions was varied from 100 µg/L to 1000 µg/L and for fluoride from 5000 µg/L to 30000 µg/L at pH 7 and adsorbent dose as 2 g/L for arsenic and 8 g/L for fluoride. This study was also conducted in order to estimate the nature and type of the adsorption isotherm.

4.9.4.1.5 *Kinetic studies*

The kinetic studies with AHNP were also conducted similarly to ABTL with similar models.

4.9.4.1.6 *Isotherm studies*

The isotherm studies with AHNP were also conducted similarly to ABTL with similar models.

4.9.4.2 Studies on the simultaneous removal of arsenic and fluoride by AHNP in bi-component system

The binary adsorption experiments were conducted at pH 7 for 300 min with 8 g/L adsorbent dose and the initial concentration of arsenic and fluoride were varied as shown in Table 4.2.

Table 4.2 Variations in the initial concentration of arsenic and fluoride for bi-component system

$C_{0,\ fluoride}$ (µg/L)	$C_{0,\ arsenic}$ (µg/L)
2500	0
5000	0
7500	0
10000	0
0	100
2500	100
5000	100
7500	100
10000	100
0	200
2500	200
5000	200
7500	200
10000	200
0	300

2500	300
5000	300
7500	300
10000	300
0	400
2500	400
5000	400
7500	400
10000	400
0	500
2500	500
5000	500
7500	500
10000	500

4.9.4.2.1 *Multicomponent isotherm modeling*

The multicomponent isotherm modeling study with AHNP was also conducted similarly to ABTL with similar models.

4.9.4.2.2 *Calculation of the error function*

For checking the accuracy and adequacy of data fitted for binary adsorption isotherms models, similar method was followed as provided in Section 4.9.1.3.2.

4.9.5 Studies on the Removal of Arsenic and Fluoride from Real Groundwater by AHNP in Batch Reactor

The study for the removal of arsenic and fluoride from real groundwater was carried out by similar method as stated in Section 4.9.2 under optimized conditions (initial pH of solution 6.8, adsorbent dose as 20 g/L and contact time as 300 minutes).

4.9.6 Studies on the Adsorptive Removal of Arsenic and Fluoride from Synthetic Solution by AHNP Adsorbent in Column Reactor

Experiments were conducted to study the removal of arsenic and fluoride from synthetic solution in a column reactor by AHNP adsorbent similarly to ABTL adsorbent.

4.9.6.1 Studies on the effect of flow rate of influent on simultaneous removal of arsenic and fluoride

For the simultaneous removal of arsenic and fluoride, the amount of AHNP used in the column was 10 g and the bed height was taken as 20 cm. The flow rate of the solution was varied from 100 ml/hr to 17 ml/hr with 500 µg/L arsenic and 10000 µg/L fluoride concentration.

4.9.6.2 Analysis of column adsorption data and modeling of the column adsorption process

The effect of flow rate of influent on the performance of AHNP adsorbent has been studied and the breakthrough curves were obtained. Dynamic response of the adsorption column was determined by the breakthrough time and shape of the breakthrough curve and mathematical analysis of the parameters associated with column breakthrough curves has been carried out similar to ABTL.

4.10 ECONOMIC EVALUATION OF THE ADSORBENTS

The cost of the adsorbents and the overall treatment cost of the contaminated water were estimated on the basis of the actual cost of the chemicals and electricity that was consumed for the synthesis of 1 kg of the adsorbents and subsequently treating 1 liter of contaminated water.

4.11 STUDIES ON THE MANAGEMENT OF SPENT ADSORBENTS IN THE FORM OF CLAY BRICKS

Spent adsorbents were immobilized in the form of clay bricks instead of regenerating them. For this, bricks were made by blending clay with spent adsorbents (10 % to 30 % w/w). The bricks so produced were characterized similarly to the ABTL and

AHNP, and were tested for various physical and leaching properties. The details of the tests carried over with the bricks are as follows:

4.11.1 Preparation of the Spent Adsorbents

For the preparation of spent adsorbents, experiments were carried out for simultaneous adsorption of As and F at solution pH value of 6, with contact time of 300 min and initial concentrations of arsenic and fluoride as 1000 µg/L and 100000 µg/L respectively. The dose of adsorbents was fixed as 100 g/L for ABTL and 20 g/L for AHNP as it was found in experiments that AHNP has more adsorbing capacity for both the ions as compared to ABTL. Arsenic and fluoride containing synthetic solutions were shaken in 1 L LDPE bottles (Tarsons) kept at 30 °C in an orbital shaker incubator (Metrex Scientific Instruments, New Delhi, India) at shaking speed of 150 rpm. After desired time (i.e. 300 min) the samples were filtered with Whatman filter paper (0.45 mm pore size) and the solid portion (i.e. the spent adsorbent) was dried at 105 °C and mixed with clay in varying percentage so as to make the bricks. The amount of arsenic and fluoride present on the spent adsorbent was calculated from specific uptake of the adsorbents as:

$$\text{Specific uptake, } q = \frac{(C_0 - C_e)v}{m} \qquad (4.1)$$

4.11.2 Preparation of the Bricks

The clay raw material was obtained from a local brick manufacturer located in the outskirts of Roorkee, India (GPS coordinates 29.818 N and 77.922 E). The raw clay was initially subjected to pretreatments such as drying, milling and sieving. The milling was performed in a laboratory mill to make the particle size smaller than 100 µm for brick production. For studying the final disposal of spent adsorbents, they were stabilized in the form of clay bricks. Evenly pressed compacted brick samples of approximately 60 × 33 × 27 mm size were prepared using clay and appropriate percentage (10 %, 20 % and 30 %) of spent adsorbents by adding 15 – 20 % (w/v) of water to the dry sample. The effect of sintering temperature (800 °C, 900 °C and 1000 °C) on their building characteristics and arsenic and fluoride leachability was also examined. Thus, in total 24 bricks were formed from ABTL + clay and AHNP + clay mixtures with the variation of two parameters viz. percentage of spent adsorbent in clay and sintering temperature. All

the brick samples were then air dried for 2 days at room temperature and then at 105 °C for 24 h in hot air oven for removing moisture. Finally, the bricks were sintered in an electric furnace at sintering temperature ranging from 800 °C to 1000 °C for 60 min [Chiang et al., 2008]. Such high temperature sintering forms metal oxides, which minimize the leaching of metals from the brick [Rouf and Hossain, 2003]. The rate of increase in temperature was maintained at 10 °C/minute during the sintering

4.11.3 Characterization of Clay, Bricks and Spent Adsorbents

Clay, brick specimens and spent adsorbent were characterized for mineralogical composition and morphological properties with various techniques like FTIR, XRD and FESEM-EDX similarly to adsorbents.

4.11.4 Leaching Tests of the Bricks

For checking the leaching back of arsenic and fluoride from spent adsorbent immobilized in the brick, they were tested as per the protocol of California Waste Extraction Test (WET) (Ghosh et al., 2004). The solids samples (sintered brick specimen made of pure clay or containing spent adsorbents with clay) to be evaluated for leaching of arsenic and fluoride were coarsely crushed so as to pass through a standard No.10 sieve. Then 5 g of solid mass was placed in an air tight glass container with 50 ml WET extraction solution and agitated for 48 h in incubator shaker at room temperature (25 °C). The extraction solution consisting 0.2 M sodium citrate at 5 pH was prepared by titrating AR grade citric acid in Millipore water with 4 N NaOH.

4.11.5 Testing of Other Physical Properties of the Bricks

Various physical properties of sintered brick specimen were also tested according to different standard protocols. Densities of the sintered samples were determined using dry mass to volume ratio. Volume was determined using Archimedes method [Chiang et al., 2008]. Water absorption tests were performed on all the sintered brick specimens as per Indian Standard IS 3495-1992. Efflorescence tests were performed to check the salt deposition on the sintered brick specimens as per Indian Standard IS 3495-1992. Dimensional changes (linear shrinkage) in the sintered brick specimens at various temperatures were tested as per ASTM C373 standard. Compressive strength of the

sintered brick specimens was tested as per Indian Standard IS 3495-1992 to check its suitability for construction works.

4.12 LIFE CYCLE ASSESSMENT (LCA) STUDIES OF THE DEFLUORIDATION PROCESS BY LATERITE SOIL BASED ADSORBENTS

The LCA study was performed as per the protocol of the International Organization for Standardization (ISO 14040:2006, ISO 14044:2006), which consists of four phases: (1) Defining the goal and scope of problem, (2) Life cycle inventory analysis, (3) Life cycle impact assessment, and (4) Interpretation of results (ISO 14040:2006). The scope of the present study includes all the stages starting from the mining/collection of raw laterite soil to final disposal in the form of clay bricks. The assumptions and system boundaries, inventory analysis, impact assessment are provided below.

4.12.1 Assumptions, System Boundaries and Inventory Analysis

The following assumptions were made for the present LCA study:

1) Mining/collection of raw laterite from the site is assumed to be carried out through human labor and not with the help of any type of mechanical drillers or excavating machines. Thus, the possible emissions associated with this step are neglected.
2) The transportation of quarried out raw laterite soil is carried out with the help of diesel engine trucks. Further, the average transportation distance from the mining site to the processing site is assumed as 5 km.
3) All the laterite soil collected is assumed to have uniform physical and chemical composition. Therefore, any pre-processing of the raw laterite to convert it into a usable form is not considered.
4) Heating of the laterite samples for drying after washing steps and while giving it acid treatment is assumed to be carried out in hot air ovens having a capacity to dry up to 50 kg of material at a time and the calculations related to emissions from these processes are done accordingly.
5) It is assumed that during acid-base treatment step (for producing ABTL), the effluent does not consist of any leftover acid or base. This assumption is based on

the fact that during the acid-base treatment, all the leftover acid is neutralized by the NaOH. Further, the amount of HCl and NaOH used in the process is very less. Thus, the environmental impacts associated with the synthesis of these chemicals are not considered.

6) The application step of the adsorbent for treating water is assumed not to contribute significantly towards any of the impacts and therefore this step is also not considered.
7) Losses in the mass of laterite soil in the form of undersized particles and water vapors generated during drying and surface modification of laterite are assumed not to produce any significant impact on the environment and human health.
8) The environmental impacts imparted by the refinery for producing diesel, which has been used for the transportation of raw laterite is not considered. This is due to the fact that the LCA of production of diesel fuel from the crude oil is beyond the scope of the present study and should be carried out separately.
9) Biogas from biomass has been selected for generating electricity for sintering the bricks which were made from spent adsorbent and clay as it is assumed that biomass is available in abundant quantities in developing countries like India [weblink 1] and it would not be economically feasible to use electricity from grid mix. Moreover, the usage of direct burning of materials like coal and other fossil fuels is also avoided as it may result in even higher impacts to the environment.

The usage phase is excluded from the study and it is assumed that the total waste emissions associated with this stage are negligible. The system boundaries considered for the defluoridation process with TTL, ATL and ABTL are shown through Figure 4.2 (a) to (c). The basis of all the calculations for inventory analysis was defined considering the amount of adsorbent required to reduce the fluoride concentration of 720 liters of water from 10000 µg/L to 1500 µg/L. Selection of 720 liter water as a basis is based on the idea of developing a water filtration unit containing the present adsorbent, which can successfully work for 30 days to meet the drinking water requirement of a family with 4 members assuming 6 liters of drinking water consumption per capita per day. The preparation of the above mentioned surface modified laterite soil based adsorbents have been discussed in Section 4.4.1.

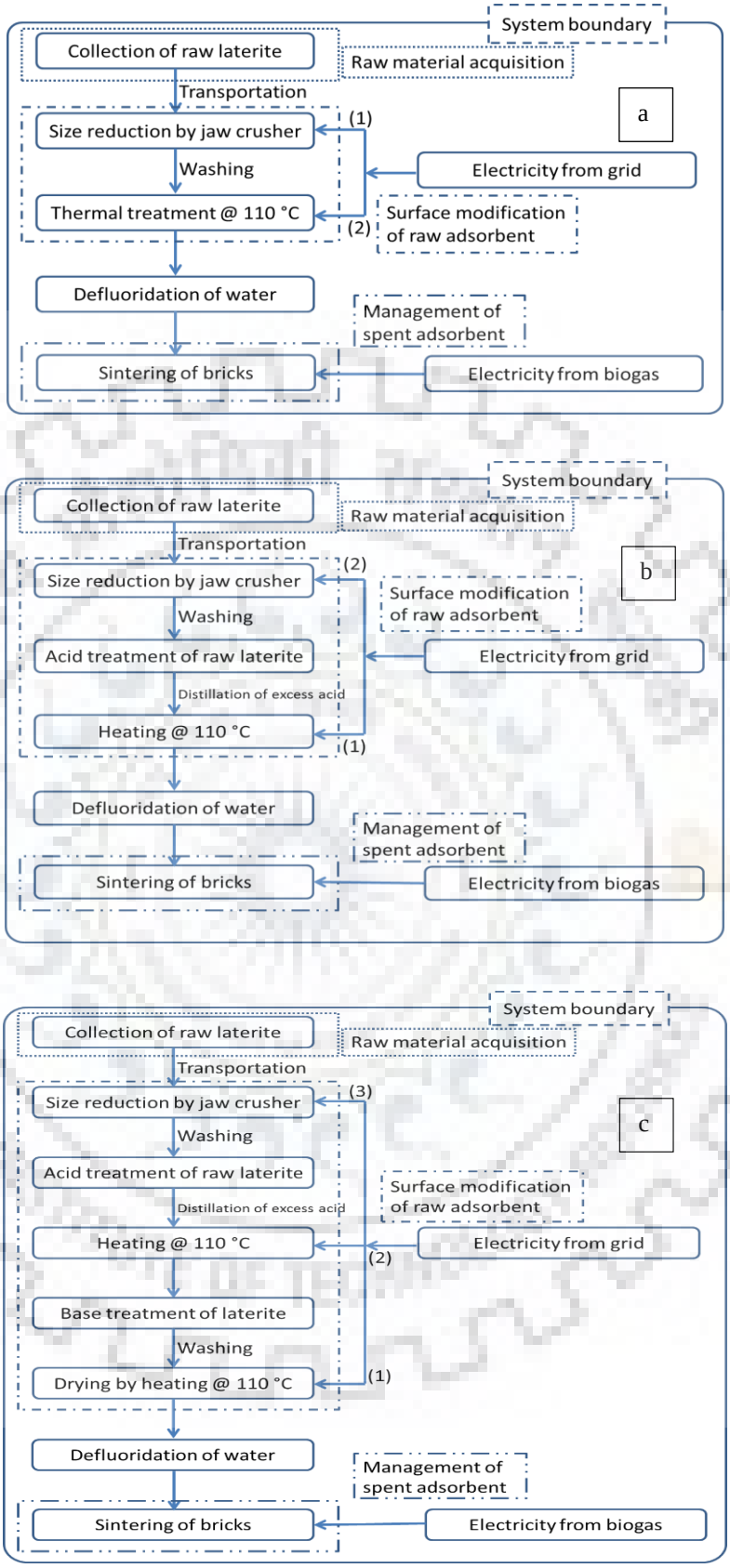

Figure 4.2 System boundaries for TTL (a), ATL (b) and ABTL (c)

The fluoride adsorption capacity at an equilibrium dissolved fluoride concentration of 1500 µg/L (referred to hereafter as $Q_{1.5}$, with units of µg F^-/g adsorbent), which is a crucial factor for comparing the magnitude of environmental impacts, was determined as per Eq. 4.2, whereas, the mass of adsorbent required was computed by using Eq. 4.3 [Yami et al., 2015]. and the values are summarized in Table 4.3.

$$Q_{1.5}\left(\mu g/g\right) = Q_{max}bC_{e1.5}/(1 + bC_e) \quad (4.2)$$

$$\text{Total mass of the adsorbent required (g)} = (C_0 - C_e)V/Q_{1.5} \quad (4.3)$$

Table 4.3 Langmuir isotherm constants for different adsorbents and their total mass required to lower the concentration of fluoride from 10000 µg/L to 1500 µg/L in 720 L water

Adsorbent	Langmuir isotherm constants	$Q_{1.5}$ (µg/g)	Total mass of adsorbent required for treating 720 L of water (in kg)
ABTL	Q_{max} = 520 µg/g b = 0.0015 L/µg	220	27.8
ATL	Q_{max} = 400 µg/g b = 0.0004 L/µg	160	38.2
TTL	Q_{max} = 270.14 µg/g b = 0.0005 L/µg	110	55.6

For preparing 55.6 kg TTL, 38.2 kg ATL, and 27.8 kg ABTL, the amount of raw laterite required were found as approximately 382 kg, 310 kg, and 370 kg respectively. Further, for producing the required adsorbents, the energy requirements and loss of laterite during each treatment steps were calculated as shown through Figure 4.3 to Figure 4.5.

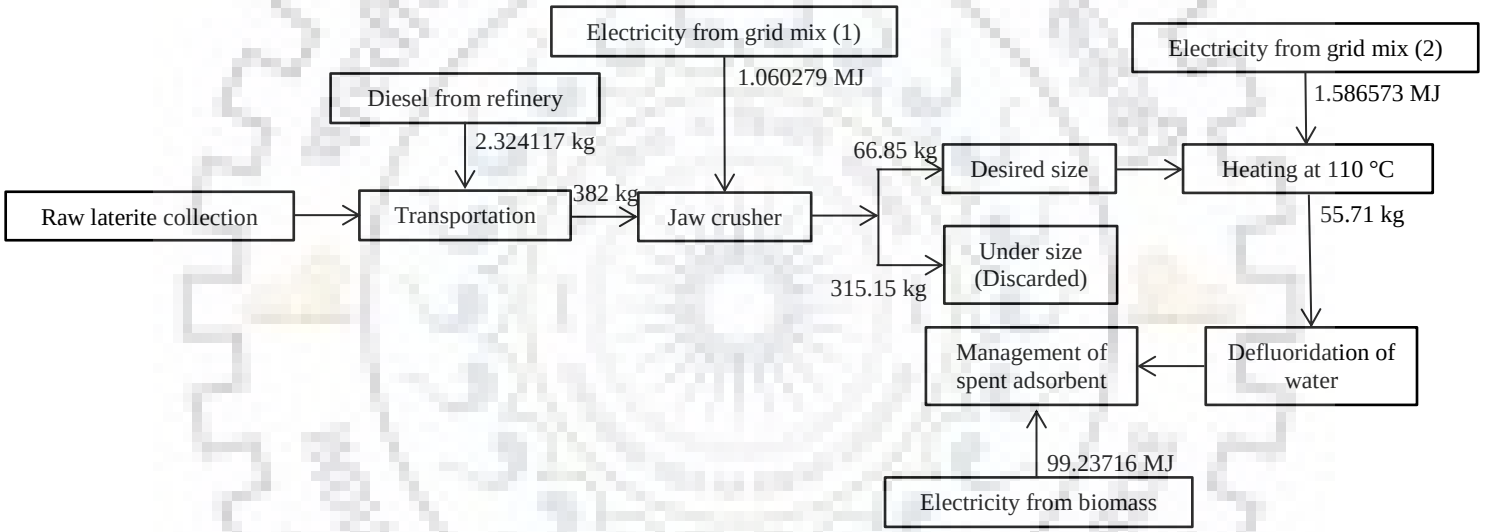

Figure 4.3 Flow diagram for the synthesis of TTL (with values of mass and energy input during various processing steps)

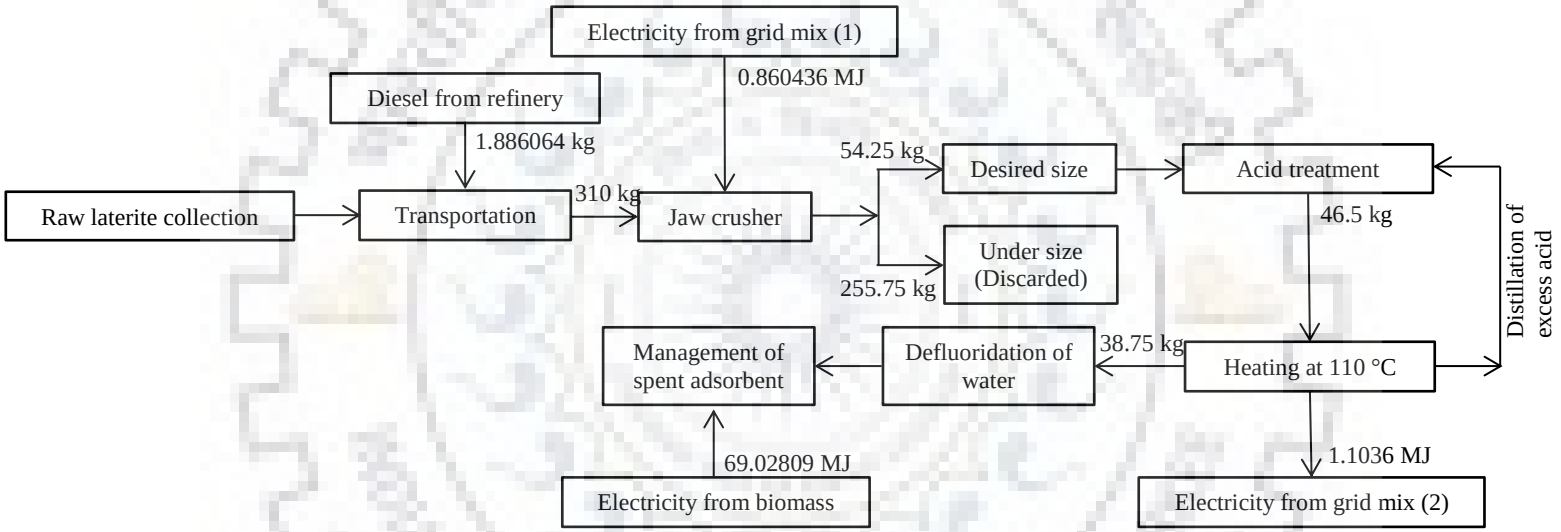

Figure 4.4 Flow diagram for the synthesis of ATL (with values of mass and energy input during various processing steps)

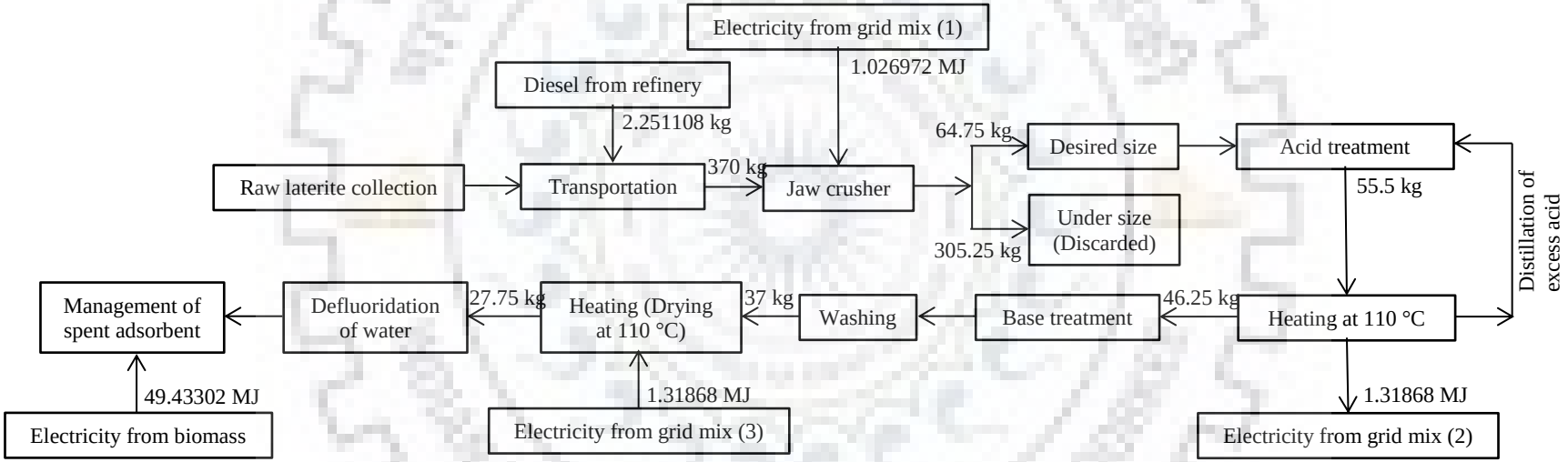

Figure 4.5 Flow diagram for the synthesis of ABTL (with values of mass and energy input during various processing steps)

4.12.2 Environmental Impact Assessment Methodologies

Different life cycle impact assessment methods may lead to distinct results in terms of values, impact categories, units etc. [Monteiro and Freire 2012]. Therefore, in order to interpret the environmental impacts, two different methods viz. CML 2001 and TRACI have been used in the present study. The main purpose of considering two different impact assessment methodologies is to compare the results obtained through these methodologies and to verify their consistency for the present system. Characterization factors of these two methodologies may vary as these are based on different geographical conditions. Therefore, a consistency in results of the environmental impacts interpreted by the above-mentioned methodologies may ascertain their application in Indian context also.

4.12.3 Sensitivity Analysis of the LCA Process

Sensitivity analysis was conducted in order to identify and evaluate the process steps with maximum contributions on various impact categories as well as to find out the alternative options to decrease the impacts varying their input values. For carrying sensitivity analysis, the impacts to the environment and human health were quantified through CML 2001 method for all the adsorbents. On reviewing the quantified data of initial LCI analysis, it was observed that the transportation of the raw material was one of the major contributors in the impact categories like Global Warming Potential (GWP), acidification potential and eutrophication potential due to emission of greenhouse gases and other gases like SOx, NOx etc., as indicated in the report of GaBi 6.0 software. Therefore, various options were considered to lower the impacts due to transportation step by varying the loading capacity of the truck trailer and the assumed distance between the mining site and the processing site. In the originally considered scenario, a truck trailer of 27 tons capacity was selected and the distance between the mining site and the processing site was assumed as 5 km. Alternatively, various other scenarios were considered, which are as follows:

1) A truck trailer having 5 ton carrying capacity and the distance between the mining site and the processing site is assumed as 5 km.
2) A truck trailer having 5 ton carrying capacity and the distance between the mining site and the processing site is assumed as 10 km.

3) A truck trailer having 12.4 ton carrying capacity and the distance between the mining site and the processing site is assumed as 5 km.

4) A truck trailer having 12.4 ton carrying capacity and the distance between the mining site and the processing site is assumed as 10 km.

5) A truck trailer having 17.3 ton carrying capacity and the distance between the mining site and the processing site is assumed as 5 km.

6) A truck trailer having 17.3 ton carrying capacity and the distance between the mining site and the processing site is assumed as 10 km.

The carrying capacities of the vehicles were selected from the database of the GaBi 6.0 software and the other properties of emissions were kept similar to the originally considered scenario (like the composition of diesel used as fuel, emission standard of the vehicle was taken as Euro IV, etc.).

4.12.4 Limitations of the Procedure

The major limitation of the LCA study was lack of availability of the data in Indian context. Hence, for the present study, most of the data considered is based on German or Global context as provided in the database of GaBi software.

CHAPTER 5

RESULTS AND DISCUSSION

This Chapter covers the discussion and interpretation of results of the present investigations. Studies embodied in this Chapter have been divided into seven sections as stated below:

Section 5.1 Studies on the selection of laterite soil based adsorbents

Section 5.2 Characteristics of ABTL and AHNP adsorbents

Section 5.3 Studies on adsorptive removal of arsenic and fluoride from synthetic solution by ABTL adsorbent in batch and column reactor

Section 5.4 Studies on adsorptive removal of arsenic and fluoride from synthetic solution by AHNP adsorbent in batch and column reactor

Section 5.5 Economic evaluation of the adsorbents

Section 5.6 Studies on the management of spent adsorbents in form of clay bricks

Section 5.7 LCA studies of the defluoridation process by laterite soil based adsorbents

Experiments conducted in the present study have been distributed into 15 experimental sets and have been presented in different groups as shown in Table 3.4 of Section 3.3. The range of process and input parameters are shown in Table 3.5 of Section 3.3. Detail procedures to conduct these experiments are provided in Chapter 4 and the experimental set-up used in the present study are described in Chapter 3. In the present study, adsorptive removal of arsenic and fluoride from synthetic solution as well as real groundwater has been investigated.

Further, the spent adsorbent management studies in the form of clay bricks have also been carried out followed by LCA study of defluoridation of aqueous solution by laterite soil based adsorbents.

The compositions of synthetic solution and real groundwater are provided in Table 3.2 and 3.3 of Section 3.1.1 and 3.1.2 respectively. LCA study of the defluoridation process has been carried out with the help of GaBi software and the

environmental implications of the process have been addressed. Details of analytical instruments and calibration curves are provided in Appendix A and Appendix C, respectively. Photographs of the analytical instruments and auxiliary equipments are provided in Appendix B. Details of chemicals used in the present study are provided in Appendix D

5.1 STUDIES ON THE SELECTION OF LATERITE SOIL BASED ADSORBENTS

The laterite soil originally collected from the site was not having much adsorbing capacity for arsenic or fluoride in its native state. Hence, it was given different physical and chemical treatments to prepare three different types of surface modified laterite soil based adsorbents (namely TTL, ATL and ABTL) as mentioned in Section 4.4.1. These surface modified laterite soil based adsorbents were subjected for the adsorptive removal of fluoride from synthetic solution. The detailed procedure along with different parameters is described in Section 4.9.1.1. Effects of different surface modification on the defluoridation capacity of the laterite soil based adsorbents are presented in Figure 5.1.

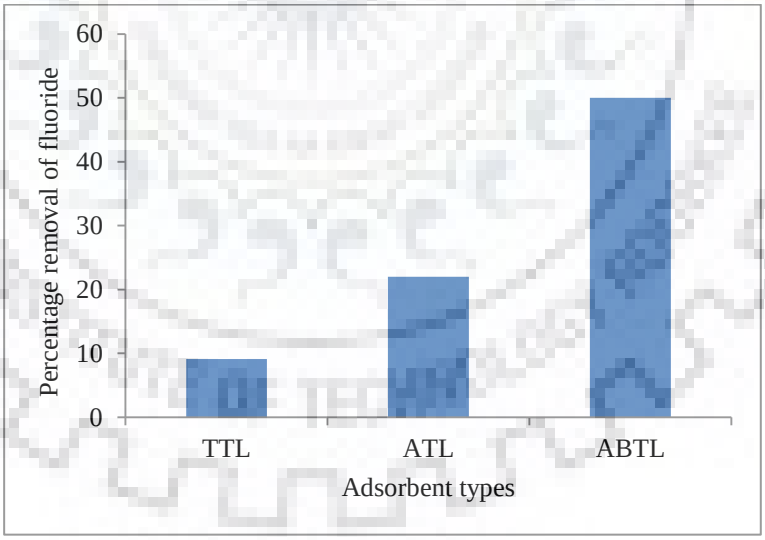

Figure 5.1 Comparison of fluoride removal capacity of laterite soil based adsorbents (TTL, ATL and ABTL)

From Figure 5.1, the following points are evident:

i. The percentage removal of fluoride by TTL, ATL and ABTL are obtained as 9.1 %, 22 % and 55 % respectively.
ii. The defluoridation capability of ATL is higher than TTL, whereas, ABTL showed highest fluoride removal capability.

Observations given in point (i) and (ii) can be explained as follows:

The increase in the percentage removal of fluoride by acid treatment can be attributed to the fact that acid treatment of the laterite is helpful in development of positive charges on its surface due to the formation of amorphous silica from the destruction of the soil structure and/or dissolution of Al layers and subsequent attachment of H^+ ions with the silica (impurities) present on the adsorbent surface, which facilitates the adsorption of F^- ions from the solution [Maiti et al. 2010, Jozefaciuk 2002].

Further, addition of base to this acid laterite-slurry, converts iron and aluminum ions leached out during acid treatment, to respective metal hydroxides [Maiti et al 2011]. It is also well reported in the literature that metal hydroxides possess significant adsorption capacities for arsenic and fluoride from water [Rathore et al. 2016]. Hence, ABTL showed maximum adsorption towards fluoride and was selected for further studies.

5.2 CHARACTERISTICS OF ABTL AND AHNP ADSORBENTS

Characterization of ABTL and AHNP, was carried out using sophisticated instruments like BET surface area analyzer, FTIR, FESEM-EDX and XRD to get information about surface morphology and chemical composition of the adsorbents. The point of zero charge (pH_{PZC}) of AHNP was determined through salt addition method by plotting ΔpH (difference between initial and final pH of suspension) against initial pH value [Tan et al., 2008] as described in Section 4.5. The point of zero charge (pH_{PZC}) of individual oxides present in ABTL was considered to explain the effect of pH of adsorption and respective values were collected from published literature. The important characteristics of these adsorbents are discussed below:

BET surface area and pore volume of virgin and spent ABTL

The procedure for the determination of BET surface area and pore volume of the virgin and spent ABTL are described in Section 4.5. The results obtained are as follows:

Table 5.1 BET surface area and pore volume of virgin and spent ABTL adsorbent

Property	Virgin ABTL	Spent ABTL
BET Surface area (m^2/g)	36.7004	21.628
Pore volume (m^3/g)	0.0444	0.0255

It is observed that the specific surface area and pore volume of virgin ABTL are more than that of spent ABTL, which indicates that the arsenic and fluoride ions are adsorbed on the surface of the adsorbent.

FTIR analysis of the virgin and spent ABTL adsorbent

FTIR analysis of the virgin and spent ABTL adsorbent was carried out as mentioned in Section 4.5. The results obtained are as follows:

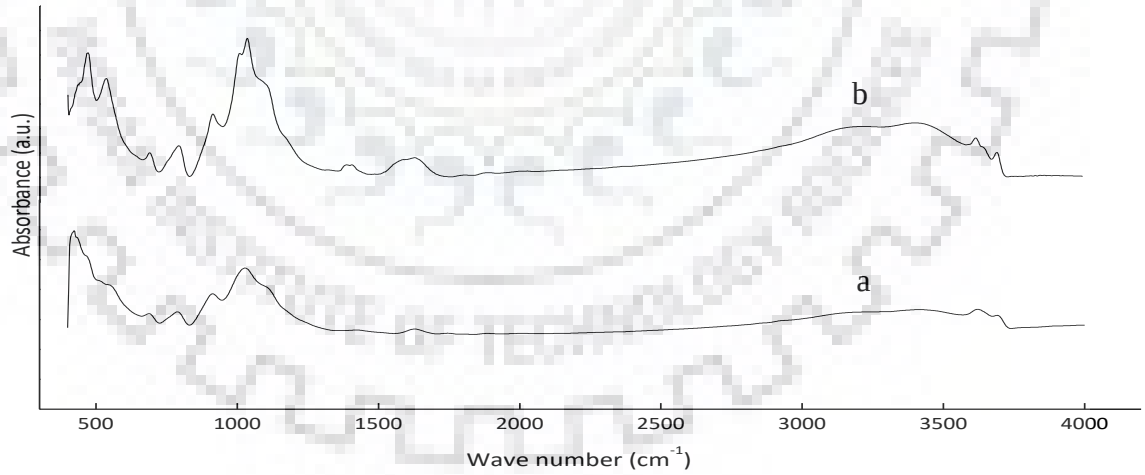

Figure 5.2 FTIR of virgin (a) and spent (b) ABTL adsorbent

The presence of iron, aluminum and silica oxides or hydroxides gets confirmed by studying these spectral patterns. The presence of Al-O-H stretching is indicated by absorbance band present near 3680 cm^{-1}. The absorption band within the range of 3370 to 3405 cm^{-1} was attributed to OH group of Fe, Al and Si minerals. The absorption band

near 1620 cm^{-1} is assigned to H-O-H bending of water molecule on the surface of laterite. A strong absorption band near 1030 cm^{-1} indicates the presence of Si-O stretching. The absorbance band at wave number 912 cm^{-1} indicates Al-OH bond stretching. The band near 790 cm^{-1} is attributed to cristobalite which is a polymorph of quartz and near 690 cm^{-1} due to Si-O quartz. The absorbance bands from 542 to 474 cm^{-1} are anticipated due to Fe-O bond stretching, Fe_2O_3 and Si-O-Al stretching. The Fe-O bond stretching near 534 and 466 cm^{-1} are highly intensified in ABTL. The wavenumber ranging from 750 to 450 cm^{-1} indicates the presence of Mn_2O_3 related stretching and bending vibrations. The increase in intensity of bands of ABTL further confirms the presence of higher amount of oxyhydroxides on its surface.

XRD analysis of the virgin and spent ABTL adsorbent

Figure 5.3 gives XRD patterns for virgin and spent ABTL. The peak at $2\theta = 26$ and 67 are due to the presence of Fe_2O_3. Whereas the presence of FeO can be anticipated by the peak at $2\theta = 36$. Peaks at $2\theta = 39$, 67 and 73 represent Al_2O_3. Other peaks at $2\theta =$ 20, 26, 36, 63 and 67 corresponds to SiO_2. The peaks at $2\theta = 26$, 49, 59, 63, 73 and 79 are probably due to Mn_3O_4. Further, broadening of the XRD peaks is associated with the formation of nanostructures of Fe and Al oxyhydroxide deposited on the surface of laterite during treatment process [Yogamalar et al. 2009]. The peaks at $2\theta = 26$, 50 and 75 in the spectra of spent ABTL adsorbent are due to the presence of $AlAsO_4$.

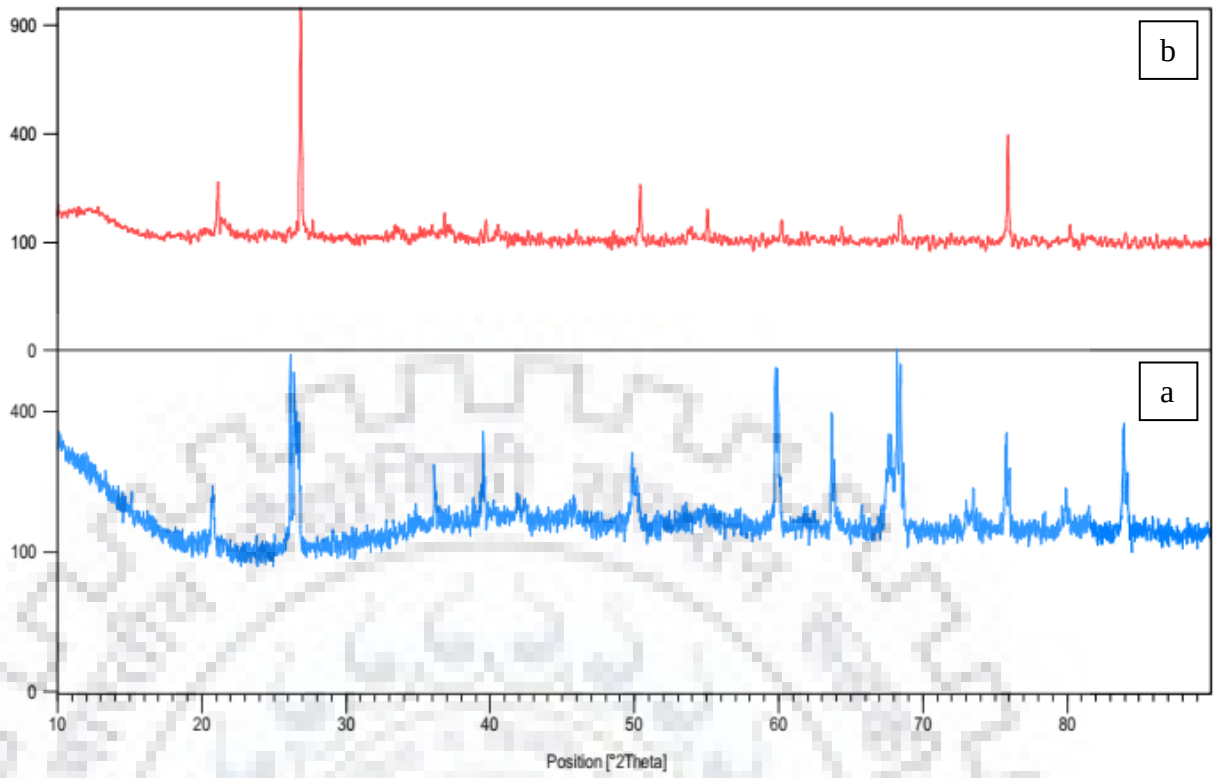

Figure 5.3 XRD of virgin (a) and spent (b) ABTL adsorbent

FESEM-EDX analysis of the virgin and spent ABTL adsorbent

The FESEM images of virgin and spent ABTL are given in Figure 5.4 (a) and 5.4 (b) respectively and EDX patterns are given in Figure 5.5 (a) and 5.5 (b) respectively. On comparing the FESEM images, it is evident that the surface morphology of the virgin ABTL has changed due to the adsorption of arsenic and fluoride on it. The surface morphology of the ABTL became more heterogeneous after the adsorption of arsenic and fluoride. Further, on comparing the EDX of the virgin and the spent adsorbent it can be observed that there is no considerable change in the elemental composition in them. It may be due to the fact that during the adsorption process, the adsorbent does not undergo any change in its elemental composition. Moreover, peaks of arsenic and fluoride are visible (in EDX pattern) on the surface of spent ABTL which confirms the adsorption of these ions during the process.

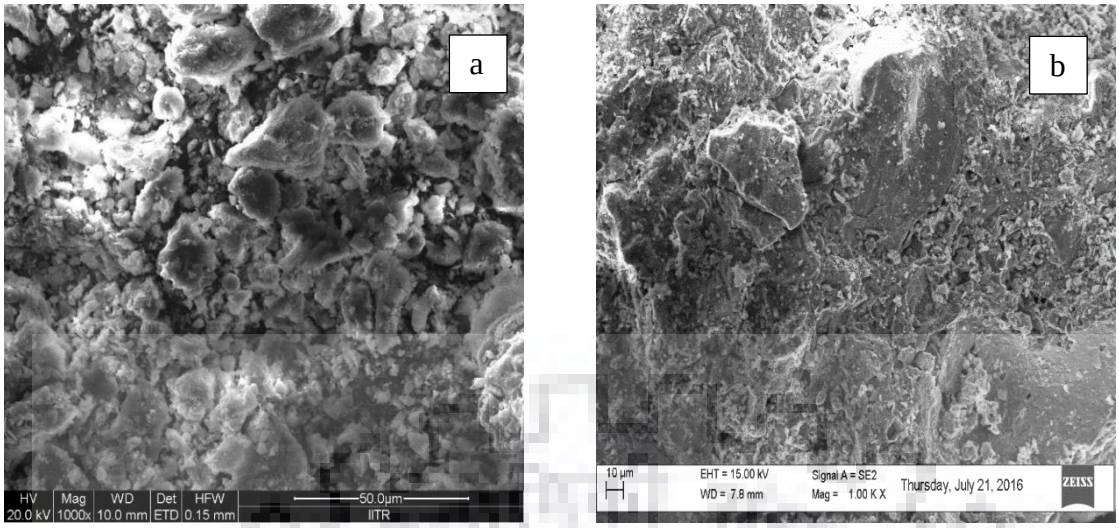

Figure 5.4 FESEM of virgin (a) and spent (b) ABTL adsorbent

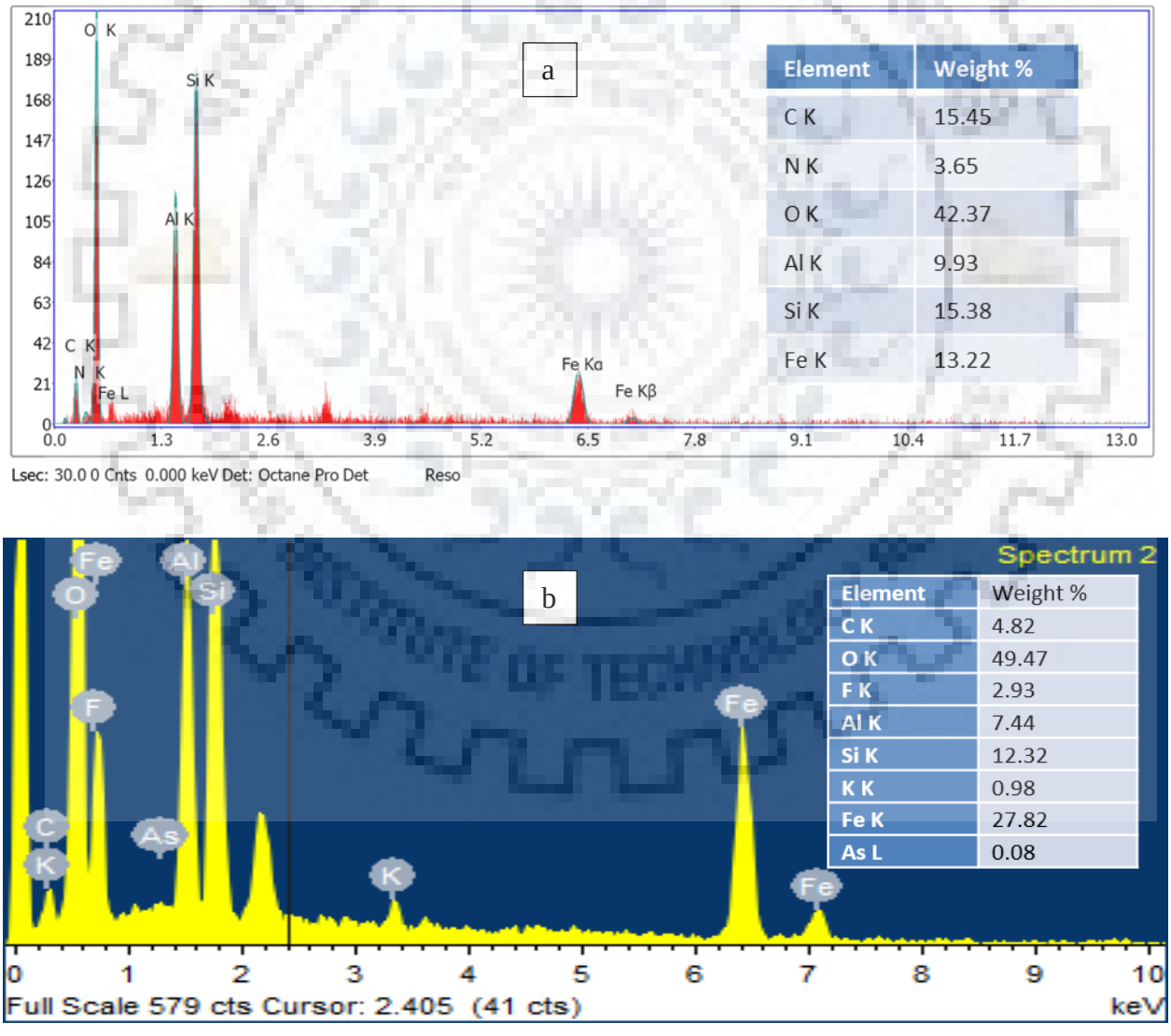

Figure 5.5 EDX of virgin (a) and spent (b) ABTL adsorbent

BET surface area and pore volume of virgin and spent AHNP

The values of the surface area and the pore volume of the virgin and the spent adsorbent are given in Table 5.2. It is observed that the specific surface area and pore volume of virgin AHNP are more than that of spent AHNP, which indicates that the arsenic and fluoride ions are adsorbed on the surface of the adsorbent. Further, it is also observed that in the present study, AHNP tends to agglomerate during the adsorption process, which is also responsible for the reduction in the surface area and pore volume of the adsorbent.

Table 5.2 BET surface area and pore volume of virgin and spent AHNP adsorbent

Property	Virgin AHNP	Spent AHNP
BET Surface area (m^2/g)	253.16	226.81
Pore volume (m^3/g)	0.296	0.266

FTIR analysis of the virgin and spent AHNP adsorbent

FTIR analysis of the virgin and spent AHNP adsorbent was carried as mentioned in Section 4.5. The results obtained are as follows:

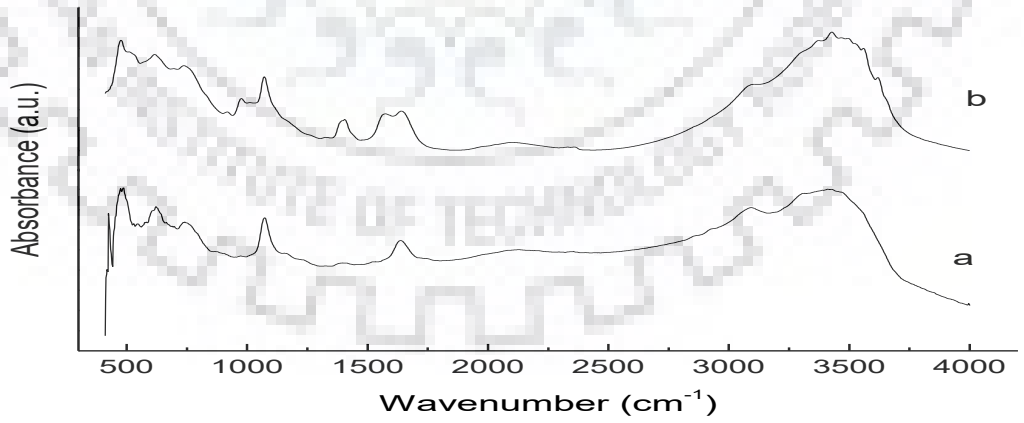

Figure 5.6 FTIR of virgin (a) and spent (b) AHNP adsorbent

The presence of aluminum oxides or hydroxides gets confirmed by studying these spectral patterns. The presence of Al-O-H stretching is indicated by absorbance band present near 3680 cm^{-1}. The absorption band within the range of 3370 to 3405 cm^{-1}

attributed to OH group of aluminum minerals. The absorption band near 1620 cm^{-1} is assigned to H-O-H bending of water molecule on the surface of AHNP. The absorbance band at wave number 912 cm^{-1} indicates Al-OH bond stretching.

XRD analysis of the virgin and spent AHNP adsorbent

Crystallographic study of the adsorbent was carried out with the help of XRD pattern, which is presented in Figure 5.7. From the Figure, it is revealed that AHNP is poorly crystalline or amorphous in nature. In this data, the peaks at 2θ = 18.46, 20.18, 20.50, 21.11, 22.78, 27.91, 37.52, 39.66, 44.98, and 55.26 are due to the presence of nordstrandite ($Al(OH)_3$), whereas the presence of aluminum oxyhydroxide (AlO(OH)) can be anticipated by the peak at 2θ = 13.69, 27.91, 38.43, 49.12, 55.26, and 64.79. Peaks at 2θ = 18.46, 20.50, 38.43, 40.51, 49.12, and 64.79 represent bayerite (Al_2O_3). Further, a sharp peak obtained at 2θ = 60.13 is due to corundum, which is an allotrope of Al_2O_3.

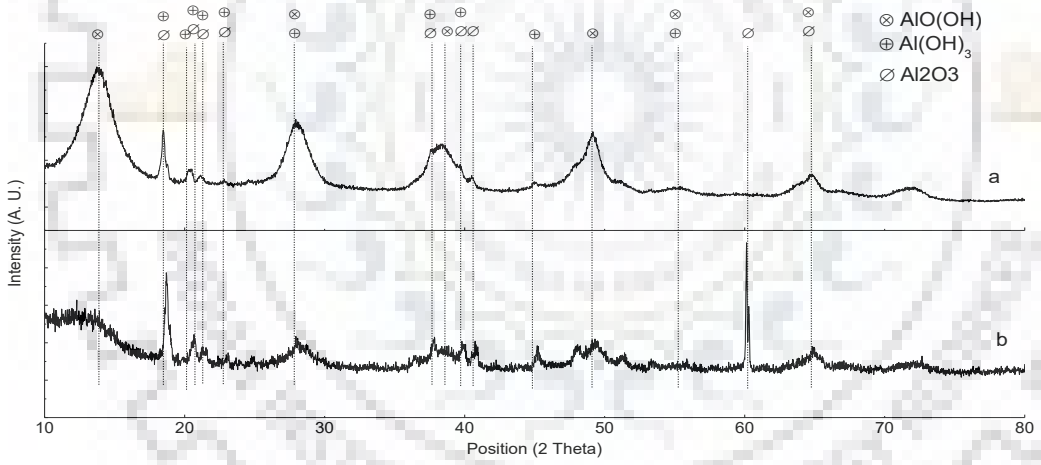

Figure 5.7 XRD of virgin (a) and spent (b) AHNP adsorbent

FESEM-EDX analysis of the virgin and spent AHNP adsorbent

Figure 5.8 (a) and 5.8 (b) shows the FESEM images of the virgin and spent adsorbents respectively, while Figure 5.9 (a) and 5.9 (b) shows the results of EDX analysis of virgin and spent adsorbent, respectively. As shown in Figure 5.8 (a), the nanoparticles of aluminum oxide/hydroxide appears in the form of large clusters and have rough and heterogeneous structures on the surface. This fact also supports the high

surface area and amorphous nature of the material. Further, as per the results of the FESEM analysis of virgin AHNP adsorbent, the size of nanoparticles is found to be between 14.6 and 19.4 nm. However, in the case of the spent adsorbents, these clusters of nanoparticles further agglomerates after the adsorption process and forms even larger clusters of the nanoparticles (Figure 5.8 (b)). This also supports the fact of reduction in the surface area and pore volume of the adsorbents after the removal of arsenic and fluoride. The EDX analysis shown in Figure 5.9 (a) and 5.9 (b) confirms the presence of only aluminum and oxygen in the materials, which indicates that the material is free from any other type of impurities for both the virgin and spent adsorbents. In the case of EDX analysis of spent adsorbents (Figure 5.9 (b)), some quantity of arsenic and fluoride are also observed over the surface of the adsorbent, which confirms the presence of the adsorbate on the surface of the adsorbent.

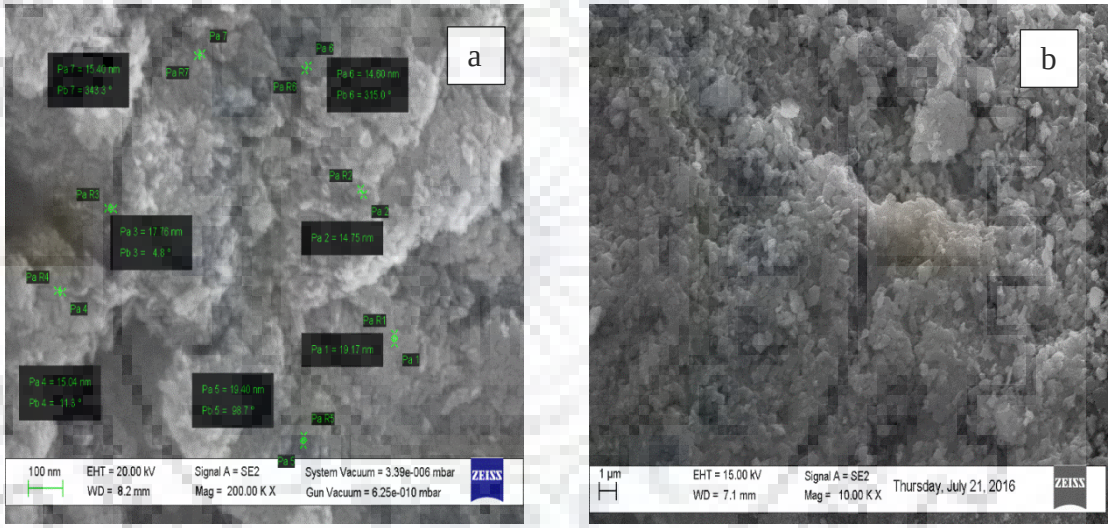

Figure 5.8 FESEM of virgin (a) and spent (b) AHNP adsorbent.

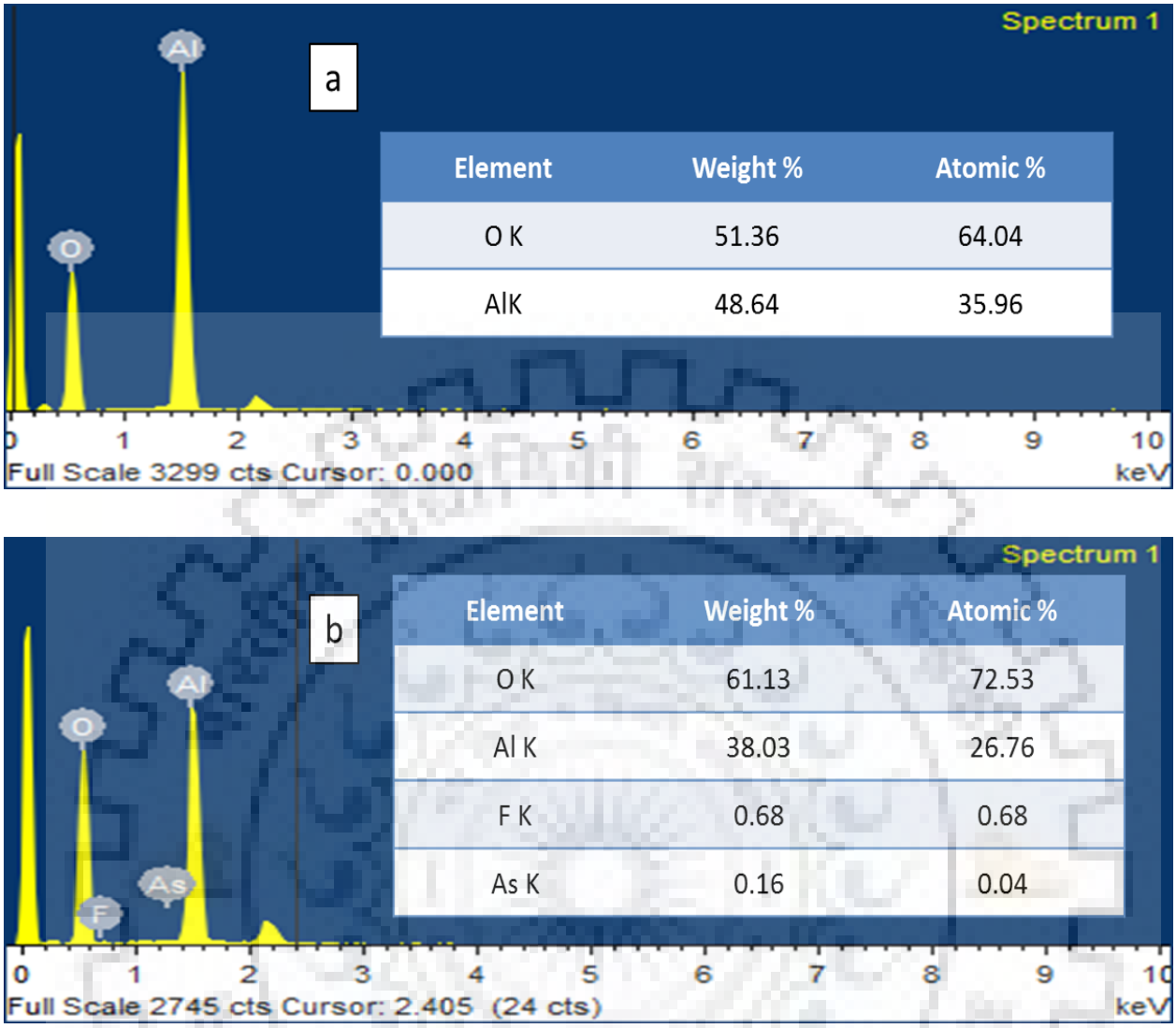

Figure 5.9 EDX of virgin (a) and spent (b) AHNP adsorbent.

Determination of point of zero charge (pH_{PZC}) of AHNP

The pH_{PZC} of any adsorbent is an essential factor in adsorption process. It is that value of pH of solution, in which, the adsorbent when kept, the net charge on the adsorbent surface is zero. If the pH of the solution in which the adsorbent is kept is more than 7, the net charge on the surface of the adsorbent is negative and is more suitable for the adsorption of the cations and vice versa. For the present case, ΔpH is negative up to initial pH value of 7.52 and positive when the initial pH value is higher than 7.52. At the pH value of 7.52 the ΔpH value is zero. Thus, the pH_{PZC} of the AHNP adsorbent is 7.52. It is because of the fact that the coagulant contains different form of aluminum hydroxides. It is well known that when a metal oxide/hydroxide (M-OH) comes in aqueous solution at lower pH (pH < pHzpc), it is converted to positively charged moiety

by capturing H^+ ion as per the Equation 5.1, consequently the H^+ ion concentration decreases in the solution resulting in increase in solution pH.

$$M - OH + H^+ \rightarrow M - OH_2^+ \quad (5.1)$$

Due to this reason ΔpH is negative. However, when the solution pH is higher (pH > pHzpc), the (M-OH) captures OH^- as per Equation 5.2 and forms negatively charged moiety, consequently the OH^- ion concentration in the solution decreases, resulting in decrease in solution pH.

$$M - OH + OH^- \rightarrow M - O^- + H_2O \quad (5.2)$$

Due to this reason ΔpH is positive. When initial pH of the solution is equal to pHzpc, both Equation 5.1 and Equation 5.2 perform in equal extent, as a result, no change in the solution pH is observed and zero ΔpH value is obtained (Figure 5.10). In the present case the pHzpc is observed as 7.52, which gives zero ΔpH value.

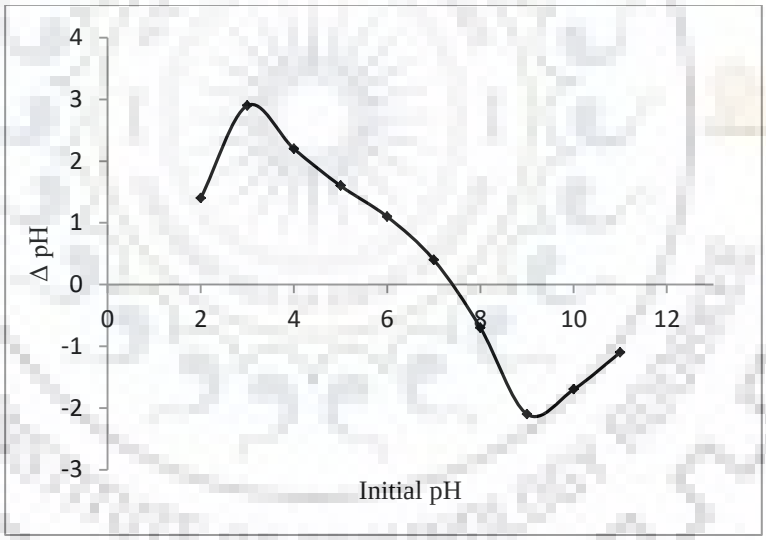

Figure 5.10 pH_{PZC} of the virgin AHNP

5.3 STUDIES ON THE ADSORPTIVE REMOVAL OF ARSENIC AND FLUORIDE FROM SYNTHETIC SOLUTION BY ABTL ADSORBENT

Based on the results of selection for best laterite soil based adsorbents presented in Section 5.1, ABTL was considered for all the further studies. Studies on the removal of arsenic and fluoride from synthetic solution in single component and bi-component system have been performed in batch as well as column reactor. Details of synthetic

solution are listed in Section 3.1. Studies have been conducted in batch reactor to find out the effects of process parameters such as initial pH, adsorbent dose, contact time and initial concentration of arsenic or fluoride on their removal. The removal of these contaminants has been studied in the column reactor to assess the applicability in the continuous process. Results are depicted in the form of percentage removal of the contaminants at given process conditions.

5.3.1 Batch Studies

The experiments for determination of the optimum conditions have been performed by following the method of sequential optimization of the parameters. In this process, one parameter is varied at a time to get its optimum value, while keeping all the other parameters constant. The effect of various parameters on the adsorption of arsenic and fluoride are as follows:

5.3.1.1 Effect of initial pH on the removal of arsenic and fluoride

Experiments have been conducted in batch reactor to study the effect of initial pH of the solution on the removal of arsenic and fluoride by ABTL adsorbent and to get the optimum value of pH. Effects of initial pH of the solution on the removal of arsenic and fluoride are presented through Figure 5.11.

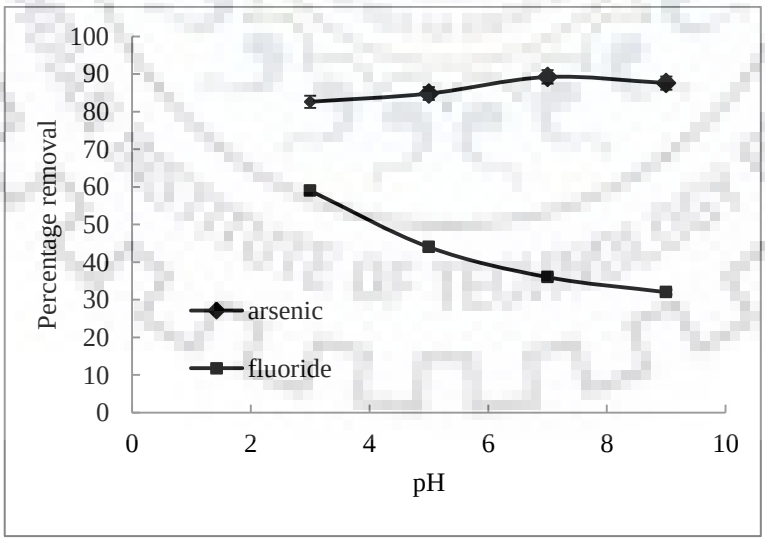

Figure 5.11 Effect of initial pH of the solution on percentage removal of arsenic and fluoride

From the Figure 5.11, the following points are evident:

i. The percentage removal of arsenic does not differ much within the pH range of 3 to 9. Although, the maximum removal percentage of arsenic of 89.2 % is obtained at the pH value around 7

ii. The percentage removal of fluoride is observed to be maximum at lower values of pH (pH = 3), however, a decreasing trend is observed in the percentage removal as the pH of the solution is increased.

The dependency on pH of both arsenic and fluoride to get adsorbed on the adsorbent surface can be explained with the help of speciation chemistry of these ions as well as with the help of surface charge of the adsorbent at different values of initial pH of solution. The speciation chemistry of arsenic and fluoride are given in the speciation diagram prepared with the help of Visual MINTEQ Ver.3.1 software (Figure 5.12 for arsenic and 5.13 for fluoride).

Observation given in point (i) can be explained as follows:

As shown in Figure 5.12, As (III) is predominately present in the form of H_3AsO_3 in the pH range 3 to 8, at pH 9 some of H_3AsO_3 converts to $H_2AsO_3^-$. The concentration of $H_2AsO_3^-$ species of arsenic reaches maximum at pH 12 and then starts to decrease with further increase in pH, which favors its conversion to $HAsO_3^{-2}$ till pH 14.

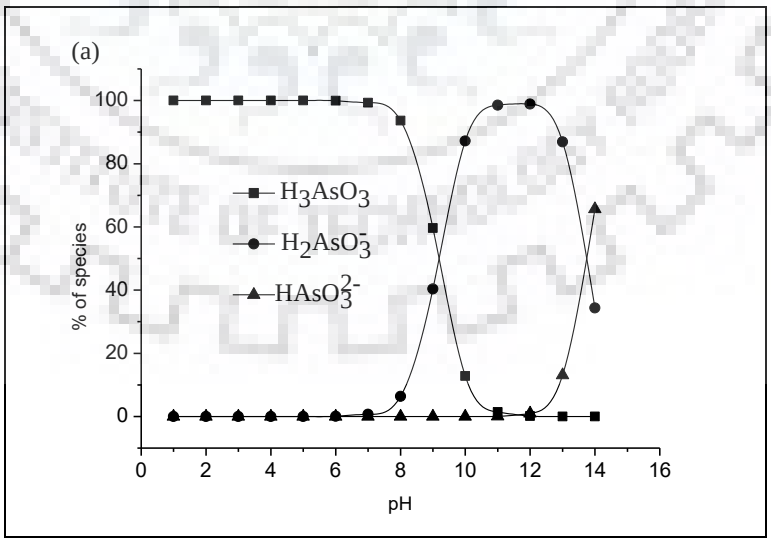

Figure 5.12 Speciation diagrams of arsenic in solution at various values of pH

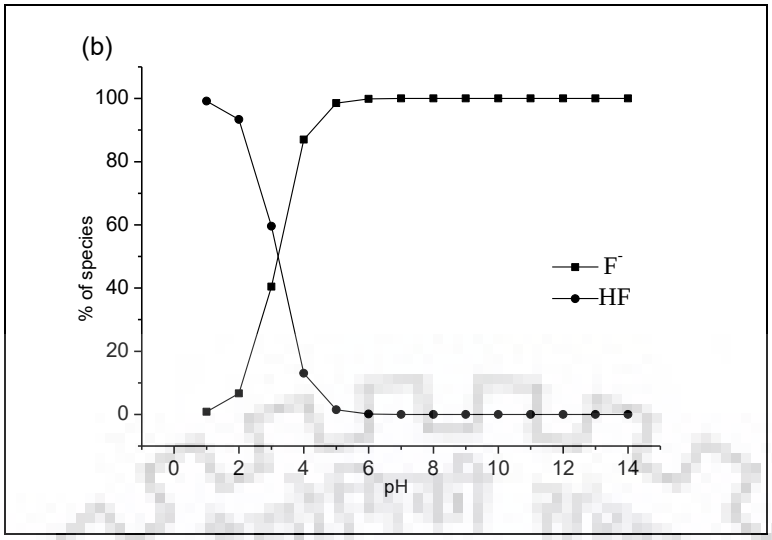

Figure 5.13 Speciation diagrams of fluoride in solution at various values of pH

Further, if we consider the molar concentration of different metal oxides in ABTL and their point of zero charge (pH_{PZC}), the behavior of these metal oxides seems to behave differently at different values of solution pH. In the present case, in 50 ml of arsenic or fluoride solution, 1 g of ABTL (having almost SiO_2 ~27.4 %, Fe_2O_3 ~47.9 %, Al_2O_3 ~20.7 %, Mn_2O_3 ~1 % etc.) by mass [Maiti et al. 2011] is taken. The presence of these compounds is also confirmed with the help of FTIR and XRD analysis. Thus, moles of SiO_2, Fe_2O_3, Al_2O_3, and Mn_2O_3 present in 1 g laterite soil are 0.0044, 0.0029, 0.0019 and 6.33×10^{-5} respectively. The values of pH_{PZC} of SiO_2, Fe_2O_3, Al_2O_3 and Mn_2O_3 are 2.2, 8, 8.3 and 4 respectively [Mondal et al. 2009, Srivastava et al. 2006]. On the basis of above data, Figure 5.14 can be developed to explain the changes on the surface of adsorbent with variation in solution pH. From this data it can be said that, the adsorbent surface is predominately positively charged at pH less than 2.2, whereas predominately negatively charged at pH more than 8.3. As the surface of the adsorbent is predominately positively charged at lower pH, it can adsorb the anions better in the acidic conditions rather than in basic condition. Further, by looking at the composition by mass of ABTL, we find that there is considerable amount of Fe_2O_3 and Al_2O_3 present in the ABTL which are helpful in adsorption of arsenic and fluoride.

Since, As (III) exists as neutral species up to pH = 9.2 and the overall pH_{PZC} of the reported material is approximately 7.5 [Maiti et al. 2010], the electrostatic interaction does not play much important role in arsenic removal, rather ligand exchange is

responsible for removal. The mechanism of removal by ligand exchange is as follows [Maiti et al. 2010]:

$$MOH_{(S)} + H_3AsO_{3(aq)} \rightarrow MH_2AsO_{3(aq)} \quad (5.3)$$

Observation given in point (ii) can be explained as follows:

Similarly, from the speciation diagram of fluoride (Figure 5.14), it is evident that fluoride is present in the form of HF predominately (nonionic form) at pH values between 1 to 3.5 and keeps on decreasing as the pH is increased, whereas, the concentration of F^- (ionic species) keeps on increasing as the pH is increased and it becomes predominant after pH 5.

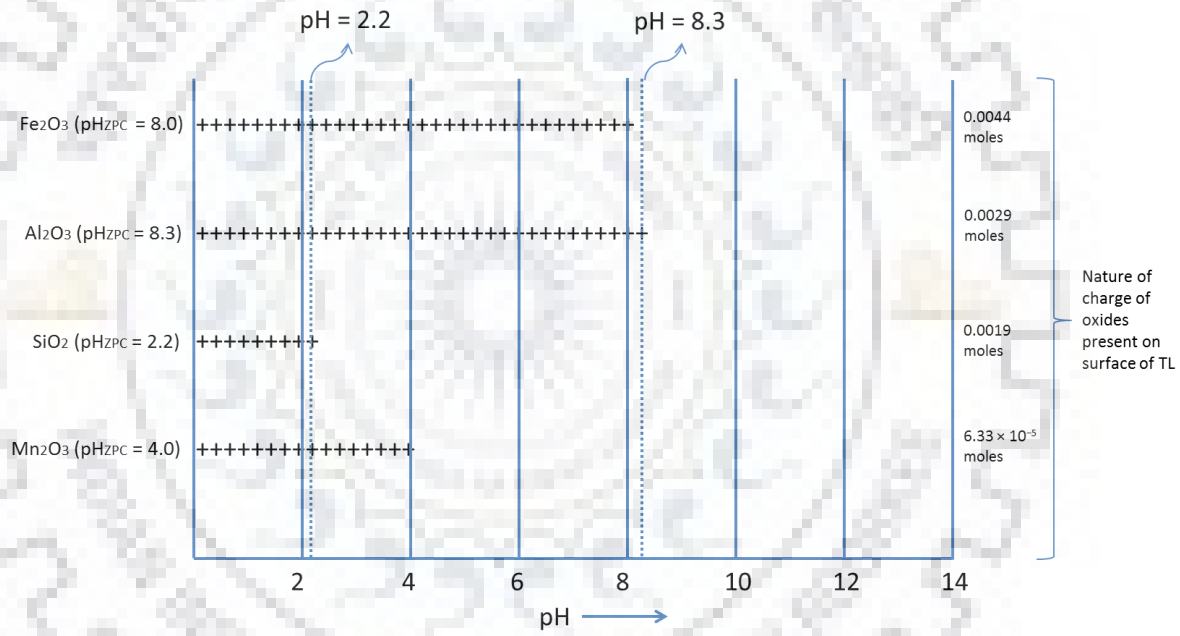

Figure 5.14 Contribution of various oxides of ABTL on the overall surface charge at various pH

The removal of fluoride decreases with increasing pH of solution. This may be due to the fact that, at low pH the surface of the adsorbent is positively charged and fluoride is also present in the form of F^- thereby facilitating the removal of fluoride anions by electrostatic attraction, whereas, the removal of fluoride gradually decreases with increasing pH of the solution. This may be due to two possible reasons:

i. Availability of less number of positively charged sites for the adsorption of negatively charged fluoride ions.

ii. Competition between hydroxyl OH^- ions with F^- ions for the positively charged sites present on the adsorbent surface.

The pH dependent interaction between fluoride and metal oxides can be represented schematically as follows:

$$= MOH + H^+ \rightarrow = MOH_2^+ \quad (5.4)$$

$$= MOH_2^+ + F^- \rightarrow = MOH_2 - F \quad (5.5)$$

$$= MOH_2^+ + F^- \rightarrow = MF + H_2O \quad (5.6)$$

$$2[= MOH] + 2F^- \rightarrow = MOF + H_2O \quad (5.7$$
$$|$$
$$= MF$$

Similar observations are also reported in various literatures, where, electrostatic attraction mechanism was considered responsible for the higher uptake of fluoride at lower pH [Maiti et al. 2010, Maiti et al. 2011, Tang et al. 2010].

5.3.1.2 Effect of adsorbent dose on the removal of arsenic and fluoride

Experiments have been conducted in batch reactor to study the effect of adsorbent dose on the removal of arsenic and fluoride from synthetic solution by ABTL adsorbent and to get the optimum value of adsorbent dose. The details of the experimental setup are provided in Section 3.4.1. In order to perform this study, the adsorbent dose was varied from 2 to 30 g/L. The detailed procedure is described in Section 4.9.1.2.2. Effect of adsorbent dose on the removal of arsenic and fluoride is presented in Figure 5.15.

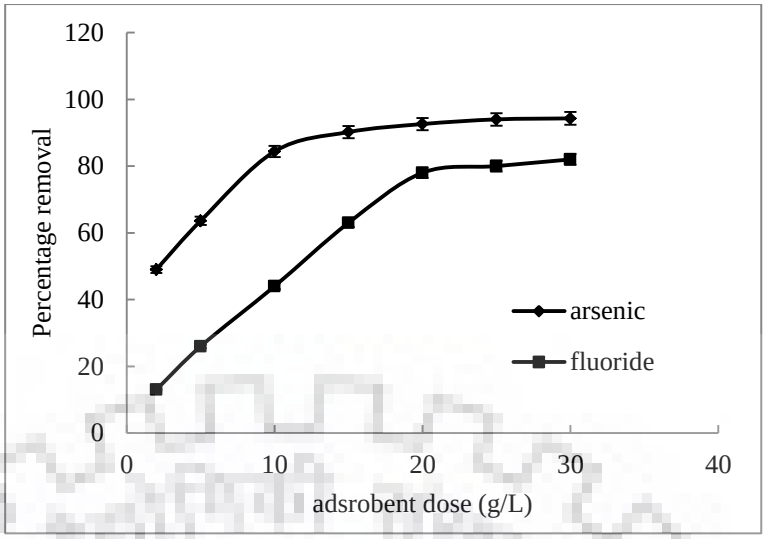

Figure 5.15 Effect of adsorption dose on percentage removal of arsenic and fluoride

From Figure 5.15, the following point is evident:

i. The removal percentage of both arsenic and fluoride initially increases with increasing dose of adsorbent (up to 20 g/L) and thereafter remains almost constant.

Observation given in point (i) can be explained as follows:

The increase in the percentage removal of both arsenic and fluoride with increase in adsorbent dose is due to increase in the availability of sorption sites on its surface. Higher adsorption of arsenic may also be attributed to the fact that the initial concentration of arsenic (500 µg/L) was very low (20 times) as compared to initial concentration of fluoride (10000 µg/L). As adsorbent dose is further increased up to 30 g/L, no significant change in removal percentage is observed as the equilibrium is achieved. Thus, all other experiments for the single matrixes were conducted using 20 g/L adsorbent dose, which yielded 92.6 % and 78 % removal for arsenic and fluoride respectively.

5.3.1.3 Effect of contact time on the removal of arsenic and fluoride

Experiments have been conducted in batch reactor to study the effect of contact time on the removal of arsenic and fluoride from synthetic solution by ABTL adsorbent. These studies were carried out to get the optimum value of contact time and to perform the kinetic studies. The details of the experimental setup are provided in Section 3.4.1. In

order to perform this study, the contact time of the adsorbent with arsenic and fluoride containing solution was varied from 15 min to 780 min. The detailed procedure is described in Section 4.9.1.2.3. Effects of contact time on the removal of arsenic and fluoride are presented through Figure 5.16.

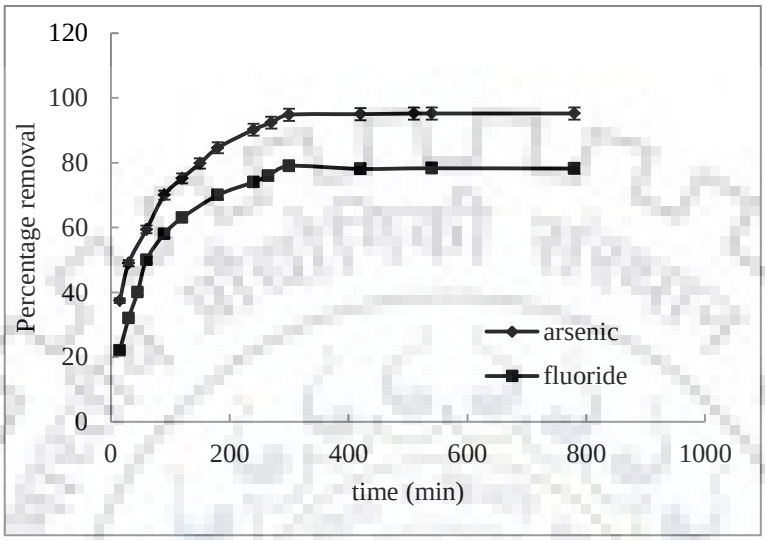

Figure 5.16 Effect of contact time on percentage removal of arsenic and fluoride

From Figure 5.16, the following point is evident:

i. The removal percentage of both arsenic and fluoride initially increases up to around 300 min, and after that it remains almost constant.

Observation given in point (i) can be explained as follows:

This is because of the fact that in the beginning, all the active sites remain free for adsorbing ions (arsenic and fluoride) and their availability decreases gradually as adsorption proceeds with time. Further, the concentration of arsenic and fluoride ions in the solution also decreases with adsorption in due course of time. Due to this fact driving force decreases gradually with time, whereas the agitation remains constant (i.e. 150 rpm) leading the system towards equilibrium where no further adsorptive removal is possible with respect to time. Therefore, 300 min agitation period is considered as an optimum agitation period.

5.3.1.4 Effect of initial concentration of arsenic and fluoride on their removal

Experiments have been conducted in batch reactor to study the effect of initial concentration of arsenic and fluoride on their removal from synthetic solution by ABTL adsorbent. These studies were carried out to get the optimum values of initial concentration of arsenic and fluoride and to perform the isotherm studies. The details of the experimental setup are provided in Section 3.4.1. In order to perform this study, the initial concentration of arsenic and fluoride ions were varied from 100 µg/L to 1000 µg/L for arsenic and 5000 µg/L to 15000 µg/L for fluoride. The detailed procedure is described in Section 4.9.1.2.4. Effects of initial concentration of arsenic and fluoride on their respective percentage removal and specific uptake are presented through Figure 5.17 and Figure 5.18.

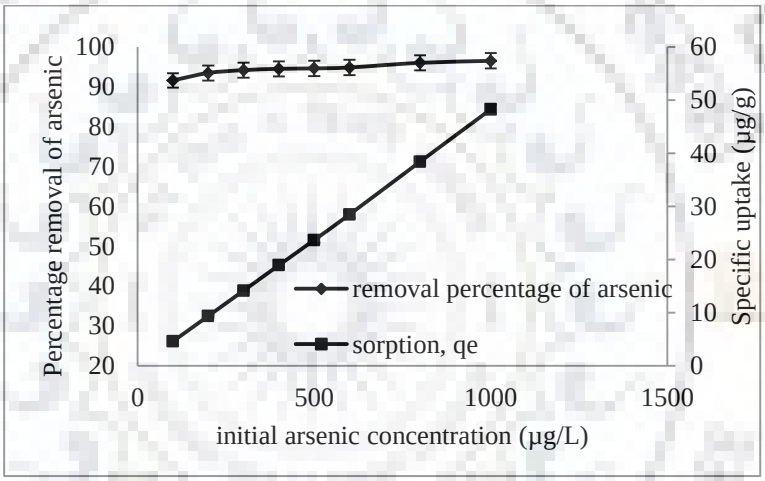

Figure 5.17 Effect of initial concentration of arsenic on percentage removal and specific uptake

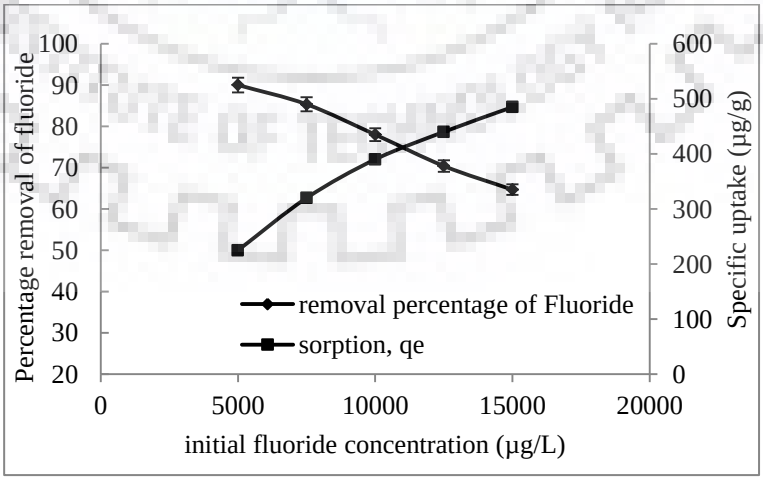

Figure 5.18 Effect of initial concentration of fluoride on percentage removal and specific uptake

From Figure 5.17 and Figure 5.18, the following points are noteworthy:

i. The specific uptake of arsenic increases from 4.58 µg/g to 48.25 µg/g by increasing initial arsenic concentration from 100 to 1000 µg/L, whereas, for fluoride, it increases from 225 µg/g to 485 µg/g due to the increase in initial fluoride concentration from 5000 to 15000 µg/L.
ii. The percentage removal of arsenic increases from 91.6% to 96.5% by increasing initial arsenic concentration from 100 to 1000 µg/L. Whereas, for fluoride, it decreases from 90% to 64.66% by increasing initial fluoride concentration from 5000 to 15000 µg/L.

Observation given in point (i) and (ii) can be explained as follows:

With increase in concentration of arsenic and fluoride in the solution, the driving force increases, which results into more adsorption of these ions, whereas, the adsorbent dose remains same and hence specific uptake increases with increase in initial concentration for both arsenic and fluoride. Further, with increase in driving force although adsorption of ions increases, the ratio of the ions adsorbed to ions present in solution may not increase in a similar fashion under all circumstances. Sometimes it may increase like arsenic and in some cases it may decrease like fluoride in the present case. The decrease in the ratio of fluoride adsorbed on adsorbent surface to the total fluoride present in the solution with increase in initial fluoride concentration is probably because of the lower fluoride adsorption capacity of ABTL and very high concentration of fluoride with respect to arsenic. Thus, unlike arsenic, the percentage removal of fluoride decreases with increase in initial concentration.

5.3.1.5 Kinetic studies for the removal of arsenic and fluoride

To determine the kinetic parameters for the adsorption of arsenic and fluoride on ABTL, the results of experiments reported in Section 5.3.1.3 have been processed further using various kinetic models as described in Section 2.3.5. Kinetic parameters for the adsorption of arsenic and fluoride on ABTL, computed by various kinetic models, are reported in Table 5.3. For getting the details of intra particle diffusion, q_t vs. $t^{1/2}$ plots have been developed, as shown in Figure 5.19 (a) and 5.19 (b) for fluoride and arsenic respectively.

Table 5.3 Kinetic parameters for adsorption of arsenic and fluoride on ABTL for single component system

Model	R^2	q_e (µg/g) (calculated)	q_e (µg/g) (experimental)	Kinetic parameters
Arsenic				
Pseudo first order	0.984	18.17	23.7	k_1 (sec^{-1}) = 0.0002
Pseudo second order	0.994	25.77	23.7	k_2 (gm/µg.min) = 0.001
Intra particle diffusion	0.977	-	-	K_{id} (µg/g.$sec^{0.5}$) = 0.139 C (µg/g) = 6.312
Fluoride				
Pseudo first order	0.994	331	395	k_1 (sec^{-1}) = 0.0002
Pseudo second order	0.999	454	395	k_2 (gm/µg.min) = 4.4 x 10^{-5}
Intra particle diffusion	0.939	-	-	K_{id} (µg/g.$sec^{0.5}$) = 2.915 C (µg/g) = 49.179

From the Table 5.3, following observations are noted:

i. All the three models namely, pseudo first order model, pseudo second model and intra particle model have R^2 values ranging from 0.977 to 0.994 for arsenic and 0.939 to 0.999 for fluoride, which indicate the extent of suitability of these models for describing the kinetics of the adsorption of arsenic and fluoride. However, the value of R^2 is observed highest for both arsenic and fluoride for pseudo second order model.

ii. The values of R^2 are almost similar for both pseudo first order as well as pseudo second order model. However, the difference between experimental and calculated values of q_e are less (8.7 % for arsenic and 14.9 % for fluoride) for pseudo second order kinetics as compared to pseudo first order kinetics (23.3 % for arsenic and 15.3 % for fluoride), which shows that the pseudo second order

kinetic model is more suitable than pseudo first order kinetic model to explain the adsorption process.

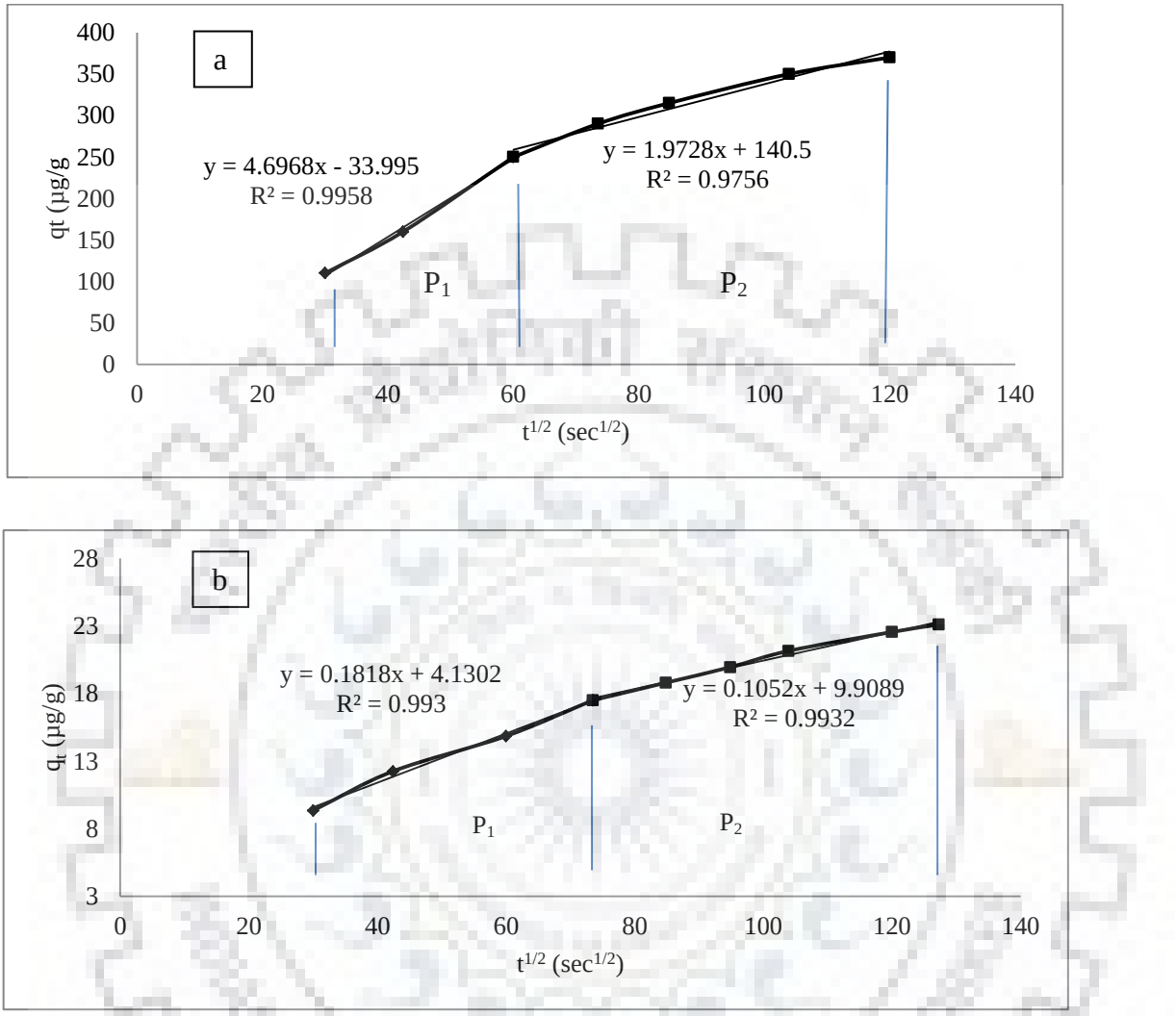

Figure 5.19 Intraparticle diffusion model for adsorption of fluoride (a) and arsenic (b) on ABTL

From Figures 5.19 (a) and 5.19 (b), following observations are noted:

i. Each plot can be considered to have two linear parts (P_1 and P_2), which indicates that the adsorption phenomena takes place in more than one step. This implies that the intra particle diffusion does not solely control the adsorption of arsenic and fluoride. The steepest part, P_1 is the initial stage of adsorption when most of the sites of adsorbent are available for adsorption. The region P_1 is attributed to boundary layer diffusion or external mass transfer effects. Whereas the second

part P_2 depict pore diffusion. From Figure 5.19 (a) and 5.19 (b), it is evident that arsenic and fluoride does not tend to adsorb in the pores of ABTL adsorbent.

ii. The values of pore diffusion coefficient (D_p) and film diffusion coefficient (D_f) so obtained are 3.94×10^{-8} cm^2/s and 1.36×10^{-8} cm^2/s for both arsenic and fluoride (as the value of first order rate constant, K_1 = 0.0002 s^{-1} is same for both the anions). For pore diffusion to be the rate limiting step, its value (D_p) should lie between 10^{-11} and 10^{-13} and if film diffusion to be the rate limiting step, its value (D_f) should lie between 10^{-6} and 10^{-8} for anions [Mondal et al. 2009]. As the value of D_f lies in the range mentioned for film diffusion, it can be said that the film diffusion is the rate limiting step for the adsorption of both the ions.

5.3.1.6 Isotherm studies for the removal of arsenic and fluoride

To determine the adsorption isotherm parameters for the adsorption of arsenic and fluoride on ABTL, the results of experiments reported in Section 5.3.1.4 have been processed further using various single component isotherm models as described in Section 2.3.5. Single component isotherm parameters for the adsorption of arsenic and fluoride on ABTL, computed by various single component isotherm models are reported in Table 5.4.

Table 5.4 Characteristic parameters of different isotherm models for the adsorption of arsenic and fluoride by ABTL for single component system

	Arsenic		**Fluoride**	
Model	**R^2**	**Isotherm constants**	**R^2**	**Isotherm constants**
Langmuir isotherm	0.996	R_L = 0.568 - 0.929 q_o (µg/g) = 769 b_L (μg^{-1}) = 0.000759	0.995	R_L = 0.04 – 0.12 q_o (µg/g) = 526 b_L (μg^{-1}) = 0.0014
Freundlich isotherm	0.986	K_F ($\mu g/g(L/\mu g)^{1/n}$) = 0.755 1/n = 0.912	0.980	K_F ($\mu g/g(L/\mu g)^{1/n}$) = 32.75 1/n = 0.317

From the Table 5.4, following observations are noted:

i. Both the Langmuir isotherm and Freundlich isotherm models have R^2 values of 0.996 and 0.986 for arsenic and 0.995 and 0.98 for fluoride respectively, which indicate the extent of suitability of these models for describing the equilibrium of the adsorption of arsenic and fluoride. However, the values of R^2 are observed highest for both arsenic and fluoride for Langmuir isotherm model.
ii. The value of Langmuir maximum adsorption capacity (q_0) of ABTL is found to be 769 µg/g and 526 µg/g for arsenic and fluoride respectively.
iii. The value of separation factor R_L associated with the Langmuir isotherm lies in the range of 0.568 to 0.929 for arsenic and 0.04 to 0.12 for fluoride. These values are in the range between 0 and 1, which indicates a favorable adsorption process.
iv. The value of 1/n should lie between 0 and 1 for favorable adsorption process. It is also noteworthy that, in this case the value of 1/n which indicates the favorability of adsorption is 0.912 for arsenic and 0.317 for fluoride respectively, which also supports the favorability of adsorption of both arsenic and fluoride on the ABTL presented in this work.

5.3.1.7 Simultaneous removal of arsenic and fluoride by ABTL in bi-component system

Experiments have been conducted in batch reactor to study the competitive effect between arsenic and fluoride in bi-component system by ABTL adsorbent. The details of the experimental setup are provided in Section 3.4.1. In order to perform this study, the concentration of one of the contaminant was increased gradually while keeping the concentration of the other contaminant constant. The detailed procedure is described in Section 4.9.1.3. Effect of presence of one contaminant on the adsorptive removal of other has been presented in the form of specific uptake of contaminants in the bi-component system in Table 5.5.

Table 5.5 Comparison of binary equilibrium sorption found at different fluoride concentration in the absence and presence of increasing concentrations of arsenic onto ABTL

$C_{o,\ fluoride}$ (µg/L)	$C_{o,\ arsenic}$ (µg/L)	$C_{e,\ fluoride}$ (µg/L)	$C_{e,\ arsenic}$ (µg/L)	$q_{e,\ fluoride}$ (µg/g)	$q_{e,\ arsenic}$ (µg/g)
5000	0	500	0	225	0
7500	0	1100	0	320	0
10000	0	2200	0	390	0
0	100	0	8	0	4.6
5000	100	507	8.7	224	4.56
7500	100	1300	9.8	310	4.51
10000	100	2500	10	375	4.5
0	300	0	23	0	13.85
5000	300	510	16.5	224	14.17
7500	300	1400	16.5	305	14.17
10000	300	2800	22	360	13.9
0	500	0	38	0	23.1
5000	500	530	28	223	23.6
7500	500	1600	28.5	295	23.575
10000	500	3100	30	345	23.5

From the Table 5.5, following observations are noted:

i. The specific uptake of fluoride decreases from 390 µg/g when no arsenic is present to 345 µg/g when arsenic concentration is 500 µg/L keeping initial fluoride concentration same (10000 µg/L).

ii. The specific uptake of arsenic increases from 23.1 µg/g to 23.5 µg/g due to the increase in fluoride concentration from 0 to 10000 µg/L with initial arsenic concentration of 500 µg/L.

The observations given in point (i) and (ii) can be explained on the basis of synergistic and antagonistic effects of ions in binary system as described in Section 4.9.1.3. It seems that arsenic removal is influenced by slight synergistic effect whereas fluoride removal is influenced by antagonistic effect.

To determine the bi-component adsorption isotherm parameters for simultaneous adsorption of arsenic and fluoride on ABTL, the results of experiments reported in this section have been processed further using various bi-component isotherm models as described in Section 2.3.5. Bi-component isotherm parameters for the adsorption of arsenic and fluoride on ABTL, computed by various models, are reported in Table 5.6.

Table 5.6 Binary adsorption isotherm parameter values for the simultaneous removal of arsenic and fluoride by ABTL

		Adsorbate	
Bi-component isotherm model		**Arsenic - Fluoride**	**Fluoride - Arsenic**
Non modified competitive Langmuir model	MPSD	311.31	46.76
Modified competitive Langmuir model	η_i	0.67	13.97
	η_j	2.98	-4535.89
	MPSD	109.38	62.9
Extended Langmuir model	b_i	0.14	17.51
	b_j	0.05	2.87
	q_{max}	5.98	0.413
	MPSD	92.26	0.36
Extended Freundlich model	x	1.43	-0.54
	y	0.0012	17.88
	z	0.47	1.44
	MPSD	13.56	1.08

From the Table 5.6, following points are noteworthy:

i. The binary non modified competitive Langmuir model shows poor fit to experimental data (with MPSD value of 311.31 for arsenic and 46.76 for fluoride) as it depicts the competitive effects in the adsorption process in binary system.

ii. In modified competitive Langmuir model the MPSD values change (MPSD value of 109.38 for arsenic and of 62.9 for fluoride) due to the introduction of interaction factor η.

iii. For extended Langmuir model, the MPSD values for arsenic and fluoride are 92.26 and 0.36 respectively. It is attributed to the fact that this model considers the non-interacting effects between the species present in binary system. This also supports the synergistic behavior of arsenic shown in the system.

iv. Extended Freundlich model shows very low values of MPSD for both arsenic and fluoride (MPSD value of 13.56 for arsenic and 1.08 for fluoride). Therefore, the binary adsorption of arsenic and fluoride ions onto ABTL can be represented satisfactorily and adequately by the extended Freundlich model.

5.3.1.8 Removal of arsenic and fluoride from real groundwater by ABTL in batch reactor

Experiments have been conducted in batch reactor to study the removal of arsenic and fluoride from real groundwater collected from Rajnandgaon District, Chhattisgarh, India by using ABTL adsorbent. The physico-chemical characteristics of the real groundwater have been discussed in Section 4.3. The details of the experimental setup are provided in Section 3.4.1. In order to perform this study, the values of different parameters kept have been described in Section 3.3 and the detailed procedure is described in Section 4.9.2. The results have been reported in the form of percentage removal in Table 5.7.

Table 5.7 Removal of arsenic and fluoride from real groundwater by ABTL

Contaminant	Initial concentration	Final concentration	Percentage removal
Arsenic (µg/L)	512	5	99.02
Fluoride (µg/L)	6300	1000	84.13

From the Table 5.7, following observations are noted:

i. The removal of both arsenic and fluoride present in the real groundwater sample was carried out satisfactorily at the optimum conditions evaluated through the studies mentioned in Section 5.3.1.1 to Section 5.3.1.3. The results reveal that the concentration of both the contaminants has decreased and is brought down to below the permissible limit as per Indian Standard (IS 10500).

5.3.2 Column Reactor Studies

Studies have been conducted to evaluate the performance of the ABTL adsorbent for the simultaneous removal of arsenic and fluoride from synthetic solution in column reactor. Schematic diagram of the column reactor is shown in Figure 3.2. Detailed procedure is described in Section 4.9.3. The output data is reported in the form of time vs. ratio of initial concentration and final concentration.

5.3.2.1 Effect of flow rate of influent on simultaneous removal of arsenic and fluoride

In order to perform this study, the flow rate of the influent was varied from 17 ml/hr to 50 ml/hr. Other conditions like concentration of the ions, mass of the adsorbent and bed height are provided in the Table 3.5. The effect of flow rate of influent on the removal of arsenic and fluoride are presented in the form of breakthrough curve in Figure 5.20.

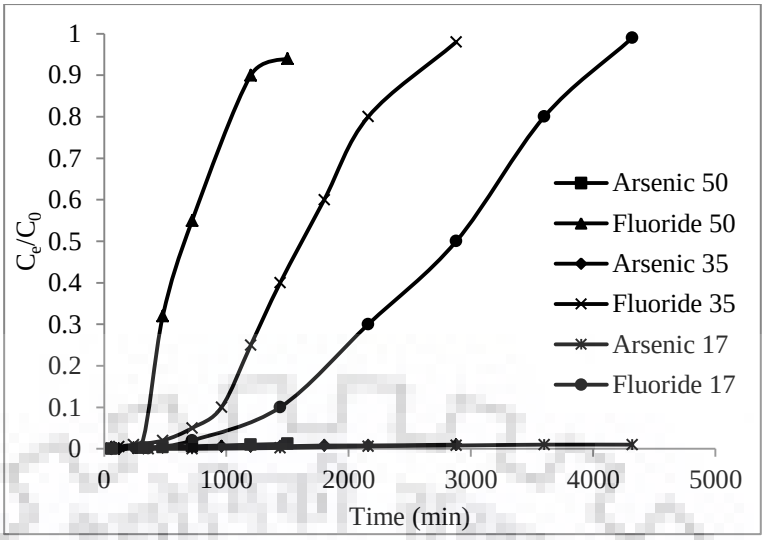

Figure 5.20 Breakthrough curves for the removal of arsenic and fluoride by ABTL at various flow rates

From Figure 5.20, following points are evident:

i. The increase in flow rate tended to speed up the exhaustion of the column.
ii. Time required for the column to reach the output concentration of fluoride at the permissible limit as per the Indian Standard (IS 10500) were approximately 360 min (at 50 ml/hr flow rate), 1100 min (at 35 ml/hr flow rate) and 1800 min (at 17 ml/hr flow rate).
iii. The column exhausted for fluoride in approximately 1500 min, 2880 min and 4320 min when the flow rate is 50 ml/hr, 35 ml/hr and 17 ml/hr respectively, however, the concentration of arsenic in the effluent was observed still to be below the permissible limit as per the Indian Standard (IS 10500).

Observations given in the above points can be explained as follows:

With increase in flowrate, more amount of water is passed through the adsorbent bed during a certain time period, thus more pollutants come in contact with the adsorbents, which results more adsorption and consequently the faster exhaustion of the bed. The amount of water treated during this time to achieve fluoride concentration in treated water as 1.5 mg/L is approximately 300 ml, 642 ml and 510 ml when the flow rate is 50 mL/hr, 35 mL/hr and 17 mL/hr respectively. However, the residence time of the influent decreases from 24.93 min to 8.51 min as the value of flow rate is increased

from 17 ml/hr to 50 ml/hr. Thus, with fixed rate constant value of different pollutants, the time required for exhaustion of column is different.

Moreover, the performance of column is found to be satisfactory for the removal of arsenic at all the above mentioned flow rates. This may be due to the fact that, the concentration of arsenic in the solution is very low (20 times less) as compared to that of fluoride and the adsorption capacity of ABTL is higher for arsenic than fluoride (769 µg/g for arsenic as compared to 526 µg/g for fluoride). Thus the concentration of arsenic remains below the permissible limit as per the Indian Standard (IS 10500) even after the column gets exhausted for fluoride.

5.3.2.2 Column adsorption kinetic studies for the removal of arsenic and fluoride

To determine the effect of flow rate on breakthrough curves, the results of experiments reported in this section have been processed further using various kinetic models as described in Section 2.3.5. The kinetic parameters for the adsorption of arsenic and fluoride on ABTL, computed by various models, are reported in Table 5.8 and 5.9 respectively:

Table 5.8 Value of model parameters for the adsorption of arsenic on ABLT

Thomas model			
Q (ml/min)	k_{Th} (ml/min.µg)	q_m (µg/g)	R^2
0.83	0.0048	51.65505	0.74
0.58	0.0026	60.37368615	0.76
0.28	0.0016	52.6089925	0.86
Yoon-Nelson model			
Q (ml/min)	k_{YN} (min^{-1})	τ (min)	R^2
0.83	0.0024	3111.75	0.74
0.58	0.0013	5177.846	0.76
0.28	0.0008	9294.875	0.86
Adam-Bohart model			
Q (ml/min)	k_{AB} (L/µg.min)	N_0 (µg/L)	R^2
0.83	0.0000048	183514.19	0.74
0.58	0.0000026	213803.15	0.76
0.28	0.0000016	186362.35	0.86

Table 5.9 Value of model parameters for the adsorption of fluoride on ABLT

Thomas model			
Q (ml/min)	k_{Th} (ml/min.µg)	q_m (µg/g)	R^2
0.83	0.00062	293.1	0.85
0.58	0.00035	384.01	0.97
0.28	0.00024	307.89	0.94
Yoon Nelson model			
Q (ml/min)	k_{YN} (min^{-1})	τ (min)	R^2
0.83	0.0062	882.84	0.86
0.58	0.0035	1646.68	0.97
0.28	0.0024	2719.83	0.94
Adam Bohart model			
Q (ml/min)	k_{AB} (L/µg.min)	N_0 (µg/L)	R^2
0.83	0.00000040	1470600	0.69
0.58	0.00000023	1858539	0.83
0.28	0.00000015	1472183	0.8

From the Table 5.8 and Table 5.9, following observations are noted:

i. In the case of Thomas model, the value of coefficient of determination (R^2) ranged between 0.74 and 0.86 for arsenic and 0.85 to 0.97 for fluoride, indicating good fits of the experimental data. As the flow rate of the influent is decreased from 0.83 ml/min (50 ml/hr) to 0.28 ml/min (17 ml/hr), the value of q_m increased form 51.65 µg/g to 52.60 µg/g but the value of k_{Th} decreased from 0.0048 ml/min.µg to 0.0016 ml/min.µg for arsenic. Similarly, for fluoride, the value of q_m increased form 293.1 µg/g to 307.89 µg/g but the value of k_{Th} decreased from 0.00062 ml/min.µg to 0.00024 ml/min.µg. It is also noteworthy that the value of maximum adsorption capacity for both the ions is obtained lower in column

adsorption as compared to batch adsorption. This may be attributed to the following facts:

(a) The ions were not getting sufficient time to get adsorbed on the surface of the adsorbent due to high flow rate of the solution.

(b) While calculating the Langmuir maximum adsorption capacity through the batch adsorption experiments, presence of only single ion is considered in the system, whereas in the present case both the ions were present simultaneously in the system.

ii. In case of Yoon-Nelson model, the value of coefficient of determination R^2 ranged between 0.74 to 0.86 for arsenic and 0.86 to 0.97 for fluoride, indicating good fits of the experimental data. The value of τ (which is the time taken (in min) to reduce the concentration of the contaminant to half of the initial concentration) increases from 3111.75 min to 9294.87 min for arsenic and 882.84 min to 2719.83 min for fluoride, whereas, the value of k_{YN} reduces from 0.0024 min^{-1} to 0.0008 min^{-1} for arsenic and from 0.0062 min^{-1} to 0.0024 min^{-1} for fluoride as the flow rate of the influent is reduced from 0.83 ml/min (50 ml/hr) to 0.28 ml/min (17 ml/hr). This indicates that at higher flow rate the column is getting exhausted at faster rate.

iii. In the case of Adam–Bohart model, the value of coefficient of determination (R^2) ranged between 0.74 and 0.86 for arsenic and 0.69 to 0.83 for fluoride, indicating not so good fit of the experimental data as compared to previous models. The value of Adam-Bohart rate constant (k_{AB}) decreases from 0.0000048 (L/µg.min) to 0.0000016 (L/µg.min) for arsenic and from 0.00000040 (L/µg.min) to 0.00000015 (L/µg.min) for fluoride as the flow rate of the influent is reduced from 0.83 ml/min (50 ml/hr) to 0.28 ml/min (17 ml/hr). At lower flow rate, less amount of water is treated per unit time per reactor length and hence the column requires more time to get exhausted consequently the service time of the column is increased. However, the values of N_0 (maximum saturation concentration, in µg/L) varied from 183514.19 µg/L to 213803.15 µg/L for arsenic and 1470600 µg/L to 1858539 µg/L for fluoride. The maximum value of N_0 is observed when the flow rate of the influent is 0.58 ml/min (35 ml/hr) which indicates its optimum value for the column operation.

5.3.3 Comparison of the Adsorbents with Other Similar Reported Materials

A comparison is given in Tables 5.10 for the removal of arsenic and fluoride with the help of various mineral based adsorbents like laterite soil.

Table 5.10 List of few mineral based adsorbents used for adsorptive removal of arsenic and fluoride in single component system.

Arsenic					
Adsorbent	**Arsenic species taken**	**C_o, arsenic (µg/L)**	**Optimum pH**	**q_{max} (µg/g)**	**Reference**
Calcinated bauxite	As(III)	1000	2 - 5	1362	Ayoob et al. 2007
Iron oxide coated sand	As(III)	100	7.5	28.57	Gupta et al. 2005
Ferruginous manganese ore	As(III)	100	2 - 8	680	Chakravarty et al. 2002
Fe modified beidellite (0.4 - 0.6 mm particle size)	As(III)	800	8	834	Bektas et al. 2011
	As(V)	800	2 - 8	841	
Fe modified sepiolite (0.4 - 0.6 mm particle size)	As(III)	800	8	512	
	As(V)	800	2 - 8	558	
Fe and Ce modified zeolite (0.4 - 0.6 mm particle size)	As(III)	800	8	540	
	As(V)	800	2 - 8	553	
Raw laterite	As(III)	1000	3 - 11	127.8	Glocheux et al. 2013
	As(V)	1000	3	301.2	
Sulphuric acid acidified laterite (ALS)	As(III)	1000	8.5	171.1	
	As(V)	1000	2 - 6	923.6	
Acid-base treated laterite	As(III)	100	5	769	**present study**

Fluoride				
Adsorbent	**$C_{o,\ fluoride}$ (µg/L)**	**Optimum pH**	**q_{max} (µg/g)**	**Reference**
Acid treated spent bleaching earth	20000	3.5	784	Mahramanlioglu et al. 2002
Red mud	83910	5.5	870	Çengeloglu et al. 2002
Activated titanium rich bauxite	10000	6	3800	Das et al. 2005
Raw laterite soil (0.5 mm size)	10000	2	201.4	Sarkar et al. 2006
Raw Kaolinite	3000	3	120	Meenakshi et al. et al. 2008
Mechanochemically activated kaolinites	3000	3	134	Meenakshi et al. et al. 2008
Waste mud	80000	2 - 8	1500	Kemer et al. 2009
20 % HCl treated waste mud	80000	2 - 8	1000	Kemer et al. 2009
Granular red mud	15000	4.7	2201	Tor et al. 2009
Lanthanum modified bentonite clay	5000	5	4240	Kamble et al. 2009
Granular acid-treated bentonite	5000	4.95	94	Ma et al. 2011
Acid-Base treated laterite	10000	5	526	**present study**

It is evident from the above mentioned Table 5.10, that the adsorbing capacity of the present material (ABTL) is competitive to some of the recently reported adsorbents.

5.4 STUDIES ON THE ADSORPTIVE REMOVAL OF ARSENIC AND FLUORIDE FROM SYNTHETIC SOLUTION BY AHNP ADSORBENT IN BATCH REACTOR

Experiments have been conducted on the removal of arsenic and fluoride from synthetic solution as well as from real groundwater by the help of AHNP adsorbent also similarly to ABTL adsorbent. The details of the batch reactor setup are provided in Section 3.4.1 and the experimental planning is also presented in Section 3.3.

5.4.1 Batch Studies

The experiments for determination of the optimum conditions have been performed by following the method of sequential optimization of the parameters in a similar way to ABTL. The effect of various parameters on the adsorption of arsenic and fluoride are as follows:

5.4.1.1 Effect of initial pH on the removal of arsenic and fluoride

Experiments have been conducted in batch reactor to study the effect of initial pH on the removal of arsenic and fluoride from synthetic solution by AHNP adsorbent and to get the optimum value of pH. In order to perform this study, the initial pH of the solution was varied from 4 to 9 in order to assess both acidic and basic scenario. The detailed procedure is described in Section 4.9.4.1.1. Effects of initial pH of the solution on the removal of arsenic and fluoride are presented through Figure 5.21.

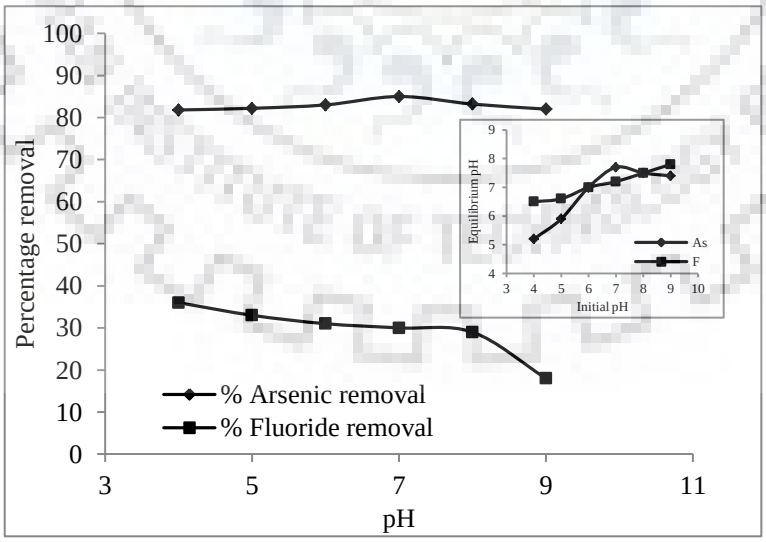

Figure 5.21 Effect of initial pH of the solution on percentage removal of arsenic and fluoride by using AHNP

From Figure 5.21, the following points are evident:

i. The percentage removal of arsenic increases slightly from 81.8 % to 85 % as the pH of the solution is increased from 4 to 7 and attains a maximum % removal of arsenic as 85 % at the pH value around 7 and again declines slightly to 82 % as the pH of the solution is further increased to 9.
ii. The % removal of fluoride is observed to be maximum (36 %) at lower values of pH (pH = 4), however, a decreasing trend is observed in the percentage removal as the pH of the solution is increased.

The dependency on pH of both arsenic and fluoride to get adsorbed on the adsorbent surface can be explained with the help of speciation chemistry of these ions as well as with the help of surface charge of the adsorbent at different values of initial pH of solution. The speciation chemistry of arsenic and fluoride are given in the speciation diagram prepared with the help of Visual MINTEQ Ver.3.1 software (Figure 5.13 and Figure 5.14 for arsenic and fluoride, respectively).

Observation given in point (i) can be explained as follows:

The increase in the percentage removal of arsenic as the initial pH of the solution is increased from 4 to 7 is due to the fact that during the adsorption process the equilibrium pH becomes slightly higher than the initial pH when its value is less than 8 due to the addition of AHNP adsorbent. However, at the initial pH value above ~8, the equilibrium pH is slightly reduced. This change in pH can be attributed to the amphoteric nature of aluminum hydroxide. At the initial pH value of 7 the changes in solution pH during adsorption is very less. Further, since the overall pH_{ZPC} of the reported material is approximately 7.52, its surface is predominantly negatively charged when solution pH is > 7.52. As the As (III) exists as neutral species up to solution pH ~9 and the overall pH_{ZPC} of AHNP is approximately 7.52, the electrostatic interaction may not play a much important role in arsenic removal; rather the ligand exchange seems to be responsible for the uptake.

The probable mechanism for the adsorption of arsenic can be presented through following equation.

$$\equiv \mathrm{M-OH} + \mathrm{H_3AsO_3} \leftrightarrow \equiv \mathrm{MH_2AsO_3} + \mathrm{H_2O} \quad (5.8)$$

Observation given in point (ii) can be explained as follows:

The adsorption of fluoride on the surface of AHNP can also be explained in the similar way as that for ABTL. In case of AHNP also the maximum adsorption of fluoride is observed at lower values of pH (pH = 4) and the percentage adsorption reduces as the pH of the solution is increased up to 9. This can also be explained as fluoride ions remain mostly in the form of HF (non-ionic form) from pH 1 to 3.5 and their percentage reduces gradually as the pH of the solution is increased. As the pH of the solution approaches to nearly 4, the percentage of species of F^- ions starts to predominate in the solution. Further, the pH_{PZC} of the adsorbent is found to be as 7.52. It facilitates the adsorption of fluoride ions at lower values of pH due to electrostatic attraction. However, as the pH of the solution is increased, the percentage adsorption of fluoride decreases. This may be due to the following two reasons:

i. Availability of less number of positively charged sites for the adsorption of negatively charged fluoride ions.
ii. Competition between hydroxyl OH^- ions with F^- ions for the positively charged sites present on the adsorbent surface.

The pH dependent interaction between fluoride and metal oxides can be represented schematically as follows:

$$= MOH + H^+ \rightarrow = MOH_2^+ \quad (5.9)$$

$$= MOH_2^+ + F^- \rightarrow = MOH_2 - F \quad (5.10)$$

$$= MOH_2^+ + F^- \rightarrow = MF + H_2O \quad (5.11)$$

$$2[= MOH] + 2F^- \rightarrow \begin{array}{c} = MOF \\ | \\ = MF \end{array} + H_2O \quad (5.12)$$

Similar observations are also reported in various literatures, where, electrostatic attraction mechanism was considered responsible for the higher uptake of fluoride at lower pH.

The increase in the percentage removal of arsenic as the initial pH of the solution is increased from 4 to 7 can be explained with the similar as explained in the case of ABTL. Similarly, decrease in the percentage removal of fluoride by AHNP can also be explained with the help of similar mechanism as proposed for ABTL.

5.4.1.2 Effect of adsorbent dose on the removal of arsenic and fluoride

Experiments have been conducted in batch reactor to study the effect of adsorbent dose on the removal of arsenic and fluoride from synthetic solution by AHNP adsorbent and to get the optimum value of adsorbent dose. The details of the experimental setup are provided in Section 3.4.1. In order to perform this study, the adsorbent dose was varied from 0.5 to 3.5 g/L for arsenic and 0.5 to 9 g/L for fluoride. The detailed procedure is described in Section 4.9.4.1.2. Effect of adsorbent dose on the removal of arsenic and fluoride is presented through Figure 5.22.

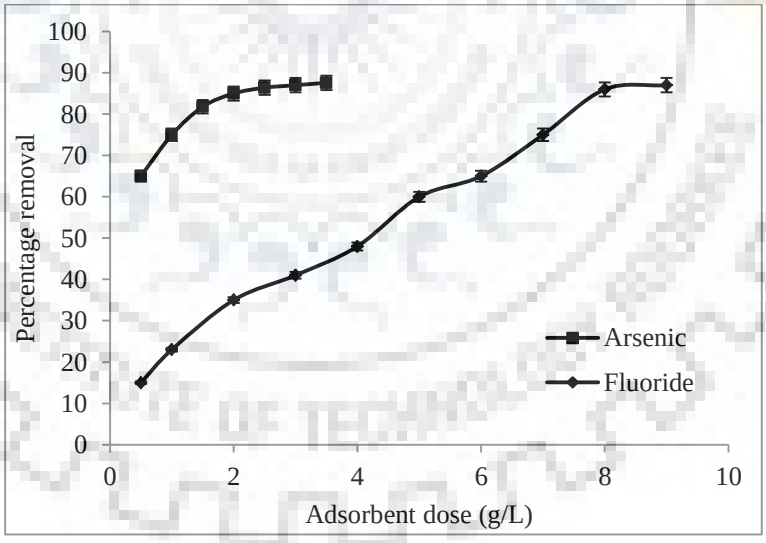

Figure 5.22 Effect of adsorbent dose on percentage removal of arsenic and fluoride

From Figure 5.22, the following points are evident:

i. The percentage removal of arsenic increases from 65 % to 85 % gradually as the adsorbent dose is increased from 0.5 g/L to 2 g/L. However, as the adsorbent dose is increased further till 3.5 g/L, no significant change in the value of

percentage removal of arsenic is observed and it remains almost constant (~87.6 %).

ii. The percentage removal of fluoride increases from 15 % to 86 % gradually as the adsorbent dose is increased from 0.5 g/L to 8 g/L. However, as the adsorbent dose is increased further till 9 g/L, no significant change in the value of percentage removal of fluoride is observed and it remains almost constant (~87 %).

Observations given in points (i) and (ii) can be explained as follows:

The increase in the percentage removal of both arsenic and fluoride with increase in adsorbent dose can be explained similarly to ABTL adsorbent. In this case also, it is due to increase in the availability of sorption sites on the surface of AHNP in the form of hydroxides. Higher adsorption of arsenic can also be attributed to the fact that the initial concentration of arsenic (500 µg/L) was very low (20 times) as compared to initial concentration of fluoride (10000 µg/L). As the adsorbent dose is further increased up to 3 g/L for arsenic and 8 g/L for fluoride, no significant change in removal percentage is observed as the equilibrium is achieved. Thus, all remaining experiments for the single matrix were conducted using 2 g/L adsorbent dose for arsenic and 8 g/L for fluoride, which yielded 85 % and 86 % removal for arsenic and fluoride respectively.

5.4.1.3 Effect of contact time on the removal of arsenic and fluoride

Experiments have been conducted in batch reactor to study the effect of contact time on the removal of arsenic and fluoride from synthetic solution by AHNP adsorbent and optimize its value to perform the kinetic studies. The details of the experimental setup are provided in Section 3.4.1. In order to perform this study, the contact time of the adsorbent with the arsenic and fluoride ions was varied from 15 min to 300 min. The detailed procedure is described in Section 4.9.4.1.3. Effects of contact time on the removal of arsenic and fluoride are presented through Figure 5.23.

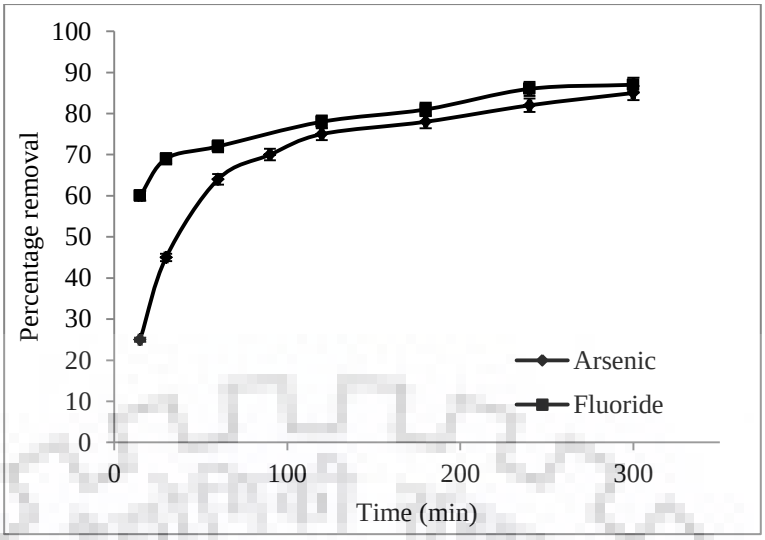

Figure 5.23 Effect of contact time on percentage removal of arsenic and fluoride

From Figure 5.23, the following points are evident:

i. The removal percentage of arsenic increases form 25 % to 85 % as the contact time is increased form 15 min to 300 min. At 240 min, the percentage removal is 82 % and at 300 min it increases very slightly to 85 %. Hence, 300 min is taken as optimum contact time for arsenic as no significant change in the percentage removal is observed beyond it.

ii. The removal percentage of fluoride increases form 60 % to 87 % as the contact time is increased form 15 min to 300 min. At 240 min, the percentage removal is 86 % and at 300 min it increases very slightly to 87 %. Hence, 300 min is taken as optimum contact time for fluoride also as no significant change in the percentage removal is observed beyond it.

Observations given in points (i) and (ii) can be explained as follows:

These can also be explained similarly to ABTL adsorbent as at the beginning of the experiment, all the active sites remain free for adsorbing ions (arsenic and fluoride) and their concentration decreases gradually as adsorption proceeds with time. Further, the concentration of arsenic and fluoride ions in the solution also decreases with adsorption in due course of time. Due to this fact driving force decreases gradually with time, whereas the agitation remains constant (i.e. 150 rpm) leading the system towards equilibrium where no further adsorptive removal is possible with respect to time. Therefore, 300 min agitation period is considered as an optimum agitation period.

5.4.1.4 Effect of initial concentration of arsenic and fluoride on their removal

Experiments have been conducted in batch reactor to study the effect of initial concentration of arsenic and fluoride on their removal from synthetic solution by AHNP to optimize it and to perform the isotherm studies. The details of the experimental setup are provided in Section 3.4.1. In order to perform this study, the initial concentration of arsenic and fluoride ions were varied from 100 µg/L to 1000 µg/L for arsenic and 5000 µg/L to 30000 µg/L for fluoride. The detailed procedure is described in Section 4.9.4.1.4. Effects of initial concentration of arsenic and fluoride on their respective percentage removal are presented through Figure 5.24 and Figure 5.25.

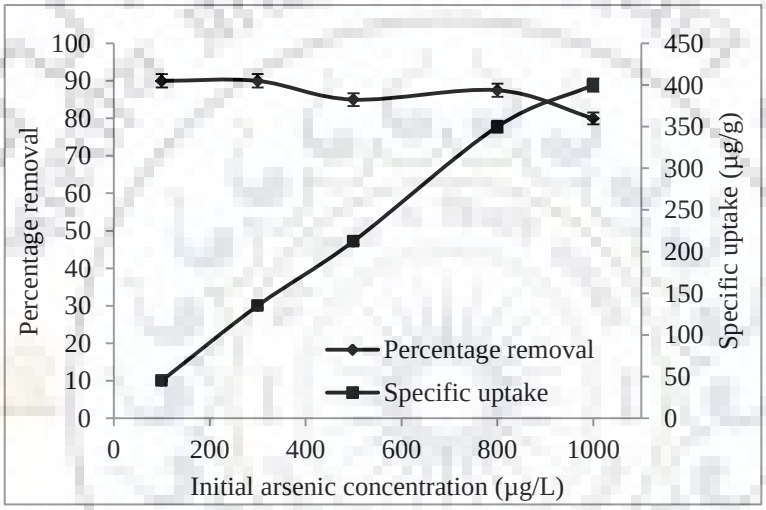

Figure 5.24 Effect of initial arsenic concentration on percentage removal and specific uptake

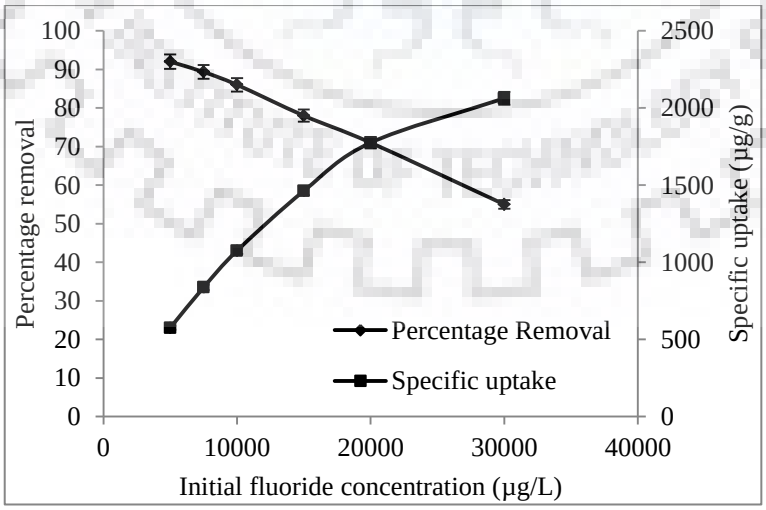

Figure 5.25 Effect of initial fluoride concentration on percentage removal and specific uptake

From Figure 5.24 and 5.25, the following points are evident:

i. The specific uptake of arsenic increases from 45 µg/g to 400 µg/g by increasing initial arsenic concentration from 100 to 1000 µg/L, whereas, for fluoride, it increases from 575 µg/g to 2062.5 µg/g due to the increase in initial fluoride concentration from 5000 to 30000 µg/L.

ii. The percentage removal of arsenic decreased from 90 % to 80 % by increasing initial arsenic concentration from 100 to 1000 µg/L. Whereas for fluoride, it decreases from 92 % to 55 % by increasing initial fluoride concentration from 5000 to 30000 µg/L.

Observations given in points (i) and (ii) can be explained as follows:

The increase in specific uptake of arsenic with increase in its initial concentration can be explained through the fact that, as the concentration of arsenic is increased the driving force for the adsorption is increased and the percentage removal is also increased whereas the number of active sites for the adsorption remained the same due to fixed value of adsorbent dose. Thus, the specific uptake of the arsenic is increased with the increase in its concentration. The increase in specific uptake of fluoride indicates the fact that increase in initial fluoride concentration increased the driving force which helped in adsorption of fluoride on the adsorbent, whereas, the number of active sites (adsorbent dose) remained constant.

The percentage removal of arsenic remained almost constant as the initial concentration of arsenic is increased from 100 µg/L to 800 µg/L. This can be explained on the basis of the fact that AHNP possesses good adsorption capacity for arsenic and hence displayed similar percentage removal for arsenic till its concentration reached upto 800 µg/L. However, as the initial concentration is further increased up to 1000 µg/L, the percentage removal decreases as the number of active sites for adsorption remained the same due to fixed value of adsorbent dose. The decrease in removal percentage of fluoride with increasing initial concentration may be because of the increasing number of fluoride ions in the solution with same number of adsorption sites. As a result, lesser number of active sites was available for the adsorption of fluoride which decreased the percentage removal of fluoride.

5.4.1.5 Kinetic studies for the removal of arsenic and fluoride

To determine the kinetic parameters for the adsorption of arsenic and fluoride on AHNP, the results of experiments reported in Section 5.4.1.3 have been processed further using various kinetic models as described in Section 2.3.5. Kinetic parameters for the adsorption of arsenic and fluoride on AHNP, computed by various kinetic models, are reported in Table 5.11. For getting the details of intraparticle diffusion, q_t vs. $t^{1/2}$ plots have been developed, as shown in Figure 5.26 (a) and (b) for fluoride and arsenic respectively.

Table 5.11 Kinetic parameters for adsorption of arsenic and fluoride on AHNP for single component system

Model	**R^2**	**q_e (calculated)**	**q_e (experimental)**	**Kinetic parameters**
		Arsenic		
Pseudo first order	0.962	135.490 µg/g	212.5 µg/g	k_1 (sec^{-1}) = 0.0002
Pseudo second order	0.997	232.558µg/g	212.5 µg/g	k_2 (gm/µg.min) = 1.29×10^{-4}
Intra particle diffusion	0.847	-	-	K_{id} (µg/g.$min^{0.5}$) = 11.374 C (µg/g) = 48.823
		Fluoride		
Pseudo first order	0.908	415.632 µg/g	1087.5 µg/g	k_1 (sec^{-1}) = 0.0002
Pseudo second order	0.997	1111.111 µg/g	1087.5 µg/g	k_2 (gm/µg.min) = 8.0198×10^{-5}
Intra particle diffusion	0.948	-	-	K_{id} (µg/g.$min^{0.5}$) = 24.878 C (µg/g) = 659.99

From Table 5.11, following observations are noted:

i. All the three models namely, pseudo 1st order model, pseudo 2nd model and intra particle diffusion model have R^2 values between 0.847 to 0.997 for arsenic and

0.908 to 0.997 for fluoride, which indicates the extent of suitability of these models for describing the kinetics of the adsorption of arsenic and fluoride. However, the value of R^2 is observed highest for both arsenic and fluoride for pseudo 2^{nd} order model which shows that the pseudo second order kinetic model is more suitable than pseudo first order kinetic model to explain the adsorption process.

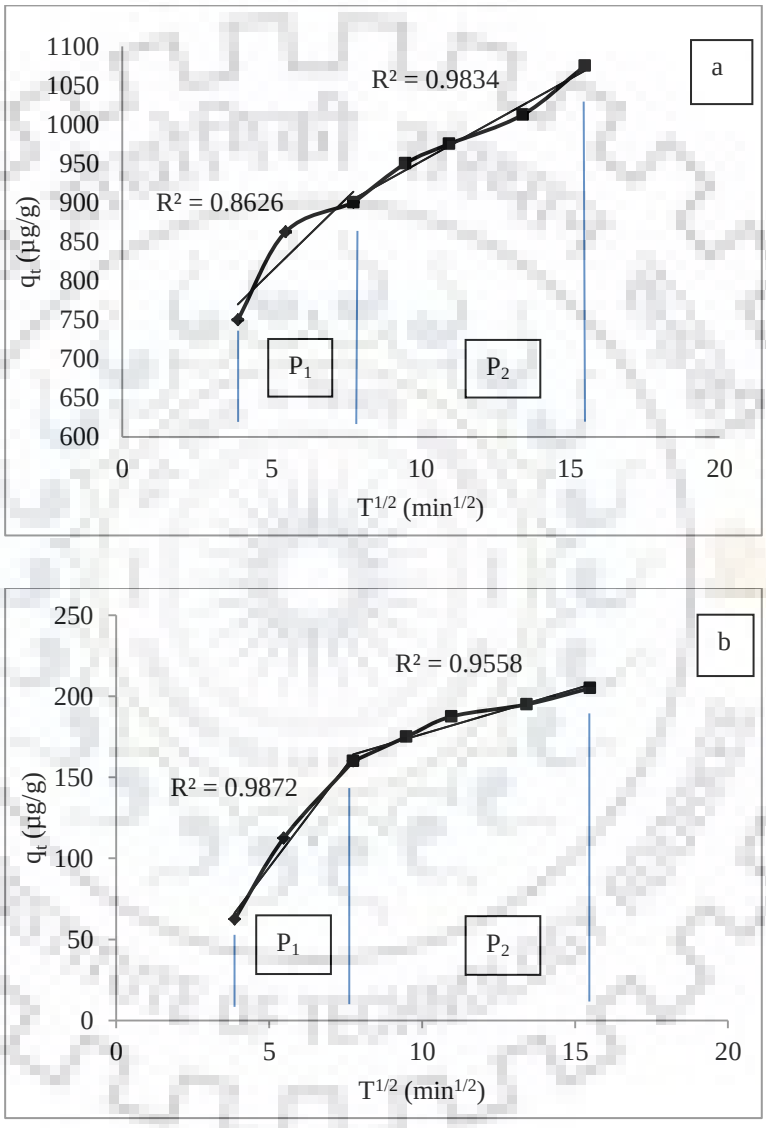

Figure 5.26 Intra particle diffusion model for adsorption of fluoride (a) and arsenic (b) on AHNP

From Figure 5.26 (a) and Figure 5.26 (b), following observations are noted

i. From Figure 5.26 (a) and (b), it is observed that the each plot can be considered as two linear parts (P_1 and P_2), which indicates that the adsorption phenomena

takes place in more than one step. This implies that the intra particle diffusion does not solely control the adsorption of arsenic and fluoride. The steepest part, P_1 is the initial stage of adsorption when most of the sites of adsorbent are available for adsorption. The region P_1 is attributed to boundary layer diffusion or external mass transfer effects.

ii. The values of pore diffusion coefficient (D_p) obtained through Eq. 2.4 is 3.94×10^{-6} cm^2/s for both arsenic and fluoride (as the value of first-order rate constant, $K_1 = 0.0002$ s^{-1} is same for both the anions), whereas the values of film diffusion coefficient (D_f) is obtained through Eq. 2.5 as 2.538×10^{-7} cm^2/s for arsenic and 4.70097×10^{-7} cm^2/s for fluoride. For pore diffusion to be the rate limiting step, its value (D_p) should lie between 10^{-11} and 10^{-13}, and if film diffusion to be the rate limiting step, its value (D_f) should lie between 10^{-6} and 10^{-8} for anions [Mondal et al. 2009]. As the value of D_f lies in the range mentioned for film diffusion, we can say that the film diffusion is the rate limiting step for the adsorption of both the two ions.

5.4.1.6 Isotherm studies for the removal of arsenic and fluoride

To determine the adsorption isotherm parameters for the adsorption of arsenic and fluoride on AHNP, the results of experiments reported in Section 5.3.1.4 have been processed further using various single component isotherm models as described in Section 2.3.5. Single component isotherm parameters for the adsorption of arsenic and fluoride computed by various single component models are reported in Table 5.12

Table 5.12 Characteristic parameters of different isotherm models for the adsorption of arsenic and fluoride by AHNP for single component system.

Model	Arsenic		Fluoride	
	R^2	Isotherm constants	R^2	Isotherm constants
Langmuir isotherm	0.995	R_L = 0.1492 to 0.6369 q_o (µg/g) = 833.33 b_L ($µg^{-1}$) = 0.0057	0.988	R_L = 0.033 to 0.169 q_o (µg/g) = 2000 b_L ($µg^{-1}$) = 9.819×10^{-4}
Freundlich isotherm	0.961	K_F (µg/g(L/µg)$^{1/n}$) = 9.1632 1/n = 0.745	0.971	K_F (µg/g(L/µg)$^{1/n}$) = 71.5145 1/n = 0.365

From the Table 5.12, following observations are noted:

i. Both Langmuir isotherm and Freundlich isotherm models have R^2 values of 0.995 and 0.961 for arsenic and 0.995 and 0.98 for fluoride respectively, which indicates the extent of suitability of these models for describing the equilibrium of the adsorption of arsenic and fluoride. However, the value of R^2 is observed highest for both arsenic and fluoride for Langmuir isotherm model.

ii. The value of Langmuir maximum adsorption capacity (q_0) of AHNP is found to be 833.33 µg/g and 2000 µg/g for arsenic and fluoride respectively.

iii. The value of separation factor R_L associated with the Langmuir isotherm lies in the range of 0.1492 to 0.6369 for arsenic and 0.033 to 0.169 for fluoride and are in the range $0 < RL < 1$, which indicates a favorable adsorption process.

iv. The value of 1/n should lie between 0 and 1 for favorable adsorption process. It is also noteworthy that, the value of 1/n which indicates the favorability of adsorption is 0.745 for arsenic and 0.365 for fluoride respectively, which also supports the favorability of adsorption of both arsenic and fluoride on the AHNP presented in this work.

5.4.1.7 Simultaneous removal of arsenic and fluoride by AHNP in bi-component system

Experiments have been conducted in batch reactor to study the competitive effect between arsenic and fluoride in bi-component system by using AHNP adsorbent. The details of the experimental setup are provided in Section 3.4.1. In order to perform this study, the concentration of one of the contaminant was increased gradually while keeping the concentration of the other contaminant constant. The detailed procedure is described in Section 4.9.4.2. Effect of presence of one contaminant on the adsorptive removal of other has been presented in the form of percentage removal of contaminants in the bi-component system in Table 5.13.

Table 5.13 Comparison of binary equilibrium sorption found at different fluoride concentrations in the absence and presence of increasing concentrations of arsenic onto AHNP

$C_{0,\ fluoride}$ (µg/L)	$C_{0,\ arsenic}$ (µg/L)	$C_{e,\ fluoride}$ (µg/L)	$C_{e,\ arsenic}$ (µg/L)	$q_{e,\ fluoride}$ (µg/g)	$q_{e,\ arsenic}$ (µg/g)
2500	0	700	0	900	0
5000	0	1800	0	1600	0
7500	0	3300	0	2100	0
10000	0	5500	0	2250	0
0	100	0	10	0	45
2500	100	840	12	830	44
5000	100	2460	13	1270	43.5
7500	100	4080	13	1710	43.5
10000	100	6000	14	2000	43
0	200	0	20	0	90
2500	200	840	20	830	90
5000	200	2520	21	1240	89.5
7500	200	3960	21	1770	89.5
10000	200	6000	24	2000	88
0	300	0	30	0	135
2500	300	960	32	770	134
5000	300	2400	32	1300	134
7500	300	4080	33	1710	133.5
10000	300	6000	35	2000	132.5
0	400	0	38	0	181
2500	400	1020	40	740	180
5000	400	2460	41	1270	179.5

7500	400	4080	42	1710	179
10000	400	6000	43	2000	178.5
0	500	0	75	0	212.5
2500	500	1020	80	740	210
5000	500	2340	82	1330	209
7500	500	4140	84	1680	208
10000	500	6000	90	2000	205

From Table 5.13, following observations are noted:

i. The specific uptake of fluoride decreases from 2250 µg/g when no arsenic is present to 2000 µg/g when arsenic concentration is 500 µg/L keeping initial fluoride concentration same (10000 µg/L).

ii. The specific uptake of arsenic also decreases from 212.5 µg/g to 205 µg/g due to the increase in fluoride concentration from 0 to 10000 µg/L with initial arsenic concentration of 500 µg/L.

The observations (i) and (ii) can be explained on the basis of synergistic and antagonistic effects of ions in binary system as described in Section 4.9.1.3. It seems that both arsenic and fluoride removal is influenced by antagonistic effect where the percentage removal of ions is getting affected by the presence of other ion. It is also noteworthy that this antagonistic behavior is more prominent in the case of fluoride as its concentration is much higher in the solution as compared to arsenic ions.

To determine the bi-component adsorption isotherm parameters for simultaneous adsorption of arsenic and fluoride on AHNP, the results of experiments reported in Section 5.4.1.7 have been processed further using various bi-component isotherm models as described in Section 2.3.5. Bi-component isotherm parameters for the adsorption of arsenic and fluoride on AHNP, computed by various models, are reported in Table 5.14.

Table 5.14 Binary adsorption isotherm parameter values for the simultaneous removal of arsenic and fluoride by AHNP

		Adsorbate	
Binary adsorption isotherm model		**Arsenic – Fluoride**	**Fluoride – Arsenic**
Non modified competitive Langmuir model	MPSD	190.48	178.95
Modified competitive Langmuir model	η_i	0.15	0.37
	η_j	12.58	7.36
	MPSD	9.08	6.72
Extended Langmuir model	b_i	0.017	0
	b_j	0	0.001
	q_{max}	384.661	2911.049
	MPSD	43.73	3.826
Extended Freundlich model	x	-4.0135	3.8045
	y	0	0.5420
	z	0.0664	-1.1724
	MPSD	16.53	173.6

From the Table 5.14, following observations are noted:

i. The binary non modified competitive Langmuir model shows poor fit to experimental data (with MPSD value of 190.48 for arsenic and 178.95 for fluoride) as it depicts the competitive effects in the adsorption process in binary system.

ii. In modified competitive Langmuir model the MPSD values changes (MPSD value of 9.08 for arsenic and of 6.72 for fluoride) due to the introduction of interaction factor η. Therefore, the binary adsorption of arsenic and fluoride ions onto AHNP can be represented satisfactorily and adequately by the modified competitive Langmuir model.

iii. For extended Langmuir model, the MPSD values for arsenic and fluoride are 43.73 and 3.826 respectively. It is attributed to the fact that this model considers the non-interacting effects between the species present in binary system. This also supports the synergistic behavior of arsenic shown in the system.

iv. Extended Freundlich model shows higher values of MPSD for both arsenic and fluoride (MPSD value of 16.53 for arsenic and 173.6 for fluoride).

5.4.1.8 Removal of arsenic and fluoride from real groundwater by AHNP in batch reactor

Experiments have been conducted in batch reactor to study the removal of arsenic and fluoride from real groundwater by AHNP adsorbent. The details of the process for the identification of site and collection of contaminated groundwater are reported in Section 3.1.2. The physico-chemical characteristics of the real groundwater have been discussed in Section 4.3 with details of the experimental setup being provided in Section 3.4.1. Results have been reported in the form of percentage removal in Table 5.15.

Table 5.15 Removal of arsenic and fluoride from real groundwater by AHNP

Contaminant	Initial concentration	Final concentration	Percentage removal
Arsenic (µg/L)	512	7	98.63
Fluoride (µg/L)	6300	1000	84.13

From Table 5.15, following observations are noted:

i. The removal of both arsenic and fluoride present in the real groundwater sample is carried out satisfactorily at the optimum conditions evaluated through the studies mentioned in Section 4.9.4.1.1 to Section 4.9.4.1.4. The results reveal that the concentration of both the contaminants have decreased and are brought down to below the respective permissible limit as per Indian Standard (IS 10500).

5.4.2 Column Reactor Studies

Studies have been conducted to evaluate the performance of the AHNP adsorbent for the simultaneous removal of arsenic and fluoride from synthetic solution in column

reactor. Schematic diagram of the column reactor is shown in Figure 3.2. Detail procedure is described in Section 4.9.6. The output data is reported in the form of time vs. ratio of initial concentration and final concentration.

5.4.2.1 Effect of flow rate of influent on simultaneous removal of arsenic and fluoride

Experiment has been conducted in column reactor containing AHNP to study the effect of flow rate of the influent on the simultaneous removal of arsenic and fluoride and to get the optimum value of flow required for the adsorption process to take place. In order to perform this study, the flow rate of the influent was varied from 17 ml/hr to 100 ml/hr. Other conditions like concentration of the ions, mass of the adsorbent and bed height are provided in the Table 3.5. The effect of flow rate of influent on the removal of arsenic and fluoride are presented in the form of breakthrough curve in Figure 5.27.

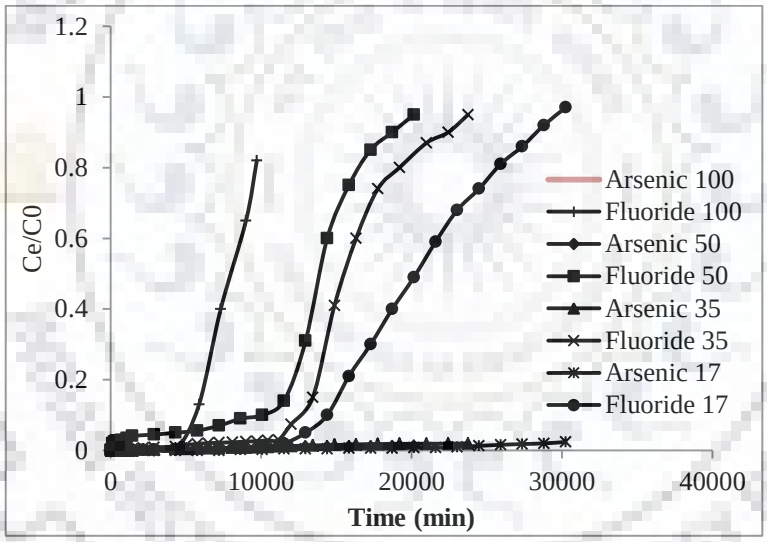

Figure 5.27 Breakthrough curves for the removal of arsenic and fluoride by AHNP at various flow rates

From Figure 5.27, following points are evident:

i. The increase in flow rate tends to speed up the exhaustion of the column.

ii. The run times required for the column to reach the output concentration of fluoride above the permissible limit as per the Indian Standard (IS 10500) are approximately 5880 min (at 100 ml/hr flow rate), 11520 min (at 50 ml/hr flow rate), 13440 min (at 35 ml/hr flow rate) and 15360 min (at 17 ml/hr flow rate).

iii. The column is exhausted for fluoride in approximately 9720 min, 20160 min, 23760 min and 30240 min when the flow rate is 100 ml/hr, 50 ml/hr, 35 ml/hr and 17 ml/hr respectively, however, the concentration of arsenic in the effluent is observed still to be below the permissible limit as per the Indian Standard (IS 10500).

Observations from the above points are as follows:

The observation in above points can also be explained similarly to column adsorption experiments with ABTL adsorbent. Here also, with increase in flowrate, more amount of water is passed through the adsorbent bed during a certain time period, thus more pollutants come in contact with the adsorbents, which results more adsorption and consequently the faster exhaustion of the bed. The amount of water treated during this time to achieve fluoride concentration in treated water as 1.5 mg/l is approximately 9800 ml, 9800 ml, 7840 ml and 4350 ml when the flow rate is 100 ml/hr, 50 ml/hr, 35 ml/hr and 17 ml/hr respectively. However, the residence time of the influent decreases from 18.28 min to 3.12 min as the value of flow rate is increased from 17 ml/hr to 100 ml/hr. Thus, with fixed rate constant value of different pollutants, the time required for exhaustion of column is different.

Moreover, in this case also the performance of the column is found to be satisfactory for the removal of arsenic at all the above mentioned flow rates. This may be due to the fact that the concentration of arsenic in the solution is very low (20 times less) as compared to that of fluoride. Thus the concentration of arsenic remains below the permissible limit as per the Indian Standard (IS 10500) even after the column gets exhausted for fluoride.

5.4.2.2 Column adsorption kinetic studies for the removal of arsenic and fluoride

To determine the effect of flow rate on breakthrough curves, the results of experiments reported in 5.4.2.1 have been processed further using various kinetic models as described in Section 2.3.5. The kinetic parameters for the adsorption of arsenic and fluoride on AHNP, computed by various models, are reported in Table 5.16 and 5.17 as follows:

Table 5.16 Mathematical description of column parameters for the adsorption of arsenic on AHNP

Thomas model			
Q (ml/min)	k_{Th} (ml/min.µg)	q_m (µg/g)	R^2
1.67	0.0004	3313.5	0.84
0.83	0.0004	18323.7	0.78
0.58	0.0002	2565.31	0.8
0.28	0.0002	1309.75	0.93
Yoon Nelson model			
Q (ml/min)	k_{YN} (min^{-1})	τ (min)	R^2
1.67	0.0002	39683	0.84
0.83	0.0002	44153.5	0.78
0.58	0.0001	88453	0.8
0.28	0.0001	93554	0.93
Adam Bohart model			
Q (ml/min)	k_{AB} (L/µg.min)	N_0 (µg/L)	R^2
1.67	0.0000004	3143835	0.84
0.83	0.0000004	1748958.2	0.78
0.58	0.0000002	2452589.8	0.8
0.28	0.0000002	1259956.58	0.93

Table 5.17 Mathematical description of column parameters for the adsorption of fluoride on AHNP

Thomas model			
Q (ml/min)	k_{Th} (ml/min.µg)	q_m (µg/g)	R^2
1.67	0.00008	13390.89	0.85
0.83	0.00004	10045.28	0.85
0.58	0.00004	9478.41	0.96
0.28	0.00004	5334.27	0.98
Yoon Nelson model			
Q (ml/min)	k_{YN} (min^{-1})	τ (min)	R^2
1.67	0.0008	8037.75	0.85
0.83	0.0004	12102.75	0.85
0.58	0.0004	16258	0.96
0.28	0.0004	18849	0.98
Adam Bohart model			
Q (ml/min)	k_{AB} (L/µg.min)	N_0 (µg/L)	R^2
1.67	0.00000006	16072503	0.82
0.83	0.00000003	12146803	0.76
0.58	0.00000003	15862962	0.93
0.28	0.00000003	13708316	0.95

From the Table 5.16 and Table 5.17, following observations are noted:

i. In the case of Thomas model, the value of coefficient of determination (R^2) ranged between 0.78 and 0.93 for arsenic and between 0.85 and 0.98 for fluoride, indicating good fits of the experimental data. As the flow rate of the influent is decreased from 1.67 ml/min (100 ml/hr) to 0.28 ml/min (17 ml/hr), the value of q_m increases form 1309.75 µg/g to 3313.5 µg/g but the value of k_{Th} decreases from 0.0004 ml/min.µg to 0.0002 ml/min.µg for arsenic. Similarly, for fluoride,

the value of q_m increases form 5334.27 µg/g to 13390.89 µg/g but the value of k_{Th} decreases from 0.00008 ml/min.µg to 0.00004 ml/min.µg.

ii. In case of Yoon-Nelson model, the value of coefficient of determination (R^2) ranged between 0.78 and 0.93 for arsenic and between 0.85 and 0.98 for fluoride, indicating good fits of the experimental data. The value of τ (which is the time taken (in min) to reduce the concentration of the contaminant to half of the initial concentration) increases from 39683 min to 93554 min for arsenic and 8037.75 min to 18849 min for fluoride, whereas, the value of k_{YN} reduces from 0.0002 min^{-1} to 0.0001 min^{-1} for arsenic and from 0.0008 min^{-1} to 0.0004 min^{-1} for fluoride as the flow rate of the influent is reduced from 1.67 ml/min (100 ml/hr) to 0.28 ml/min (17 ml/hr). This indicates that, at higher flow rate the column is getting exhausted at faster rate.

iii. In the case of Adam–Bohart model, the value of coefficient of determination (R^2) ranged between 0.78 and 0.93 for arsenic and between 0.76 and 0.95 for fluoride, indicating good fit of the experimental data. The value of Adam-Bohart rate constant (k_{AB}) decreases from 0.0000004 (L/µg.min) to 0.0000002 (L/µg.min) for arsenic and from 0.00000006 (L/µg.min) to 0.00000003 (L/µg.min) for fluoride as the flow rate of the influent is reduced from 1.67 ml/min (100 ml/hr) to 0.28 ml/min (17 ml/hr). This indicates that at lower flow, the solution is getting treated at lower rates and hence the service time of the column is increased. However, the values of N_0 (maximum saturation concentration, in µg/L) varies from 3143835 µg/L to 1259956.58 µg/L for arsenic and 16072503 µg/L to 12146803 µg/L for fluoride. The maximum value of N_0 is observed when the flow rate of the influent is 0.28 ml/min (17 ml/hr) for arsenic and 1.67 ml/min (100 ml/min) for fluoride, which indicates its optimum value for the column operation.

5.4.3 Comparison of the Adsorbents with Other Similar Reported Materials

A comparison of some metal oxides based adsorbents, used for the removal of As and F, are given in Table 5.18 for the removal of arsenic and fluoride with the help of various aluminum based adsorbents.

Table 5.18 List of few aluminum based adsorbents used for adsorptive removal of arsenic and fluoride.

Arsenic				
Adsorbent	**$C_{o,\ arsenic}$ (µg/L)**	**Optimum pH**	**q_{max} (µg/g)**	**Reference**
Iron oxide coated sand	100	7.5	28.57	Gupta et al. 2005
Ferruginous manganese ore	120	2 to 8	536.7	Chakravarty et al. 2002
Iron oxide coated sand IOCS	100	-	136	Thirunavukkarasu et al. 2005
Activated alumina	1000	7.6	180	Singh and Pant 2004
Polymetallic sea nodule	0 to 700	6	690	Maity et al. 2005
Aluminum oxide/hydroxide nanoparticles	500	7	833.33	**Present study**

Fluoride				
Adsorbent	**$C_{o,\ fluoride}$ (µg/L)**	**Optimum pH**	**q_{max} (µg/g)**	**Reference**
Al–Mn hybrid material	2500 to 30000	4 to 7	2852	Maliyekkal et al. 2006
Activated alumina	2500 to 30000	4 to 7	1080	Maliyekkal et al. 2006

Aluminum-impregnated chitosan biopolymer	1000 to 10000	1730	6700	Swain et al. 2009
Al impregnated activated carbon	500 to 15000	3	1070	Leyva-Ramos et al. 1999
Activated alumina (Grade OA-25)	2500 to 14000	7	2000	Ghorai and Pant 2004
Aluminum oxide/hydroxide nanoparticles	10000	4 to 7	2000	**Present study**

From Table 5.18, it is evident that the present material is well comparable for the removal of both arsenic and fluoride with some of the recently reported materials in the literature. In case of fluoride, the AHNP has shown removal capacity equivalent to commercially available activated alumina (Activated alumina (Grade OA-25)).

5.5 ECONOMIC EVALUATION OF THE ADSORBENTS

The economic evaluation of the adsorbents was carried out to assess the economic viability of the adsorbents in practical field application. To carry out this study, the synthesis cost of the adsorbents was calculated in ₹/kg of adsorbent. Calculations related to the consumption of electricity and chemicals in various steps of synthesis are provided in Appendix F and details of estimation of cost of the adsorbents are as follows:

Cost of ABTL

The cost of ABTL adsorbent (in ₹/kg) is determined by adding the cost of chemicals required and the cost of electricity required during its synthesis.

Thus, total cost of synthesis = Cost of 2 N HCl + Cost of 4 N NaOH + Electricity

For the present case, the ABTL adsorbent was prepared in batches of 50 g.

Therefore, for preparing 50 gm ABTL, we need approximately 80 ml of 2 N HCl (as 60 % of the HCl is recovered through distillation out of 200 ml HCl taken initially)

Volume of conc. HCl required to make 80 ml of 2 N HCl = 13.7 ml (taking the normality of concentrated HCl (~ 36 %) as 11.67)

Cost of 1 ton concentrated HCl (commercially available) = ~200 $ = ~ ₹13000 [Weblink 2]

Cost of 1 liter of HCl = 11.72 (considering the density of 33 % HCl is 1.16 g/cm^3)

Therefore, cost of 13.7 ml HCl = ₹0.16

Further,

Volume of 4 N NaOH required = 120 ml

Amount of NaOH pallets required to prepare 120 ml 4 N NaOH solution = 19.2 gm

Cost of 1 ton NaOH (commercially available) = ~400 $ = ~ ₹25800 [Weblink 3]

Cost of 500 gm NaOH = ₹ 12.92 (approximately)

Therefore, cost of 19.2 gm NaOH = ₹ 0.49

Electricity consumed for preparation (acid treatment + base treatment + drying) of 1 kg ABTL = 1 kWh (approximately)

Cost of 1 kWh electricity in India = ₹ 4 [Weblink 4]

Total cost for production of 1 kg ABTL = Cost of 2 N HCl + Cost of 4 N NaOH + cost of electricity

Therefore, total cost of production (per kg) = 20 (0.16 + 0.49) + 4 = ₹ 17.1 (approx.)

Transportation and handling cost = 10 % of total cost of production

Total cost of ABTL = 18.83 ₹/kg

Cost of AHNP

The cost of AHNP adsorbent (in ₹/kg) is determined by adding the cost of chemicals required and the cost of electricity required during its synthesis.

The cost of AHNP adsorbent (in ₹/kg) is determined by adding the cost of aluminum consumed in the preparation of the aluminum hydroxide nanoparticles by electrochemical (EC) method, cost of electricity consumed during the EC process, and the cost of electricity used for the sintering of the fresh aluminum hydroxide nanoparticles.

The total cost of synthesis of AHNP adsorbent in a single batch can be calculated as

Total cost of synthesis = $a \times (C_{electrode}) + b \times (C_{electricity})$

Where, $C_{electrode}$ (kg of aluminum) and $C_{electricity}$ (kWh) are the amount of electrodes consumed and amount of electricity consumed in the EC process as well as for sintering

of the fresh adsorbents, respectively, while ‘a’ and ‘b’ are the coefficients of cost, respectively,

Cost of aluminum (per kg) = ₹ 123 (‘a’) [weblink 5]

Amount of aluminum consumed in 1 run of EC process = 5 g

Cost of aluminum consumed per run = ₹ 0.625

Amount of aluminum hydroxide nanoparticles produces per run = 14.5 g

Amount of electricity consumed during the synthesis of AHNP = electricity consumed per batch in the EC process + electricity consumed during sintering of aluminum hydroxide nanoparticles

The amount of electricity consumed per batch of EC process = voltage × current × runtime

For the present case, the electrolysis was carried out by supplying DC power with a constant current of 4 A and potential difference of 19 V (average).

Run time of EC process (per batch) = 2 hours

Thus, total electricity consumed during the synthesis of aluminum hydroxide nanoparticles per batch = ~0.152 kWh.

Cost of 1kWh electricity in India = ₹ 4 (approximately) (‘b’)

Therefore, cost of 0.152 kWh of electricity = ₹ 0.58

Power rating of the electric furnace used in the present case for sintering of aluminum hydroxide nanoparticles = 9 kWh

Capacity of the electric furnace used for sintering of aluminum hydroxide nanoparticles = 10 kg material per batch

Thus, the total electricity consumed for the sintering of 1 kg of aluminum hydroxide nanoparticles = ~0.9 kWh

Cost of calcination of 1 kg of aluminum hydroxide nanoparticles = ₹ 3.6

Cost of calcination of 14.5 g of aluminum hydroxide nanoparticles = ₹ 0.005

Therefore, total cost of synthesis (per batch) of AHNP = 0.625 + 0.58 + 0.05 = ₹ 1.25

Hence, cost of synthesis of 1 kg of AHNP = ~ ₹86

5.6 STUDIES ON THE MANAGEMENT OF SPENT ADSORBENTS IN THE FORM OF CLAY BRICKS

In the present study, the spent adsorbent has been managed in the form of clay bricks. ABTL and AHNP spent adsorbents were considered for this study. The spent adsorbents were obtained after simultaneous adsorption of arsenic and fluoride from the synthetic solution. Details of synthesis of the spent adsorbents, characterization of the spent adsorbents and the adsorption study for the simultaneous removal of arsenic and fluoride have been discussed in Section 4.11. The range of concentration of the spent adsorbents in the bricks and sintering temperature are shown in Table 3.5 of Section 3.3. Results of tests for physico-chemical characterization of the brick samples and leaching test of the bricks are discussed hereunder.

5.6.1 Characteristics of the Clay, Sintered Brick Specimens and Spent Adsorbents

Characterization of the clay, sintered brick specimens and spent adsorbents has been carried out similarly to the characterization studies of the fresh adsorbents as described in Section 4.5. The characteristics of the spent adsorbents have been discussed already; hence, they are not presented here. The brick specimens considered in the present study are sintered at 800 °C, 900 °C and 1000 °C.

XRD analysis of the clay and sintered brick specimen

XRD analysis of the raw clay and brick specimens sintered at various temperatures was carried out as mentioned in Section 4.11.3. The XRD patterns of various samples are shown in Figure 5.28.

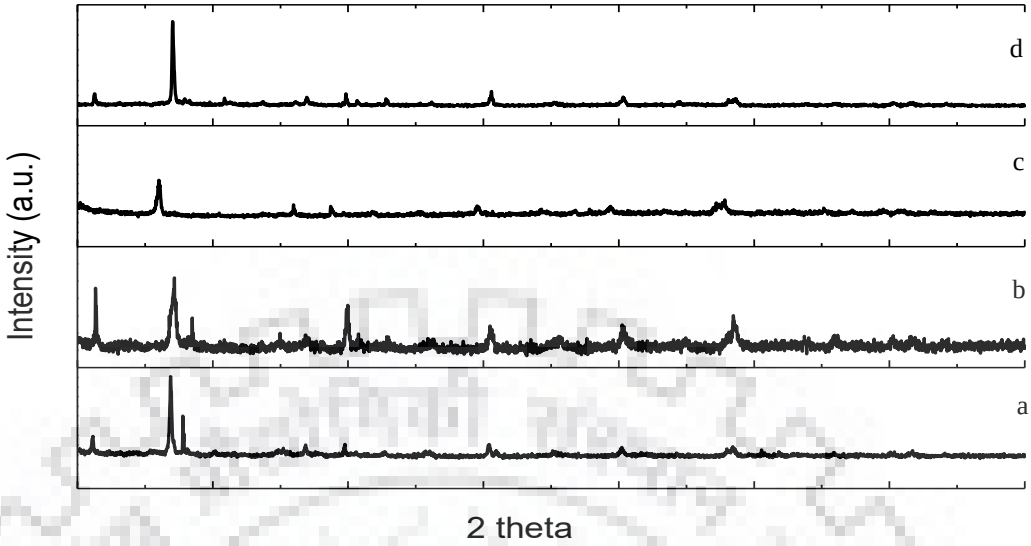

Figure 5.28 XRD of raw clay (a), brick specimen sintered at 800 °C (b), brick specimen sintered at 900 °C (c) and brick specimen sintered at 1000 °C (d).

From Figure 5.28, it is evident that the brick specimens sintered at different temperatures have almost similar patterns for values of 2θ. It is also observed that as the sintering temperature of the specimen is increased, more sharp peaks are obtained. This is due to the fact that, at higher temperature the sintered brick specimen tends to convert into more crystalline form. The analysis of sintered brick specimens shows peaks at 2θ = 21 and 27 which indicate the presence of SiO_2. The peaks at 2θ = 39, 42 and 60 indicate the presence of Al_2O_3. The presence of various forms of iron oxides (Fe_3O_4, Fe_2O_3 and FeO) can be anticipated by the peaks at 2θ = 36, 42, 55, 60 and 65. The peaks obtained at 2θ = 36, 40, 42, 55, 65 and 68 indicate the presence of various forms of oxides of manganese (MnO, Mn_2O_3 and Mn_3O_4). Presence of arsenic is also identified in the form of As_2O_3 by peaks present at 2θ = 27, 39, 48 and 55 and in the form of NiAs by the peaks present at 2θ = 33, 46, 50 and 64.

FTIR analysis of the clay and sintered brick specimen

FTIR analysis of the raw clay and brick specimens sintered at various temperatures was carried as mentioned in Section 4.11.3. The FTIR spectra of the samples are shown in Figure 5.29.

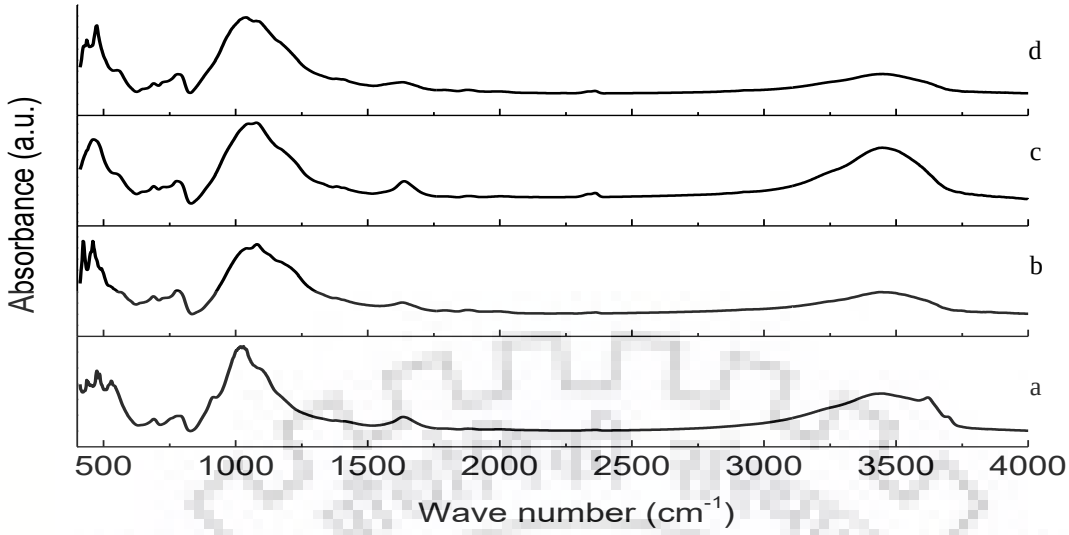

Figure 5.29 FTIR of raw clay (a), brick specimen sintered at 800 °C (b), brick specimen sintered at 900 °C (c) and brick specimen sintered at 1000 °C (d).

From Figure 5.29, it is evident that the brick specimens sintered at different temperatures have almost similar spectral patterns. The presence of iron, aluminum and silica oxides gets confirmed by studying these spectral patterns. The absorption band within the range of 3370 – 3405 cm^{-1} are attributed to OH group of Fe, Al and Si minerals, whereas, the absorption band near 1620 cm^{-1} is assigned to H – O – H bending of water molecule on the surface of clay. A strong absorption band near 1030 cm^{-1} indicates the presence of Si – O stretching present in clay minerals. At wave number 912 cm^{-1}, the absorbance band indicates Al – OH bond stretching. The band near 790 cm^{-1} in clay and sintered brick specimen is attributed to cristobalite, which is a polymorph of quartz and near 690 cm^{-1} due to Si – O quartz. The absorbance bands from 542 to 474 cm^{-1} are anticipated due to Fe – O bond stretching, Fe_2O_3 and Si – O – Al stretching [Maiti et al. 2010, Saikia and Parthasarathy 2010, Julien et al. 2004]. The peaks corresponding to wavenumber ranging from 750 cm^{-1} to 450 cm^{-1} indicates the presence of Mn_2O_3 related stretching and bending vibrations. Peak at wavenumber 878 cm^{-1} is observed in all the spectra of clay and sintered brick specimen which is associated with presence of arsenic complex ($AsO_2(OH)$) in clay and sintered brick specimens [Goldberg and Johnston 2001].

FESEM-EDX analysis of the clay and sintered brick specimen

FESEM-EDX analysis of the raw clay and brick specimens sintered at various temperatures was carried out as mentioned in Section 4.11.3. The FESEM images and EDX data are shown through Figure 5.30 (a) to (d) and Figure 5.31 (a) to (d).

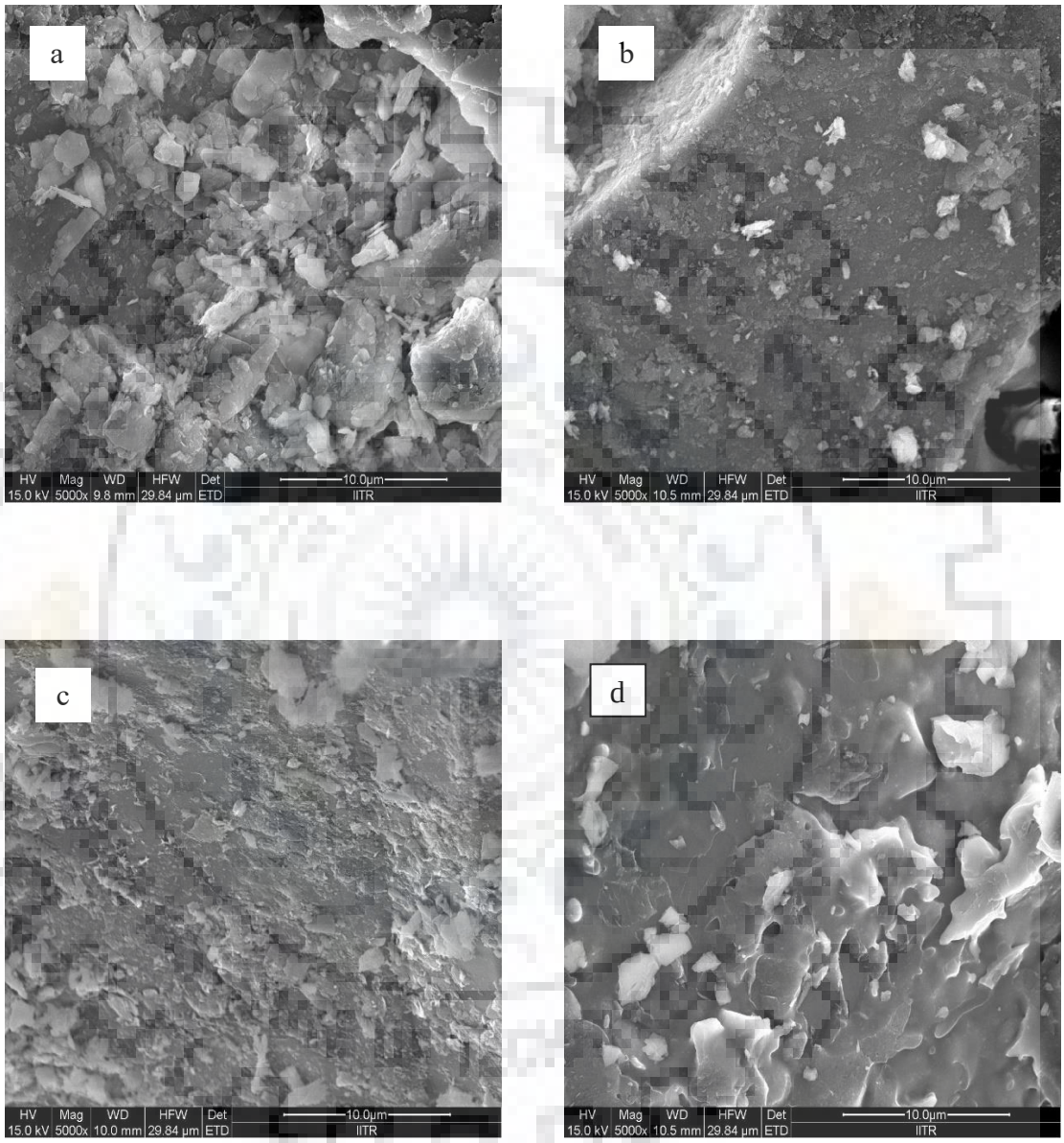

Figure 5.30 FESEM image of raw clay (a), brick specimen sintered at 800 °C (b), brick specimen sintered at 900 °C (c) and brick specimen sintered at 1000 °C (d).

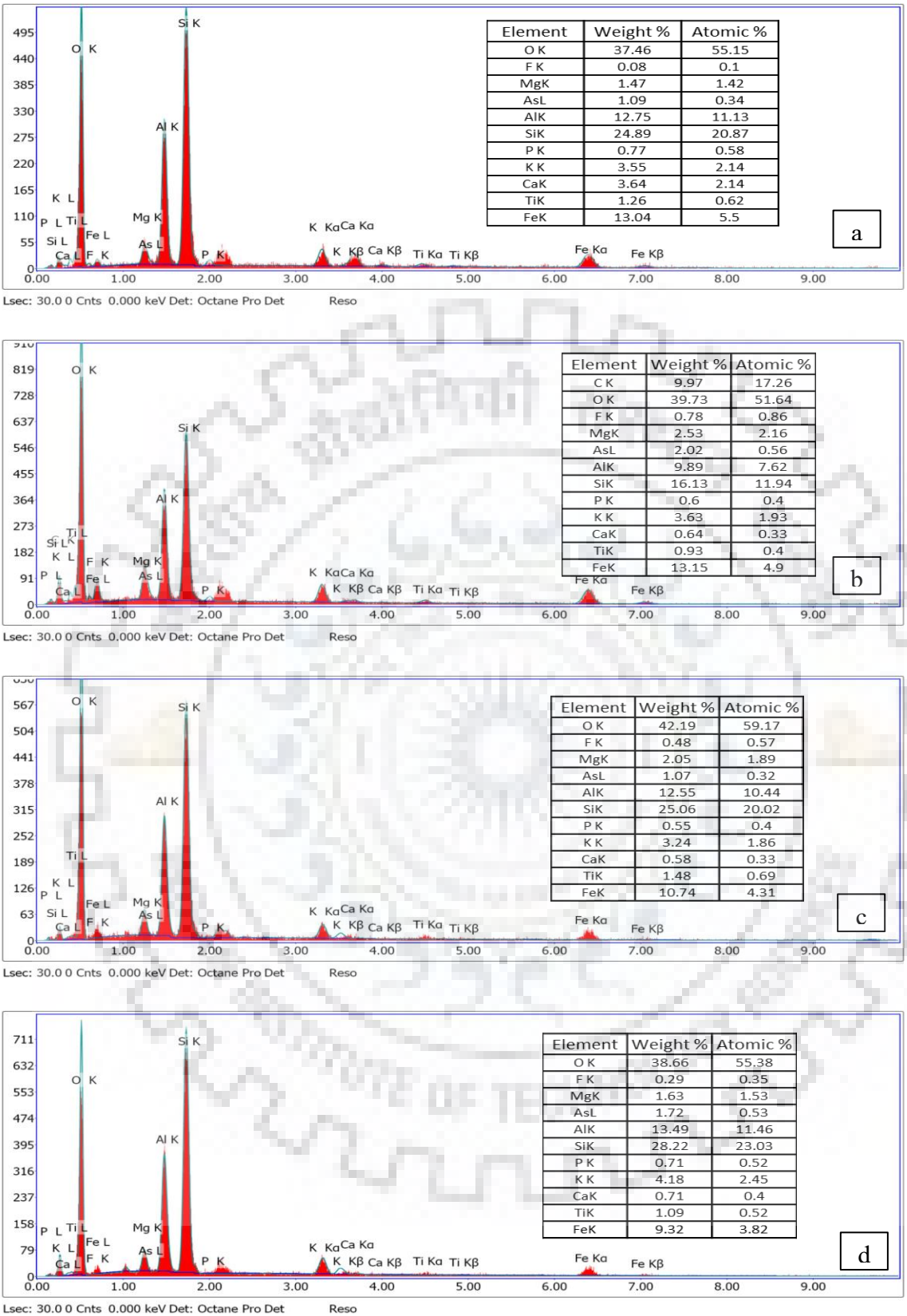

Figure 5.31 EDX analysis of raw clay (a), specimen sintered at 800 °C (b), specimen sintered at 900 °C (c) and specimen sintered at 1000 °C (d)

Figure 5.30 (a) to Figure 5.30 (d) illustrates the FESEM images of raw clay, brick specimen sintered at 800 °C, brick specimen sintered at 900 °C and brick specimen sintered at 1000 °C respectively. The FESEM image of clay shows heterogeneous surface. Further, FESEM images of sintered brick specimen at different temperatures show that their surface is getting smoother with increase in temperature and is showing signs of vitrification at elevated temperature.

Figure 5.31 (a) to Figure 5.31 (d) shows the EDX analysis of raw clay, brick specimen sintered at 800 °C, brick specimen sintered at 900 °C and brick specimen sintered at 1000 °C respectively. Presence of many types of elements commonly found in clay is observed in EDX analysis. The composition of elements in the sintered brick specimen are also found to be almost similar to that of clay sample as sintering only changes the internal structure of samples and does not affect its composition.

5.6.2 Effects of Spent Adsorbent (ABTL and AHNP) Concentration and Sintering Temperature on Physico-Chemical Properties of Bricks

In this study, the effect of concentration of spent adsorbent in the bricks and the sintering temperature of the bricks on its physico-chemical properties has been carried out. The details of the experimental setup are provided in Section 3.4.3. In order to perform this study, the concentration of the spent (ABTL and AHNP) adsorbent was varied from 0 % to 30 % and the sintering temperature was varied from 800 °C to 1000 °C. The detailed procedure is described in Section 4.11.1. Effect of above mentioned parameters on the physico-chemical properties of bricks are presented through Figure 5.32 to Figure 5.36.

Effect on density of bricks

The effects of concentration of spent (ABTL and AHNP) adsorbents and the sintering temperature on density of bricks have been shown in Figure 5.32 (a) and (b).

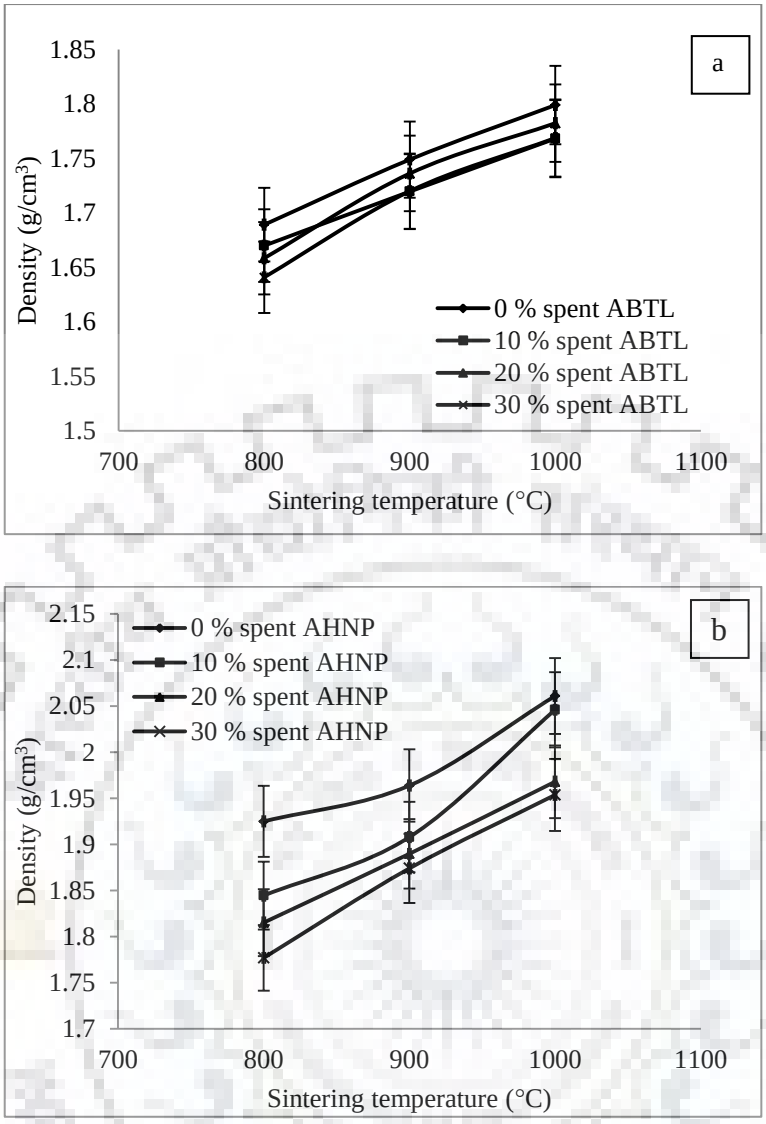

Figure 5.32 Effects of concentration of spent adsorbent (ABTL (a) and AHNP (b)) and sintering temperature on density of bricks

From Figure 5.32, the following points are evident:

i. The density of the sintered brick specimen increases as the sintering temperature is increased. The density of the sintered brick specimens containing spent ABTL ranges from ~1.64 to ~1.8 g/cm^3 whereas the density of the sintered brick specimens containing spent AHNP adsorbent ranges from ~1.82 g/cm^3 to ~2.06 g/cm^3 within sintering temperature ranging from 800 °C to 1000 °C. The density of some of the sintered brick specimens (sintered at 1000 °C) are almost equal to 1.8 g/cm^3, which is the normal range of density of clay bricks (1.8 to 2 g/cm^3) as reported by [Lin 2006].

ii. The density of the sintered brick specimen decreases (in case of both types of spent adsorbent containing specimens) marginally as the percentage of spent adsorbent is increased.

Observation given in point (i) can be explained as follows:

Densification of sintered brick specimen increases with sintering temperature as the clay brick tends to shrink slightly with increase in the sintering temperature. This shrinkage is due to the vitrification or consolidation between particles of the sintered brick specimen at higher temperatures [Sutcu et al. 2015] as well as the loss of chemically and mechanically bound water to the clay and the spent adsorbents [Weng et al. 2003]. However, the contribution of the water loss is very less with respect to vitrification.

Observation given in point (ii) can be explained as follows:

The density of the sintered brick specimen decreases because of difference in the composition of the clay and spent adsorbent. As evident from XRD and EDX analysis of clay and spent adsorbent containing bricks (Figure 5.28 and Figure 5.31), high proportion of silicon is present in ABTL in the form of SiO_2 in clay whereas in the spent AHNP adsorbent high proportion of aluminum is present in the form of Al_2O_3. The melting point of SiO_2 is ~1600 °C whereas it is ~2072 °C for Al_2O_3. Thus, the presence of high amount of Al_2O_3 and SiO_2 in the spent adsorbent may produce lesser vitrification due to their higher melting points.

Water absorption

The effect of concentration of spent (ABTL and AHNP) adsorbents and the sintering temperature on water absorption capacity of bricks has been shown in Figure 5.33 (a) and (b).

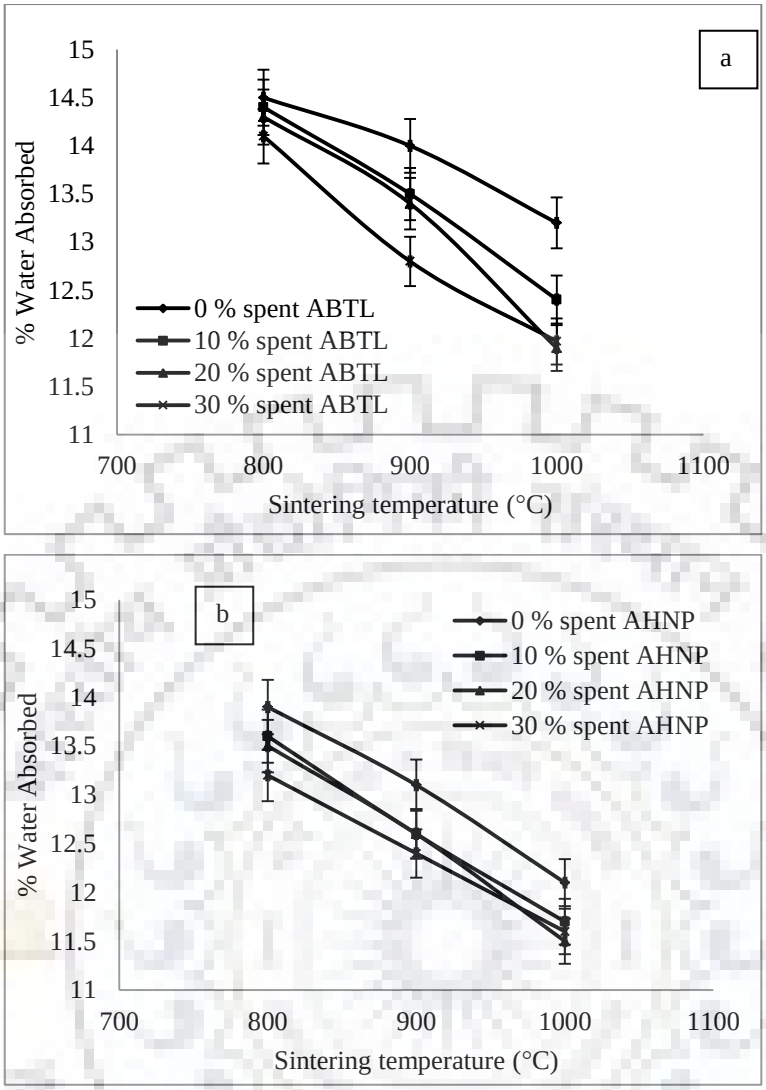

Figure 5.33 Effects of concentration of spent (ABTL (a) and AHNP (b)) adsorbent and sintering temperature on water absorption capacity of bricks

From Figure 5.33, the following points are evident:

i. The water absorption capacity of the sintered brick specimen decreases as the sintering temperature is increased. The water absorption capacity of the sintered brick specimens containing spent ABTL adsorbent ranges from ~14.5 % to 11.9 % whereas the water absorption capacity of the sintered brick specimens containing spent AHNP adsorbent ranges from ~11.5 % to 13.9 % with sintering temperature ranging from 800 °C to 1000 °C. The water absorption capacity of the brick specimens is in compliance with the Indian Standard (IS 1077-1992) for building brick criteria (i.e., below 15%).

ii. The water absorption capacity of the sintered brick specimen decreases (in case of both types of spent adsorbent containing specimens) marginally as the percentage of spent adsorbent is increased.

Observation given in point (i) can be explained as follows:

The decrease in water absorption capacity of the sintered brick specimen with the increase in sintering temperature is due to the fact that, porosity of sintered brick specimens decreases significantly with increasing sintering temperature [Nowok et al., 1990]. It also suggests that at higher temperature local liquid-phase sintering occurs, which contributes to a decrease in the pore volume and thus the water absorption rate [Lin, 2006]. High water absorption capacity of the sintered brick specimen indicates that the sintered brick specimen has large number of open pores. This can also be considered as a function of compressive strength and the density of the sintered brick specimen.

Observation given in point (ii) can be explained as follows:

The decrease in water absorption capacity of the sintered brick specimen as the percentage of spent adsorbent is increased may be because of the decrease in density of the sintered brick specimen with increase in spent adsorbent concentration.

Change in dimension (shrinkage)

The effect of concentration of spent (ABTL and AHNP) adsorbent and the sintering temperature on shrinkage of bricks has been shown in Figure 5.34 (a) and (b).

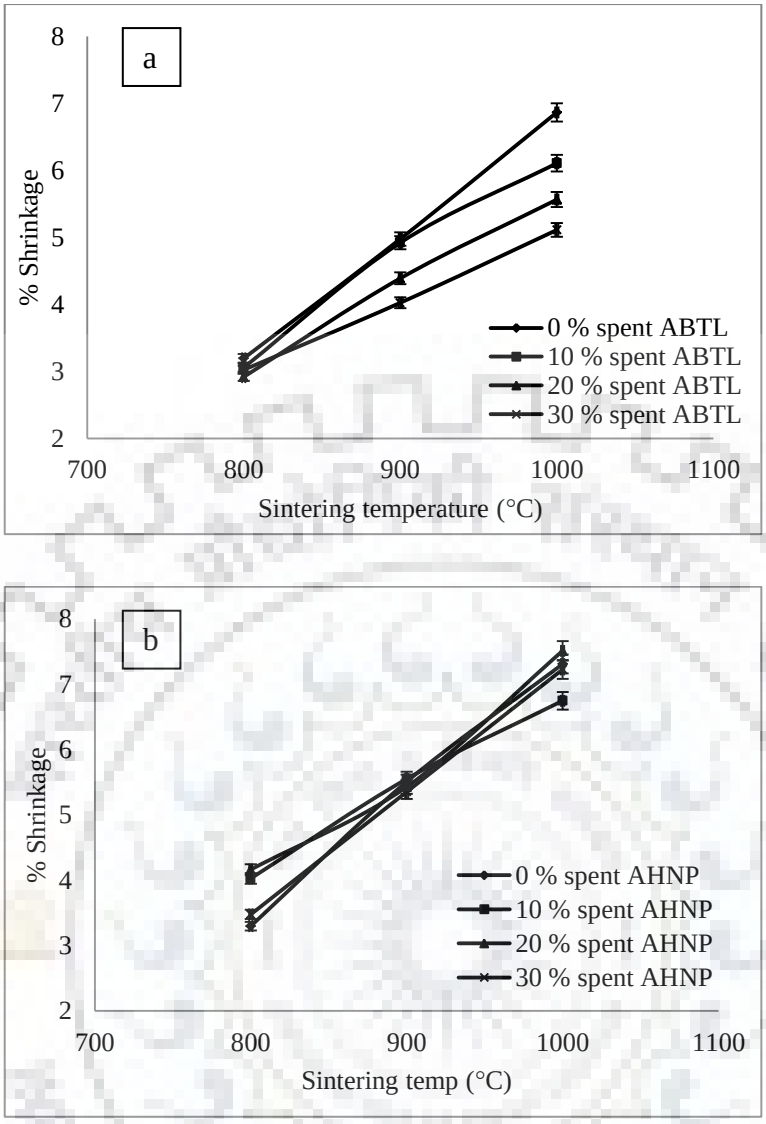

Figure 5.34 Effects of concentration of spent (ABTL (a) and AHNP (b)) adsorbent and sintering temperature on shrinkage of bricks

From Figure 5.34, the following points are evident:

i. The shrinkage of the sintered brick specimen increases as the sintering temperature is increased. Shrinkage of the sintered brick specimens containing spent ABTL adsorbent ranges from 2.91 % to 6.87 % whereas the shrinkage of the sintered brick specimens containing spent AHNP adsorbent ranges from 3.3 % to 7.5 % with sintering temperature ranging from 800 °C to 1000 °C.

ii. The shrinkage of the sintered brick specimen decreases (in case of both types of spent adsorbent containing specimens) marginally as the percentage of spent adsorbent is increased.

Observation given in point (i) can be explained as follows:

The densification of sintered brick specimens mainly occurs due to increase in the shrinkage of the sintered brick specimens. Shrinkage in the sintered brick specimen is associated with the loss of chemically and mechanically bound water to the clay as well as to the spent adsorbents [Weng et al., 2003]. The increase in shrinkage with increase in sintering temperature is also consistent with results showing increase in density of sintered brick specimens with sintering temperature. Accordingly, a contrary trend between the dimensional change (shrinkage) and water absorption with respect to sintering temperature is observed for sintered brick specimens (as shown in Figure 5.33).

Observation given in point (ii) can be explained as follows:

When the percentage of spent adsorbent is increased, a marginal decrease in the percentage shrinkage is observed for all the spent adsorbents. Reduction in percentage shrinkage with increase in percentage of spent adsorbent may be attributed to the fact that, the spent adsorbent does not tend to shrink as compared to pure clay.

Compressive strength

The effect of concentration of spent (ABTL and AHNP) adsorbent and the sintering temperature on the compressive strength of bricks has been shown in Figure 5.35 (a) and (b).

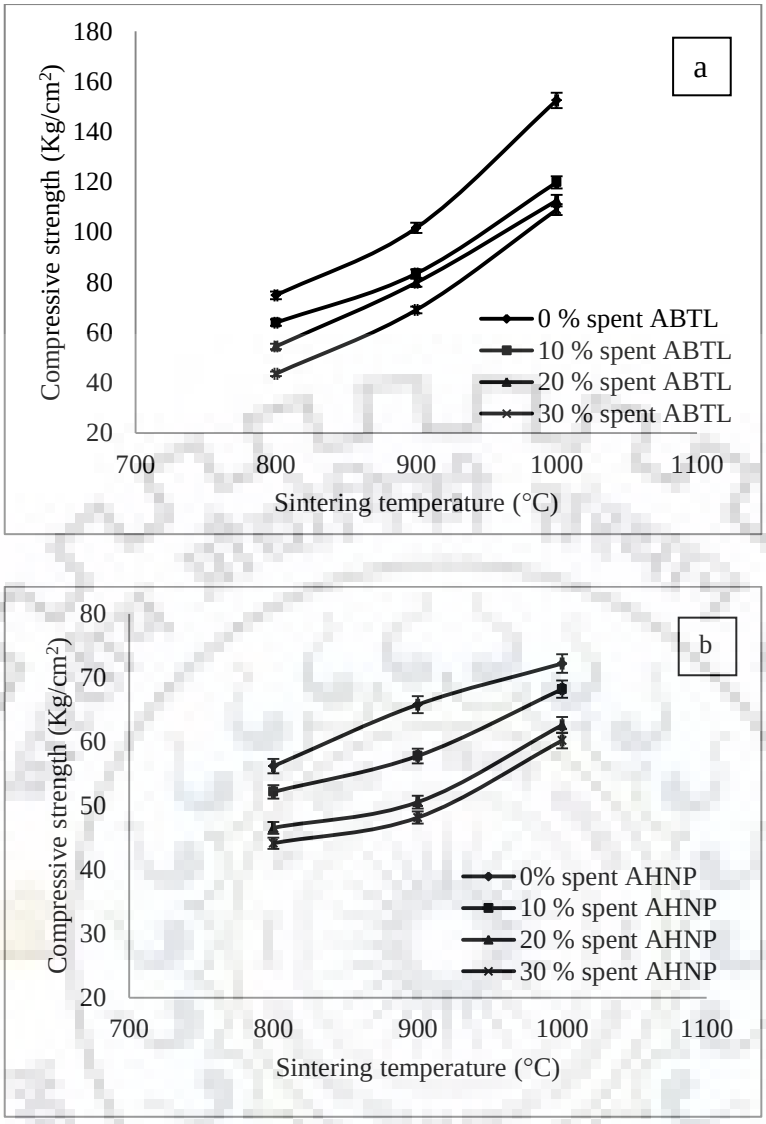

Figure 5.35 Effects of concentration of spent (ABTL (a) and AHNP (b)) adsorbent and sintering temperature on the compressive strength of bricks

From Figure 5.35, the following points are evident:

i. The compressive strength of the sintered brick specimen increases as the sintering temperature is increased. The compressive strength of the sintered brick specimens containing spent ABTL adsorbent ranges from 43.57 kg/cm^2 to 152.49 kg/cm^2 whereas compressive strength of the sintered brick specimens containing spent AHNP adsorbent ranges from 44.15 kg/cm^2 to 72.25 kg/cm^2 with sintering temperature ranging from 800 °C to 1000 °C. The compressive strength of various sintered brick specimen falls in the range set by Indian Standards (IS 1077-1992) for bricks and can be used for various types of building purposes.

ii. The compressive strength of the sintered brick specimen decreases (in case of both types of adsorbents) as the percentage of spent adsorbent is increased.

Observation given in point (i) can be explained as follows:

The increase in sintering temperature increases the compressive strength due to two possible reasons:

a. Enhanced vitrification of the clay and the spent adsorbent materials at higher temperatures as shown in the FESEM images (Figure 5.30).
b. Increase in bulk density of the sintered brick specimen due to reduction in porosity at higher temperature [Bhatnagar and Goel, 2002].

Further, the results obtained for change in dimensions (shrinkage) in the present study are also consistent with this observation.

Observation given in point (ii) can be explained as follows:

The decrease in the compressive strength of the bricks with increase in the percentage of spent adsorbent may be due to the fact that the binding capacity of the clay is not very good with the spent adsorbent present in it.

Efflorescence

Efflorescence test is carried out on the bricks containing spent (both ABTL and AHNP) adsorbent in order to determine the amount of soluble salts present in the sintered brick specimen. When the sintered brick specimen comes in contact with water, the dissolved salt bearing water moves towards the surface of a structure, where air evaporates the moisture leaving the salt behind. In the present case, no efflorescence is observed on any of the brick specimen. The results are in compliance with the Indian Standards for bricks which prefers 'Nil' efflorescence for good quality bricks (IS 1077-1992).

Leaching test of arsenic and fluoride

Experiments have been conducted to study the leaching back of arsenic and fluoride from the sintered brick specimens (containing spent ABTL and spent AHNP adsorbent) to understand their environmental viability. The detailed procedure is

described in Section 4.11.4. Effects of concentration of spent (ABTL and AHNP) adsorbent and sintering temperature on leaching back of arsenic and fluoride are presented through Figure 5.36 (a) and (b) and Figure 5.37 (a) and (b) respectively.

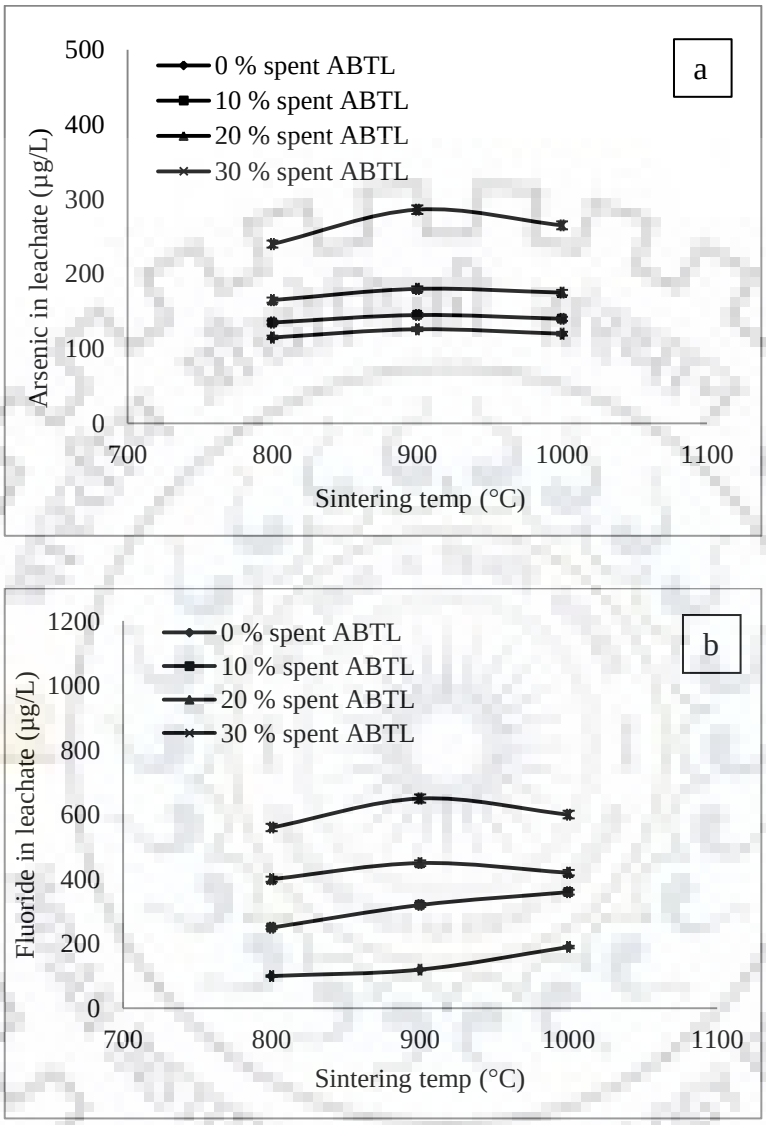

Figure 5.36 Concentration of arsenic (a) and fluoride (b) in leachate of sintered specimen containing spent ABTL adsorbent

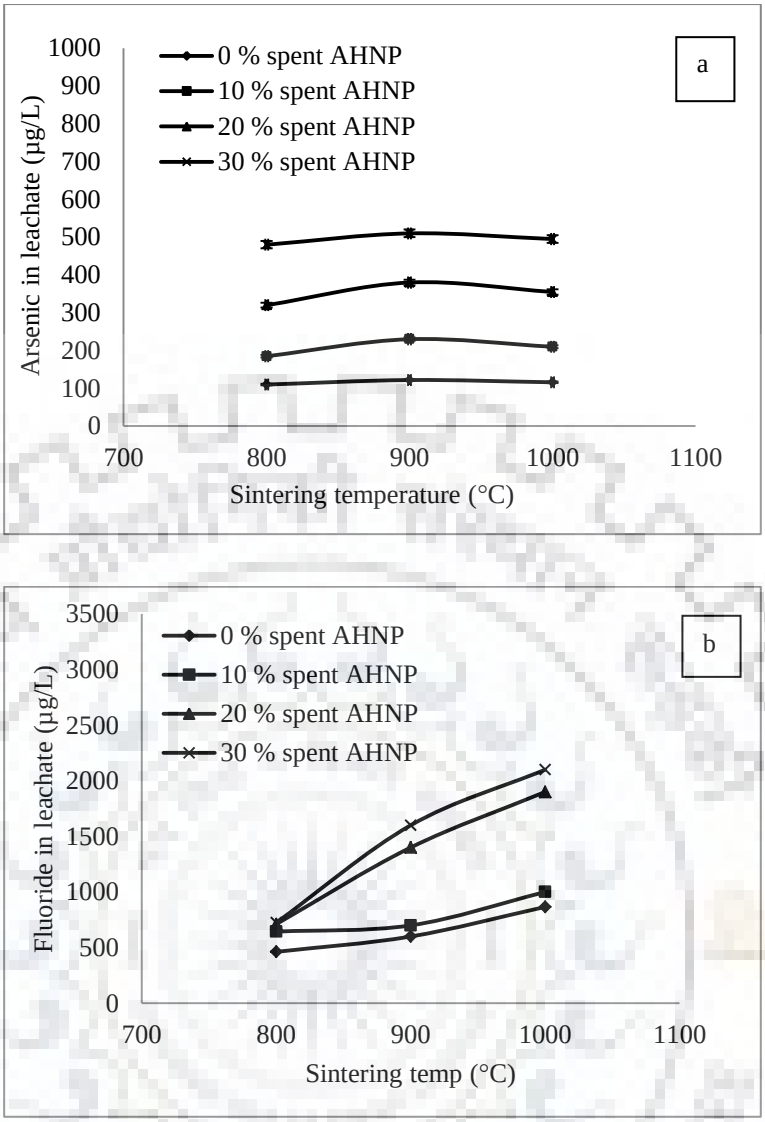

Figure 5.37 Concentration of arsenic (a) and fluoride (b) in leachate of sintered specimen containing spent AHNP adsorbent

From Figure 5.36, the following points are evident:

i. In case of ABTL, the concentration of arsenic and fluoride in the leachate is not affected much with the sintering temperature of the brick specimen and it remains almost constant at all sintering temperatures.

ii. In case of AHNP, the concentration of arsenic in the leachate is not affected much with the sintering temperature of the brick specimen. However, an increase in the concentration of fluoride in the leachate is observed with increasing sintering temperature.

iii. The concentration of arsenic and fluoride in the leachate is found to be highly dependent on the concentration of spent (ABTL and AHNP) adsorbent in the sintered brick specimen. The concertation of the contaminants increases as the concentration of the spent adsorbent is increased in the bricks.

Observation given in point (i) can be explained as follows:

The leaching of arsenic and fluoride is not dependent on the sintering temperature of the bricks due to the fact that the ABTL get fused in the brick samples and does allow the contaminants to leach back. Moreover, it may also be due to lesser adsorbing capacity of the ABTL adsorbent.

Observation given in point (ii) can be explained as follows:

The leaching of arsenic and fluoride is not dependent on the sintering temperature of the bricks due to the fact that the AHNP did not got fused much in the brick samples and allowed the contaminants (arsenic and fluoride) to leach back. The increase in the concentration of fluoride in the leachate of bricks sintered at higher temperature is not well understood.

Observation given in point (iii) can be explained as follows:

The increase in the concentration of arsenic and fluoride in the leachate is observed as the concentration of the spent (ABTL or AHNP) adsorbent is increased in the bricks as the leaching of these contaminants is proportional to their concentration in the bricks. However, the concentration of both arsenic and fluoride in the leachate are well below the permissible limits according to US-EPA standard of 48000 µg/L for fluoride [Dou et al., 2011] and according to US-EPA, EHSO standard of 5000 µg/L for arsenic [EHSO, 2015] even when the concentration of spent (ABTL or AHNP) adsorbent is 30 % in the bricks. The maximum concentration of arsenic and fluoride in the leachate are found to be 286 µg/L and 650 µg/L for spent ABTL adsorbent whereas they are found to be 510 µg/L and 2100 µg/L for spent AHNP adsorbent.

5.7 LIFE CYCLE ASSESSMENT (LCA) STUDIES OF THE DEFLUORIDATION PROCESS BY LATERITE SOIL BASED ADSORBENTS

Life cycle assessment (LCA) of defluoridation of water by laterite soil based adsorbents has also been studied for understanding the environmental implications of the defluoridation process. Three surface-modified laterite soil based adsorbents, viz. thermally treated laterite (TTL), acid treated laterite (ATL) and acid-base treated laterite (ABTL) were synthesized and used to remove excess fluoride from water to meet the WHO recommended quality of drinking water, i.e., maximum fluoride concentration of 1500 µg/L. the arsenic and fluoride removal capacity of adsorbents have been considered. The scope of LCA study consists of cradle to grave approach (i.e., from the acquisition of raw materials to the management of spent adsorbent). Environmental impacts associated with the defluoridation process are interpreted with the help of two different types of assessment techniques namely, CML 2001 and TRACI using GaBi 6.0 software.

The goal and scope for the LCA study have been discussed in Section 4.12 along with the system boundaries for treating 720 L of water which can be used by a family of 4 members for a month with per capita daily consumption of 6 L/day. The amount of raw laterite soil required for the synthesis of different types of surface modified laterite soil adsorbents were determined using the formula mentioned in Section 4.12 along with details for performing the inventory analysis. Major assumptions that were made during the study have been given in the Section 4.12.1. The LCA study has been conducted using two different methods viz. CML 2001 and TRACI. The details of these methods have been discussed in Section 4.12.2. Sensitivity analysis of the LCA process has been carried out to identify the processes with maximum contributions on various impact categories as well as to find out the alternative options to decrease the impacts varying their input values. The details of sensitivity analysis have been given in the Section 4.12.3.

5.7.1 Assessment of Impacts Due to TTL, ATL and ABTL by CML 2001 and TRACI Method

The contribution of different operations such as transportation of raw materials (truck trailer), crushing of raw laterite (electricity from grid mix 2), drying of adsorbents (electricity from grid mix 1) and management of the spent adsorbents (electricity from biogas) on environmental impacts under different impact categories (indicators) for TTL, ATL and ABTL are shown in Figure 5.38 (a), 5.39 (a) and 5.40 (a), respectively which are calculated by CML 2001 method and in Figure 5.38 (b), 5.39 (b) and 5.40 (b), respectively which are calculated by TRACI method.

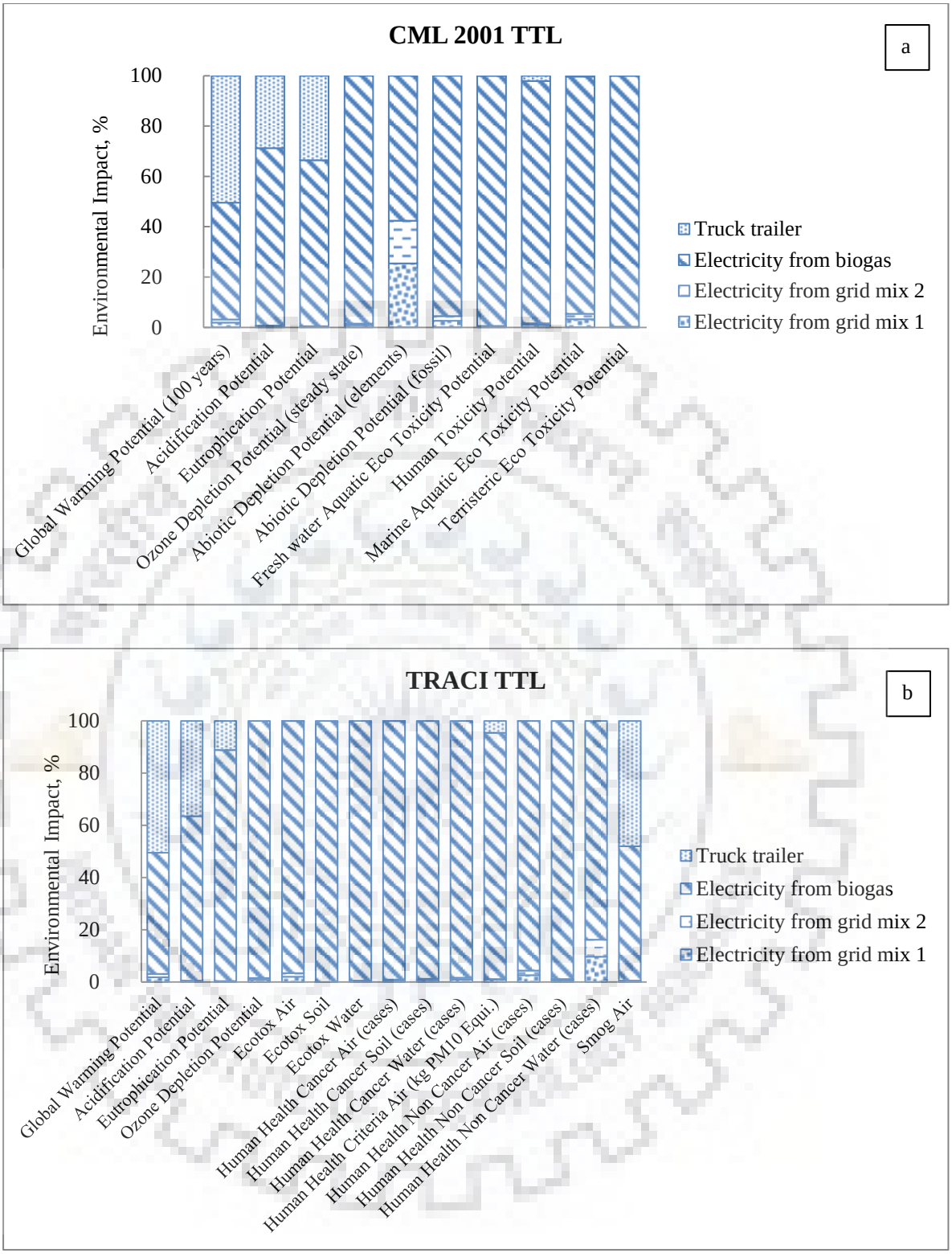

Figure 5.38 Assessment of impacts by TTL estimated by CML 2001 (a) and TRACI (b) method

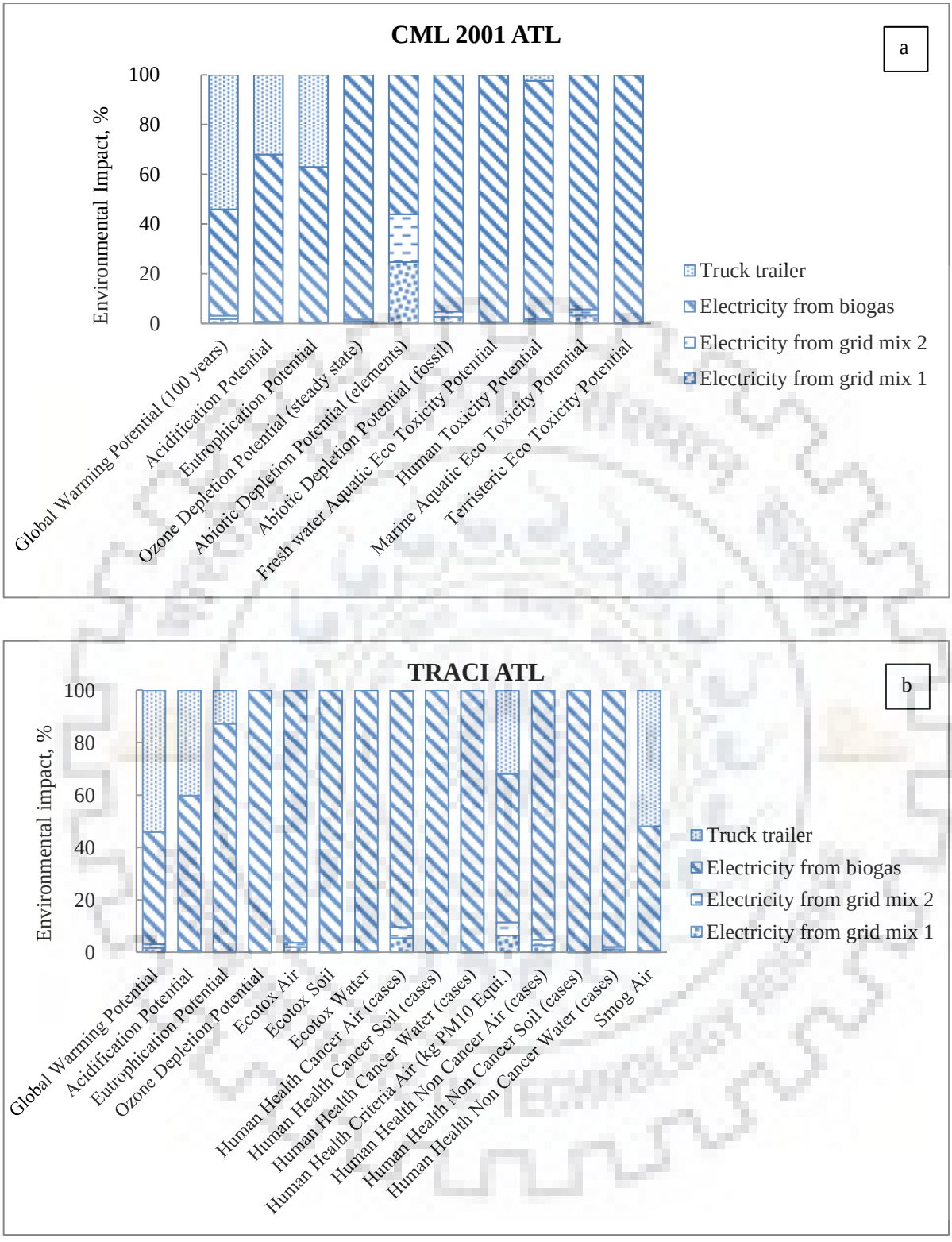

Figure 5.39 Assessment of impacts by ATL estimated by CML 2001 (a) and TRACI (b) method

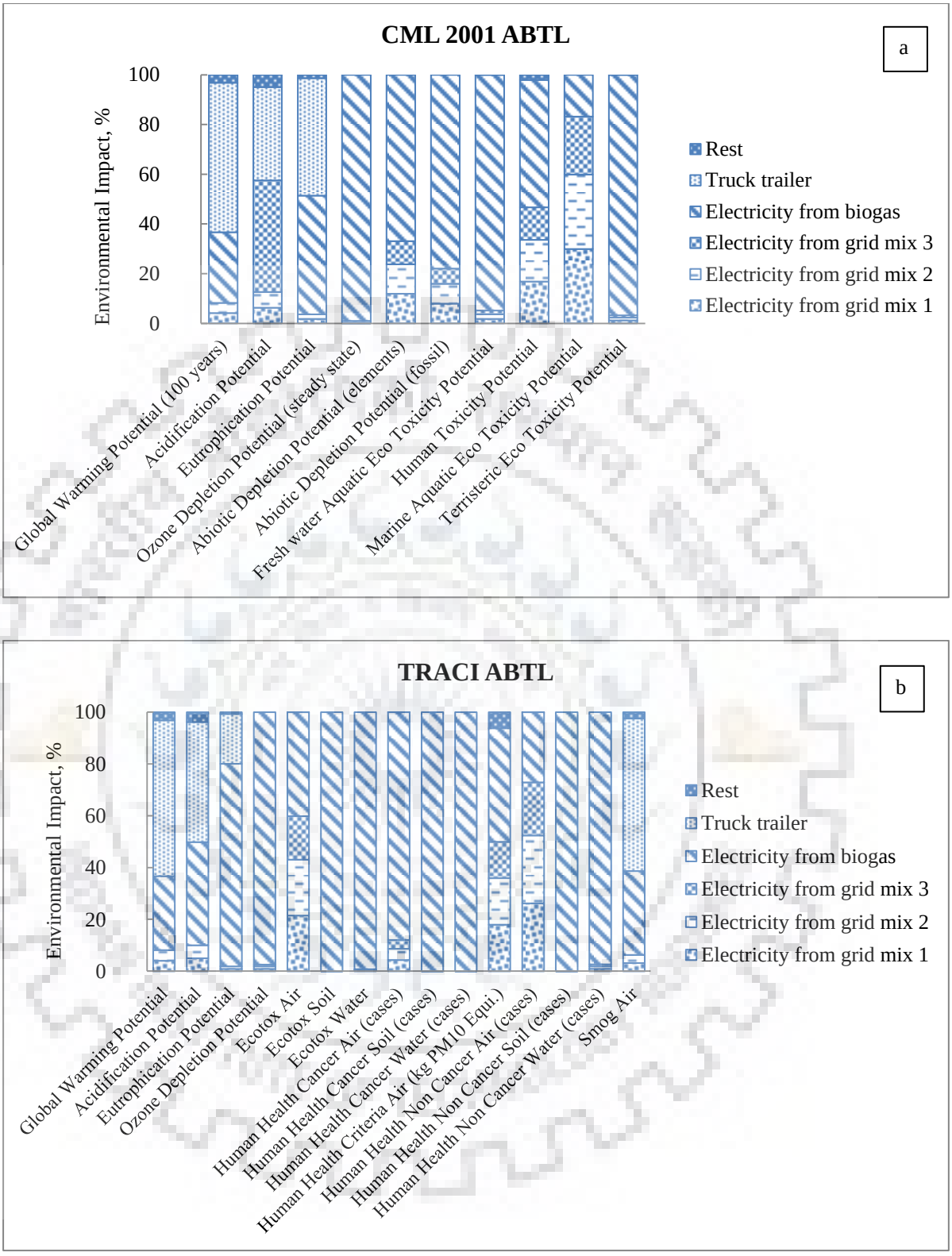

Figure 5.40 Assessment of impacts by ABTL estimated by CML 2001 (a) and TRACI (b) method

From Figure 5.38, Figure 5.39 and Figure 5.40, the following points are evident:

Transportation of raw materials (by the truck trailer) and management of the spent adsorbents (with electricity from biogas) together contributes to more than 90 % of the impacts for all the indicators except Abiotic Depletion Potential (ADP) elements. In this case (for ADP elements) contribution of the truck trailer is not available and only electricity from biogas and grid mixes are contributing to impacts. It is obvious as the truck is operated by diesel, which is a fossil fuel and hence it contributes ADP fossils in spite of ADP elements (which is generally associated with extraction of metals and their remaining reserves) as shown in Figure 5.38 (a), 5.39 (a) and 5.40 (a). It is interesting to note that, the trend in the contribution of different operations on different impact categories for TTL and ATL are similar, however, for ABTL it is different for many impact categories such as ADP fossils, Human Toxicity Potential (HTP) and Marine Aquatic Eco-Toxicity Potential (MAETP). In the case of ABTL; ADP fossils, HTP and MAETP have significant contributions from electricity production through grid mixes along with electricity production from biogas. This is due to the fact that for the ABTL, surface modification of more mass of laterite soil is needed as compared to TTL and ATL, which in turn consumes more coal to produce required electricity for grid mixes. Further, a larger amount of wastes is produced during surface modification in case of ABTL, which accounts for higher values of HTP and MAETP.

From Figure 5.38 (b), 5.39 (b) and 5.40 (b), it is evident that when impacts are calculated with TRACI method for TTL and ATL, the contribution of transportation of raw materials (truck trailer) and management of the spent adsorbents (electricity from biogas) on the different indicators are also more than 90 %, however, for ABTL it is less than 90 % for the indicators like Ecotox Air, and Human Health Non Cancer air. In this case, other operations like electricity from grid mix play a significant role due to the addition of more drying step in case of ABTL production, unlike other adsorbents. Since, electricity production emits acutely toxic gasses into the air, the values of Ecotox Air as well as Human Health Non-Cancer air are influenced by electric grid mix. It is interesting to note that in the case of TRACI, for ABTL, one extra contributor (Rest) is observed (Figure 5.40 (b)), which is probably due to the use of more number of treatment steps and material loss.

5.7.2 Normalization of the Impacts Due to Laterite Soil Based Adsorbents Estimated by CML 2001

The normalized value of the impacts of different categories for TTL, ATL, and ABTL obtained through CML 2001 and TRACI methods are shown in Figure 5.41 (a) and (b), respectively.

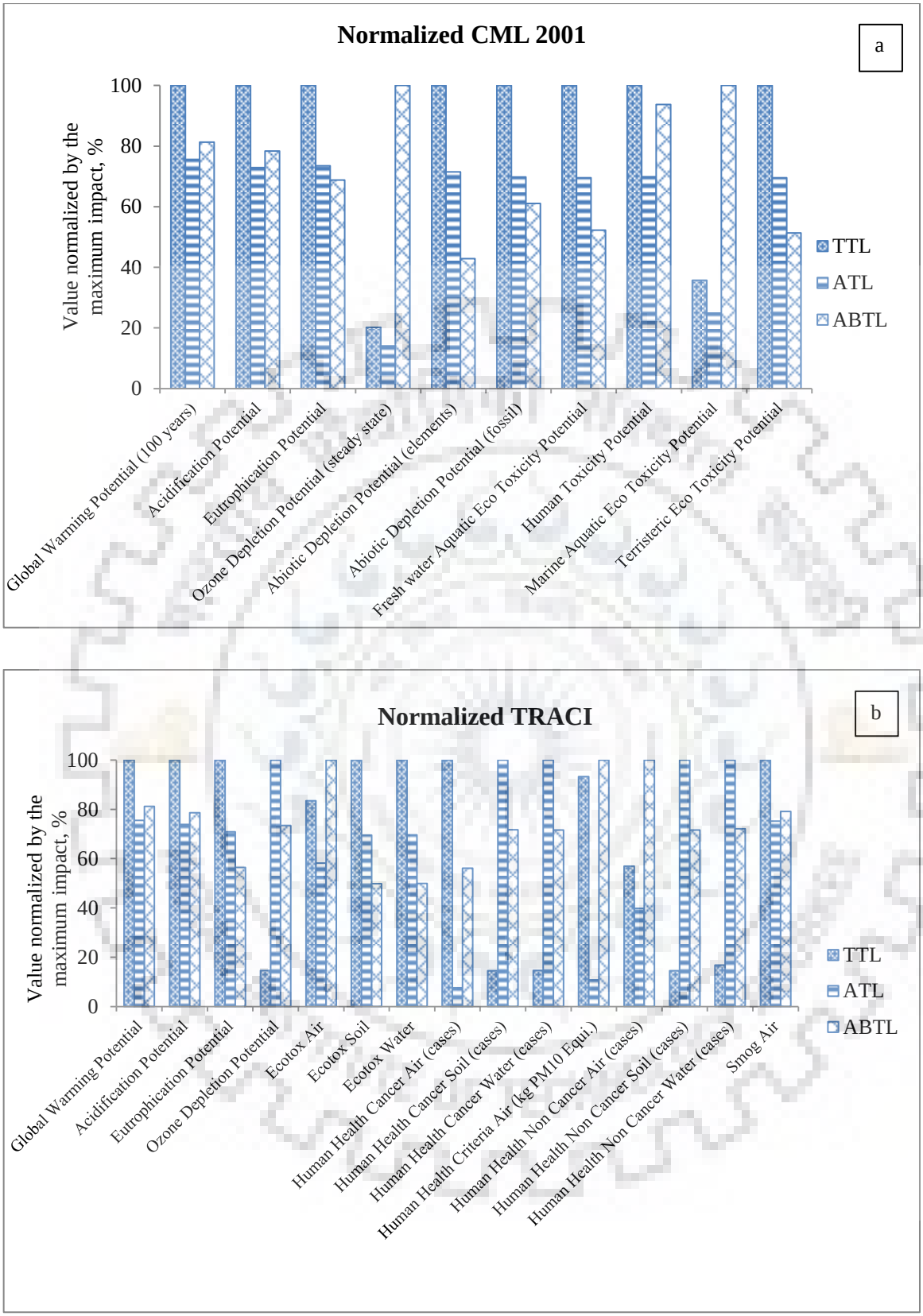

Figure 5.41 Impact comparison using CML 2001 (a) and TRACI (b) method. The y-axis value for the adsorbent that had the maximum impact in each category was set equal to 100 %, and other values were normalized to this maximum value

From Figure 5.41, the following points are evident:

The indicator values (CML 2001) are maximum either for TTL or ABTL in most of the cases. The impacts of ATL are in between TTL and ABTL. To produce the stipulated amount of TTL (55.63 kg), which is required to treat 720 L of fluoride contaminated water, approximately 382 kg raw laterite is required. The transportation of large quantities of raw laterite requires combustion of fossil fuels, which produces greenhouse gases and consequently gives higher values of ODP, ADP (both elemental and fossil), FAETP and TETP in impact assessment by CML 2001 method. Comparatively less amount of raw laterite is required to produce sufficient amount of ATL for treating the same amount of water, so it creates less impact in these categories. Similarly, the requirement of raw laterite for the production of ABTL for the treatment of same amount of water is also high as a considerable amount of laterite soil is lost during the chemical processing steps. Moreover, both energy and chemicals are needed for the surface modification of raw laterite to produce ABTL, which leads to its large contribution in the form of GWP, AP, EP, HTP, and MAETP in impact assessment by CML 2001 method.

Further, almost similar trends are observed in impact assessment by TRACI method also for all the adsorbents (Figure 5.41 (b)). The TTL shows maximum impacts in several categories, which include GWP, AP, EP, Ecotox Soil, Ecotox Water, Human Health Cancer Air and Smog Air. Similarly, ABTL shows maximum impacts in Ecotox Air, Human Health Criteria Air, and Human Health Non Cancer Air, whereas, ATL shows maximum impacts in remaining categories like ODP, Human Health Cancer Soil, Human Health Cancer Water, Human Health Non Cancer Soil and Human Health Non Cancer Water. The highest contribution of ATL in these categories is observed due to the usage of HCl acid for surface modification of laterite soil. Although HCl is used for ABTL also, it is further neutralized by the base and thus the contribution of ABTL on these indicators is less than ATL.

On the basis of the above discussions, it seems that the overall environmental impacts of TTL, ATL, and ABTL as determined by the LCA study, follows the following order TTL>ABTL>ATL. It can be explained by the fact that the adsorption capacity of TTL is very small as compared to ABTL (50 % as compared to ABTL), therefore, it accounts for usage of large quantity (382 kg) of raw materials to produce

sufficient quantity (55.63 kg) of adsorbent required to treat 720 liters of water. Further, in post adsorption process, about 55.63 kg of spent adsorbent needs to be immobilized in the form of clay bricks (as it is assumed that there is no loss in adsorbent mass during the defluoridation process). Further, it is also observed that more laterite soil is required for the production of the required amount of ABTL than that of ATL to treat 720 liters water. The requirement of more amount of raw laterite for ABTL is due to some additional treatment steps for its production than ATL. On the other hand, it is observed that the specific uptake of three adsorbents for fluoride increases in the following order ABTL>ATL>TTL. Considering both environmental impacts and specific uptake, ABTL is found to be a suitable adsorbent for fluoride removal from the contaminated water.

5.7.3 Sensitivity Analysis of the LCA Process

Sensitivity analysis of the process is conducted in order to identify and evaluate the process steps with maximum contributions on various impact categories as well as to find out the alternative options to decrease the impacts by varying their input values. The details of the method adopted for calculating the environmental data are given in Section 4.12.3 along with the different scenarios considered for carrying out the sensitivity analysis.

On performing the sensitivity analysis, it is observed that the transportation of the raw material was one of the major contributors in the impact categories like GWP, acidification potential and eutrophication potential due to emission of greenhouse gases and other gases like SOx, NOx etc. A comparison is done between original scenario and the revised scenario in the above mentioned impact categories and is shown through Figure 5.42 (a) to (c).

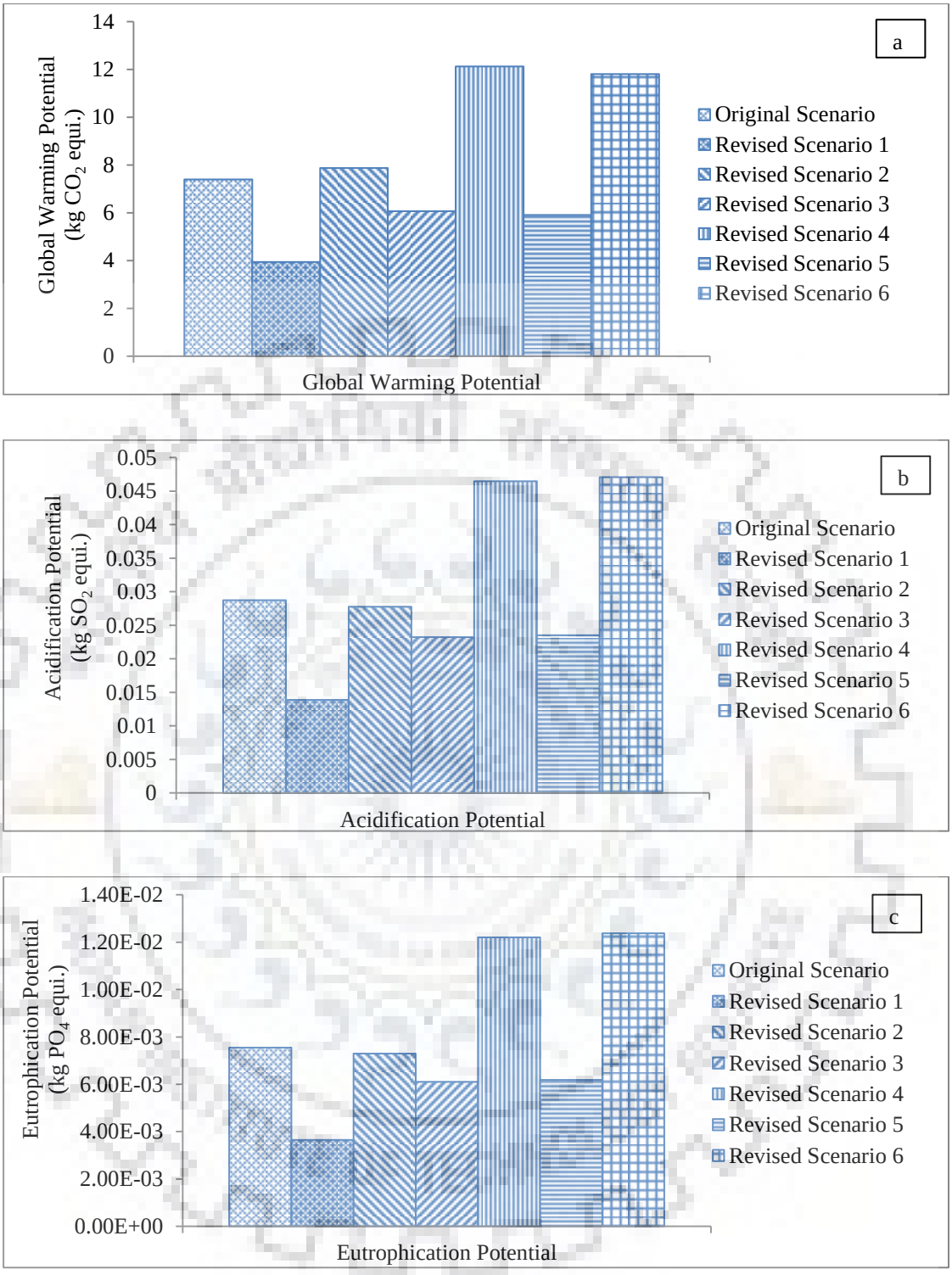

Figure 5.42 Comparison of effects of variation in transportation capacity of the truck trailer and the transportation distance on the global warming potential (a), acidification potential (b) and eutrophication potential (c) under different scenarios

From Figure 5.42, the following points are evident:

On comparing the alternative scenarios with the originally presented scenario, a decrease in the impacts is observed in all three above mentioned categories when the distance of carrying load is kept 5 km. In the case of a vehicle having 5 ton loading capacity and transportation distance as 5 km, the impacts are reduced to nearly 50 % and by increasing the transportation distance to 10 km, it had almost similar impacts as compared to original scenario in all the three categories.

Moreover, for the present case, maximum amount of raw material required is 382 kg for the synthesis of sufficient adsorbent (in case of TTL) for the treatment of stipulated amount (720 liters) of contaminated water and a truck trailer having a default capacity of 5 tons would be sufficient to carry enough raw material to last for synthesis of 13 batches of TTL adsorbent. Similarly, a higher number of batches of ATL (~16) and ABTL (~13.5) can be synthesized from 5 tons of raw laterite soil. By using light engine vehicles, the emissions are less due to their high fuel economy and hence lesser emissions [Sivak and Schoettle 2012, National Research Council, 2010].

Alternate modes of transportation of raw material like railway or by air were not considered as the distance between the mining site and the processing site is assumed to be very less (5 km) and hence it would not be economically feasible to use these.

Moreover, the total impacts caused by each of the treatment steps under original scenario (using a truck trailer of 27 tons capacity and the distance between the mining site and the processing site taken as 5 km) is also given in Table 5.19 and Table 5.20.

Table 5.19 Total impact caused by each treatment step as per the CML 2001 method

	GWP 100 years (kg CO_2 equi.)	AP (kg SO_2 equi.)	EP (kg phosphate equi.)	ODP, steady state (kg R-11 equi.)	ADP elements (kg Sb equi.)	ADP fossil (MJ)	FAETP (kg DCB equi.)	HTP (kg DCB equi.)	MAETP (kg DCB equi.)	TETP (kg DCB equi.)
TTL	14.67	0.1	2.25E-2	2.57E-10	2.60E-07	1.05E2	1.13E-1	1.09	9.70E+2	2.21E-1
ATL	11.09	0.07	0.02	1.79E-10	1.86E-07	73.45	0.08	0.76	674.46	0.154
ABTL	11.93	0.08	0.02	1.27E-09	1.12E-07	64.29	0.06	1.02	2712.05	0.11

Table 5.20 Total impact caused by each treatment step as per the TRACI method

	GWP (kg CO_2 equi.)	AP (kg H^+ moles equi.)	EP (kg N equi.)	ODP (kg CFC-11 equi.)	Ecotox Air (PAF m^3day/kg)	Ecotox Soil (PAF m^3day/kg)	Ecotox Water (PAF m^3day/ kg)	Human Health Cancer Air (cases)	Human Health Cancer Soil (cases)	Human Health Cancer Water (cases)	Human Health Criteria Air (kg PM10 Equi.)	Human Health Non-Cancer Air (cases)	Human Health Non-Cancer Soil (cases)	Human Health Non-Cancer Water (cases)	Smog Air (kg O_3 equi.)
TTL	14.68	6.34	2.30E-2	2.74E-10	0.12	2.86	1.47	8.93E-9	1.13E-9	2.10E-9	9.84E-3	3.44	7.10E-7	6.82E-9	1.95
ATL	11.09	4.68	0.02	1.87E-9	0.08	1.99	1.03	6.82E-10	7.79E-9	1.43E-8	0.001	2.4	4.88E-6	4.05E-8	1.47
ABTL	11.93	4.98	0.01	1.37E-9	0.14	1.42	0.74	5.00E-9	5.58E-9	1.02E-8	0.011	6.03	3.5E-6	2.92E-8	1.55

CHAPTER 6

CONCLUSIONS AND RECOMMANDATIONS

Conclusions of the present work along with some scopes for further investigation are provided below:

6.1 CONCLUSIONS

From the present investigation on the simultaneous and individual removal of arsenic and fluoride from synthetic and real groundwater through batch and continuous adsorption on laterite soil based and aluminum oxide/hydroxide nanoparticles based adsorbents; spent adsorbent management studies and the LCA studies for the defluoridation of water using laterite soil based adsorbents; the following conclusions have been drawn:

6.1.1. Removal of Arsenic and Fluoride by the Adsorbents

- Out of different laterite soil based adsorbents, ABTL is found to be most efficient.
- For single component system, the optimal conditions for maximum removal of arsenic and fluoride are found at pH 5, adsorbent dose 20 g/L and contact time 300 min for ABTL; and pH 7, adsorbent dose 2 g/L and 8 g/L for As and F respectively and contact time as 300 min for AHNP.
- Both Langmuir and Freundlich isotherms fitted the equilibrium data well; however Langmuir isotherm described the adsorption process better for single component system for both the adsorbents.
- The maximum Langmuir adsorption capacities are found to be 769 µg/g and 526 µg/g for arsenic and fluoride respectively for ABTL and 833.33 and 2000 µg/g for arsenic and fluoride, respectively for AHNP.
- Both the anions followed pseudo second order kinetics for adsorption.
- In the binary system, extended Freundlich model fitted best the experimental data for both arsenic and fluoride for ABTL and modified competitive Langmuir model for AHNP.
- The binary adsorbate mixture having arsenic and fluoride in varying concentration indicates the antagonistic behavior for fluoride and slight synergistic behavior for arsenic for both the adsorbents.

- Adsorption capacity (specific uptake) of ABTL in column is not improved whereas the adsorption capacity (specific uptake) of AHNP increases in column reactor.
- ABTL can be suitable for As only whereas, AHNP can be suitable for both As and F.

6.1.2. Management of the Spent Adsorbents

- The density of the sintered brick specimens is found to range between 1.81 and 2.3 g/cm^3 whereas, the percentage water absorption and percentage shrinkage for the sintered brick specimen are found to range between 11.4 % to 14.5 % and 1.3 % to 10.2 % respectively.
- Compressible strengths of the sintered brick specimen varies from 35 to 150 kg/cm^2 within a variation of percentage of spent adsorbents and sintering temperature.
- It is observed that the ratio of spent adsorbent to clay should remain below 30:70 (w/w) in the bricks so as to achieve compressive strengths as per the Indian Standards.
- Leaching test of arsenic and fluoride from the sintered brick specimen are also conducted. The maximum concentration of arsenic and fluoride in the leachate are found as 510 µg/L and 2100 µg/L respectively which are below the prescribed limit of USEPA.

6.1.3. LCA study of the defluoridation process by laterite soil based adsorbents

- In the LCA of defluoridation process, the environmental impacts are found to be proportional to raw material requirement and inversely proportional to the adsorption capacity of the adsorbent.
- Almost similar patterns of impacts are observed when the impacts are calculated with CML 2001 and TRACI method.
- In order to reduce the environmental and human impact, the adsorption capacity of the adsorbents should be increased and transportation of the raw materials should be minimized. Further, the sensitivity analysis of the present LCA study revealed that the environmental impacts may be reduced by using a vehicle having lower carrying capacity and reducing the distance between the mining site of the raw laterite and the processing site.

6.2 RECOMMENDATIONS

On the basis of present investigations, some of the important recommendations that can be useful for the future researchers and for interest of knowledge are as follows:

- Investigations on thermodynamic studies for the removal of arsenic and fluoride by both the adsorbents in batch mode of operation.
- Investigations on isotherm and kinetic study with the help of more models in batch as well as column mode of operation.
- Investigations on assessing the performance of adsorbents with real groundwater from more contaminated sites.
- Investigations on column studies by varying concentration of arsenic and fluoride in the influent and also by varying the bed depth of the column.
- Investigation on LCA study of the dearsination process should also be carried out with the help of ABTL adsorption.
- Investigations on LCA study of the defluoridation and dearsination process should also be carried out with the help of AHNP adsorbents.

APPENDIX-A

DETAILS OF SOME IMPORTANT ANALYTICAL INSTRUMENTS USED IN THE PRESENT INVESTIGATION

Name of Instrument	Model & Make	Operating Conditions	Remarks
ICP-MS (for detection of arsenic)	Perkin Elmer ICP-MS, model ELAN-DRC-e	Foreword power: 1100 W, extraction voltage: 200 V, Argon gas pressure: 4-5 kg/cm^2 , plasma gas flow rate: 15 L/min, nebulizer gas flow rate: 0.93 L/min auxiliary gas flow rate: 1.2 L/min	Detection limit: 0.026 µg/L Accuracy: 98 ±1%
Ion meter	Orlab India, model-OR930, India	TISAB solution: 1:1 (v/v) with sample pH: 5-8	Detection limit: F: 0.02 mg/l Accuracy: ± 1 mV
FESEM-EDX	FE-SEM QUANTA 200 FEG from FEI Netherlands	Resolution: <2 nm @ 30 kV-high vacuum –with SED Magnification: 12 X-1000 kX, Acceleration voltage: 200V- 30 kV	Sample thickness < 1cm
FTIR	Thermo FT-IR Spectrometer Model: Nicolet 6700	KBR Plate method, around 10 mg of dried sample was dispersed in 100 mg of spectroscopic grade.	Detection limit: Able to detect qualitatively the presence of few µg of element in sample.
X-Ray Diffractometer (X-ray diffraction pattern of adsorbents)	Bruker, Model D8 Advance	Cu target X-ray diffraction with 2θ: 5-100 degree, Working voltage: 10-100 kV, Tube current: 4 to 80 mA	Can work within 2θ: 0-150 degree

Peristaltic pump	Peristaltic pump, model: Miclins PP20 and Miclins PP20 EX	Flow range: 0.5 ml/min to 2110 ml/min No of channels: 1 No of rollers: 3 and 4 Tube size: ID:2 mm to 8 mm WT:1.5 mm	Accuracy: ±2%
Weighing machine	Weighing Machine, model AUW220D, Shimadzu Corporation, Kyoto, Japan	Maximum capacity : 220g Minimum capacity: 0.1mg Pan size (mm): 80 diameter	Repeatability (standard deviation) : ≤ 0.05 mg

APPENDIX-B

PHOTOGRAPHS OF IMPORTANT ANALYTICAL INSTRUMENTS AS WELL AS SOME AUXILIARY INSTRUMENTS USED IN THE PRESENT STUDY

FTIR, Thermo model Nicolet 6700

ICP-MS, Perkin Elmer model ELAN-DRC-e

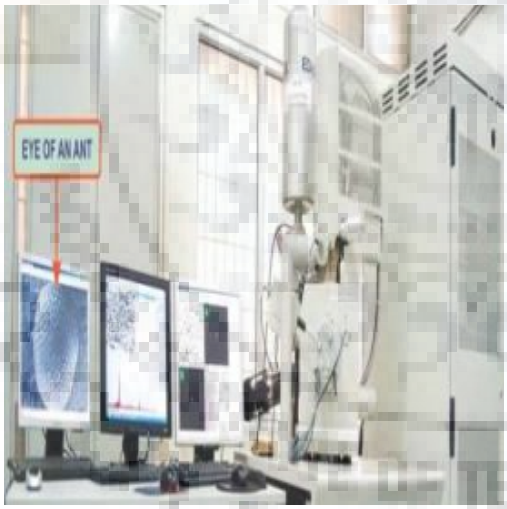

FE-SEM QUANTA 200 FEG from FEI Netherlands

Ion meter. Orlab India, model-OR930

X-Ray Diffractometer, Bruker, model D8 Advance

Some Auxiliary Instruments Used in the Present Investigation

Milli-Q water unit, Millipore Corp.

APPENDIX-C

IMPORTANT CALIBRATION GRAPHS USED IN THE PRESENT INVESTIGATION

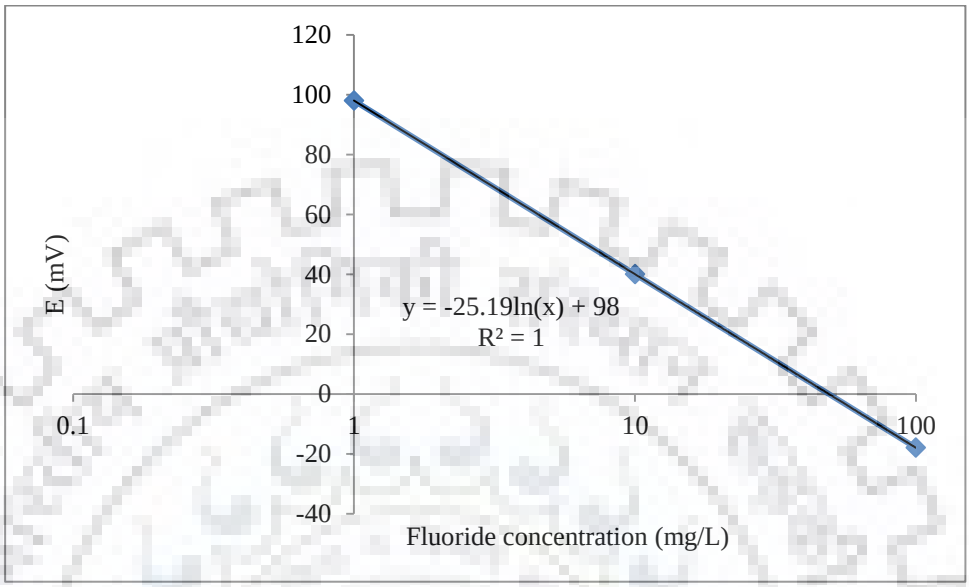

Figure C-1 Calibration curve for the detection of fluoride

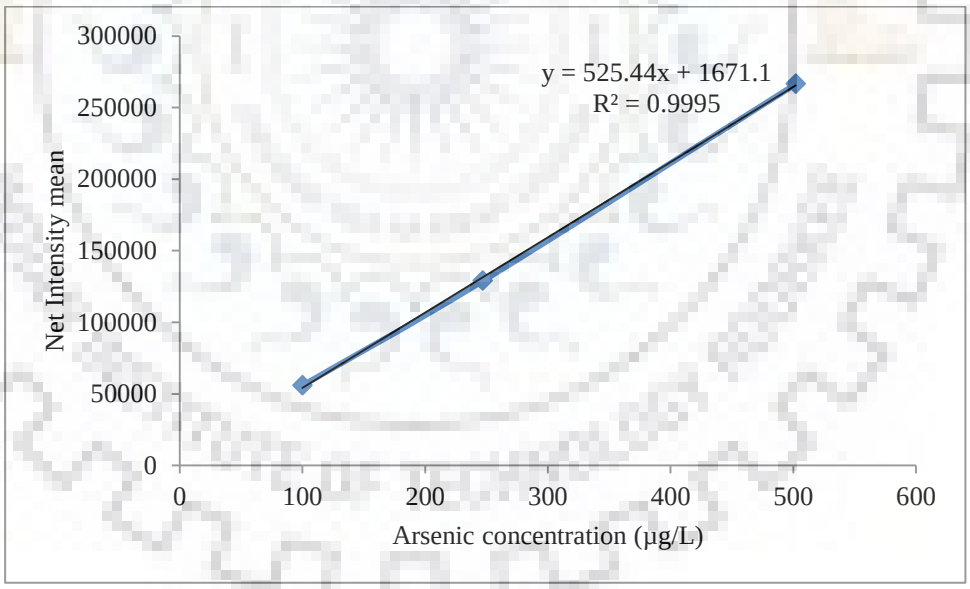

Figure C-2 Calibration curve for the detection of arsenic

APPENDIX-D

DETAILS OF SOME IMPORTANT REAGENTS USED AND THEIR SPECIFICATION

Table D-1 Reagents used in the present investigation and their specification

Chemical (s)	Molecular weight	Make	Assay/ Purity (%)
Sodium arsenite, $NaAsO_2$	129.91	Loba chemie	98.0
Sodium fluoride NaF	41.99	Thomas baker	98.5
Sodium chloride NaCl	58.44	Do	99.5
Hydrochloric acid, HCl	36.46	Do	35.4
Sodium hydroxide, NaOH	40.00	Do	98
Nitric acid, HNO_3	63.01	Do	69-72

APPENDIX-E

PREPARATION OF STOCK SOLUTIONS

Preparation of Stock As (III) Solution (1000 mg/l)

1.734 g $NaAsO_2$ was added in the 100 ml of Milli-Q water in a 1000 ml volumetric flask. It was dissolved by shaking and the volume was made up to the mark. Arsenite concentration of this solution was 1000 mg/l

Preparation of stock F solution (1000 mg/l)

2.211 g of NaF was added in 100 ml of Milli-Q water in a 1000 ml volumetric flask. It was dissolved by shaking and the volume was made up to the mark. Fluoride concentration of this solution was 1000 mg/l

PREPARATION OF STANDARD SOLUTIONS FROM STOCK SOLUTIONS

Primary and secondary standards of the above solutions were prepared by dilutions with Milli-Q water.

REFERENCES

1. Ahmaruzzaman, M. (2011). Industrial wastes as low-cost potential adsorbents for the treatment of wastewater laden with heavy metals. *Advances in colloid and interface science*, *166*(1-2), 36-59.
2. Aiuppa, A., Dongarrà, G., Capasso, G., & Allard, P. (2000). Trace elements in the thermal groundwaters of Vulcano Island (Sicily). *Journal of Volcanology and Geothermal Research*, *98*(1-4), 189-207.
3. Aksu Z, Açikel Ü, Kutsal T. Investigation of simultaneous biosorption of copper (II) and chromium (VI) on dried Chlorella Vulgaris from binary metal mixtures: Application of multicomponent adsorption isotherms. Separation Science and Technology, 1999, 34(3): 501–524.
4. Ali, I., ALOthman, Z. A., & Sanagi, M. M. (2015). Green synthesis of iron nano-impregnated adsorbent for fast removal of fluoride from water. *Journal of Molecular Liquids*, *211*, 457-465.
5. Andjelkovic, I., Tran, D. N., Kabiri, S., Azari, S., Markovic, M., & Losic, D. (2015). Graphene aerogels decorated with α-FeOOH nanoparticles for efficient adsorption of arsenic from contaminated waters. *ACS applied materials & interfaces*, *7*(18), 9758-9766.
6. Aredes, S., Klein, B., & Pawlik, M. (2012). The removal of arsenic from water using natural iron oxide minerals. *Journal of Cleaner Production*, *29*, 208-213.
7. Arena, N., Lee, J., & Clift, R. (2016). Life Cycle Assessment of activated carbon production from coconut shells. *Journal of Cleaner Production*, *125*, 68-77.
8. Armienta, M. A., & Segovia, N. (2008). Arsenic and fluoride in the groundwater of Mexico. *Environmental Geochemistry and Health*, *30*(4), 345-353.
9. Ayoob, S., & Gupta, A. K. (2006). Fluoride in drinking water: a review on the status and stress effects. *Critical Reviews in Environmental Science and Technology*, *36*(6), 433-487.
10. Ayoob, S., Gupta, A. K., & Bhakat, P. B. (2007). Performance evaluation of modified calcined bauxite in the sorptive removal of arsenic (III) from aqueous environment. *Colloids and Surfaces A: Physicochemical and Engineering Aspects*, *293*(1-3), 247-254.

11. Bahar, M. M., Mahbub, K. R., Naidu, R., & Megharaj, M. (2018). As (V) removal from aqueous solution using a low-cost adsorbent coir pith ash: Equilibrium and kinetic study. *Environmental Technology & Innovation*.
12. Baig, S. A., Sheng, T., Hu, Y., Lv, X., & Xu, X. (2013). Adsorptive removal of arsenic in saturated sand filter containing amended adsorbents. *Ecological engineering*, *60*, 345-353.
13. Balasubramanian, N., Kojima, T., & Srinivasakannan, C. (2009). Arsenic removal through electrocoagulation: kinetic and statistical modeling. *Chemical Engineering Journal*, *155*(1-2), 76-82.
14. Banerjee, P., Chakrabarti, S., Maitra, S., & Dutta, B. K. (2012). Zinc oxide nano-particles–sonochemical synthesis, characterization and application for photo-remediation of heavy metal. *Ultrasonics sonochemistry*, *19*(1), 85-93.
15. Basha, C. A., Selvi, S. J., Ramasamy, E., & Chellammal, S. (2008). Removal of arsenic and sulphate from the copper smelting industrial effluent. *Chemical Engineering Journal*, *141*(1-3), 89-98.
16. Bednar, A. J., Garbarino, J. R., Ranville, J. F., & Wildeman, T. R. (2002). Presence of organoarsenicals used in cotton production in agricultural water and soil of the southern United States. *Journal of agricultural and food chemistry*, *50*(25), 7340-7344.
17. Bektaş, N., Aydın, S., & Öncel, M. S. (2011). The adsorption of arsenic ions using beidellite, zeolite, and sepiolite clays: a study of kinetic, equilibrium and thermodynamics. *Separation Science and Technology*, *46*(6), 1005-1016.
18. Bharali, R. K., & Bhattacharyya, K. G. (2015). Biosorption of fluoride on Neem (Azadirachta indica) leaf powder. *Journal of Environmental Chemical Engineering*, *3*(2), 662-669.
19. Bhargavi, R. J., Maheshwari, U., & Gupta, S. (2015). Synthesis and use of alumina nanoparticles as an adsorbent for the removal of Zn (II) and CBG dye from wastewater. *International Journal of Industrial Chemistry*, *6*(1), 31-41.
20. Bhatnagar, J. M., & Goel, R. K. (2002). Thermal changes in clay products from alluvial deposits of the Indo–Gangetic plains. *Construction and Building Materials*, *16*(2), 113-122.
21. Bhaumik, M., Noubactep, C., Gupta, V. K., McCrindle, R. I., & Maity, A. (2015). Polyaniline/Fe0 composite nanofibers: An excellent adsorbent for the removal of arsenic from aqueous solutions. *Chemical Engineering Journal*, *271*, 135-146.

22. Bibi, S., Farooqi, A., Hussain, K., & Haider, N. (2015). Evaluation of industrial based adsorbents for simultaneous removal of arsenic and fluoride from drinking water. *Journal of cleaner production*, *87*, 882-896.
23. Bibi, S., Farooqi, A., Ramzan, M., & Javed, A. (2015). Health risk of arsenic in the alluvial aquifers of Lahore and Raiwind, Punjab Province, Pakistan: an investigation for safer well water. *Toxicological & Environmental Chemistry*, *97*(7), 888-907.
24. Bissen, M., & Frimmel, F. H. (2003). Arsenic—a review. Part II: oxidation of arsenic and its removal in water treatment. *CLEAN–Soil, Air, Water*, *31*(2), 97-107.
25. Biswas, K., Gupta, K., & Ghosh, U. C. (2009). Adsorption of fluoride by hydrous iron (III)–tin (IV) bimetal mixed oxide from the aqueous solutions. *Chemical Engineering Journal*, *149*(1-3), 196-206.
26. Biswas, K., Gupta, K., Goswami, A., & Ghosh, U. C. (2010). Fluoride removal efficiency from aqueous solution by synthetic iron (III)–aluminum (III)–chromium (III) ternary mixed oxide. *Desalination*, *255*(1-3), 44-51.
27. Borah, K. K., Bhuyan, B., & Sarma, H. P. (2010). Lead, arsenic, fluoride, and iron contamination of drinking water in the tea garden belt of Darrang district, Assam, India. *Environmental monitoring and assessment*, *169*(1-4), 347-352.
28. Brahman, K. D., Kazi, T. G., Afridi, H. I., Naseem, S., Arain, S. S., Wadhwa, S. K., & Shah, F. (2013). Simultaneously evaluate the toxic levels of fluoride and arsenic species in underground water of Tharparkar and possible contaminant sources: a multivariate study. *Ecotoxicology and environmental safety*, *89*, 95-107.
29. Brahman, K. D., Kazi, T. G., Baig, J. A., Afridi, H. I., Khan, A., Arain, S. S., & Arain, M. B. (2014). Fluoride and arsenic exposure through water and grain crops in Nagarparkar, Pakistan. *Chemosphere*, *100*, 182-189.
30. Buamah, R., Oduro, C. A., & Sadik, M. H. (2016). Fluoride removal from drinking water using regenerated aluminum oxide coated media. *Journal of Environmental Chemical Engineering*, *4*(1), 250-258.
31. Bureau of Indian Standards, Drinking Water Specification, IS 10500, 2012, New Delhi
32. Cai, H. M., Chen, G. J., Peng, C. Y., Zhang, Z. Z., Dong, Y. Y., Shang, G. Z., ... & Wan, X. C. (2015). Removal of fluoride from drinking water using tea waste loaded with Al/Fe oxides: A novel, safe and efficient biosorbent. *Applied Surface Science*, *328*, 34-44.

33. Canales, R. M., Guan, H., Bestland, E., Hutson, J., & Simmons, C. T. (2013). Particle-size effects on dissolved arsenic adsorption to an Australian laterite. *Environmental earth sciences*, *68*(8), 2301-2312.
34. Chakravarty, S., Dureja, V., Bhattacharyya, G., Maity, S., & Bhattacharjee, S. (2002). Removal of arsenic from groundwater using low cost ferruginous manganese ore. *Water research*, *36*(3), 625-632.
35. Chandra Srivastava, V., Deo Mall, I., & Mani Mishra, I. (2006). Modelling individual and competitive adsorption of cadmium (II) and zinc (II) metal ions from aqueous solution onto bagasse fly ash. *Separation science and technology*, *41*(12), 2685-2710.
36. Chatterjee, S., & De, S. (2017). Adsorptive removal of arsenic from groundwater using chemically treated iron ore slime incorporated mixed matrix hollow fiber membrane. *Separation and Purification Technology*, *179*, 357-368.
37. Chaurasia, S. C., Sahayam, A. C., Venkateswarlu, G., Dhavile, S. M., Thangavel, S., & Rastogi, L. (2012). Groundwater contamination problems in rural India: detection and remediation at the household level. *Barc Newsletter*, *324*, 39-45.
38. Chen, A. S., Sorg, T. J., & Wang, L. (2015). Regeneration of iron-based adsorptive media used for removing arsenic from groundwater. *Water research*, *77*, 85-97.
39. Chen, L., Zhang, K. S., He, J. Y., Xu, W. H., Huang, X. J., & Liu, J. H. (2016). Enhanced fluoride removal from water by sulfate-doped hydroxyapatite hierarchical hollow microspheres. *Chemical Engineering Journal*, *285*, 616-624.
40. Chiang, K. Y., Chien, K. L., & Hwang, S. J. (2008). Study on the characteristics of building bricks produced from reservoir sediment. *Journal of Hazardous Materials*, *159*(2-3), 499-504.
41. Choong, T. S., Chuah, T. G., Robiah, Y., Koay, F. G., & Azni, I. (2007). Arsenic toxicity, health hazards and removal techniques from water: an overview. *Desalination*, *217*(1-3), 139-166.
42. Christina, E., & Viswanathan, P. (2015). Development of a novel nano-biosorbent for the removal of fluoride from water. *Chinese Journal of Chemical Engineering*, *23*(6), 924-933.
43. Çiftçi, T. D., & Henden, E. (2015). Nickel/nickel boride nanoparticles coated resin: A novel adsorbent for arsenic (III) and arsenic (V) removal. *Powder Technology*, *269*, 470-480.

44. CPCB standard, 1986. General standards for discharge of environmental pollutant, Part A: Effluents as per Schedule VI of the Environmental (Protection) Rules 1986, (http://cpcb.nic.in/GeneralStandards.pdf, access date 28.01.17)

45. Creed, J.T., Brockhoff, C.A. and Martin, T.D., 1994. Determination of trace elements in waters and wastes by inductively coupled plasma–mass spectrometry, Method 200.8. Environmental Monitoring Systems Laboratory. Office of Research and Development. US Environmental Protection Agency. Cincinnati, OH. Rev 5.

46. Cui, J., Jing, C., Che, D., Zhang, J., & Duan, S. (2015). Groundwater arsenic removal by coagulation using ferric (III) sulfate and polyferric sulfate: a comparative and mechanistic study. *Journal of Environmental Sciences*, *32*, 42-53.

47. Das, N., Pattanaik, P., & Das, R. (2005). Defluoridation of drinking water using activated titanium rich bauxite. *Journal of Colloid and Interface Science*, *292*(1), 1-10.

48. Das, S., Mehta, B. C., Das, P. K., Srivastava, S. K., & Samanta, S. K. (1999). Sources of high fluoride in ground water around Anugul, Dhenkenal District, Orissa. *POLLUTION RESEARCH*, *18*(1), 21-28.

49. Das, S., Metha, B. C., Das, P. K., Srivastava, S. K., & Samanta, S. K. (1998). Source of High Fluoride in Ground Water Around Anugul, Dhenkenal District, Orissa. *Pollution Research*, *17*, 385-392.

50. Dash, S. S., Sahu, M. K., Sahu, E., & Patel, R. K. (2015). Fluoride removal from aqueous solutions using cerium loaded mesoporous zirconium phosphate. *New Journal of Chemistry*, *39*(9), 7300-7308.

51. Dayananda, D., Sarva, V. R., Prasad, S. V., Arunachalam, J., & Ghosh, N. N. (2014). Preparation of CaO loaded mesoporous Al2O3: Efficient adsorbent for fluoride removal from water. *Chemical Engineering Journal*, *248*, 430-439.

52. Dayananda, D., Sarva, V. R., Prasad, S. V., Arunachalam, J., Parameswaran, P., & Ghosh, N. N. (2015). Synthesis of MgO nanoparticle loaded mesoporous Al2O3 and its defluoridation study. *Applied Surface Science*, *329*, 1-10.

53. Deng, H., & Yu, X. (2012). Adsorption of fluoride, arsenate and phosphate in aqueous solution by cerium impregnated fibrous protein. *Chemical Engineering Journal*, *184*, 205-212.

54. Deng, H., & Yu, X. (2015). Fluoride removal from drinking water by zirconium-impregnated fibrous protein. *Desalination and Water Treatment*, *54*(6), 1594-1603.

55. Ding, M., Szymczyk, A., & Ghoufi, A. (2015). On the structure and rejection of ions by a polyamide membrane in pressure-driven molecular dynamics simulations. *Desalination*, *368*, 76-80.
56. Dominguez-Ramos, A., Chavan, K., García, V., Jimeno, G., Albo, J., Marathe, K. V., ... & Irabien, A. (2014). Arsenic removal from natural waters by adsorption or ion exchange: an environmental sustainability assessment. *Industrial & Engineering Chemistry Research*, *53*(49), 18920-18927.
57. Dong, S., & Wang, Y. (2016). Characterization and adsorption properties of a lanthanum-loaded magnetic cationic hydrogel composite for fluoride removal. *Water research*, *88*, 852-860.
58. Dou, X., Zhang, Y., Wang, H., Wang, T., & Wang, Y. (2011). Performance of granular zirconium–iron oxide in the removal of fluoride from drinking water. *Water research*, *45*(12), 3571-3578.
59. Drinking Water Standards and Health Advisories, EPA 822-S-12–001, Office of Water, U.S Environmental Protection Agency, 2012 Edition, Washington, DC
60. Dugo, G., Pellicano, T. M., La Pera, L., Turco, V. L., Tamborrino, A., & Clodoveo, M. L. (2007). Determination of inorganic anions in commercial seed oils and in virgin olive oils produced from de-stoned olives and traditional extraction methods, using suppressed ion exchange chromatography (IEC). *Food chemistry*, *102*(3), 599-605.
61. Ekka, B., Dhaka, R. S., Patel, R. K., & Dash, P. (2017). Fluoride removal in waters using ionic liquid-functionalized alumina as a novel adsorbent. *Journal of Cleaner Production*, *151*, 303-318.
62. Elwakeel, K. Z., & Guibal, E. (2015). Arsenic (V) sorption using chitosan/Cu (OH) 2 and chitosan/CuO composite sorbents. *Carbohydrate polymers*, *134*, 190-204.
63. Essadki, A. H., Gourich, B., Vial, C., Delmas, H., & Bennajah, M. (2009). Defluoridation of drinking water by electrocoagulation/electroflotation in a stirred tank reactor with a comparative performance to an external-loop airlift reactor. *Journal of hazardous materials*, *168*(2-3), 1325-1333.
64. Fan, L., Zhang, S., Zhang, X., Zhou, H., Lu, Z., & Wang, S. (2015). Removal of arsenic from simulation wastewater using nano-iron/oyster shell composites. *Journal of environmental management*, *156*, 109-114.
65. Fang, F., Jia, Y., Wu, P. Y., Zhang, Q. Y., Jiang, Y. P., Zhou, S. S., & Peng, D. Y. (2015). Facile one-pot preparation of goethite/parabutlerite nanocomposites and

their removal properties and mechanism toward As (V) ions. *Applied Surface Science*, *324*, 355-362.

66. Farooqi, A., Masuda, H., & Firdous, N. (2007). Toxic fluoride and arsenic contaminated groundwater in the Lahore and Kasur districts, Punjab, Pakistan and possible contaminant sources. *Environmental Pollution*, *145*(3), 839-849.
67. Fritz W, Schluender E U. Simultaneous adsorption equilibria of organic solutes in dilute aqueous solutions on activated carbon. Chemical Engineering Science, 1974, 29(5): 1279-1282.
68. Gai, W. Z., Deng, Z. Y., & Shi, Y. (2015). Fluoride removal from water using high-activity aluminum hydroxide prepared by the ultrasonic method. *RSC Advances*, *5*(102), 84223-84231.
69. Ghorai, S., & Pant, K. K. (2004). Investigations on the column performance of fluoride adsorption by activated alumina in a fixed-bed. *Chemical Engineering Journal*, *98*(1-2), 165-173.
70. Ghorai, S., & Pant, K. K. (2005). Equilibrium, kinetics and breakthrough studies for adsorption of fluoride on activated alumina. *Separation and purification technology*, *42*(3), 265-271.
71. Ghosal, P. S., Kattil, K. V., Yadav, M. K., & Gupta, A. K. (2018). Adsorptive removal of arsenic by novel iron/olivine composite: Insights into preparation and adsorption process by response surface methodology and artificial neural network. *Journal of environmental management*, *209*, 176-187.
72. Glocheux, Y., Pasarín, M. M., Albadarin, A. B., Allen, S. J., & Walker, G. M. (2013). Removal of arsenic from groundwater by adsorption onto an acidified laterite by-product. *Chemical Engineering Journal*, *228*, 565-574.
73. Gogoi, S., & Dutta, R. K. (2016). Fluoride removal by hydrothermally modified limestone powder using phosphoric acid. *Journal of Environmental Chemical Engineering*, *4*(1), 1040-1049.
74. Goldberg, S., & Johnston, C. T. (2001). Mechanisms of arsenic adsorption on amorphous oxides evaluated using macroscopic measurements, vibrational spectroscopy, and surface complexation modeling. *Journal of colloid and Interface Science*, *234*(1), 204-216.
75. Gomez, M. L., Blarasin, M. T., & Martínez, D. E. (2009). Arsenic and fluoride in a loess aquifer in the central area of Argentina. *Environmental Geology*, *57*(1), 143-155.

76. Goswami, A., & Purkait, M. K. (2011). Kinetic and equilibrium study for the fluoride adsorption using pyrophyllite. *Separation Science and Technology*, *46*(11), 1797-1807.
77. Greenwood, N. N., & Earnshaw, A. (2012). *Chemistry of the Elements*. Elsevier.
78. Guo, L., Ye, P., Wang, J., Fu, F., & Wu, Z. (2015). Three-dimensional Fe3O4-graphene macroscopic composites for arsenic and arsenate removal. *Journal of hazardous materials*, *298*, 28-35.
79. Gupta, V. K., Saini, V. K., & Jain, N. (2005). Adsorption of As (III) from aqueous solutions by iron oxide-coated sand. *Journal of colloid and interface science*, *288*(1), 55-60.
80. Hashim, M. A., Mukhopadhyay, S., Sahu, J. N., & Sengupta, B. (2011). Remediation technologies for heavy metal contaminated groundwater. *Journal of environmental management*, *92*(10), 2355-2388.
81. Hazarika, S., & Bhuyan, B. (2013). Fluoride, arsenic and iron content of groundwater around six selected tea gardens of Lakhimpur District, Assam, India. *Arch Appl Sci Res*, *5*(1), 57-61.
82. He, J., Ma, T., Deng, Y., Yang, H., & Wang, Y. (2009). Environmental geochemistry of high arsenic groundwater at western Hetao plain, Inner Mongolia. *Frontiers of Earth Science in China*, *3*(1), 63.
83. He, J., Siah, T. S., & Chen, J. P. (2014). Performance of an optimized Zr-based nanoparticle-embedded PSF blend hollow fiber membrane in treatment of fluoride contaminated water. *Water research*, *56*, 88-97.
84. He, J., Zhang, K., Wu, S., Cai, X., Chen, K., Li, Y., ... & Kong, L. (2016). Performance of novel hydroxyapatite nanowires in treatment of fluoride contaminated water. *Journal of hazardous materials*, *303*, 119-130.
85. Hjaila, K., Baccar, R., Sarrà, M., Gasol, C. M., & Blánquez, P. (2013). Environmental impact associated with activated carbon preparation from olive-waste cake via life cycle assessment. *Journal of environmental management*, *130*, 242-247.
86. Hu, X., Ding, Z., Zimmerman, A. R., Wang, S., & Gao, B. (2015). Batch and column sorption of arsenic onto iron-impregnated biochar synthesized through hydrolysis. *water research*, *68*, 206-216.

87. Huang, P. P., Cao, C. Y., Wei, F., Sun, Y. B., & Song, W. G. (2015). MgAl layered double hydroxides with chloride and carbonate ions as interlayer anions for removal of arsenic and fluoride ions in water. *RSC Advances*, *5*(14), 10412-10417.
88. Huong, P. T. L., Phan, V. N., Huy, T. Q., Nam, M. H., Lam, V. D., & Le, A. T. (2016). Application of Graphene Oxide-MnFe 2 O 4 Magnetic Nanohybrids as Magnetically Separable Adsorbent for Highly Efficient Removal of Arsenic from Water. *Journal of Electronic Materials*, *45*(5), 2372-2380.
89. Indu, R., Krishnan, S., & Shah, T. (2007). Impacts of groundwater contamination with fluoride and arsenic: affliction severity, medical cost and wage loss in some villages of India. *International Journal of Rural Management*, *3*(1), 69-93.
90. Iriel, A., Bruneel, S. P., Schenone, N., & Cirelli, A. F. (2018). The removal of fluoride from aqueous solution by a lateritic soil adsorption: Kinetic and equilibrium studies. *Ecotoxicology and environmental safety*, *149*, 166-172.
91. Ismail, Z. Z., & AbdelKareem, H. N. (2015). Sustainable approach for recycling waste lamb and chicken bones for fluoride removal from water followed by reusing fluoride-bearing waste in concrete. *Waste management*, *45*, 66-75.
92. Jagtap, S., Yenkie, M. K., Labhsetwar, N., & Rayalu, S. (2012). Fluoride in drinking water and defluoridation of water. *Chemical reviews*, *112*(4), 2454-2466.
93. Jiang, L., Xiao, S., & Chen, J. (2015). Removal behavior and mechanism of Co (II) on the surface of Fe–Mn binary oxide adsorbent. *Colloids and Surfaces A: Physicochemical and Engineering Aspects*, *479*, 1-10.
94. Jin, H., Ji, Z., Yuan, J., Li, J., Liu, M., Xu, C., ... & Hou, S. (2015). Research on removal of fluoride in aqueous solution by alumina-modified expanded graphite composite. *Journal of Alloys and Compounds*, *620*, 361-367.
95. Jing, C., Cui, J., Huang, Y., & Li, A. (2012). Fabrication, characterization, and application of a composite adsorbent for simultaneous removal of arsenic and fluoride. *ACS applied materials & interfaces*, *4*(2), 714-720.
96. Jozefaciuk, G. (2002). Effect of acid and alkali treatments on surface-charge properties of selected minerals. *Clays and Clay Minerals*, *50*(5), 647-656.
97. Julien, C. M., Massot, M., & Poinsignon, C. (2004). Lattice vibrations of manganese oxides: Part I. Periodic structures. *Spectrochimica Acta Part A: Molecular and Biomolecular Spectroscopy*, *60*(3), 689-700.

98. Kang, D., Tong, S., Yu, X., & Ge, M. (2015). Template-free synthesis of 3D hierarchical amorphous aluminum oxide microspheres with broccoli-like structure and their application in fluoride removal. *RSC Advances*, *5*(25), 19159-19165.
99. Kang, D., Yu, X., Tong, S., Ge, M., Zuo, J., Cao, C., & Song, W. (2013). Performance and mechanism of Mg/Fe layered double hydroxides for fluoride and arsenate removal from aqueous solution. *Chemical engineering journal*, *228*, 731-740.
100. Karmakar, S., Dechnik, J., Janiak, C., & De, S. (2016). Aluminium fumarate metal-organic framework: a super adsorbent for fluoride from water. *Journal of hazardous materials*, *303*, 10-20.
101. Kaygusuz, H., Uzaşçı, S., & Erim, F. B. (2015). Removal of fluoride from aqueous solution using aluminum alginate beads. *CLEAN–Soil, Air, Water*, *43*(5), 724-730.
102. Kemer, B., Ozdes, D., Gundogdu, A., Bulut, V. N., Duran, C., & Soylak, M. (2009). Removal of fluoride ions from aqueous solution by waste mud. *Journal of hazardous materials*, *168*(2-3), 888-894.
103. Khan, H., Sharma, C. R., & Sharma, S. (2017). Fabrication of sustainable organometallic polymeric adsorbents for remediation of fluoride from water: A novel approach. *Journal of Water Process Engineering*, *20*, 149-159.
104. Kilianová, M., Prucek, R., Filip, J., Kolařík, J., Kvítek, L., Panáček, A., ... & Zbořil, R. (2013). Remarkable efficiency of ultrafine superparamagnetic iron (III) oxide nanoparticles toward arsenate removal from aqueous environment, *Chemosphere*, *93*(11), 2690-2697.
105. Kim, S. H., Kim, K., Ko, K. S., Kim, Y., & Lee, K. S. (2012). Co-contamination of arsenic and fluoride in the groundwater of unconsolidated aquifers under reducing environments. *Chemosphere*, *87*(8), 851-856.
106. Kumar, M., Kumar, P., Ramanathan, A. L., Bhattacharya, P., Thunvik, R., Singh, U. K., ... & Sracek, O. (2010). Arsenic enrichment in groundwater in the middle Gangetic Plain of Ghazipur District in Uttar Pradesh, India. *Journal of Geochemical Exploration*, *105*(3), 83-94.
107. Kundu, S., & Gupta, A. K. (2008). Immobilization and leaching characteristics of arsenic from cement and/or lime solidified/stabilized spent adsorbent containing arsenic. *Journal of hazardous materials*, *153*(1-2), 434-443.

108. Lan, B., Wang, Y., Wang, X., Zhou, X., Kang, Y., & Li, L. (2016). Aqueous arsenic (As) and antimony (Sb) removal by potassium ferrate. *Chemical Engineering Journal*, *292*, 389-397.
109. Lee, H., Kim, D., Kim, J., Ji, M. K., Han, Y. S., Park, Y. T., ... & Choi, J. (2015). As (III) and As (V) removal from the aqueous phase via adsorption onto acid mine drainage sludge (AMDS) alginate beads and goethite alginate beads. *Journal of hazardous materials*, *292*, 146-154.
110. Lescano, M. R., Passalía, C., Zalazar, C. S., & Brandi, R. J. (2015). Arsenic sorption onto titanium dioxide, granular ferric hydroxide and activated alumina: Batch and dynamic studies. *Journal of Environmental Science and Health, Part A*, *50*(4), 424-431.
111. Li, L., Li, J., Shao, C., Zhang, K., Yu, S., Gao, N., ... & Yin, D. (2014). Arsenic removal in synthetic ground water using iron electrolysis. *Separation and Purification Technology*, *122*, 225-230.
112. Li, W., Cao, C. Y., Wu, L. Y., Ge, M. F., & Song, W. G. (2011). Superb fluoride and arsenic removal performance of highly ordered mesoporous aluminas. *Journal of hazardous materials*, *198*, 143-150.
113. Li, Z., Tang, X., Liu, K., Huang, J., Peng, Q., Ao, M., & Huang, Z. (2018). Fabrication of novel sandwich nanocomposite as an efficient and regenerable adsorbent for methylene blue and Pb (II) ion removal. *Journal of environmental management*, *218*, 363-373.
114. Lin, K. L. (2006). Feasibility study of using brick made from municipal solid waste incinerator fly ash slag. *Journal of Hazardous Materials*, *137*(3), 1810-1816.
115. Liu, R., Gong, W., Lan, H., Yang, T., Liu, H., & Qu, J. (2012). Simultaneous removal of arsenate and fluoride by iron and aluminum binary oxide: Competitive adsorption effects. *Separation and purification technology*, *92*, 100-105.
116. Loganathan, P., Vigneswaran, S., Kandasamy, J., & Naidu, R. (2013). Defluoridation of drinking water using adsorption processes. *Journal of hazardous materials*, *248*, 1-19.
117. Ma, Y., Shi, F., Zheng, X., Ma, J., & Gao, C. (2011). Removal of fluoride from aqueous solution using granular acid-treated bentonite (GHB): Batch and column studies. *Journal of hazardous materials*, *185*(2-3), 1073-1080.

118. Mahmood, S. J., Taj, F., Parveen, F., Usmani, T. H., Azmat, R., & Uddin, F. (2007). Arsenic, fluoride and nitrate in drinking water: the problem and its possible solution. *Research Journal of Environmental Sciences*, *1*(4), 179-184.
119. Mahramanlioglu, M., Kizilcikli, I., & Bicer, I. O. (2002). Adsorption of fluoride from aqueous solution by acid treated spent bleaching earth. *Journal of Fluorine Chemistry*, *115*(1), 41-47.
120. Maiti, A., Basu, J. K., & De, S. (2010). Removal of arsenic from synthetic and natural groundwater using acid-activated laterite. *Environmental Progress & Sustainable Energy*, *29*(4), 457-470.
121. Maiti, A., Basu, J. K., & De, S. (2011). Chemical treated laterite as promising fluoride adsorbent for aqueous system and kinetic modeling. *Desalination*, *265*(1-3), 28-36.
122. Maiti, A., Sharma, H., Basu, J. K., & De, S. (2009). Modeling of arsenic adsorption kinetics of synthetic and contaminated groundwater on natural laterite. *Journal of hazardous materials*, *172*(2-3), 928-934.
123. Maity, S., Chakravarty, S., Bhattacharjee, S., & Roy, B. C. (2005). A study on arsenic adsorption on polymetallic sea nodule in aqueous medium. *Water Research*, *39*(12), 2579-2590.
124. Maji, S. K., Pal, A., & Pal, T. (2008). Arsenic removal from real-life groundwater by adsorption on laterite soil. *Journal of Hazardous Materials*, *151*(2-3), 811-820.
125. Malakootian, M., Javdan, M., & Iranmanesh, F. (2015). Fluoride removal study from aqueous solutions using Jajarm bauxite: case study on Koohbanan water. *Fluoride*, *48*(2), 113.
126. Maliyekkal, S. M., Sharma, A. K., & Philip, L. (2006). Manganese-oxide-coated alumina: a promising sorbent for defluoridation of water. *Water research*, *40*(19), 3497-3506.
127. Maliyekkal, S. M., Shukla, S., Philip, L., & Nambi, I. M. (2008). Enhanced fluoride removal from drinking water by magnesia-amended activated alumina granules. *Chemical Engineering Journal*, *140*(1-3), 183-192.
128. Malwal, D., & Gopinath, P. (2017). Silica Stabilized Magnetic-Chitosan Beads for Removal of Arsenic from Water. *Colloid and Interface Science Communications*, *19*, 14-19.
129. Mamindy-Pajany, Y., Hurel, C., Marmier, N., & Roméo, M. (2009). Arsenic adsorption onto hematite and goethite. *Comptes Rendus Chimie*, *12*(8), 876-881.

130. Mariappan, R., Vairamuthu, R., & Ganapathy, A. (2015). Use of chemically activated cotton nut shell carbon for the removal of fluoride contaminated drinking water: kinetics evaluation. *Chinese Journal of Chemical Engineering*, *23*(4), 710-721.
131. Marquardt, D. W. (1963). An algorithm for least-squares estimation of nonlinear parameters. *Journal of the society for Industrial and Applied Mathematics*, *11*(2), 431-441.
132. McQuaker, N. R., & Gurney, M. (1977). Determination of total fluoride in soil and vegetation using an alkali fusion-selective ion electrode technique. *Analytical Chemistry*, *49*(1), 53-56.
133. Meenakshi, S., Sundaram, C. S., & Sukumar, R. (2008). Enhanced fluoride sorption by mechanochemically activated kaolinites. *Journal of hazardous materials*, *153*(1-2), 164-172.
134. Mehta, D., Mondal, P., & George, S. (2016). Utilization of marble waste powder as a novel adsorbent for removal of fluoride ions from aqueous solution. *Journal of Environmental Chemical Engineering*, *4*(1), 932-942.
135. Melidis, P. (2015). Fluoride removal from aluminium finishing wastewater by hydroxyapatite. *Environmental Processes*, *2*(1), 205-213.
136. Mendoza-Castillo, D. I., Rojas-Mayorga, C. K., García-Martínez, I. P., Pérez-Cruz, M. A., Hernández-Montoya, V., Bonilla-Petriciolet, A., & Montes-Morán, M. A. (2015). Removal of heavy metals and arsenic from aqueous solution using textile wastes from denim industry. *International Journal of Environmental Science and Technology*, *12*(5), 1657-1668.
137. Min, L. L., Yuan, Z. H., Zhong, L. B., Liu, Q., Wu, R. X., & Zheng, Y. M. (2015). Preparation of chitosan based electrospun nanofiber membrane and its adsorptive removal of arsenate from aqueous solution. *Chemical Engineering Journal*, *267*, 132-141.
138. Moghal, A. A. B., Reddy, K. R., Mohammed, S. A. S., Al-Shamrani, M. A., & Zahid, W. M. (2017). Retention studies on arsenic from aqueous solutions by lime treated semi-arid soils. *Int J Geomate*, *12*(29), 17-24.
139. Moghal, B., Reddy, K. R., Mohammed, S. A. S., Al-Shamrani, M. A., & Zahid, W. M. (2016) Sorptive Response of Chromium (Cr6) and Mercury (Hg2) From Aqueous Solutions Using Chemically Modified Soils, ASTM Journal of Testing and Evaluation

140. Mohammod, M., Sen, T. K., Maitra, S., & Dutta, B. K. (2011). Removal of Zn 2+ from aqueous solution using castor seed hull. *Water, Air, & Soil Pollution*, *215*(1-4), 609-620.
141. Mohan, D., & Pittman Jr, C. U. (2007). Arsenic removal from water/wastewater using adsorbents—a critical review. *Journal of hazardous materials*, *142*(1-2), 1-53.
142. Mohapatra, D., Mishra, D., Chaudhury, G. R., & Das, R. P. (2007). Arsenic (V) adsorption mechanism using kaolinite, montmorillonite and illite from aqueous medium. *Journal of Environmental Science and Health Part A*, *42*(4), 463-469.
143. Mohapatra, M., Anand, S., Mishra, B. K., Giles, D. E., & Singh, P. (2009). Review of fluoride removal from drinking water. *Journal of environmental management*, *91*(1), 67-77.
144. Mohseni-Bandpi, A., Kakavandi, B., Kalantary, R. R., Azari, A., & Keramati, A. (2015). Development of a novel magnetite–chitosan composite for the removal of fluoride from drinking water: adsorption modeling and optimization. *Rsc Advances*, *5*(89), 73279-73289.
145. Mondal P, Mohanty B, Majumder C B, Bhandari N. Removal of arsenic from simulated groundwater by GAC-Fe: A modeling approach. AIChE Journal, 2009, 55(7): 1860–1871.
146. Mondal, N. K., Bhaumik, R., & Datta, J. K. (2015). Removal of fluoride by aluminum impregnated coconut fiber from synthetic fluoride solution and natural water. *Alexandria Engineering Journal*, *54*(4), 1273-1284.
147. Monteiro, H., & Freire, F. (2012). Life-cycle assessment of a house with alternative exterior walls: comparison of three impact assessment methods. *Energy and Buildings*, *47*, 572-583.
148. Morillo, D., Uheida, A., Pérez, G., Muhammed, M., & Valiente, M. (2015). Arsenate removal with 3-mercaptopropanoic acid-coated superparamagnetic iron oxide nanoparticles. *Journal of colloid and interface science*, *438*, 227-234.
149. National Research Council, 2010. Technologies and Approaches to Reducing the Fuel
Consumption of Medium-and Heavy-duty Vehicles. National Academies Press.
150. Nguyen, V. T., Vigneswaran, S., Ngo, H. H., Shon, H. K., & Kandasamy, J. (2009). Arsenic removal by a membrane hybrid filtration system. *Desalination*, *236*(1-3), 363-369.

151. Nicolli, H. B., Bundschuh, J., Blanco, M. D. C., Tujchneider, O. C., Panarello, H. O., Dapeña, C., & Rusansky, J. E. (2012). Arsenic and associated trace-elements in groundwater from the Chaco-Pampean plain, Argentina: results from 100 years of research. *Science of the total Environment*, *429*, 36-56.
152. Nowok, J. W., Benson, S. A., Jones, M. L., & Kalmanovitch, D. P. (1990). Sintering behaviour and strength development in various coal ashes. *Fuel*, *69*(8), 1020-1028.
153. Ouzounis, K., Katsoyiannis, I., Zouboulis, A., & Mitrakas, M. (2015). Is the coagulation-filtration process with Fe (III) efficient for As (III) removal from groundwaters?. *Separation Science and Technology*, *50*(10), 1587-1592.
154. Öztel, M. D., Akbal, F., & Altaş, L. (2015). Arsenite removal by adsorption onto iron oxide-coated pumice and sepiolite. *Environmental Earth Sciences*, *73*(8), 4461-4471.
155. Padungthon, S., German, M., Wiriyathamcharoen, S., & SenGupta, A. K. (2015). Polymeric anion exchanger supported hydrated Zr (IV) oxide nanoparticles: a reusable hybrid sorbent for selective trace arsenic removal. *Reactive and Functional Polymers*, *93*, 84-94.
156. Pal, S., Tak, Y. K., & Song, J. M. (2007). Does the antibacterial activity of silver nanoparticles depend on the shape of the nanoparticle? A study of the gram-negative bacterium Escherichia coli. *Applied and environmental microbiology*, *73*(6), 1712-1720.
157. Patel, K. S., Sahu, B. L., Dahariya, N. S., Bhatia, A., Patel, R. K., Matini, L., ... & Bhattacharya, P. (2017). Groundwater arsenic and fluoride in Rajnandgaon District, Chhattisgarh, northeastern India. *Applied Water Science*, *7*(4), 1817-1826.
158. Patra, G., Das, P., Chakraborty, S., & Meikap, B. C. (2018). Removal of fluoride from wastewater using HCl-treated activated alumina in a ribbed hydrocyclone separator. *Journal of Environmental Science and Health, Part A*, *53*(7), 601-608.
159. Piñón-Miramontes, M., Bautista-Margulis, R. G., & Pérez-Hernández, A. (2003). Removal of arsenic and fluoride from drinking water with cake alum and a polymeric anionic flocculent. *Fluoride*, *36*(2), 122-128.
160. Prabhu, S. M., & Meenakshi, S. (2015). A dendrimer-like hyper branched chitosan beads toward fluoride adsorption from water. *International journal of biological macromolecules*, *78*, 280-286.

161. Pradhan, S. K., Panwar, J., & Gupta, S. (2017). Enhanced heavy metal removal using silver-yttrium oxide nanocomposites as novel adsorbent system. *Journal of Environmental Chemical Engineering*, *5*(6), 5801-5814.
162. Qi, J., Zhang, G., & Li, H. (2015). Efficient removal of arsenic from water using a granular adsorbent: Fe–Mn binary oxide impregnated chitosan bead. *Bioresource technology*, *193*, 243-249.
163. Qiao, J., Cui, Z., Sun, Y., Hu, Q., & Guan, X. (2014). Simultaneous removal of arsenate and fluoride from water by Al-Fe (hydr) oxides. *Frontiers of Environmental Science & Engineering*, *8*(2), 169-179.
164. Ramos, R. L., Ovalle-Turrubiartes, J., & Sanchez-Castillo, M. A. (1999). Adsorption of fluoride from aqueous solution on aluminum-impregnated carbon. *Carbon*, *37*(4), 609-617.
165. Rathore, V. K., Dohare, D. K., & Mondal, P. (2016). Competitive adsorption between arsenic and fluoride from binary mixture on chemically treated laterite. *Journal of Environmental Chemical Engineering*, *4*(2), 2417-2430.
166. Raul, P. K., Devi, R. R., Umlong, I. M., Thakur, A. J., Banerjee, S., & Veer, V. (2014). Iron oxide hydroxide nanoflower assisted removal of arsenic from water. *Materials Research Bulletin*, *49*, 360-368.
167. Reddy, K. R. (2010). Technical challenges to in-situ remediation of polluted sites. *Geotechnical and Geological Engineering*, *28*(3), 211-221.
168. Reddy, K. R., & Cameselle, C. (2009). *Electrochemical remediation technologies for polluted soils, sediments and groundwater*. John Wiley & Sons.
169. Reyes-Gómez, V. M., Alarcón-Herrera, M. T., Gutiérrez, M., & López, D. N. (2015). Arsenic and fluoride variations in groundwater of an endorheic basin undergoing land-use changes. *Archives of environmental contamination and toxicology*, *68*(2), 292-304.
170. Riahi, F., Bagherzadeh, M., & Hadizadeh, Z. (2015). Modification of Fe 3 O 4 superparamagnetic nanoparticles with zirconium oxide; preparation, characterization and its application toward fluoride removal. *RSC Advances*, *5*(88), 72058-72068.
171. Rojas-Mayorga, C. K., Silvestre-Albero, J., Aguayo-Villarreal, I. A., Mendoza-Castillo, D. I., & Bonilla-Petriciolet, A. (2015). A new synthesis route for bone chars using CO2 atmosphere and their application as fluoride adsorbents. *Microporous and Mesoporous Materials*, *209*, 38-44.

172. Rouf, M. A., & Hossain, M. D. (2003). Effects of using arsenic-iron sludge in brick making. *Fate of Arsenic in the Environment*, 193-208.
173. Saikia, B. J., & Parthasarathy, G. (2010). Fourier transform infrared spectroscopic characterization of kaolinite from Assam and Meghalaya, Northeastern India. *Journal of Modern Physics*, *1*(04), 206.
174. Sarkar, M., Banerjee, A., Pramanick, P. P., & Sarkar, A. R. (2006). Use of laterite for the removal of fluoride from contaminated drinking water. *Journal of colloid and interface science*, *302*(2), 432-441.
175. Saxena, V., & Ahmed, S. (2001). Dissolution of fluoride in groundwater: a water-rock interaction study. *Environmental geology*, *40*(9), 1084-1087.
176. Sen, T. K. (2012). Agricultural by-product biomass for removal of pollutants from aqueous solution by adsorption. *Journal of Environmental Research And Development Vol*, *6*(3).
177. Sen, T. K., & Sarzali, M. V. (2008). Removal of cadmium metal ion (Cd2+) from its aqueous solution by aluminium oxide (Al2O3): a kinetic and equilibrium study. *Chemical Engineering Journal*, *142*(3), 256-262.
178. Sen, T. K., Mahajan, S. P., & Khilar, K. C. (2002). Colloid-Associated contaminant transport in porous media: 1. Experimental studies. *AIChE journal*, *48*(10), 2366-2374.
179. Sen, T. K., Shanbhag, S., & Khilar, K. C. (2004). Subsurface colloids in groundwater contamination: a mathematical model. *Colloids and Surfaces A: Physicochemical and Engineering Aspects*, *232*(1), 29-38.
180. Senior, L. A., & Sloto, R. A. (2006). *Arsenic, boron, and fluoride concentrations in ground water in and near diabase intrusions, Newark Basin, Southeastern Pennsylvania* (No. 2006-5261). US Geological Survey.
181. Shih, Y. J., Huang, R. L., & Huang, Y. H. (2015). Adsorptive removal of arsenic using a novel akhtenskite coated waste goethite. *Journal of Cleaner Production*, *87*, 897-905.
182. Singh, A. K., Raj, B., Tiwari, A. K., & Mahato, M. K. (2013). Evaluation of hydrogeochemical processes and groundwater quality in the Jhansi district of Bundelkhand region, India. *Environmental earth sciences*, *70*(3), 1225-1247.
183. Singh, C. K., Sahu, J. N., Mahalik, K. K., Mohanty, C. R., Mohan, B. R., & Meikap, B. C. (2008). Studies on the removal of Pb (II) from wastewater by

activated carbon developed from Tamarind wood activated with sulphuric acid. *Journal of Hazardous Materials*, *153*(1-2), 221-228.

184. Singh, T. S., & Pant, K. K. (2006). Solidification/stabilization of arsenic containing solid wastes using portland cement, fly ash and polymeric materials. *Journal of Hazardous Materials*, *131*(1-3), 29-36.
185. Sivak, M., & Schoettle, B. (2012). Eco-driving: Strategic, tactical, and operational decisions of the driver that influence vehicle fuel economy. *Transport Policy*, *22*, 96-99.
186. Smedley, P. L., & Kinniburgh, D. G. (2002). A review of the source, behaviour and distribution of arsenic in natural waters. *Applied geochemistry*, *17*(5), 517-568.
187. Smedley, P. L., Nicolli, H. B., Macdonald, D. M. J., Barros, A. J., & Tullio, J. O. (2002). Hydrogeochemistry of arsenic and other inorganic constituents in groundwaters from La Pampa, Argentina. *Applied geochemistry*, *17*(3), 259-284.
188. Srinivasan, R. (2011). Advances in application of natural clay and its composites in removal of biological, organic, and inorganic contaminants from drinking water. *Advances in Materials Science and Engineering*, *2011*.
189. Sujana, M. G., & Anand, S. (2010). Iron and aluminium based mixed hydroxides: a novel sorbent for fluoride removal from aqueous solutions. *Applied Surface Science*, *256*(23), 6956-6962.
190. Suriyaraj, S. P., Bhattacharyya, A., & Selvakumar, R. (2015). Hybrid Al 2 O 3/bio-TiO 2 nanocomposite impregnated thermoplastic polyurethane (TPU) nanofibrous membrane for fluoride removal from aqueous solutions. *RSC Advances*, *5*(34), 26905-26912.
191. Sutcu, M., Alptekin, H., Erdogmus, E., Er, Y., & Gencel, O. (2015). Characteristics of fired clay bricks with waste marble powder addition as building materials. *Construction and Building Materials*, *82*, 1-8.
192. Swain, S. K., Dey, R. K., Islam, M., Patel, R. K., Jha, U., Patnaik, T., & Airoldi, C. (2009). Removal of fluoride from aqueous solution using aluminum-impregnated chitosan biopolymer. *Separation Science and Technology*, *44*(9), 2096-2116.
193. Tabelin, C. B., Igarashi, T., Arima, T., Sato, D., Tatsuhara, T., & Tamoto, S. (2014). Characterization and evaluation of arsenic and boron adsorption onto natural geologic materials, and their application in the disposal of excavated altered rock. *Geoderma*, *213*, 163-172.

194. Talat, M., Mohan, S., Dixit, V., Singh, D. K., Hasan, S. H., & Srivastava, O. N. (2018). Effective removal of fluoride from water by coconut husk activated carbon in fixed bed column: Experimental and breakthrough curves analysis. *Groundwater for Sustainable Development*, *7*, 48-55.
195. Taleb, K., Markovski, J., Milosavljević, M., Marinović-Cincović, M., Rusmirović, J., Ristić, M., & Marinković, A. (2015). Efficient arsenic removal by cross-linked macroporous polymer impregnated with hydrous iron oxide: material performance. *Chemical Engineering Journal*, *279*, 66-78.
196. Tan, W. F., Lu, S. J., Liu, F., Feng, X. H., He, J. Z., & Koopal, L. K. (2008). Determination of the point-of-zero charge of manganese oxides with different methods including an improved salt titration method. *Soil Science*, *173*(4), 277-286.
197. Tang, D., & Zhang, G. (2016). Efficient removal of fluoride by hierarchical Ce–Fe bimetal oxides adsorbent: thermodynamics, kinetics and mechanism. *Chemical Engineering Journal*, *283*, 721-729.
198. Tang, W., Li, Q., Gao, S., & Shang, J. K. (2011). Arsenic (III, V) removal from aqueous solution by ultrafine α-Fe2O3 nanoparticles synthesized from solvent thermal method. *Journal of hazardous materials*, *192*(1), 131-138.
199. Tang, Y., Wang, J., & Gao, N. (2010). Characteristics and model studies for fluoride and arsenic adsorption on goethite. *Journal of Environmental Sciences*, *22*(11), 1689-1694.
200. Tchieda, V. K., D'Amato, E., Chiavola, A., Parisi, M., Chianese, A., Amamra, M., & Kanaev, A. (2016). Removal of arsenic by alumina: effects of material size, additives, and water contaminants. *Clean–Soil, Air, Water*, *44*(5), 496-505.
201. Teimouri, A., Nasab, S. G., Habibollahi, S., Fazel-Najafabadi, M., & Chermahini, A. N. (2015). Synthesis and characterization of a chitosan/montmorillonite/ZrO 2 nanocomposite and its application as an adsorbent for removal of fluoride. *RSC Advances*, *5*(9), 6771-6781.
202. Teychene, B., Collet, G., Gallard, H., & Croue, J. P. (2013). A comparative study of boron and arsenic (III) rejection from brackish water by reverse osmosis membranes. *Desalination*, *310*, 109-114.
203. The EPA, 2015. TCLP: Toxicity Characteristic Leaching Procedure and Characteristic

Wastes (D-codes). Available online at: http://www.ehso.com/cssepa/TCLP.htm. Accessed on 16 August 2016.

204. Thirunavukkarasu, O. S., Viraraghavan, T., Subramanian, K. S., Chaalal, O., & Islam, M. R. (2005). Arsenic removal in drinking water—impacts and novel removal technologies. *Energy sources*, *27*(1-2), 209-219.
205. Togarcheti, S. C., kumar Mediboyina, M., Chauhan, V. S., Mukherji, S., Ravi, S., & Mudliar, S. N. (2017). Life cycle assessment of microalgae based biodiesel production to evaluate the impact of biomass productivity and energy source. *Resources, Conservation and Recycling*, *122*, 286-294.
206. Tor, A., Danaoglu, N., Arslan, G., & Cengeloglu, Y. (2009). Removal of fluoride from water by using granular red mud: batch and column studies. *Journal of hazardous materials*, *164*(1), 271-278.
207. Tresintsi, S., Simeonidis, K., Katsikini, M., Paloura, E. C., Bantsis, G., & Mitrakas, M. (2014). A novel approach for arsenic adsorbents regeneration using MgO. *Journal of hazardous materials*, *265*, 217-225.
208. Tressaud, A. (2006). *Fluorine and the environment: agrochemicals, archaeology, green chemistry and water* (Vol. 2). Elsevier.
209. Tripathy, S. S., & Raichur, A. M. (2008). Enhanced adsorption capacity of activated alumina by impregnation with alum for removal of As (V) from water. *Chemical Engineering Journal*, *138*(1-3), 179-186.
210. Van Vinh, N., Zafar, M., Behera, S. K., & Park, H. S. (2015). Arsenic (III) removal from aqueous solution by raw and zinc-loaded pine cone biochar: equilibrium, kinetics, and thermodynamics studies. *International journal of environmental science and technology*, *12*(4), 1283-1294.
211. Vences-Alvarez, E., Velazquez-Jimenez, L. H., Chazaro-Ruiz, L. F., Diaz-Flores, P. E., & Rangel-Mendez, J. R. (2015). Fluoride removal in water by a hybrid adsorbent lanthanum–carbon. *Journal of colloid and interface science*, *455*, 194-202.
212. Verbinnen, B., Block, C., Van Caneghem, J., & Vandecasteele, C. (2015). Recycling of spent adsorbents for oxyanions and heavy metal ions in the production of ceramics. *Waste management*, *45*, 407-411.
213. Villanueva, C. M., Kogevinas, M., Cordier, S., Templeton, M. R., Vermeulen, R., Nuckols, J. R., & Levallois, P. (2014). Assessing exposure and health

consequences of chemicals in drinking water: current state of knowledge and research needs. *Environmental Health Perspectives*, *122*(3), 213.

214. Vivek Vardhan, C. M., & Srimurali, M. (2016). Defluoridation of drinking water using a novel sorbent: lanthanum-impregnated green sand. *Desalination and Water Treatment*, *57*(1), 202-212.
215. Vu, T. A., Le, G. H., Dao, C. D., Dang, L. Q., Nguyen, K. T., Nguyen, Q. K., ... & Lee, G. D. (2015). Arsenic removal from aqueous solutions by adsorption using novel MIL-53 (Fe) as a highly efficient adsorbent. *Rsc Advances*, *5*(7), 5261-5268.
216. Waghmare, S. S., Arfin, T., Manwar, N., Lataye, D. H., Labhsetwar, N., & Rayalu, S. (2015). Preparation and characterization of polyalthia longifolia based alumina as a novel adsorbent for removing fluoride from drinking water. *Asian J. Adv. Basic Sci*, *4*(1), 12-24.
217. Waghmare, S., Arfin, T., Rayalu, S., Lataye, D., Dubey, S., & Tiwari, S. (2015). Adsorption behavior of modified zeolite as novel adsorbents for fluoride removal from drinking water: surface phenomena, kinetics and thermodynamics studies. *International Journal of Science, Engineering and Technology Research*, *4*(12), 4114-24.
218. Wang, J., Kang, D., Yu, X., Ge, M., & Chen, Y. (2015). Synthesis and characterization of Mg–Fe–La trimetal composite as an adsorbent for fluoride removal. *Chemical Engineering Journal*, *264*, 506-513.
219. Wasewar, K. L. (2010). Adsorption of metals onto tea factory waste: a review. *Int. J. Res. Rev. Appl. Sci.*, *3*(3), 303-322.
220. Wen, D., Zhang, F., Zhang, E., Wang, C., Han, S., & Zheng, Y. (2013). Arsenic, fluoride and iodine in groundwater of China. *Journal of Geochemical Exploration*, *135*, 1-21.
221. Wen, Z., Zhang, Y., Dai, C., Chen, B., Guo, S., Yu, H., & Wu, D. (2014). Synthesis of ordered mesoporous iron manganese bimetal oxides for arsenic removal from aqueous solutions. *Microporous and Mesoporous Materials*, *200*, 235-244.
222. Weng, C. H., Lin, D. F., & Chiang, P. C. (2003). Utilization of sludge as brick materials. *Advances in environmental research*, *7*(3), 679-685.
223. World Health Organisation, Guidelines for Drinking Water Quality, fourth ed., World Health Organisation, Geneva, 2011

224. Xu, Z., Jing, C., Li, F., & Meng, X. (2008). Mechanisms of photocatalytical degradation of monomethylarsonic and dimethylarsinic acids using nanocrystalline titanium dioxide. *Environmental science & technology*, *42*(7), 2349-2354.
225. Yami, T. L., Du, J., Brunson, L. R., Chamberlain, J. F., Sabatini, D. A., & Butler, E. C. (2015). Life cycle assessment of adsorbents for fluoride removal from drinking water in East Africa. *The International Journal of Life Cycle Assessment*, *20*(9), 1277-1286.
226. Yin, H., Kong, M., & Tang, W. (2015). Removal of fluoride from contaminated water using natural calcium-rich attapulgite as a low-cost adsorbent. *Water, Air, & Soil Pollution*, *226*(12), 425.
227. Yogamalar, R., Srinivasan, R., Vinu, A., Ariga, K., & Bose, A. C. (2009). X-ray peak broadening analysis in ZnO nanoparticles. *Solid State Communications*, *149*(43-44), 1919-1923.
228. Yu, L., Ma, Y., Ong, C. N., Xie, J., & Liu, Y. (2015). Rapid adsorption removal of arsenate by hydrous cerium oxide–graphene composite. *RSC Advances*, *5*(80), 64983-64990.
229. Yu, Y., Yu, L., Shih, K., & Chen, J. P. (2018). Yttrium-doped iron oxide magnetic adsorbent for enhancement in arsenic removal and ease in separation after applications. *Journal of colloid and interface science*, *521*, 252-260.
230. Zazouli, M. A., Mahvi, A. H., Mahdavi, Y., & Balarak, D. (2015). Isothermic and kinetic modeling of fluoride removal from water by means of the natural biosorbents sorghum and canola. *Fluoride*, *48*(1), 37.
231. Zehhaf, A., Benyoucef, A., Quijada, C., Taleb, S., & Morallon, E. (2015). Algerian natural montmorillonites for arsenic (III) removal in aqueous solution. *International Journal of Environmental Science and Technology*, *12*(2), 595-602.
232. Zhang, Y., Dou, X. M., Yang, M., He, H., Jing, C. Y., & Wu, Z. Y. (2010). Removal of arsenate from water by using an Fe–Ce oxide adsorbent: effects of coexistent fluoride and phosphate. *Journal of hazardous materials*, *179*(1-3), 208-214.
233. Zhao, X., Wang, J., Wu, F., Wang, T., Cai, Y., Shi, Y., & Jiang, G. (2010). Removal of fluoride from aqueous media by Fe3O4@ Al (OH) 3 magnetic nanoparticles. *Journal of Hazardous Materials*, *173*(1-3), 102-109.

234. Zhou, J., Zhu, W., Yu, J., Zhang, H., Zhang, Y., Lin, X., & Luo, X. (2018). Highly selective and efficient removal of fluoride from ground water by layered Al-Zr-La Tri-metal hydroxide. *Applied Surface Science*, *435*, 920-927.
235. Zhu, B. S., Jia, Y., Jin, Z., Sun, B., Luo, T., Yu, X. Y., ... & Liu, J. H. (2015). Controlled synthesis of natroalunite microtubes and spheres with excellent fluoride removal performance. *Chemical Engineering Journal*, *271*, 240-251.
236. Zhu, J., Lin, X., Wu, P., Zhou, Q., & Luo, X. (2015). Fluoride removal from aqueous solution by Al (III)–Zr (IV) binary oxide adsorbent. *Applied Surface Science*, *357*, 91-100.

WEBLINKS

1. http://mnre.gov.in/mnre-2010/offgrid/biogas-2/ (Accessed 16 September 2017).
2. https://dir.indiamart.com/delhi/hydrochloricacid.html;D.S.WaterTechnology,New Delhi
3. https://www.alibaba.com/product-detail/Sodium-Hydroxide-Caustic-Soda Flake_50035798802.html?spm=a2700.7724857.main07.69.441e6209DZUtYv
4. The Public Notice of Uttarakhand Power Corporation Limited Electrical Tariff 2014 Dated 01.04.14; Uttarakhand Power Corporation Limited: Dehradun, India, 2014; https://www.upcl.org/wss/downloads/TariffMay_8274.pdf (accessed January 02, 2015).
5. Aluminim Rate; Bennett, Coleman & Co. Ltd., 2017; http://economictimes.indiatimes.com/commoditysummary/symbolALUMINIUM.cms (accessed January 13, 2017).